



UNIVERSITAT DE
BARCELONA

IKK α modulates metastatic activity by preventing Tight Junctions stabilization and collective cell migration

Daniel Alvarez Villanueva

ADVERTIMENT. La consulta d'aquesta tesi queda condicionada a l'acceptació de les següents condicions d'ús: La difusió d'aquesta tesi per mitjà del servei TDX (www.tdx.cat) i a través del Dipòsit Digital de la UB (diposit.ub.edu) ha estat autoritzada pels titulars dels drets de propietat intel·lectual únicament per a usos privats emmarcats en activitats d'investigació i docència. No s'autoritza la seva reproducció amb finalitats de lucre ni la seva difusió i posada a disposició des d'un lloc aliè al servei TDX ni al Dipòsit Digital de la UB. No s'autoritza la presentació del seu contingut en una finestra o marc aliè a TDX o al Dipòsit Digital de la UB (framing). Aquesta reserva de drets afecta tant al resum de presentació de la tesi com als seus continguts. En la utilització o cita de parts de la tesi és obligat indicar el nom de la persona autora.

ADVERTENCIA. La consulta de esta tesis queda condicionada a la aceptación de las siguientes condiciones de uso: La difusión de esta tesis por medio del servicio TDR (www.tdx.cat) y a través del Repositorio Digital de la UB (diposit.ub.edu) ha sido autorizada por los titulares de los derechos de propiedad intelectual únicamente para usos privados enmarcados en actividades de investigación y docencia. No se autoriza su reproducción con finalidades de lucro ni su difusión y puesta a disposición desde un sitio ajeno al servicio TDR o al Repositorio Digital de la UB. No se autoriza la presentación de su contenido en una ventana o marco ajeno a TDR o al Repositorio Digital de la UB (framing). Esta reserva de derechos afecta tanto al resumen de presentación de la tesis como a sus contenidos. En la utilización o cita de partes de la tesis es obligado indicar el nombre de la persona autora.

WARNING. On having consulted this thesis you're accepting the following use conditions: Spreading this thesis by the TDX (www.tdx.cat) service and by the UB Digital Repository (diposit.ub.edu) has been authorized by the titular of the intellectual property rights only for private uses placed in investigation and teaching activities. Reproduction with lucrative aims is not authorized nor its spreading and availability from a site foreign to the TDX service or to the UB Digital Repository. Introducing its content in a window or frame foreign to the TDX service or to the UB Digital Repository is not authorized (framing). Those rights affect to the presentation summary of the thesis as well as to its contents. In the using or citation of parts of the thesis it's obliged to indicate the name of the author.

IKK α modulates metastatic activity by preventing Tight Junctions stabilization and collective cell migration

Daniel Alvarez Villanueva



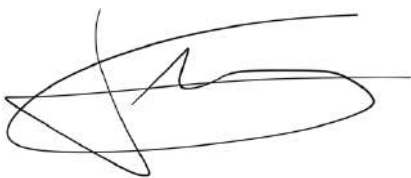
TESI DOCTORAL UB / 2024

Programa de Doctorat en Biomedicina

Programa d'Investigació del Càncer

Hospital del Mar Research Institute

Institut d'Investigació Biomèdica de Bellvitge (IDIBELL)



Directors: Dr. Lluís Espinosa Blay

Dr. Alberto Villanueva Garatachea

Tutor: Dr. Francesc Vinyals Canals

 **Hospital del Mar**
Research Institute
Barcelona

 **IDI BELL**
Institut d'Investigació
Biomèdica de Bellvitge

 
 **Universitat**
de Barcelona



UNIVERSITAT DE BARCELONA

Programa de Doctorat en Biomedicina

IKK α modulates metastatic activity by preventing tight junction stabilization and collective cell migration

TESI DOCTORAL UB / 2024

Memòria de tesi doctoral presentada per Daniel Alvarez Villanueva
per optar al grau de doctor per la Universitat de Barcelona,
realitzat sota la direcció del Dr. Lluís Espinosa Blay
i del Dr. Alberto Villanueva Garatachea

Barcelona, 2024

ACKNOWLEDGEMENTS

ACKNOWLEDGEMENTS/AGRADECIMIENTOS

Muchos dicen que el doctorado es una etapa muy dura a la vez que muy desafiante en la que aprendes muchísimas cosas tanto a nivel profesional como personal. Lo que no había escuchado tanto es que, en medio de todo ese “caos”, también tienes la sensación de estar viviendo una de las mejores etapas de tu vida, en la que ir a trabajar no se te hace ni mucho menos una montaña e incluso te levantas con ganas de ir a ver cómo van las cosas. Todo eso, en gran parte, es por la gente que te acompaña en el camino y por eso, esta tesis va dedicada a todas esas personas que han hecho que estos cuatro años hayan sido geniales.

Para empezar, me gustaría agradecerle a ti, Alberto. Porque sin ti seguramente no estaría escribiendo estos agradecimientos de la tesis (aún me cuesta creérmelo), ni seguramente trabajando de lo que de verdad me apasiona. Hace unos cuantos años ya, me llevaste a ver de qué trabajabas (sí, los ratones y los gusanos) y desde entonces supe que lo que de verdad quería ser era científico. En ti vi lo que realmente era la pasión por tu trabajo y que si haces lo que de verdad te gusta la rutina no tiene por qué ser algo negativo, sino que se convierte en algo fantástico. Gracias por ayudarme a darme cuenta de que lo más importante era estudiar algo que me gustara sin importar las salidas que pudiera tener en el futuro. Y cómo olvidarme que gracias a ti pude hacer el doctorado (aunque la resolución de la beca fuera con suspense y medio de rebote). Por todo eso y mucho más, quería dedicarte a ti el primero esta tesis. Espero que, aunque sea la última que diriges (o eso dices), sea especial y la sientas también tuya.

La meva arribada al BigSpin lab va ser fa molt de temps ja, jo era un estudiant de carrera que buscava un lloc on fer el treball de fi de grau i, perquè no, quedar-m'hi després per fer un doctorat? Encara recordo el primer dia que vaig coincidir amb vosaltres, Lluís i Anna. Tot i que estava molt perdut vaig tenir la sensació que aquell havia de ser el meu lloc. Des de el primer dia m'heu fet sentir com a casa i això és una de les coses que no oblidaré mai. Lluís, m'agradaria que sabessis lo afortunat que em sento per haver-me donat la oportunitat d'unir-me al laboratori. Des de l'inici vas confiar en mi per portar un projecte que, a dia d'avui, es el centre d'aquesta tesi (“lo bueno, si breve, dos veces bueno” però s'ha allargat una mica la història...). Sempre has valorat el meu treball en positiu però també amb un esperit molt crític que, en part, m'ha ajudat a ser molt exigent amb mi mateix i la feina que faig, t'ho agraeixo de veritat. Fer el doctorat sota la vostra direcció ha estat un luxe, no ho canviaria per res.

La culpa de que este viaje haya sido genial es, sin duda, de mis compañeros de laboratorio. Me gustaría agradecerlos el haberme aguantado durante todo este tiempo, en los días buenos, pero sobre todo en los malos. De todos vosotros me llevo el gran grupo que somos y lo fácil que es trabajar con vosotros al lado.

Josune (George de la jungle, Yusuf), que bueno coincidir con alguien como tú. No podría haber tenido una mejor compañera de desgracias, ese es el resumen. Pero también de muchísimas risas y buenos momentos que ahora echo tanto de menos, porque desde que te fuiste del lab parece que ya no es lo mismo. Seguro que todo te va a ir genial porque te lo mereces y porque eres una currante que lo hace todo genial. Aunque seas vasca y me dejaras la custodia de MEMO, siempre tendrás un amigo catalán que le tiene pavor a la lluvia y al mal tiempo. Eskerrik asko, oso ondo.

Violeta (Violet), eres una investigadora como la copa de un pino y, aunque te desearía suerte en tu nueva aventura, estoy seguro de que no la necesitas, te va a ir genial. Aunque casi te rompiera el pie de un martillazo “.”, totalmente involuntario, también eres mi postdoc favorita (como dice padre). Bueno, y la mejor contrabandista de crema de orujo del mundo, a ver si por fin la pruebo... Creo que eres la persona más inteligente que he conocido en el mundo de la ciencia y te tengo que agradecer el haberme acompañado y aconsejado durante esta aventura.

Luis (Koldo, Zuis, Hugo), la pasión por la ciencia en persona. Espero que no la pierdas nunca y la sigas transmitiendo a la gente que te rodea porque es la ostia. Eres un tío genial y es una pena que te vayas a la otra punta del mundo, literalmente, porque eso significa que ya no podremos seguir con la custodia compartida de Hugo y Bart (a Hugo te lo quedas tu). Pero también estoy seguro de que va a ser una aventura increíble y te va a ir genial. Quién sabe dónde y cuándo volveremos a coincidir (USA, ruta en burro?) pero seguro que será con una sonrisa de oreja a oreja, porque eso es lo que transmites cada día.

Ángela (Engels, Angelines), aunque no hace tanto que llegaste te has convertido en un pilar del lab. Tienes una energía muy guay que contagias a los que te rodean. Te contaría alguna historia de algún día en el lab, pero seguro que ya te las sabes todas así que prefiero que la cuentes tú, que se te da genial. Aunque debes tener cuidado, nunca sabes hacia qué lado batea la gente.

Los “real jefes” del lab, Jessi (Gonzalez) y Arnau (Agno, Arnaldo, Ronaldo, Reinildo, Ronnie, Gonnie). Mientras vosotros sigáis en el lab todo seguirá genial, porque sois unos cracks gestionándolo todo y aguantándonos a todos. Os merecéis un monumento.

A todos los miembros actuales del BigSpin lab: Laura S. (Lora), m'agradaria agrair-te tota l'ajuda des de l'inici amb els organoides i drames relacionats, les penes compartides son menys penes diuen. Patri (Patrick) eres la siguiente, así que ánimo con la tesis, aunque aún te quede "mucho" tiempo... Gayathri, I'm sure you'll have a great PhD experience, you're very kind and deserve it. Alba, acabas de empezar así que lo único que puedo decirte es que aproveches al máximo la experiencia porque es única. María, desde tu llegada todos intuimos que eras una profesional como la copa de un pino, pero al trabajar contigo codo con codo de lo que de verdad te das cuenta es de que eres una máquina. Muchísimas gracias por toda la ayuda y el tiempo que le has dedicado a mi proyecto, has sido el gel en el km 30 que te ayuda a llegar al final y acabar sin ningún desmayo. Eric, gracias por tu implicación y por tu profesionalidad. Aunque a veces haya sido muy pesado con los colores de los gráficos, espero que te lleves un buen recuerdo de nuestro trabajo juntos, como el que me llevo yo. Y también a todos los miembros que coincidieron conmigo en el BigSpin lab, en especial a Irene y Laura M. por ser mis dos teachers en el lab, tanto al inicio como cuando empecé a currar de verdad. Y también a David, que buenos momentos pasamos tú y yo "colaborando" boicoteándonos experimentos y haciendo arte contemporáneo en las poyatas. Y cómo olvidarme de Evelyn (Evelyna), aunque no formes parte del lab sabes que eres una más. Sin ti, quien sabe si yo podría enseñar alguna immuno en esta tesis. Costó mucho, muchísimo o incluso más. Pero que bonito nos quedó el rosa.

Muchas gracias a todos, habéis hecho que mi paso por el BigSpin lab haya sido increíble, no cambiaría, ni por un segundo, la elección que tomé hace ya 6 años.

Me gustaría también agradecer a todos los colaboradores que he tenido durante este tiempo, en especial a María, por haberme ayudado con toda la casquería que hay detrás de los experimentos con bichos y por ayudarme a entender el "caos organizativo" de Alberto. Eres una crack en tu trabajo y una persona genial. I també al Joan, per estar sempre estar disposat a ajudar i a fer un cop de mà fins i tot quan no tens ni un minut lliure. Els mutants són una realitat gràcies a tu. A l'equip d'AP de l'Hospital del Mar; Mar, Monica i Anna, gràcies per deixar-me anar a molestar als matins per fer un cop d'ull als talls i per fer-vos perdre una mica el temps explicant-me totes les coses que no sabia (pràcticament tot el que miràvem), m'ha encantat. También a los laboratorios vecinos, caracoles y celíacos, por haberme prestado absolutamente de todo, y hacerlo siempre entre risas.

Me gustaría agradecer también a mis amigos, a los que siempre están ahí: Albert, Jaume, Carreño, Lydia, Amparo y María. Aunque no lo sepáis, habéis contribuido a que haya llegado al final de esta aventura sin volverme loco. Me encanta pasar tiempo con vosotros y si es sufriendo en el Crossfit

(Jaume y María pa' cuando) o en una carrera en el barro, mejor. Podéis contar conmigo para lo que sea. También a Andrés y Teijeiro. Aunque no nos veamos tan a menudo sé que estáis ahí. I com oblidar-me del Joan i el Xavi, el millor que m'emporto de la uni sou vosaltres sense cap mena de dubte, sou uns genis.

A mi familia, en especial a mis padres y mis abuelos (Muninos), sin los que esta tesis hoy no sería posible. Por inculcarme los valores que tengo desde pequeño. Por enseñarme que el esfuerzo siempre tiene su recompensa, por muy dura que parezca la situación actual. A ser agradecido por todo y con todo el mundo. Espero que estéis orgullosos.

En especial a ti mama, Isabelita. Por ser faro en la tormenta y haber aguantado mil y unas conmigo al lado. Por el amor que nos das a todos los que te rodeamos. Es un regalo poder contar contigo para cualquier cosa. Gracias por aconsejarme y acompañarme en todas las decisiones que tomo. Sé que no te lo digo todo lo que debería, te quiero muchísimo. Eres mi ejemplo a seguir. A ti, en especial, te dedico esta tesis.

Per últim a tu Sara, fem camí junts des de fa uns quants anys i no podria haver desitjat una millor companya d'aventures. Crec que ens compenetrem a la perfecció. Tu sempre ho tens tot controlat i jo casi mai res, però aquí està el secret d'una barreja perfecta. Gràcies per animar-me en els moments més durs d'aquesta etapa, has estat sempre el meu gran recolzament i la que sempre ha cregut en mi, fins i tot quan ni jo mateix ho feia. En breus et tocarà a tu preparar i defensar la tesi i allà estaré, com el teu màxim hooligan per veure com triomfes i ho petes. Qui sap què ens depararà la pròxima aventura, el que si que sé es que amb tu al costat, tota la resta només serà un petit detall. Ets genial, no canviïs mai. Podria estar escrivint un milió de pàgines sobre les coses bones i lo agraït que estic a la vida de compartir-la amb tu, però no es gaire el meu estil, així que ho resumiré molt breument: t'estimo molt.

M'agradaria tancar amb la frase que més cops m'ha repetit el meu jefe durant aquests quatre anys de tesi:

“Dani, t’ho passes tan bé al lab que hauries de pagar per venir a treballar!!!”

I quina raó té...

MOLTES GRÀCIES A TOTS!!!

ABSTRACT

ABSTRACT

The IKK α kinase was previously found to activate multiple oncogenic and therapy-resistance pathways, including ATM/DDR, BRD4, and JAK/STAT3, independently of canonical NF- κ B signaling. Here, we show that suppression of IKK α , either genetically or pharmacologically, imposes a pro-metastatic activity on colorectal cancer (CRC) patient-derived organoid (PDO) cells, which is linked to an increase in the protein levels of the tight junction protein ZO-1 and CLDN2, and a shift in their migratory mode towards collective migration. Analysis of single-cell (sc)RNAseq data revealed an accumulation of the tight junction signature in the metastatic populations. Specifically, PDO cells contain three distinct epithelial cell clusters (C2, C4 and C8) with concomitant enrichment of the tight junction and metastasis-associated EpiHR signatures, whose unique genetic signatures are upregulated upon depletion of IKK α and enriched in PDO-derived metastases. CLDN2 inhibition or depletion abolishes the metastatic activity of IKK α KO PDO cells *in vivo*. By analyzing human paraffin-embedded CRC specimens, we have detected the presence of vascular tumor infiltrates with cluster-like or glandular phenotypes and high levels of ZO-1 and CLDN2-positive junctions.

Collectively, our results suggest that high levels of tight junction proteins in CRC cells imposes a pro-metastatic collective CRC cell migration, which can be detected in the vascular infiltrates at diagnosis. We propose that after validation, this type of exploration could be standardized in the clinical routine.

RESUMEN

Estudios previos han asociado la quinasa IKK α con la activación de múltiples vías de señalización y mecanismos de resistencia a la terapia contra el cáncer, como ATM/DDR, BRD4 y JAK/STAT, de manera independiente a la vía de señalización canónica NF- κ B. En este trabajo, demostramos que la supresión de la función de IKK α , tanto genética como farmacológicamente, induce una actividad pro-metastática en los organoides derivados de paciente (PDOs), asociada a un aumento en los niveles de las proteínas de las uniones estrechas ZO-1 y CLDN2, además de un cambio hacia la migración colectiva. El análisis de los datos de secuenciación de ARN de célula única (scRNA-seq) reveló una acumulación de la firma de uniones estrechas en las poblaciones metastáticas. En particular, las células secuenciadas de PDO contienen tres conjuntos celulares epiteliales distintos (C2, C4 y C8) con un enriquecimiento significativo de la firma de uniones estrechas y de la firma EpiHR, asociada a la metástasis. Ambas firmas genéticas se incrementan tras la eliminación de IKK α y se encuentran enriquecidas en las metástasis derivadas de los PDOs. La inhibición o eliminación de la proteína CLDN2 suprime la actividad metastática de las células PDO con IKK α eliminada en modelos *in vivo*. En el análisis de muestras de tumores colorrectales incluidos en parafina, se detectaron infiltrados tumorales vasculares con morfología colectiva, presentando agrupaciones celulares sólidas o glandulares con altos niveles de uniones positivas para ZO-1 y CLDN2.

En conjunto, nuestros resultados sugieren que los altos niveles de proteínas de uniones estrechas en las células de cáncer colorrectal promueven una migración celular colectiva pro-metastática, detectable en infiltrados vasculares en el momento del diagnóstico. Finalmente, proponemos que, tras su validación, este tipo de análisis se estandarice en la práctica clínica.

RESUM

Estudis previs han relacionat la quinasa IKK α amb l'activació de múltiples vies de senyalització i mecanismes de resistència a la teràpia contra el càncer, incloent ATM/DDR, BRD4 i JAK/STAT, independentment a la via de senyalització canònica NF- κ B. En aquest treball, demostrem que la supressió de la funció d'IKK α , tant genètica com farmacològica, imposa una activitat pro-metastàtica en organoids derivats de pacient (PDOs), el que està vinculat a un augment dels nivells de les proteïnes ZO-1 i CLDN2, presents en les unions estretes, així com el canvi en el mode migratori cap a la migració col·lectiva. L'anàlisi de les dades de seqüenciació d'ARN de cèl·lula única (scRNA-seq) va mostrar l'acumulació de la firma de unions estretes en les poblacions metastàtiques. En concret, les cèl·lules de PDO seqüenciades contenen, entre d'altres, tres conjunts cel·lulars epitelials (C2, C4 i C8) amb un enriquiment significatiu de la firma d'unions estretes i de la firma EpiHR associada a metastasi. Ambdues firmes genètiques augmenten a l'eliminar l'expressió d'IKK α i s'enriqueixen en les metastasi derivades de les cèl·lules de PDO. La inhibició o eliminació de la proteïna CLDN2 suprimeix l'activitat metastàtica de les cèl·lules IKK α KO de PDO *in vivo*. Mitjançant l'anàlisi de tumors colorectals inclosos en parafina en el moment del diagnòstic, hem detectat la presència d'infiltrats vasculars tumorals amb morfologia col·lectiva; grups cel·lulars sòlids o glandulars, als quals es detecten alts nivells d'unions cel·lulars positives per ZO-1 i CLDN2.

En conjunt, els nostres resultats suggereixen que la presència d'alts nivells de les proteïnes d'unions estretes a les cèl·lules de càncer colorectal, imposen la migració col·lectiva pro-metastàtica, que pot detectar-se als infiltrats vasculars al moment del diagnòstic. Finalment, proposem que, posterior a la seva validació, aquest tipus d'exploració s'estandarditzi a la rutina clínica.

TABLE OF CONTENTS

TABLE OF CONTENTS

ACKNOWLEDGEMENTS/AGRADECIMIENTOS	7
ABSTRACT.....	13
RESUMEN	15
RESUM	17
TABLE OF CONTENTS.....	21
FIGURES AND TABLES	29
ABBREVIATIONS AND ACRONYMS	35
INTRODUCTION	45
I1. COLORECTAL CANCER	45
I1.1 Epidemiology of colorectal cancer.....	45
I1.2 Molecular mechanisms of colorectal cancer development and progression	45
I1.3 Colorectal cancer classification.....	48
I1.4 Cancer stem cells	50
I1.5 Colorectal cancer therapeutic strategies	51
I2. TUMOR DISSEMINATION AND METASTASIS.....	52
I2.1 Metastatic origin.....	53
I2.2 Metastatic intravasation.....	53
I2.3 Metastatic extravasation	54
I2.4 Metastatic site	54
I3. CIRCULATING TUMOR CELLS NATURE	56
I3.1 EMT	56
I3.2 CTC clusters.....	57
Homotypic CTC clusters	58
Heterotypic CTC clusters.....	58
I3.3 Detection and analysis of CTCs	59
I3.4 Potential CTC-based therapies.....	60

13.5 Prognostic and predictive value of CTCs.....	60
14. NF-κB SIGNALING PATHWAY	61
14.1 NF- κ B family, structure and classification.....	61
NF- κ B transcription factors.....	61
Inhibitor of NF- κ B (I κ B)	61
I κ B kinase complex (IKK complex).....	62
14.2 Activation of NF- κ B signaling pathway.....	63
Classical NF- κ B pathway (canonical)	63
Alternative NF- κ B pathway (non-canonical)	64
14.3 NF- κ B independent IKK α functions and cancer association.....	65
15. TIGHT JUNCTIONS.....	68
15.1 Tight junction structure	68
Junctional plaque components.....	68
Transmembrane proteins	69
15.2 Tight junctions in cancer	70
ZO-1	71
CLDN2	71
15.3 Tight junction elements in cancer treatment	72
OBJECTIVES	77
MATERIALS AND METHODS	81
MM1. CELL LINES AND REAGENTS.....	81
MM2. PDOs GENERATION	81
MM3. PDOs CULTURE AND PASSAGING	83
MM3.1 Mechanical disaggregation	84
MM3.2 Disaggregation to single cells.....	84
MM4. CELL TRANSFECTION	85
MM5. CELL INFECTION	86
MM5.1 Viral production	87
MM5.2 Viral infection.....	88

Cell lines viral infection.....	88
PDOs viral infection	88
MM6. CRISPR-Cas9 GENE MODIFICATION	89
MM7. CELL LYSATES	91
MM8. WOUND-HEALING ASSAY.....	92
MM9. TRANSWELL	92
MM10. CELL CLUSTERING <i>IN VITRO</i>	93
MM11. PDOs ADHESION AND MIGRATION ASSAY	93
MM12. CHROMATIN IMMUNOPRECIPITATION ASSAY (ChIP) AND ChIPseq	94
MM13. GST-FUSION PROTEIN AND PULLDOWN ASSAY	97
MM14. CO-IMMUNOPRECIPITATION.....	99
MM15. WESTERN BLOT	100
MM16. IMMUNOFLUORESCENCE	102
MM17. RNA ISOLATION	103
MM18. RT-qPCR.....	105
MM19. TUMOR INITIATING CAPACITY <i>IN VITRO</i>	106
MM20. CRYSTAL VIOLET STAINING	107
MM21. PARAFFIN EMBEDDING OF TUMOR SAMPLES	107
MM22. IMMUNOHISTOCHEMISTRY.....	108
MM23. HAEMATOXYLIN AND EOSIN STAINING.....	109
MM24. ANIMAL STUDIES	110
MM25. BULK RNA-seq DATA ANALYSIS	110
MM26. SINGLE CELL RNA-seq DATA ANALYSIS.....	112
MM27. CRC PATIENTS METACOHORT	113
MM28. QUANTIFICATION AND STATISTICAL ANALYSIS.....	115
RESULTS	119
PART I	119
R1. Regulation of the tight junction proteins ZO-1 and CLDN2 by the IKK α kinase.....	119
R2. Functional depletion of IKK α alters the migratory behavior of cancer cells.....	125

R3. Accumulation of the tight junction signature in CRC IKK α KO cells is linked to a higher metastatic activity	129
R4. Accumulation of high relapse and tight junction signature in two different clusters of PDO5, that are characterized by TFF3 expression are increased in IKK α KO cells	133
R5. Targeting CLDN2 activity reverts the migratory mode imposed by IKK deficiency	137
R6. Different modes of vascular invasion and tight junction distribution are detected in primary human CRC samples. ZO-1 and CLDN2 as candidate IHC biomarkers in the invasive clusters	141
R7. Activation of the MAPK pathway linked to downregulation of DUSPs in IKK α KO tumor cells increases metastatic growth.....	143
PART II	150
R8. A common domain of I κ B α binds to p65 and histones H2A and H4.....	150
R9. Two different aminoacidic clusters in I κ B α define NF- κ B and chromatin interaction ..	153
R10. I κ B α mutants display separation of function (SOF) activity in intestinal cells	156
R11. The I κ B α SOF ^{ΔNF-κB} mutant N108A rescues the Goblet Cell differentiation I κ B α depleted cells linked to repression of the ISC program	158
R12. I κ B α binds to genomic regions at genes involved in cell development and neuronal signaling.....	161
DISCUSSION	165
PART I	165
D1. Pro-tumorigenic vs anti-metastatic functions of IKK α	165
D2. Tight junction elements as key modulators of cancer cell migration mode	166
D3. CHUK and TJP1 as novel biomarkers of relapse risk in CRC patients.....	167
D4. CLDN2 inhibition as a potential new anti-metastatic therapeutic strategy in CRC	168
D5. MEK inhibitors slow the growth of hepatic metastases but do not reduce liver colonization	169
D6. A deeper understanding of CTC vulnerabilities could lead to more precise treatments for mCRC.....	170
D7. Following steps: how CT affects CTC cluster formation and tight junction dynamics?	171

PART II	173
D8. Separation-of-function mutants reveal the NF- κ B-independent involvement of I κ B α in the regulation of intestinal stemness	173
CONCLUSIONS	177
BIBLIOGRAPHY	181

FIGURES AND TABLES

FIGURES AND TABLES

INTRODUCTION

Figure I1. The adenoma-carcinoma sequence	46
Figure I2. Schematic representation of MAPK oncogenic signaling.....	47
Figure I3. Staging of CRC	48
Table I1. Classification of CRC according to TNM stages	49
Figure I4. Stepwise progression of the metastatic cascade	52
Figure I5. EMT states in the metastatic context	57
Figure I6. CTC cluster types.....	59
Figure I7. NF- κ B pathway	64
Figure I8. NF- κ B independent IKK α function in DDR.....	67
Figure I9. Tight junction structure	70

MATERIALS AND METHODS

Table MM1. List of CRC PDOs used.....	81
Table MM2. List of DF12 ⁺⁺⁺ medium factors	82
Table MM3. List of complete medium factors.....	82
Table MM4. Factors used for tumor disaggregation	83
Table MM5. Vectors used for knock-down virus production	86
Table MM6. sgRNA used for IKK α KO generation	90
Table MM7. Antibodies used for ChIP and ChIP-seq	96
Table MM8. Antibodies used in Co-IP experiments.....	99
Table MM9. Antibodies used in WB	101
Table MM10. Antibodies used in IF/IHC	103
Table MM11. Primers used for RT-qPCR.....	106

RESULTS

PART I

Table R1. Tight junction elements identified as putative direct phosphorylation targets of IKK α	119
Figure R1. ZO-1 distribution is altered, in CRC cell lines, in response to IKK α depletion, either genetically or pharmacologically.....	120
Figure R2. ZO-1 distribution is altered in IKK α KO CRC PDOs	120

Figure R3. IKK α modulates ZO-1 levels at protein level.....	121
Figure R4. IKK α and pIKK co-localize with residual ZO-1 at the cell membrane of peripheral WT cells.....	122
Table R2. IKK α KO cells present altered expression in several tight junction elements and canonical adherens junction component	123
Figure R5. IKK α KO cells showed increased CLDN2 levels.....	123
Figure R6. CDH1 is downregulated and re-localized upon IKK α depletion	124
Figure R7. IKK α KO cells showed increased stemness and reduced differentiation.....	125
Figure R8. IKK α depleted CRC cell lines, either genetically or pharmacologically, showed decreased cell migration <i>in vitro</i>	126
Figure R9. IKK α depleted CRC PDOs, either genetically or pharmacologically, showed decreased cell migration <i>in vitro</i>	127
Figure R10. Pharmacological inhibition of IKK α in CRC cells imposes a collective cell migration behavior	128
Figure R11. Intrinsic cell clustering ability is enhanced upon IKK α depletion	129
Figure R12. Metastatic populations in mice are enriched in tight junction elements.....	130
Figure R13. IKK α depleted PDO5 cells showed higher metastatic ability	131
Figure R14. Characterization of IKK α KO PDO5-derived hepatic metastases	132
Figure R15. IKK α depleted PDO4 cells showed higher metastatic ability and tight junction accumulation	132
Figure R16. PDO5 scRNA-seq clustering data	133
Figure R17. PDO5 scRNA-seq data, cluster characterization	134
Figure R18. EpiHR and tight junction signature scores represented in PDO5 scRNA-seq data	134
Figure R19. C2, C4 and C8 marker gene signatures predict poor prognosis in CRC.....	135
Figure R20. C2, C4 and C8 marker gene signatures are enriched in PDO5-derived metastases.....	136
Figure R21. C2 and C8 marker genes are not enriched in the general IKK α KO cell populations.....	137
Figure R22. YM201636 treatment restores the migratory properties of IKK α KO CRC cell lines	138
Figure R23. YM201636 treatment reverts the adhesive/migratory properties of IKK α KO PDO5 cells.....	138

Figure R24. CLDN2 knockdown restores the migratory properties of IKK α KO CaCo-2 cells	139
Figure R25. Metastatic potential of PDO5 IKK α -depleted cells is reduced upon YM201636 treatment	140
Figure R26. CLDN2 knockdown reduces the metastatic potential of PDO5 IKK α -depleted cells	140
Figure R27. Different observed patterns of tumor vascular infiltration	141
Figure R28. Tight junction proteins ZO-1 and CLDN2 as candidate IHC biomarkers in the invasive clusters of CRC patients	142
Figure R29. ZO-1 and IKK α predict the risk of metastasis of CRC patients	143
Figure R30. IKK α KO PDO5-derived metastases present increased MAPK pathway signaling	144
Figure R31. IKK α depletion influences the transcriptional status of DUSPs in different CRC cell types	145
Figure R32. DUSPs transcriptional regulation is NF- κ B/RelA-dependent	145
Figure R33. DUSP1 and DUSP5 staining is increased in PDO5 IKK α KO-derived metastases	146
Figure R34. i-DUSPs constructs increase DUSPs presence in CaCo-2 IKK α depleted cells and block pERK activation	147
Figure R35. DUSP1 or DUSP5 overexpression reduce tumoral growth <i>in vitro</i>	147
Figure R36. MEK inhibition abrogates pERK activation and reduces the growth of PDO5 IKK α KO-derived metastases	148
Figure R37. Combination of BRAFi plus MEKi reduces metastatic potential of WT PDO5 cells	149

PART II

Figure R38. A common domain of I κ B α binds to p65 and histones H2A and H4	151
Figure R39. Structural characterization of the N-terminal tail of histone H4	152
Figure R40. Two different evolutionary conserved Aa clusters of I κ B α define NF- κ B or histone H2A and H4 binding	153
Figure R41. Two different aminoacidic clusters in I κ B α define NF- κ B and histone H4 interaction	154
Figure R42. I κ B α / β -mimic <i>in vitro</i> characterization	155
Figure R43. I κ B α mutants display separation of function (SOF) activity in intestinal cells .	156

Figure R44. Similar transcriptional induction of I κ B α WT and SOF mutants after doxycycline treatment	157
Figure R45. The I κ B α SOF ^{ΔNF-κB} mutant 108A rescues the Goblet Cell differentiation blockage imposed by I κ B α deletion	158
Figure R46. RNA-seq characterization of i-I κ B α cell lines	159
Figure R47. Transcriptional characterization of the rescue of goblet cell differentiation by the I κ B α SOF ^{ΔNF-κB} mutant 108A	160
Figure R48. i-I κ B α WT and SOF ^{ΔNF-κB} expression regulates a specific intestinal stem cell program with impact on intestinal differentiation	162

DISCUSSION

Figure D1. Proposed CTC clustering mechanism in CRC	171
---	-----

ABBREVIATIONS AND ACRONYMS

ABBREVIATIONS AND ACRNOYMS

5-FU	5-Fluorouracil
ADAM12	Disintegrin and metalloproteinase 12
ADC	Antibody-drug conjugate
Akt	AKT serine/threonine kinase 1
ANGPTL4	Angiopoietin-like protein 4
APC	Adenomatous polyposis coli
ALDH1	Aldehyde dehydrogenase 1
B3GALT5	Beta-1,3-galactosyltransferase 5
BAFF	B-cell activating factor
BCL3	B-cell lymphoma 3-encoded protein
BRAF	B-Rapidly Accelerated Fibrosarcoma
BRAFi	BRAF inhibitor
BRD4	Bromodomain containing 4
BSA	Bovine Serum Albumin
BVES	Blood vessel epicardial substance
Cas9	CRISPR-associated protein 9
CAF	Cancer-associated fibroblast
CAR	Coxsackievirus and adenovirus receptor
CBP	CREB binding protein
CCL2	Matrix metalloproteinases and CC chemokine ligand 2
CD24	Heat stable antigen
CD29	Integrin beta-1
CD40	Tumor necrosis factor receptor superfamily member 5
CD44	Homing cell adhesion molecule
CD47	Integrin-associated protein
CD133	Prominin-1
CD147	Basigin
CD166	Activated leukocyte cell adhesion molecule
CDC25C	M-phase inducer phosphatase 3
Cdc37	Hsp 90 co-chaperone Cdc37
CDK4	Cyclin-dependent kinase 4

CDKN2A	Cyclin dependent kinase inhibitor 2A
cDNA	Complementary DNA
ChEA	ChIP Enrichment Analysis
ChIP	Chromatin immunoprecipitation
CHX	Cycloheximide
ciAP	Cellular inhibitor of apoptosis
CIMP	CpG island methylation phenotype
CIN	Chromosomal instability
CLDN1	Claudin 1
CLDN2	Claudin 2
CLDN3	Claudin 3
CLDN4	Claudin 4
CLDN18.2	Claudin 18.2
CLDNi	Claudin inhibitor
CMS	Consensus molecular subtypes
Co-IP	Co-Immunoprecipitation
CRB3	Crumbs cell polarity complex component 3
CRC	Colorectal cancer
CSC	Cancer stem cell
CT	Chemotherapy
CTC	Circulating tumor cell
CTLA4	Cytotoxic T lymphocyte-associated antigen 4
CXCL1	CXC chemokine 1
CXCL12	CXC chemokine 12
CXCR4	CXC chemokine receptor 4
DAB	3,3'-Diaminobenzidine
DAPI	4,6-diamino-2-phenylindole
DDR	DNA damage response
DFS	Disease free survival
DMEM	Dulbecco's modified Eagle's medium
DNA	Deoxyribonucleic acid
DPX	Dibutylphthalate Polystyrene Xylene
DSP	Dithiobis (succinimidyl propionate)

DTC	Disseminated tumor cell
DUSP	Dual-specificity phosphatase
DUSP1	Dual-specificity phosphatase 1
DUSP3	Dual-specificity phosphatase 3
DUSP5	Dual-specificity phosphatase 5
DUSP10	Dual-specificity phosphatase 10
E2F1	E2F transcription factor 1
ECL	Electrochemiluminiscence
EDTA	Ethylenediaminetetraacetic acid
EGFR	Epidermal growth factor receptor
ELKS	Glutamate, leucine, lysine and serine
EMP1	Epithelial membrane protein 1
EMT	Epithelial-to-mesenchymal transition
EpB2	Ephrin B2 Fc chimaera protein
EpiHR	Epithelial-specific high relapse risk
ER α	Estrogen receptor alpha
ERK	Mitogen-activated protein kinase 1
FADD	FAS-associated death domain protein
FAP	Familial adenomatous polyposis
FAT1	Protocadherin Fat 1
FBS	Fetal bovine serum
GAPDH	Glyceraldehyde-3-phosphate dehydrogenase
GFP	Green fluorescent protein
GPIb-IX-V	Glycoprotein Ib–IX–V
GPVI	Glycoprotein VI
H&E	Haematoxylin and eosin
HEPES	Hydroxyethyl piperazineethanesulfonic acid
HES1	Hairy and enhancer of split 1
HES5	Hairy and enhancer of split 5
HIF1 α	Hypoxia-inducible factor 1 α
HIFPH2	HIF prolyl hydroxylase 2
HLH	Helix-loop-helix
HPSE	Heparanase

HRC	High-relapse cell
HRP	Horseradish Peroxidase
Hsp90	Heat shock protein 90
ICAM1	Intercellular adhesion molecule 1
IF	Immunofluorescence
IHC	Immunohistochemistry
IKKK	IKK kinase
IL-8	Interleukin-8
IP	Immunoprecipitation
Iri.	Irinotecan
ISC	Intestinal stem cell
ITGB1	Integrin β 1
I κ B	NF- κ B inhibitor
I κ B α	NF- κ B inhibitor subunit α
I κ B β	NF- κ B inhibitor subunit β
I κ B ϵ	NF- κ B inhibitor subunit ϵ
I κ B γ	NF- κ B inhibitor subunit γ
I κ B ζ	NF- κ B inhibitor subunit ζ
IKK α	Inhibitor of NF- κ B kinase subunit α
IKK β	Inhibitor of NF- κ B kinase subunit β
IKK γ	Inhibitor of NF- κ B kinase regulatory subunit γ
IL-1	Interleukin-1
ISC	Intestinal stem cells
JAM	Junctional adhesion molecule
JNK	Mitogen-activated protein kinase 8
KD	Kinase domain
kDa	KiloDalton
Ki67	Marker of proliferation ki67
KO	Knock-out
KRAS	Kirsten rat sarcoma viral oncogene
L1CAM	L1 cell adhesion molecule
LGR5	Leucine rich repeat containing G protein-coupled receptor 5
LPS	Lipopolysaccharide

LTβ	Lymphotoxin-β
LZ	Leucine zipper
MAPK	Mitogen-activated protein kinase
MARVELD3	MARVEL domain-containing protein 3
Maspin	Mammary serine protease inhibitor
mCRC	Metastatic colorectal cancer
MEK	Mitogen-Activated Protein Kinase Kinase 1
MEKK3	MAPK/ERK kinase kinase 3
MET	Mesenchymal-to-epithelial transition
MGMT	O ⁶ -Methylguanine-DNA Methyltransferase
MIC	Metastasis-initiating cell
MMP9	Matrix metalloproteinase 9
MMP28	Matrix metalloproteinase 28
MSI	Microsatellite Instability
MLH1	MutL homolog 1
MUC1	Mucin 1
Na ₃ VO ₄	NA-orthovanadate
NBD	NEMO-binding domain
NCoR	Nuclear receptor co-repressor
NEMO	NF-κB essential modulator
NF-κB	Nuclear Factor Kappa B
NIK	NF-κB inducing kinase
NLS	Nuclear localization signal
Notch	Notch receptor
N-terminal	Amino Terminal
NUCKS1	Nuclear casein kinase and cyclin dependent kinase substrate 1
O/N	Overnight
OS	Overall survival
P2Y2	ATP-P2Y purinoceptor 2
p38	Mitogen-activated protein kinase 14
PAK2	p21 protein-activated kinase 2
PAMP	Pathogen-associated molecular pattern
Par3	Partitioning defective protein 3

PBS	Phosphate-buffered saline
PCR	Polymerase Chain Reaction
PD1	Programmed cell death protein 1
PDL1	PD1 ligand 1
PDO	Patient-derived organoid
PDX	Patient-derived xenograft
PEI	Polyethylenimine
pERK	Phosphorylated ERK
PFA	Paraformaldehyde
PI3K	Phosphoinositide 3-kinase
PLAC8	Placenta associated 8
PLK1	Polo-like kinase 1
PLP2	Proteolipid protein 2
pMEK	Phosphorylated MEK
PMSF	Phenylmethanesulfonyl fluoride
PNK	Polynucleotide Kinase
PVDF	Polyvinylidene fluoride
PRC2	Polycomb repressive complex 2
RT-qPCR	Quantitative real time polymerase chain reaction
RANKL	Receptor activator for NF- κ B ligand
RBM38	RNA-binding motif protein 38
RHD	Rel homology domain
RIP1	Receptor interacting protein 1
RIPK1	Receptor-interacting serine/threonine protein kinase 1
RNA	Ribonucleic Acid
ROS	Reactive oxygen species
RT	Room temperature
SCC	Squamous cell carcinoma
SCR-3	Steroid receptor coactivator 3
SDD	Scaffold/dimerization domain
SDS	Sodium Dodecyl Sulphate
SDS-PAGE	SDS-polyacrylamide gel electrophoresis
sgRNA	Single guide RNA

SUMO	Small ubiquitin-related modifier
SMA	Smooth muscle actin
SMAD3/4	Small mothers against decapentaplegic family member 3/4
SMRT	Silencing mediator for retinoid and thyroid receptors
SRC	Avian Sarcoma (Schmidt-Ruppin A-2)
STAT3	Signal transducer and activator of transcription 3
SUV39h1	Suppressor of variegation 3-9 homolog 1
TAD	Transactivation domain
TAK1	TGF β -activated kinase 1
TBP	TATA-Box binding protein
TBS	Tris buffered saline
TBS-T	Tris buffered saline plus Tween20
TIC	Tumor-initiating capacity
TF	Transcription Factor
TFF1	Trefoil factor 1
TFF2	Trefoil factor 2
TFF3	Trefoil factor 3
TGF β	Transforming growth factor β
TJ	Tight junction
TLR	Toll-like receptor
TME	Tumor microenvironment
TNF α	Tumor Necrosis Factor α
TP53	Tumor Protein 53
TRADD	TNF receptor type 1-associated DEATH domain protein
TRAF3	TNF receptor associated factor 3
USP49	Ubiquitin-specific peptidase 49
VEGF	Vascular endothelial growth factor
WB	Western blot
WNT	Wingless-related integration site
WT	Wild type
ZO-1	Zonula occludens protein 1
ZO-2	Zonula occludens protein 2
ZO-3	Zonula occludens protein 3

β -ME	β -mercaptoethanol
γ H2A.X	Phospho-Histone H2A family member X

INTRODUCTION

11. COLORECTAL CANCER

The intestinal epithelium is continuously self-renewing through a combination of cellular processes involving cell proliferation, differentiation, migration and death. Maintaining the balance between these processes is complex but crucial for tissue homeostasis. Perturbation of any of these processes can lead to intestinal tumorigenesis. Colorectal cancer (CRC) is characterized by the abnormal and uncontrolled growth of colonic and rectal cells caused by the accumulation of multiple genetic and epigenetic alterations.

11.1 Epidemiology of colorectal cancer

CRC is the third most common cancer in men and women worldwide, accounting for approximately 9% of cancer-related deaths¹. In general, most CRCs (about 95%) are considered sporadic, and there are multiple risk factors (hereditary and environmental) that increase the probability of developing CRC, such as other bowel diseases, obesity, high-fat diet, sedentary lifestyle, alcohol consumption, and long-term smoking. Inherited CRCs are less common (about 5-10%) and can be classified into polyposis syndromes, such as familial adenomatous polyposis (FAP), and non-polyposis syndromes, such as Lynch syndrome².

11.2 Molecular mechanisms of colorectal cancer development and progression

Normally, CRC tumorigenesis is initiated by the transformation of normal colorectal epithelial cells through spontaneous mutations, environmental mutagens, and genetic or epigenetic alterations. The development of normal colon epithelial cells into aberrant crypt foci, followed by early and advanced polyps with subsequent progression to early and then advanced cancer has traditionally been explained by the adenoma-carcinoma sequence (**Figure I1**). In the classical model, CRC cancer arises from a dysplastic polyp in an aberrant crypt, usually carrying a driver mutation in the APC gene³, which develops into an early adenoma (<1 cm in size). The adenoma then progresses to an advanced adenoma before finally becoming a colon carcinoma and an invasive colon carcinoma. The progressive accumulation of mutations and epigenetic alterations that cause hyperproliferation, such as KRAS/BRAF, SMAD4, or TP53 mutations, allow the malignant transformation of these adenomas into colon carcinoma and metastasis^{4,5}.

Colon Cancer Progression

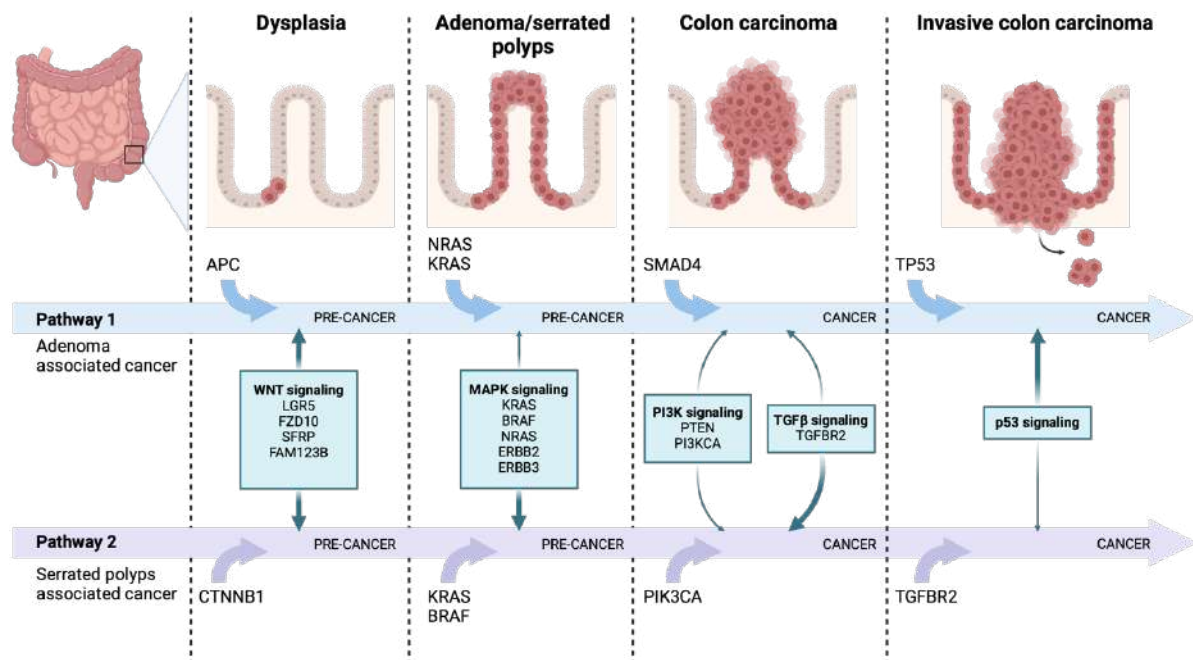


Figure I1. The adenoma-carcinoma sequence. CRC tumorigenesis is initiated by adenomas or serrated polyps, which, driven by a series of defined genetic alterations, progress to colon carcinoma and then to invasive colon carcinoma. Created with BioRender.com.

BRAF and KRAS are two of the most frequently mutated oncogenes that indicate a poor prognosis in patients and are identified in the daily routine of pathology departments. Both KRAS and BRAF are members of the mitogen-activated kinase (MAPK) pathway and are immediate downstream effectors of the epidermal growth factor receptor (EGFR). Thus, KRAS or BRAF mutations lead to constitutive activation of the MAPK pathway and cellular proliferation even in the absence of ligand-dependent stimulation of EGFR (**Figure I2**).

In addition to the multiple positive effectors of the pathway, the dual-specificity phosphatase (DUSP) family of proteins includes various phosphatases, some of which can specifically target effector kinases in the MAPK pathway (e.g., DUSP1 and DUSP5), such as mitogen-activated protein kinase 1 (ERK), mitogen-activated protein kinase 14 (p38) or mitogen-activated protein kinase 8 (JNK), thereby inhibiting their activity⁶.

Likely related to their role as negative regulators of MAPK signaling, several DUSPs, including DUSP2 and DUSP6, have been characterized for their role as tumor suppressors^{7–11}. DUSPs have also been implicated in chemotherapy resistance through various mechanisms including MAPK regulation. Several transcription factors including EYA4¹², BAF53A¹³, ELK1¹⁴ and the hypoxia-inducible factor

HIF-1 α ^{15,16} have been found to directly regulate DUSPs expression in cancer cells. Moreover, and further linking hypoxia to cancer and metastasis progression, DUSP2 levels are significantly reduced in many human cancers, including colorectal cancer, and inversely correlated with HIF-1 α , resulting in tumor stemness^{16,17}.

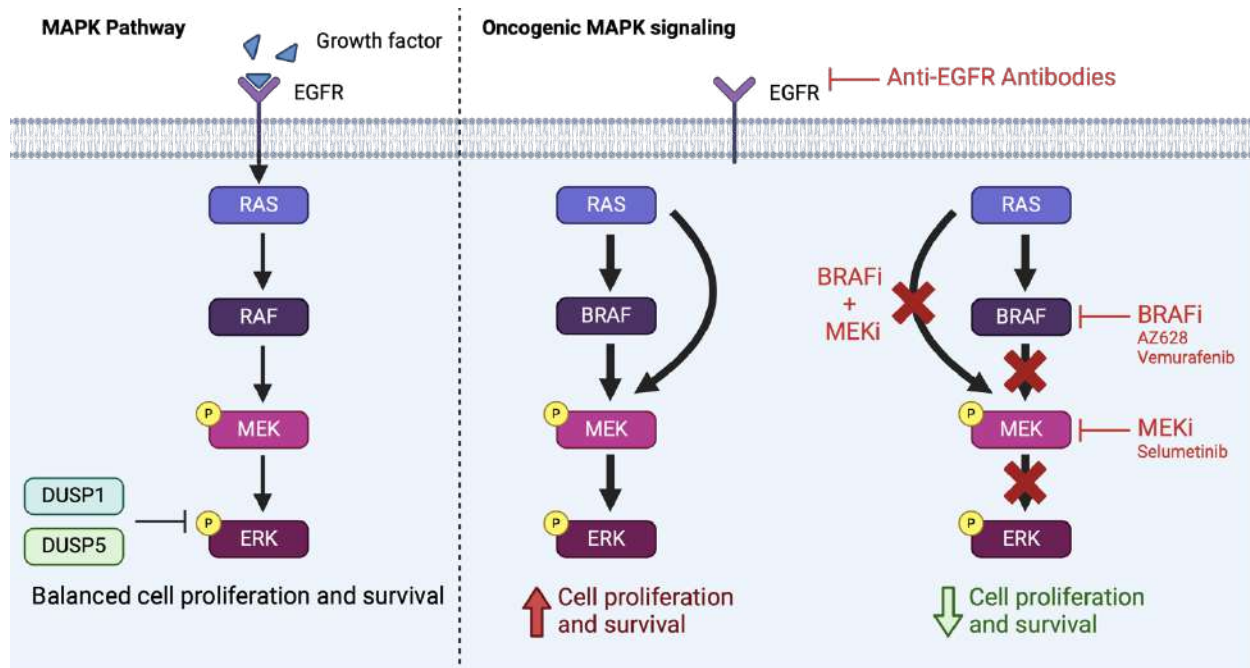


Figure I2. Schematic representation of MAPK oncogenic signaling. Upon ligand binding, the EGF receptor (among others) activates the RAS signaling cascade, which leads to RAF, MEK, and ERK activation, promoting cell growth and survival. DUSP1 and DUSP5 dephosphorylate ERK, shutting down the pathway. On the oncogenic side, several mutational scenarios can cause constant activation of the pathway, independent of ligand-receptor stimuli, and paradoxical feedback loop may increase signaling. To counter this, strategies like BRAF and MEK inhibition, or their combination, are used to block MAPK oncogenic signaling and prevent feedback loop activation. Created with BioRender.com.

At the molecular level, CRC initiation and progression are driven by three major molecular mechanisms. The most common is the chromosomal instability (CIN) mechanism, which occurs in 70-85% of sporadic CRC cases and is characterized by aneuploidy, structural chromosomal abnormalities, loss of heterozygosity at tumor suppressor genes, and chromosomal rearrangements¹⁸. Indeed, these alterations are associated with mutations in specific oncogenic or tumor suppressor genes such as APC, KRAS, BRAF, SMAD4 or TP53, which regulate cell proliferation and cell cycle¹⁹. Microsatellite instability (MSI) is another important CRC mechanism caused by dysfunctional DNA mismatch repair²⁰ and associated with genetic hypermutability²¹. The CpG island methylation phenotype (CIMP) comprises the third pathway to CRC. CIMP-positive tumors can be

classified according to their CIMP levels. CIMP-high tumors often carry mutations in BRAF, MLH1 methylation and MGMT or CDKN2A silencing. While CIMP-low tumors are associated with KRAS mutations²². These three mechanisms (CIN, MSI, CIMP) are not mutually exclusive and influence several physiological pathways, including the WNT, MAPK, PI3K, TGF β signaling, Notch, and NF- κ B pathways, among others²³. In addition, CRC cells are highly influenced by the stromal and immune cells of the tumor microenvironment (TME), in particular, TME inflammation affects CRC tumorigenesis and modulates cell polarization²⁴.

11.3 Colorectal cancer classification

Classically, CRC has been classified according to the TNM histologic criteria, which take into account the characteristics of the primary tumor (T stage), the regional lymph node involvement (N stage), and the presence of distant metastatic spread (M stage). This method allows for the overall cancer stage classification as described in **Table I1**²⁵. Using this system CRC tumors are classified in four different stages (I, II, III and IV) (**Figure I3**), with subcategories²⁶. Although TNM is currently the most widely used guideline for CRC staging and an important basis for treatment decisions, it is not a reliable tool for predicting prognosis. In fact, the outcome of CRC patients after treatment is highly variable even when patients are assigned to the same TNM category²⁷, highlighting the need for a better understanding of the molecular basis of CRC.

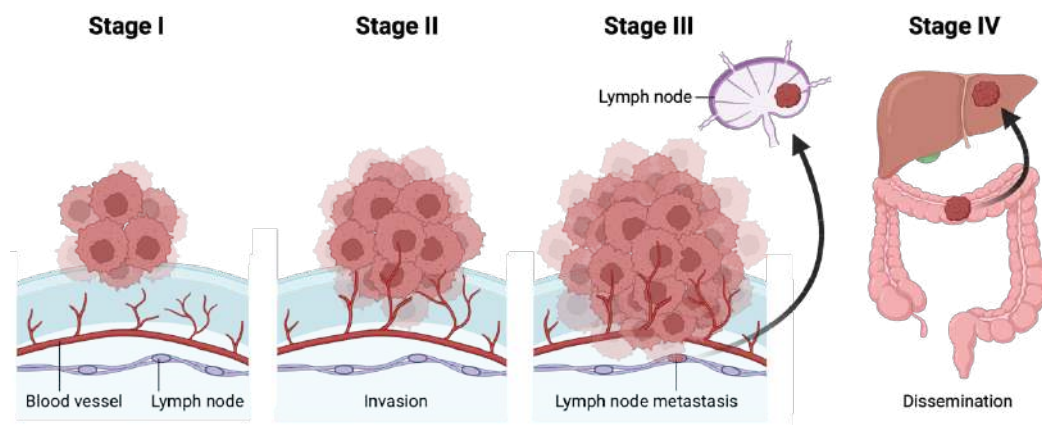


Figure I3. Staging of CRC. CRC staging, depicting the degree of tumor invasion and dissemination. Adapted from²⁸. Created with BioRender.com.

T stages	Definition
Tx	No information about local tumor infiltration available
Tis	Tumor restricted to mucosa
T1	Infiltration through mucosa into submucosa
T2	Infiltration into, but not beyond, muscularis externa
T3	Infiltration into subserosa or non-peritonealized pericolic or perirectal tissue, or both
T4a	Infiltration of the serosa
T4b	Infiltration of neighboring tissues or organs

N stages	Definition
Nx	No information about lymph node involvement available
N0	No lymph node involvement
N1a	Cancer cells detectable in 1 regional lymph node
N1b	Cancer cells detectable in 2-3 regional lymph nodes
N1c	Tumor satellites in subserosa or pericolic or perirectal fat tissue, regional lymph nodes not involved
N2a	Cancer cells detectable in 4-6 regional lymph nodes
N2b	Cancer cells detectable in 7 or greater regional lymph nodes

M stages	Definition
Mx	No information about distant metastases available
M0	No distant metastases detectable
M1a	Metastasis to 1 distant organ or distant lymph nodes
M1b	Metastasis to more than 1 distant organ or set of distant lymph nodes or peritoneal metastasis

	T	N	M
Stage 0	Tis	N0	M0
Stage I	T1/T2	N0	M0
Stage II	T3/T4	N0	M0
IIA	T3	N0	M0
IIB	T4a	N0	M0
IIC	T4b	N0	M0
Stage III	Any	N+	M0
IIIA	T1/T2	N1	M0
	T1	N2a	M0
	T3/T4a	N1	M0
IIIB	T2/T3	N2a	M0
	T1/T2	N2b	M0
	T4a	N2a	M0
IIIC	T3/T4a	N2b	M0
	T4b	N1/N2	M0
Stage IV	Any	Any	M+
IVA	Any	Any	M1a
IVB	Any	Any	M1b

Table I1. Classification of CRC according to TNM stages. Histological classification of T, N and M stages and overall classification, with characteristics of each stage indicated. Adapted from²⁵.

The advent of omics technology has allowed the integration of genetic, transcriptomic and proteomic data from different biological characteristics. Recently, a new classification system has emerged that not only integrates expression data from all published cohorts, but also considers other biological features, such as genomic aberrations and mutations, to confirm whether there is a good genomic-phenotypic correlation. Known as consensus molecular subtypes (CMS)²⁹, it classifies CRC tumors into four groups based on their molecular characteristics. CMS1 tumors are characterized by MSI, CIMP and strong immune infiltration. It is associated with a good prognosis, although the small fraction of patients who develop metastases have the poorest prognosis. CMS2 is characterized by the activation of WNT and MYC signaling pathways and is associated with the conventional CRC development pathway. Tumors in CMS2 typically exhibit chromosomal instability, leading to genetic and epigenetic alterations. CMS3 tumors exhibit a distinct metabolic profile and

are marginally enriched in KRAS-activating mutations. CMS4 tumors show stromal infiltration and TGF β activation (associated with epithelial-to-mesenchymal transition (EMT) gene signatures). Both CMS2 and CMS3 tumors are poorly immunogenic, in contrast to CMS1 tumors. Importantly, CMS4 tumors have the worst disease free (DFS) and overall survival (OS).

11.4 Cancer stem cells

Inter- and intra-tumor heterogeneity has been consistently demonstrated, but the mechanisms driving this heterogeneity are not fully understood. There are two models that try to explain these differences: the first, the stochastic model, is based on the different intrinsic and extrinsic factors to which cells are exposed and subsequently adopt heterogeneous changes. The second, the hierarchical model, explains heterogeneity based on the retention of the original hierarchical organization present in the tissue^{30,31}.

The identification of cancer stem cells (CSCs), which exhibit stem cell-like properties and are capable of self-renewal and restoring tumor heterogeneity, provides proof of concept for the hierarchical model of tumors³². CSCs are also characterized by an enhanced ability to initiate tumor growth, proliferate, invade and migrate and have superior resistance to chemotherapy³³. This implies a critical role of CSCs in cancer development and makes CSCs candidate targets for anti-cancer treatments³⁴. There are some markers that have been classically used to identify CSCs: CD44³⁵, CD133^{36,37}, Lgr5^{38,39}, ALDH1⁴⁰, CD166⁴¹, CD29 and CD24 or nuclear β -catenin⁴², some of which are shared with ISCs. However, Lgr5, considered by many scientists as the canonical intestinal stem cell marker, has been shown to be dispensable for tumor growth⁴³, particularly in a subset of CRC tumors characterized by their high biosynthetic state⁴⁴.

It is becoming clear that stem cell hierarchies may be much more plastic than previously appreciated⁴⁵, a phenomenon that complicates CRCs identification and eradication. Moreover, CSCs display considerable plasticity and are highly variable in both number and characteristics between patients and tumor regions, making it difficult to define a common CSC profile^{33,46,47}. In fact, some undifferentiated tumor types do not present a specific CSC population, as all cells exhibit some degree of stemness⁴⁸. Furthermore, it has been shown that deletion of APC specifically in the ISCs (either the Lgr5+ or the CD133+ populations) leading to aberrant Wnt signaling is sufficient to initiate the tumorigenic transformation and subsequent neoplastic expansion^{49,50}. However, other studies have shown that Wnt activation in differentiated intestinal cells can also induce the

acquisition of CSC properties⁵¹. All these data suggest that the process of tumor initiation and acquisition of CSC activity is very similar to the plasticity of the healthy intestine⁵².

11.5 Colorectal cancer therapeutic strategies

The standard guidelines for CRC treatment are surgery for complete resection of the rectum for rectal cancer and resection of the colon area containing the tumor and lymphatic vessels for colon cancer. Surgery is usually combined with radiotherapy and/or chemotherapy (CT) to reduce the risk of recurrence in invasive tumors. Neoadjuvant therapy, which refers to therapy administered before surgery, is usually indicated for stage III rectal tumors; adjuvant therapy is administered after surgery for stage III colon tumors^{5,25}.

The most commonly used chemotherapeutic agents include 5-fluorouracil (5-FU), irinotecan (Iri.), oxaliplatin, calcium folinate, and capecitabine. These agents are usually given together in various combination regimens: FOLFOX (5-FU + calcium folinate + oxaliplatin), FOLFIRI (5-FU + Iri. + calcium folinate), CALPEOX (capecitabine + oxaliplatin), and FOLFOXIRI (5-FU + Iri. + calcium folinate + oxaliplatin)⁵³.

Other therapeutic options include targeted therapies and immunotherapy. Regarding targeted therapies, anti-EGFR antibodies (cetuximab or panitumumab) for KRAS wild-type CRC^{54,55} or anti-VEGF (bevacizumab) to block angiogenesis⁵⁶ are used alone or, in advanced and metastatic CRC (mCRC), in combination with CT⁵⁷. The PD-1 inhibitors nivolumab and pembrolizumab⁵⁸ are also used as immunotherapeutic agents.

Since EGF inhibitors are not worth using in KRAS mutant tumors, other strategies have been developed in the last few years to switch off MAPK signaling in cancer cells. BRAF inhibitors (BRAFi) such as vemurafenib are another therapeutic option in combination with CT. However, it has been described that cancer cells can develop resistance to BRAFi through a process called paradoxical feedback loop activation^{59–61} which consists of overactivation of ERK bypassing BRAF in the cascade (**Figure I2**). This process can be avoided by combination treatment of BRAFi plus MEK inhibitors (MEKi) such as selumetinib^{62–64}.

12. TUMOR DISSEMINATION AND METASTASIS

Despite the advances in cancer treatment, mCRC, comprising around 45% of all CRC patients⁶⁵, is the leading cause of CRC deaths with a median survival rate of patient with mCRC of about 30 months⁶⁶.

Metastasis occurs through a multistep cascade, which includes the detachment of cancer cells from the primary tumor, local invasion into the surrounding tissue, intravasation into the blood or lymphatic vessels, extravasation, colonization of a secondary organ and growth of a secondary tumor (**Figure I4**). Each of these steps is considered to be extremely inefficient, estimating that less than 1% of cells that intravasate into the circulation, known as circulating tumor cells (CTCs), ultimately succeed to establish a distant metastasis⁶⁷. However, tumors are composed of billions of cells and, as a consequence, it is calculated that (in the case of mammary tumors) millions of individual cells may be shed into circulation from 1 gram of cancerous tissue each day⁶⁸.

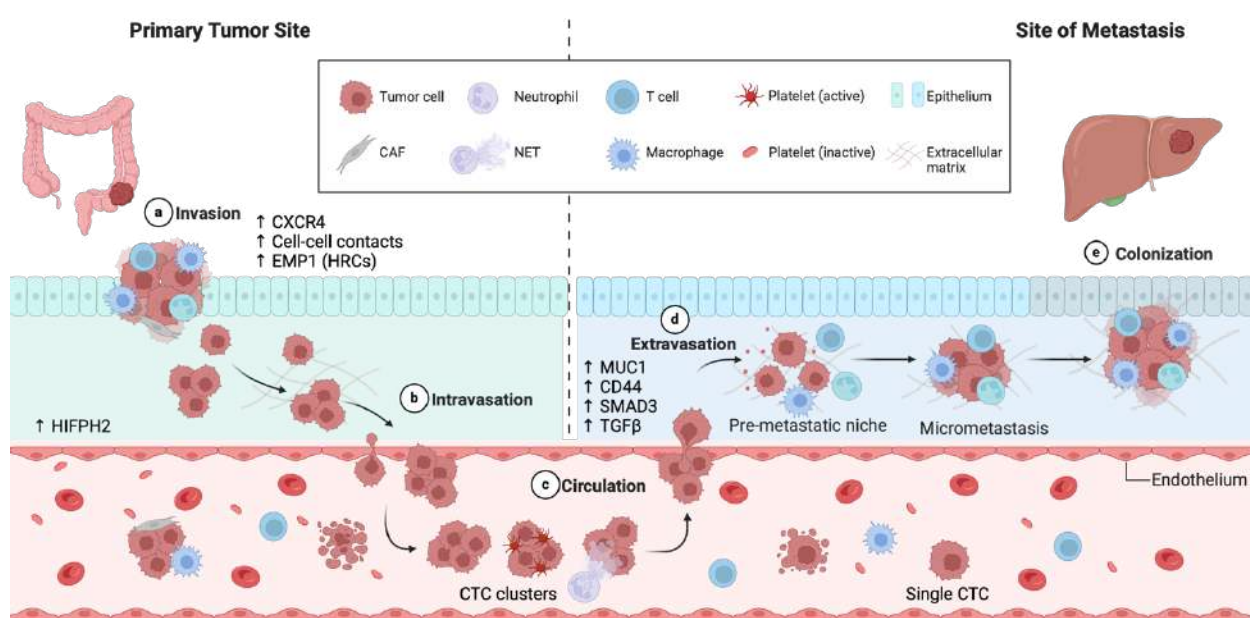


Figure I4. Stepwise progression of the metastatic cascade. Metastasis consists of a series of steps, including tumor expansion and invasion, intravasation into the circulation, survival in the circulation, followed by extravasation and expansion at distant sites. Adapted from^{69,70}. Created with BioRender.com.

I2.1 Metastatic origin

There is increasing evidence that only certain subpopulations of tumor cells, termed metastasis-initiating cells (MICs), are capable of forming metastases⁷¹. It has been recently described that a unique population of cells, called high-relapse cells (HRC), characterized by the expression of the EMP1 marker, are the origin of the metastatic process in a mouse model of colorectal cancer. This cell population is mostly undetectable in the primary CRC lesions and but it subsequently leads to metastasis. However, their identification allowed the generation of an epithelial-specific high-risk gene signature (EpiHR) that is expressed by HRCs which is associated with poor prognosis in patients⁷². In contrast to tumor initiation, which is associated with mutations in cancer drivers, no metastasis-specific mutations have been identified^{73,74}, although certain mutations may predispose to metastasis^{75,76}.

The likelihood of different types of metastases and the degree of metastatic heterogeneity are closely related to the timing of metastasis. Traditionally, metastasis has been viewed as an end product of tumor development. However, recent reports suggest that dissemination may occur early in the evolutionary history of a tumor, prior to primary tumor resection, and that primary and metastatic tumors evolve in parallel⁷³. A recent model of CRC development suggests that metastatic dissemination occurs before the primary tumor is clinically detectable in the majority of cases⁷⁷.

I2.2 Metastatic intravasation

Access to the circulation can be achieved by passive shedding or active cell invasion⁷⁸. In the case of passive shedding, tumor fluid dynamics and reduced barrier function of immature tumor neovasculature facilitate the physical expulsion of tumor cells to the periphery^{78–80}. However, the frequency and precise conditions leading to passive tumor cell shedding remain poorly understood. Active cancer cell invasion can be triggered by hypoxia⁸¹. Hypoxia-inducible factor 1 α (HIF1 α) increases expression of CXC chemokine receptor 4 (CXCR4)⁸², resulting in enhanced CTC endothelial binding and intravasation. Hypoxia has also been linked to CTC clustering and intravasation via upregulation of cell-cell adhesion molecules⁸¹. Expression of HIF prolyl hydroxylase 2 (HIFPH2) by endothelial cells promotes tumor cell escape into blood vessels by impairing endothelial integrity and vessel maturation⁸³.

12.3 Metastatic extravasation

Extravasation, like intravasation, can be promoted both actively and passively. Both mechanical trapping (with capillaries as small as a few micrometers in diameter) and active adhesion may depend on CTC configuration (e.g., single CTCs versus CTC clusters)⁸⁴, composition of CTC clusters (homotypic versus heterotypic)^{85,86} (details in I3), and geometric shape⁸⁷.

Active CTC extravasation is dependent on cytoskeletal remodeling (e.g., invadopodia formation⁸⁸) and signaling changes, including expression of ligands and receptors for direct endothelial cell wall interaction⁸⁹. For example, expression of mucin 1 (MUC1)⁹⁰ or CD44⁹¹ by cancer cells and their ligation to selectins, intercellular adhesion molecule 1 (ICAM1) or integrin β 1 (ITGB1) on endothelial cells triggers CTC rolling and subsequent adhesion, allowing transendothelial migration. Endothelial adhesion is further enhanced by inflammatory mediators such as CXC chemokine 12 (CXCL12)⁹². Reactive oxygen species (ROS) and SMAD3 enhance CTC adhesion via TGF β signaling⁹³. Secretion of ANGPTL4, VEGF, matrix metalloproteinases and CC chemokine ligand 2 (CCL2) by cancer cells or a disintegrin and metalloproteinase 12 (ADAM12) by endothelial cells increases endothelial permeability to facilitate extravasation^{94–96}. CTCs induce endothelial cell damage, mediated by receptor-interacting serine/threonine protein kinase 1 (RIPK1), providing another escape route⁹⁷.

Furthermore, several cell types other than endothelial cells support CTCs extravasation. Platelets facilitate extravasation by causing endothelial retraction via ATP-P2Y purinoceptor 2 (P2Y2) interaction⁸⁶. Neutrophils, immobilized by binding to the endothelial glycocalyx, create a pro-inflammatory microenvironment by secreting interleukin-8 (IL-8) and CXC chemokine 1 (CXCL1), leading to vascular leakiness^{98,99}, release of neutrophil extracellular traps¹⁰⁰ or matrix metalloproteinases⁹⁹ that promote dissemination.

12.4 Metastatic site

After leaving the circulation, CTCs may home to their new metastatic site as disseminated tumor cells (DTCs). Homing can be influenced by both anatomical and biological characteristics of CTCs. For example, particularly in CRC, a direct vascular connection between the primary site and the metastatic site allows rapid trapping of CTCs in the liver¹⁰¹. On the molecular side, breast CTCs can undergo chemotaxis to the bone marrow via expression of CXCR4¹⁰². When traveling as heterotypic clusters with platelets, CTC clusters can attract granulocytes that help to establish neoplastic lesions at secondary sites¹⁰³.

In the metastatic niche, the associated microenvironment exerts a critical influence on CTCs and can induce a non-proliferative state in these cells, potentially causing them to enter a dormant state.¹⁰⁴. Organ-specific cell types have been suggested to provide DTC sanctuaries and promote dormancy, including NK cells and hepatic stellate cells in the liver¹⁰⁵, perivascular osteoblasts in bone^{106,107}, astrocytes in the brain¹⁰⁸, and hematopoietic stem cells in the bone marrow¹⁰⁹. Activation and proliferation of DTCs may subsequently be promoted by inflammatory stimuli among others^{110,111}. Whether physical factors differ between organs and influence metastasis remains poorly understood.

13. CIRCULATING TUMOR CELLS NATURE

CTCs are tumor-derived pioneers responsible for the metastatic spread of cancer. However, the mechanisms by which cancer cells migrate through vessels remain controversial and poorly characterized. Epithelial cells typically undergo anoikis upon losing the physical interaction with their surrounding environment; thus, metastatic seeding is generally inefficient^{112,113}. Nevertheless, enhanced survival and tumor-seeding capacity seems to be contained within a small fraction of tumor-initiating cells with stem-like properties¹¹⁴.

There are two main models that attempt to explain the origin and behavior of CTCs in the metastatic context: epithelial-to-mesenchymal transition (EMT), which focuses on single cell behavior, and CTC clusters, which postulate a collective behavior of cancer cells in circulation.

13.1 EMT

Classically, it was assumed that these cancer cells were necessarily single cells detached from the primary tumor that underwent EMT¹¹⁵ (**Figure I5**), whereby they lose epithelial features (e.g., E-cadherin loss¹¹⁶) and acquire mesenchymal traits (e.g., increased vimentin expression), typically in a TGF β -dependent manner, through Snail and Slug activation. These changes, not only in expression but also in morphology, should give them some advantages to metastasize^{117,118}. In addition, some studies have shown that this EMT transition needs to be reverted for successful metastatic progression. The process known as mesenchymal-to-epithelial transition (MET), appears to be essential to replenish epithelial properties upon arrival in the metastatic niche. While transient overexpression of the EMT TFs Twist1 and Prrx1 promotes metastasis, constitutive overexpression of the same TFs inhibits metastasis, suggesting that MET may be important for metastasis formation^{119–121}. Indeed, some mouse metastasis assays have demonstrated the absence of metastases composed solely of mesenchymal cells¹²², suggesting that complete EMT is not essential (or even facilitative) for metastasis.

This binary view, in which cells can only be epithelial or mesenchymal, has been updated with the introduction of hybrid/transition EMT states^{123–125} (**Figure I5**). These intermediate states are characterized by the simultaneous presence of both epithelial and mesenchymal traits, cell-cell contacts are maintained, but some mesenchymal features are also present. Indeed, upon FAT1 deletion, tumor stemness and metastasis are promoted by induction of hybrid EMT states¹²⁶. Interestingly, these hybrid EMT CTCs exhibit features of non-individual cell migration, in which cells

migrate with retained cell-cell contacts and disseminate as tumor cell clusters^{127,128}, opening a window to a new view of cell migration in the context of metastasis: collective cell migration known as CTC clusters.

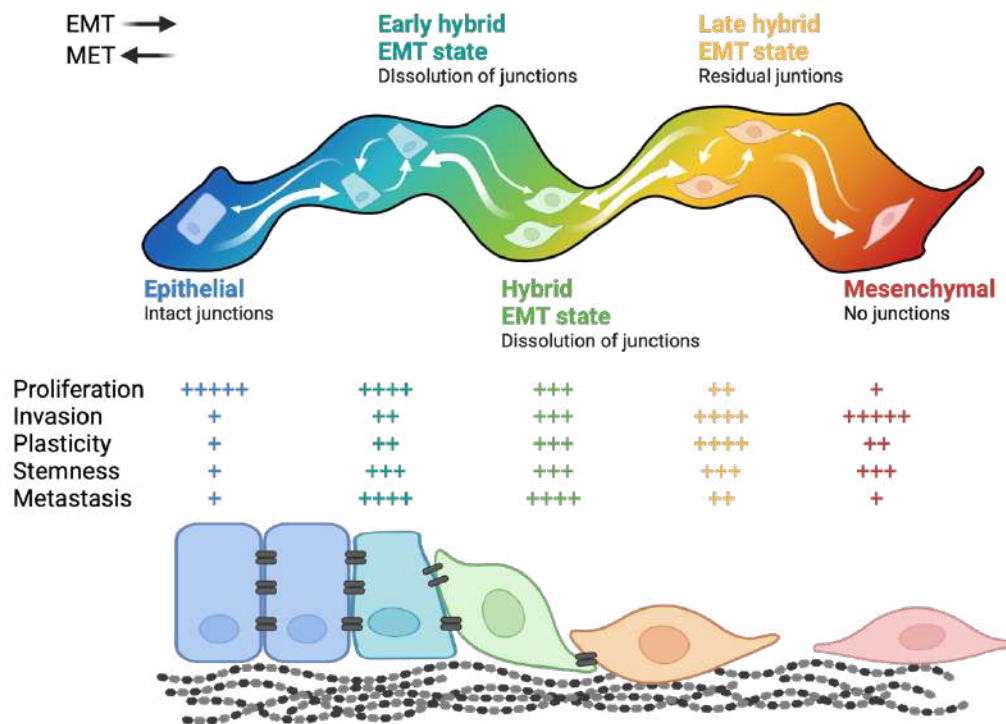


Figure I5. EMT estates in the metastatic context. EMT process dissecting the different possible cell states and the transitions between them. Adapted from¹¹⁵. Created with BioRender.com.

13.2 CTC clusters

The infrequent identification of individual invading cells during clinical examination of tumor sections (and the possibility that they represent a cross-sectioned 3D cluster¹²⁹) has led to an active but unresolved debate about whether the EMT program is required for invasion and metastasis^{130,131}. The cell-cell contact dependent, collectively migrating and highly metastatic CTC clusters, was described several decades ago¹³². The polyclonal nature of metastatic colonies in different cancer types^{133–136} and the mutually beneficial or synergistic interactions between subclones¹³⁷ suggest that cancer spread occurs preferentially via CTC clusters^{138,139}. Several studies show that CTC clusters, which represent a minority of total CTC events, have up to a 100-fold increase in metastatic potential compared to individual CTCs^{138–142}. Mathematical models suggest that cluster shape influences CTC behavior, with compact clusters flowing closer to the endothelial wall than linear clusters¹⁴³. In addition, clusters pass through narrow capillaries as "single chains"¹⁴⁴. This phenotypic plasticity influences the metastatic potential of CTC clusters.

There's growing evidence that these CTC clusters can be formed both uniquely by cancer cells (homotypic CTC clusters) or by cancer cells plus other cell types (heterotypic CTC clusters) (**Figure 16**).

Homotypic CTC clusters

Homotypic clustering enhances several cellular properties, including upregulation of stem-like features^{139,145–147} via methylation of metastasis suppressor genes¹⁴⁵. Clustering can be further enhanced by circulating galectin 3 or cancer-associated MUC1¹⁴⁸, homotypic ICAM interactions¹⁴⁷, or CD44 interacting with p21 protein-activated kinase 2 (PAK2)¹³⁹. It can also increase survival and self-renewal capacity by increasing the size or number of different cell-cell contacts: desmosomes (plakoglobin) and hemidesmosomes^{138,141} or tight junction members claudin 3 (CLDN3) and claudin 4 (CLDN4) in breast cancer¹⁴⁶.

Heterotypic CTC clusters

Cancer cells and other cell types have been found to cluster together in the circulation. These other cell types include platelets, myeloid cells, and cancer-associated fibroblasts (CAFs). Platelets rapidly interact with CTCs in the circulation¹⁴⁹ through glycoprotein Ib–IX–V (GPIb-IX-V) and glycoprotein VI (GPVI), promoting plasticity and metastasis-initiating capacity¹⁰³ via YAP1 signaling⁸⁵ or platelet-derived ATP⁸⁶. They also provide protection against T cells¹⁵⁰ and NK cells¹⁵¹. Neutrophils are another possible partner in the formation of heterotypic CTC clusters¹⁵², recruited by CXCL5 and CXCL7-dependent chemotaxis¹⁵³, and establish cell-cell contact with CTCs via vascular cell adhesion molecule 1 (VCAM1), increasing their proliferative and metastatic potential¹⁵². They also facilitate adhesion and extravasation by forming extracellular traps¹⁰⁰ or secreting IL-1 β and matrix metalloproteinases⁹⁹. Neutrophils also protect CTCs from immune surveillance^{99,154}, a benefit similarly observed for CTC clustering with myeloid-derived suppressor cells and macrophages^{155,156}. CAFs form heterotypic adherens junctions with invasive cancer cells (mediated by N-cadherin and E-cadherin, respectively), which has been shown to promote collective invasion^{157,158}.

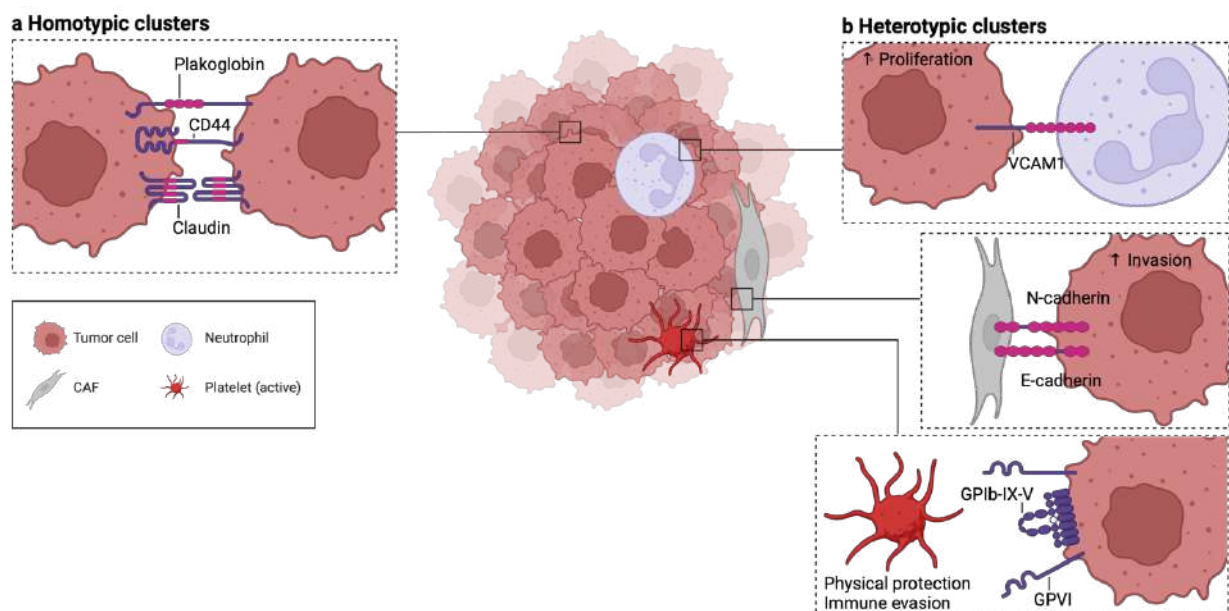


Figure 16. CTC cluster types. (A) Homotypic clustering of CTCs, kept together by cell adhesion molecules (plakoglobin, CD44, claudins and other tight junction proteins). **(B)** Heterotypic CTC clustering including tumor cells, platelets, neutrophils or CAFs, showing cell-cell interactions. Adapted from⁷⁰. Created with Biorender.com.

Regardless of the nature of CTC clusters, cell-cell contacts are one of the main points to be explored in the metastatic scenario. To date, adherens junctions, desmosomes and hemidesmosomes have been shown to play an important role. In our work, we also show that tight junctions, which were previously poorly linked to CTC clusters and never associated with CRC CTC clusters, are critical for the collective migratory phenotype of CRC cells

13.3 Detection and analysis of CTCs

The implementation of CTCs detection from liquid biopsy in the clinic would be a very useful tool, and although isolation is currently possible with different equipment, its implementation and standardization at the technical level are major challenges and difficulties. Today, these obstacles make its use in diagnosis very difficult and expensive. However, as an alternative approach, it is possible to evaluate the colonization of vessels adjacent to the primary tumor in the solid biopsy at the time of diagnosis. It is worth noting that the dynamics of CTC dissemination is emerging as an equally important element in tumor cell dissemination. Recently, it has been demonstrated that CTC release and metastatic dissemination are under the influence of circadian rhythm^{159,160}, specifically in breast cancer mouse models, the highest CTC counts were detected at night. In line with a very new concept in cancer treatment: chronotherapy, which consists in understanding the role of

circadian rhythm for tumor onset^{161–163} and growth dynamics^{164,165}. This knowledge should be considered when analyzing samples obtained at different times of the day and could potentially be applied in cancer treatment to increase drug efficacy by administering drugs at optimized times^{166–168}.

13.4 Potential CTC-based therapies

Current strategies for eliminating metastasis are identical to those used for primary tumors and consist of targeting growth and tumorigenesis rather than the metastatic process itself^{169,170}. Since metastatic cancer is the progeny of CTCs, targeting these cells at different stages of the metastatic cascade would, in principle, interrupt metastatic progression. The current potential CTC-targeting strategies are: i) Intravasation: ephrin B2 Fc chimera protein (EpB2)⁸¹, polo-like kinase 1 (PLK1) inhibitor¹⁷¹ or integrin-targeted antibodies¹⁷². ii) Cell clustering: heparanase (HPSE) inhibition¹⁷³, platelet receptor inhibitors^{153,174}, Na⁺/K⁺-ATPase inhibitors¹⁴⁶ (e.g., digoxin) or urokinase¹⁷⁵. iii) CTCs survival (metabolic interference): inhibiting pyruvate metabolism or increasing oxidative stress^{176,177}. iv) Immune checkpoint inhibition: anti-CD47, anti-PDL1/PD1 or anti-CTLA4^{178,179}. v) Engineered CTCs: cancer vaccine production using mechanically disrupted CTCs as nanolysates²²¹ or CTCs to deliver therapeutic payloads¹⁸⁰.

13.5 Prognostic and predictive value of CTCs

CTCs have been detected in the blood of patients with all major carcinomas, with proven prognostic value in colorectal, breast, prostate, and lung cancers^{181–185}. Specifically, in CRC, a higher number of CTCs detected before treatment is associated with a worse prognosis¹⁸⁶. Evaluation of CTC clusters together with single CTC counts significantly improves prognostic accuracy in breast cancer patients undergoing surgery¹⁸⁷. After surgery, CTCs can be detected 7-9 weeks before the appearance of clinical manifestations indicating their usefulness in predicting minimal residual disease, relapse, and early cancer detection¹⁸⁸.

Despite their value in risk stratification, using CTCs for therapeutic patient stratification in clinical trials has had limited success, including monitoring therapy response and resistance¹⁸⁹. CTCs have been included in the AJCC Cancer Staging Manual¹⁹⁰ as 'cM0 (i+),' indicating no overt metastasis but detectable tumor cells in blood, bone marrow, or lymph nodes. However, they are not yet part of clinical practice guidelines from major cancer societies like the European Society for Medical Oncology or the American Society for Clinical Oncology.

14. NF-κB SIGNALING PATHWAY

The nuclear factor-κB (NF-κB) signaling pathway is a central coordinator of the immune system and inflammation. It was discovered more than 30 years ago as a DNA-binding factor in the nucleus of activated B cells¹⁹¹. Further investigations revealed the involvement of the NF-κB signaling pathway in various biological processes and its contribution to tumorigenesis, both by triggering the inflammatory response and by directly modulating cellular functions such as proliferation, inhibition of apoptosis, or cellular migration^{192,193}.

14.1 NF-κB family, structure and classification

NF-κB transcription factors

The mammalian NF-κB family comprises five transcription factors (TFs): RelA (p65), RelB, c-Rel, p105/p50 (NF-κB1), and p100/p52 (NF-κB2). All members can form homodimers and heterodimers and translocate from the cytoplasm to the nucleus in response to cell stimulation. Both types of NF-κB dimers can bind to specific DNA sequences (consensus κB sites) and either induce or repress expression of target genes through the recruitment of coactivators and corepressors^{194,195}. Genes regulated by NF-κB include those controlling apoptosis, cell adhesion, proliferation, innate and adaptive immune responses, inflammation, cellular stress response, and tissue remodeling^{196,197}.

All NF-κB members share a highly conserved N-terminal Rel homology domain (RHD) that contains the nuclear localization signal (NLS) responsible for DNA binding, dimerization, and interaction with inhibitor proteins¹⁹⁸. RelA, RelB and c-Rel are synthesized in their mature form and contain a transactivation domain (TAD) necessary for positive regulation of gene expression. p50 and p52 subunits are synthesized as large precursors p105 and p100, respectively, and require proteolysis of the C-terminus (which contains multiple ankyrin repeats) to mature¹⁹⁹. Because they lack TAD, p50 and p52 may repress transcription unless associated with TAD-containing NF-κB members²⁰⁰. Despite structural similarities and their ability to bind DNA, all NF-κB subunits have distinct and non-overlapping functions.

Inhibitor of NF-κB (IκB)

In unstimulated cells, NF-κB proteins are predominantly localized in the cytoplasm bound to a family of NF-κB inhibitor proteins (IκB), which includes IκBα, IκBβ, IκBε, IκBγ, IκBζ and Bcl-3 (B-cell lymphoma 3-encoding protein). This family of proteins is characterized by the presence of C-

terminal ankyrin repeats, which are essential for their interaction with NF- κ B members. Through these motifs, they bind to NF- κ B dimers, masking their NLS, resulting in a cytoplasmic retention²⁰¹. In addition, I κ B proteins also possess their own NLS and nuclear export sequence (NES) in the N-terminus, reflecting their capacity to dynamically regulate the NF- κ B nuclear-cytoplasmic shuttling process^{198,202,203}. I κ B degradation is a rapidly induced signaling event initiated by specific phosphorylation deposited by the inhibitor of kappaB kinase (IKK) complex, which marks I κ B for ubiquitination and subsequent proteasomal degradation²⁰⁴. This process drastically alters the dynamic balance between cytoplasmic and nuclear localization signals to induce nuclear accumulation of NF- κ B factors to promote gene transcription.

Apart from NF- κ B pathway regulation, alternative nuclear functions have been identified for several I κ Bs²⁰⁵. Physical association of I κ B α with histone deacetylases (HDACs) has been described, increasing NF- κ B-independent transcription through cytoplasmic retention of HDACs^{206,207}. In addition, previous studies from our group have shown that I κ B α can also interact with chromatin at specific genomic regions to regulate gene transcription through modulation of the chromatin-editing polycomb repressive complex 2 (PRC2). Indeed, phosphorylated and SUMOylated I κ B α can directly bind to acetylated N-terminal histone tails, particularly H4, facilitating PRC2 recruitment to specific genes related to development, stemness, and tissue homeostasis^{207–210}.

IkB kinase complex (IKK complex)

The IKK kinase complex is the master regulator of the NF- κ B signaling pathway. It is composed of two catalytic subunits, IKK α and IKK β , and the regulatory subunit IKK γ /NEMO²¹¹. Biochemical purification of this complex revealed a molecular size of 700 to 900 kDa²¹² and demonstrated the presence of other components such as Hsp90, Cdc37 and ELKS, although their association with the IKK core complex is transient and stimulus-dependent^{213–215}. This core complex catalyzes the phosphorylation of I κ B on serine residues (Ser32/36 I κ B α , Ser19/23 I κ B β , Ser18/22 I κ B ϵ), leading to its degradation and inducing NF- κ B pathway activation²¹⁶. The kinases IKK α and IKK β share a similar structure (50% sequence identity) that includes an N-terminal kinase domain (KD), a scaffold/dimerization domain (SDD) with a helix-loop-helix (HLH) motif that modulates kinase activity and a leucine zipper (LZ) that allows homo- or heterodimerization of the kinases, and a C-terminal NEMO-binding domain (NBD) that allows recognition and binding to NEMO²¹⁷.

Additional nuclear functions of IKK α include phosphorylation of histone H3 at Ser10 thus facilitating the subsequent CBP-mediated histone acetylation at Lys14, modulating chromatin accessibility and

promoting NF- κ B gene expression^{218,219}; transcriptional repression of the tumor suppressor Maspin^{220,221}, regulation of keratinocyte differentiation by interacting with smad2/3²²² or suppressing squamous cell carcinoma by preventing hypermethylation of the 14-3-3 sigma gene by Suv39h1²²³.

IKK α activation is induced by phosphorylation of two serine residues in the kinase domain: Ser176/180. This event leads to a conformational change in the activation loop, which activates the catalytic function^{224,225}. However, the molecular mechanisms of IKK α activation are not fully understood. In general, TGF β -activated kinase 1 (TAK1) has been identified as an IKK kinase (IKKK). TAK1 is activated and recruited to the IKK complex together with TAB2/3 by a variety of proinflammatory mediators, which phosphorylates and activates the kinase in the cytoplasm, resulting in the initiation of NF- κ B signaling^{226,227}. In addition, receptor interacting protein 1 (RIP1) and MAPK/ERK kinase kinase 3 (MEKK3) kinases have also been postulated to play a role in IKK phosphorylation and TNF α -mediated NF- κ B activation^{228–230}.

14.2 Activation of NF- κ B signaling pathway

The NF- κ B signaling pathway can be activated by a variety of factors that elicit different responses.

Classical NF- κ B pathway (canonical)

The canonical NF- κ B pathway is mainly induced by pathogen-associated molecular patterns (PAMPs) and pro-inflammatory cytokines such as interleukin-1 (IL-1), tumor necrosis factor (TNF α) or toll-like receptor (TLR) ligands such as lipopolysaccharide (LPS). Receptor stimulation initiates the signaling cascade and the recruitment of several proteins (TRADDs, FADDs, cIAPs, LUBAC, TRAFs, RIP1, among others) that lead to the activation of TAK1^{231,232}, which catalyzes the phosphorylation of the IKK complex. Subsequently, the active IKK complex phosphorylates I κ Bs at the N-terminal serine residues²⁰⁴. The ubiquitin ligase machinery SCF (Skp-1/cullin/F-box) then recognizes the phosphorylated I κ B, inducing its polyubiquitination and proteasomal degradation²³³. Degradation of I κ Bs releases NF- κ B dimers (except for the p52/RelB dimer) that translocate to the nucleus to activate specific gene transcription¹⁷⁴ (**Figure 17**).

Alternative NF- κ B pathway (non-canonical)

Activation of non-canonical NF- κ B signaling is induced by specific members of the TNF cytokine family, including CD40 ligand, B-cell activating factor (BAFF), lymphotoxin- β (LT β) and receptor activator of NF- κ B ligand (RANKL)^{234–236}. In contrast to the canonical NF- κ B pathway, the non-canonical NF- κ B pathway is completely dependent on IKK α activity (independent of IKK β and NEMO) and specifically mediates activation of the p52/RelB NF- κ B dimer. Upon ligand induction, NF- κ B inducing kinase (NIK) is stabilized, which phosphorylates and activates IKK α ²³⁷. Under normal conditions, NIK is targeted for continuous degradation by TRAF3, which is degraded upon TNF receptor activation²³⁸. IKK α then phosphorylates the NF- κ B precursor p100, causing its proteolytic processing to the active form p52. After this processing, the p52/RelB heterodimer translocates to the nucleus and promotes the regulation of genes associated with specific immunological processes, such as lymphoid organogenesis and lymphocyte function^{239,240} (Figure 17).

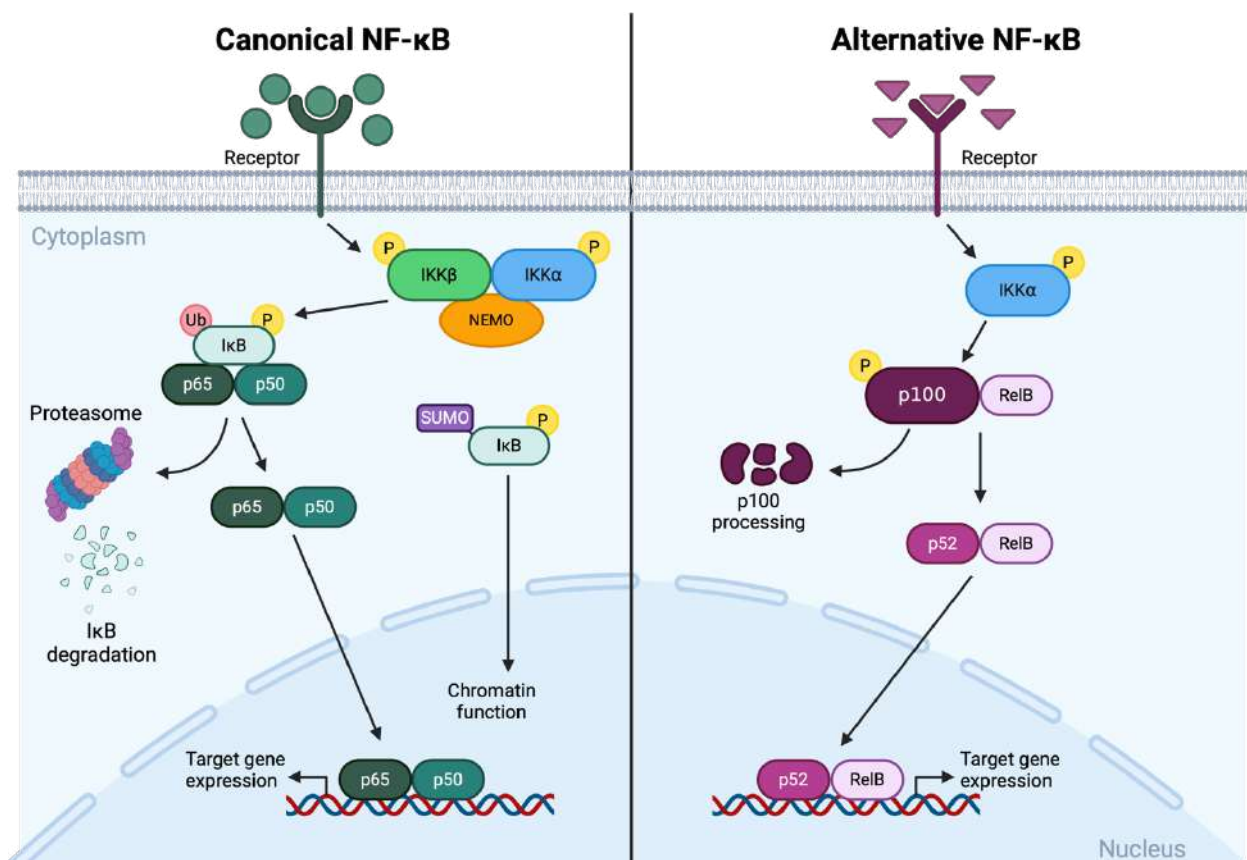


Figure 17. NF- κ B pathway. In the canonical NF- κ B pathway (left) the stimulation of multiple receptors leads to the activation of the IKK complex (IKK α , IKK β and NEMO) which catalyses the phosphorylation of the inhibitor I κ B. This phosphorylation is essential for signaling the ubiquitination and protein degradation of I κ B, leading NF- κ B members free to translocate to the nucleus and promote gene transcription. Apart from ubiquitination, the same residue can be sumoylated thus blocking I κ B proteasomal degradation, promoting

its nuclear translocation. In the alternative NF- κ B pathway (right), upon ligand induction, active IKK α phosphorylates p100, and as a result, it is processed into the active form p52 and together with RelB, translocates to the nucleus an active gene transcription. Created with BioRender.com.

14.3 NF- κ B independent IKK α functions and cancer association

The IKK complex interacts not only with I κ Bs, but also with many other proteins related to the NF- κ B pathway, such as RelA, or unrelated to NF- κ B, such as p53 thus highlighting the importance of the complex in several different physiological processes²⁴¹. In particular, IKK α (specifically nuclear) has been shown to play an important protumoral role in several cancer types.

In breast cancer, nuclear IKK α increases the phosphorylation and recruitment of estrogen-induced transcription factors, such as estrogen receptor alpha (ER α), steroid receptor coactivator 3 (SCR-3) and E2F transcription factor 1 (E2F1), to the promoter regions of cell cycle progression genes (e.g., CYCLIN D1 and C-MYC), enhancing their transcription and inducing cancer cell proliferation^{242,243}. In addition, when active, IKK α enters the nucleus of cancer cells and phosphorylates p27/Kip1, inducing its nuclear export and leading to increased cell proliferation²⁴⁴.

As mentioned, in prostate cancer nuclear IKK α negatively regulates the tumor suppressor Maspin by facilitating the recruitment of DNA methyltransferase activity to its promoter²²⁰. By a comparable mechanism, high nuclear IKK α levels are predictive of the metastatic ability in squamous cell carcinoma (SCC)²²¹.

In contrast, in keratinocytes nuclear IKK α binds to H3 at the 14-3-3 σ locus thus preventing its hypermethylation-mediated repression by SUV39h1 and acting as a tumor suppressor. Mechanistically, 14-3-3 σ induces the cytoplasmic export of the cell cycle regulatory phosphatase CDC25C and inhibits constitute cell cycle²²³.

In lung cancer, nuclear IKK α phosphorylates CREB binding protein (CBP) to increase its affinity for p65/NF- κ B. As a result, CBP-p53 association is reduced, leading to decreased p53-dependent gene expression²⁴⁵.

In CRC, nuclear IKK α phosphorylates the nuclear co-repressors silencing mediator for retinoid and thyroid receptors (SMRT) and nuclear receptor co-repressor (NCoR), leading to their cytoplasmic export by 14-3-3 σ . This export induces gene transcription, including Notch target genes such as HES1, HES5 and HERP2^{246,247}. In addition, IKK α contributes to the oncogenic transformation of the

intestine through the regulation of stemness-related genes²⁴⁸. A few years ago, our group identified a truncated form of IKK α with a predicted weight of 45 kDa that we called IKK α (p45). It is generated by proteolytic cleavage of full-length IKK α in the endosomal compartment and is present in various cell types, but particularly in the nucleus of cancer cells. We found that the majority of activated IKK α in the nucleus of cancer cells correspond to IKK α (p45), which includes the KD but lacks some regulatory domains in the C-terminal region. Therefore, we speculate that many of the described nuclear functions of IKK α are associated with this truncated form. Recently, we demonstrated that in response to damage, IKK α (p45) is phosphorylated and activated downstream BRAF/TAK1/p38 MAPK, inducing its nuclear translocation. Once in the nucleus, IKK α (p45) regulates the activation of the DNA damage response (DDR) through direct phosphorylation of ATM (**Figure 18**). Active p45-IKK α is essential for efficient DNA repair; therefore, inhibition of IKK α or BRAF abrogates the activation of key DDR elements, compromising DNA repair and synergistically potentiating the antitumor effect of chemotherapy/radiotherapy in CRC, leading to the eradication of resistant cells²⁴⁹. In addition to ATM phosphorylation, damage-induced IKK α modulates BRD4, and JAK/STAT signaling with clinical relevance in CRC²⁵⁰. Specifically, phosphorylation of BRD4 by IKK α is required for its chromatin-binding at target genes upon DNA damage. Moreover, IKK α induces the NF- κ B-dependent transcription of the cytokine LIF, leading to STAT3 activation, association with BRD4 and recruitment to specific target genes.

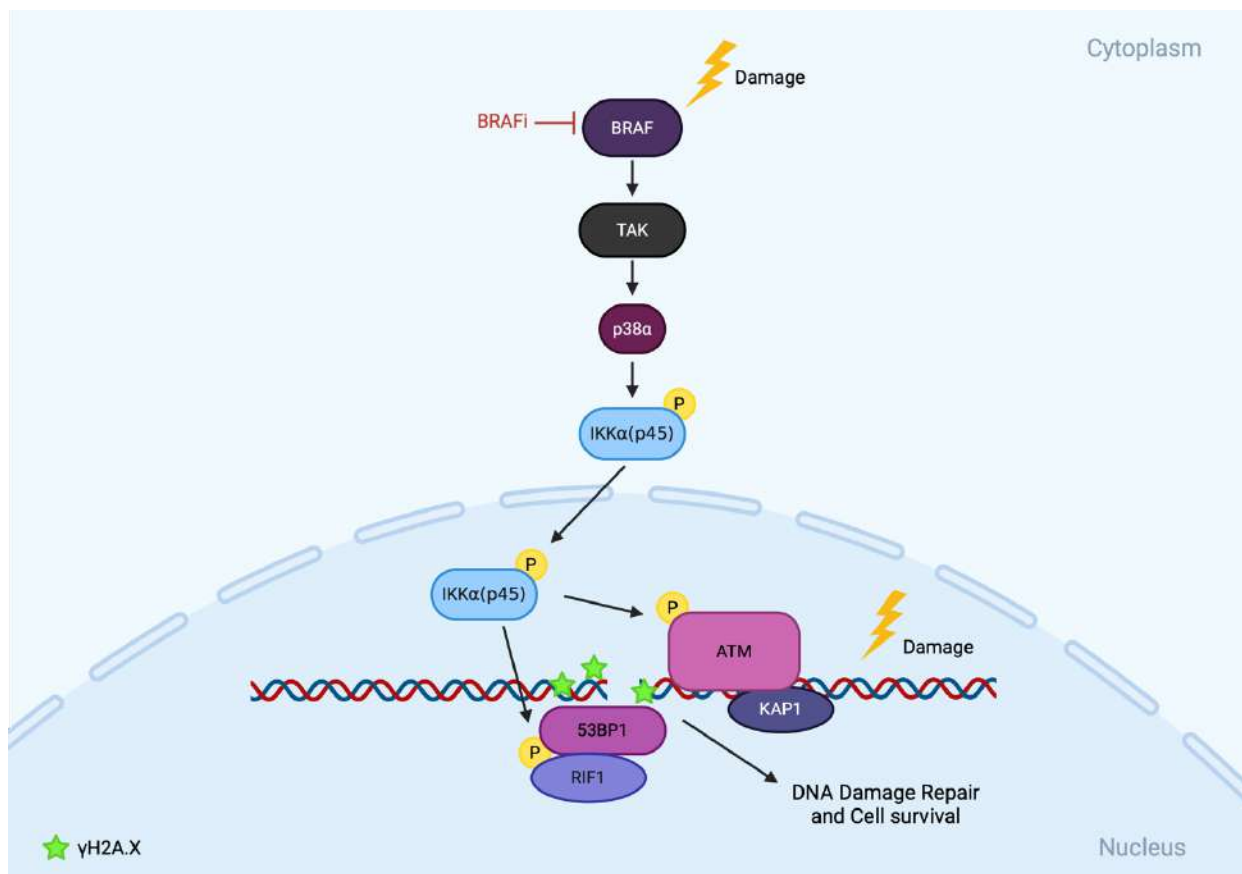


Figure I8. NF-κB independent IKKα function in DDR. The IKKα truncated form, p45-IKKα, is rapidly activated in response to DNA damage downstream BRAF, TAK1 and p38α and regulates different elements of DNA repair machinery through direct phosphorylation of ATM and 53BP1, leading to efficient DNA repair and cell survival. Created with BioRender.com.

Due to their association with tumorigenesis both inside and outside the NF-κB pathway, chemical inhibition of IKKα has become an attractive approach for cancer therapy. There are a variety of inhibitors including natural products, biomolecular and peptide inhibitors and synthetic small molecule inhibitors with different inhibition strategies²⁵¹. However, the inhibitors developed to date have shown severe toxic effects due to lack of specificity and strong interference with cellular homeostasis²⁵².

15. TIGHT JUNCTIONS

Tight junctions (TJs) are the most apical intercellular junctions of epithelial and endothelial cells, which form a regulatable semipermeable diffusion barrier between individual cells²⁵³. They are essential for establishing a barrier between different compartments of the body, and their primary physiological role is to function as paracellular gates that restrict diffusion on the basis of size and charge. Selective paracellular diffusion is an essential process for the maintenance of homeostasis in organs and tissues. TJs are composed of several interconnecting integral plasma membrane proteins that are anchored to the cytoskeleton, forming an intramembrane diffusion fence that restricts the mixing of apical and basolateral membrane components and are linked to the machinery that controls apicobasal polarization²⁵⁴. In addition, signaling networks that control diverse cell functions are connected to TJs, transmitting information to and from the cytoskeleton, nucleus and several cell adhesion complexes.

15.1 Tight junction structure

TJs are multiprotein structures that can be separated into two modules: the junctional plaque (which is located in the cytoplasmic region anchored to the cytoskeleton) and the transmembrane proteins (connecting the inside-outside of neighboring cells) (**Figure I9**).

Junctional plaque components

The cytosolic plaque is a complex protein network that interacts with the cytoplasmic domains of junctional membrane proteins as well as with F-actin and microtubules. Its major structural components are adaptor proteins that contain multiple protein-protein interaction motifs²⁵⁵ and are essential for junction formation (e.g., zonula occludens protein 1 (ZO-1), also known as tight junction protein 1). The tight junction plaque contains a large number of other adaptor proteins, many of which interact to form a protein network. Examples include ZO-2 and ZO-3, two proteins that co-immunoprecipitate with ZO-1^{256–258}. Other examples of junctional plaque proteins include the membrane-associated guanylate kinase inverted (MAGI) proteins^{259,260}, the multi-PDZ domain proteins MUPP1 (also known as MPDZ)²⁶¹ and partitioning defective 3 (PAR3) and PAR6²⁶², and protein associated with Lin-1 1 (PALS1) and PALS1-associated tight junction (PATJ)²⁶³. Anchoring to the cytoskeleton can be mediated directly by ZO proteins or through cingulin interaction²⁶⁴.

In addition, the junction contains many different signaling proteins that are recruited by binding to adaptors or membrane proteins^{265,266}. These signaling proteins include protein kinases, phosphatases, monomeric and trimeric GTP-binding proteins, and transcriptional and post-transcriptional regulators involved in various signaling pathways such as epithelial cell proliferation and migration^{267–269}.

Transmembrane proteins

The major protein components of the transmembrane strands present in TJs are tetraspan proteins, including the claudin family (26 members in humans) and the three junctional MARVEL domain proteins: occludin, tricellulin, and MARVEL domain-containing protein 3 (MARVELD3). When expressed in cells that do not form tight junctions, they have been shown to produce superficially similar strands in the case of claudins or transmembrane particles, and short strand fragments in the case of occludin^{270–273}. Similarly, some claudins and occludin are capable of mediating Ca²⁺-independent cell-cell adhesion^{273,274}.

Other transmembrane components of tight junctions include a trispan protein, blood vessel epicardial substance (BVES)²⁷⁵, and a large group of single-span transmembrane adhesion proteins with two immunoglobulin-like domains, including junctional adhesion molecules (JAMs)^{276,277}, coxsackievirus and adenovirus receptor (CAR)²⁷⁸, angulins²⁷⁹ and crumbs cell polarity complex component 3 (CRB3).

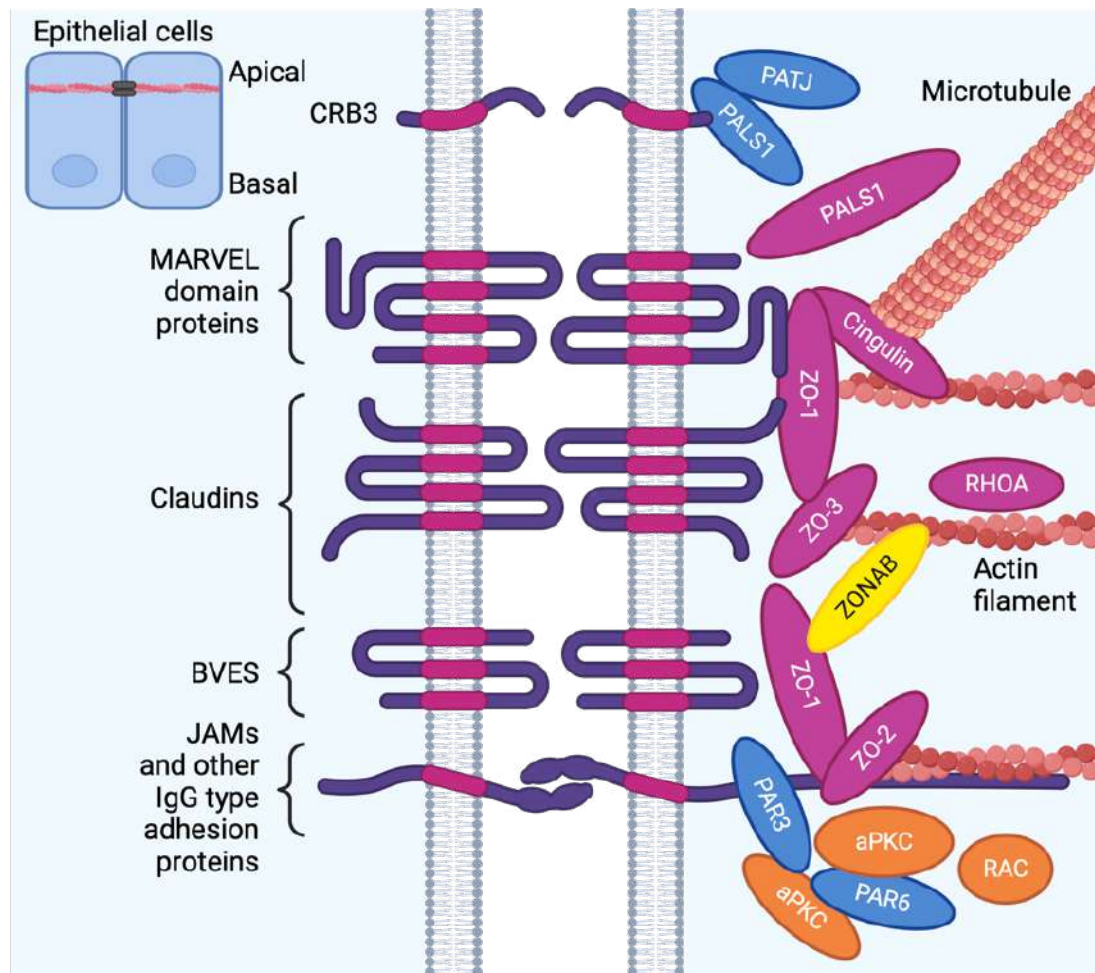


Figure 19. Tight junction structure. Overview of the types of tight junction protein, with only representatives of the main groups shown. Transmembrane proteins (shown as purple strands) include CRB3; MARVEL domain proteins such as occludin, tricellulin and MARVELD3; claudins; BVES; JAMs; and other IgG-type adhesion proteins. Adaptor proteins and cytoskeletal linkers (pink ovals), as well as polarity proteins (blue ovals), include the ZO proteins ZO-1, ZO-2 and ZO-3; cingulin; MAGI; PAR3 and PAR6; PALS1 and PATJ. Signaling components associated with tight junctions (orange ovals) include aPKC; the small RHO GTPases CDC42, RAC and RHOA. Additionally, an interaction between ZO-1 and the transcriptional regulator ZONAB is shown (yellow oval). Adapted from²⁶². Created with Biorender.com.

In summary, in a very simplistic way, TJs are formed by a cytosolic plaque formed by the core protein ZO-1 (with the possible presence of ZO-2), directly linked to the cytoskeleton (or through cingulin) and, at the same time, linked to transmembrane proteins; basically claudins or occludin.

15.2 Tight junctions in cancer

The complexity of TJ functionality is highlighted by their dual and differential expression patterns in different cancer types, where loss of expression or alternatively overexpression has been described

to promote tumorigenesis²⁸⁰. This is further confirmed in several *in vivo* animal models, where aberrant expression of TJ proteins promotes abnormal cell proliferation, neoplasia or metastasis. In addition, growing evidence suggests that tight junction proteins, in particular CLDNs, play an important role in CSC biology²⁸¹. Specifically in CRC context, CLDN1/2/3/4/7/16, occludin and tricellulin appear to be upregulated²⁸².

Among the whole list of TJ proteins and their links to tumorigenic processes, we focused on ZO-1 and claudin-2 (CLDN2) because of our experimental data.

ZO-1

Dysregulation of ZO-1 has been poorly linked to tumorigenic processes, but there are some specific situations in which ZO-1 plays a relevant role. For example, in tumoral cell cycle progression, association with ZONAB has been shown to regulate cellular proliferation and G1/S phase progression through interaction with cyclin-dependent kinase 4 (CDK4)²⁸³. CLDN1 expression confers resistance to anoikis in colon cancer cells. This is mainly dependent on the activation of Src, a tyrosine kinase identified to promote anoikis resistance, with which CLDN1 has been described to form a multi-protein complex with ZO-1²⁸⁴, leading to modulation of Akt phosphorylation and increased Bcl-2 expression. In addition, RNA-binding motif protein 38 (RBM38), a key mediator of TGF- β -induced EMT, positively regulates ZO-1 transcription in breast cancer²⁸⁵. Partitioning defective protein 3 (Par3) and ZO-1 clustering on the cell membrane are indicators of poor prognosis in lung squamous cell carcinoma²⁸⁶.

With this work, we challenge the lack of clear evidence for a tumorigenic role of ZO-1 in CRC, particularly in mediating collective migration in metastasis.

CLDN2

Conflicting roles for CLDN2 in cancer have been proposed depending on the type of cancer. In breast cancer, CLDN2 expression has been shown to be downregulated in breast tumors compared to normal tissue, and decreased levels are observed in breast cancers of increasing grade, suggesting a tumor-suppressive role²⁸⁷. In contrast, CLDN2 is important for the invasive characteristics of gastric carcinoma and is overexpressed in CRC, two tumor types that preferentially metastasize to the liver^{288,289}.

Focusing on the pro-tumorigenic functions of CLDN2, it has been linked to several cancer processes. For example, tumor cell growth. CLDN2 expression increases cancer cell proliferation, anchorage-independent growth and tumor growth *in vivo* through transactivation of epidermal growth factor receptor (EGFR), a key regulator of colorectal carcinogenesis²⁹⁰. Furthermore, inhibition of cell proliferation in lung adenocarcinoma is partly related to the decrease in CLDN2 expression upon treatment with the DNA methyltransferase inhibitor azacitidine²⁹¹, through a decrease in NF-κB phosphorylation and binding to the promoter region of CLDN2²⁹².

Regarding cell migration, CLDN2 increases the mRNA level and enzymatic activity of matrix metalloproteinase 9 (MMP9) in the human lung adenocarcinoma cell line A549²⁹³, thereby enhancing their ability to migrate.

In the context of CSCs, CLDN2 promotes CRC cell self-renewal both *in vitro* and *in vivo*, along with increasing the population of ALDH^{High} stem-like cells and favoring phenotypic transitions from ALDH^{Low} to ALDH^{High} subpopulations²⁹⁴. Furthermore, an association between high CLDN2 expression in CAFs and shorter survival in 5-FU- and oxaliplatin-treated metastatic colorectal cancer patients has been described²⁹⁵.

15.3 Tight junction elements in cancer treatment

Over the last years, several studies have shown an abnormal TJ function and expression in cancer, highlighting individual components of the TJs as promising new targets for cancer prognosis, detection and treatment.

One of the most important therapeutic approaches developed very recently is related to CLDN18.2. Expression of the tight junction protein CLDN18.2 in gastric cancer cells correlates with liver metastasis and blocking antibodies to CLDN18.2 have demonstrated efficacy in the treatment of metastatic gastric cancer^{296,297}.

In liver cancer, treatment with humanized monoclonal antibodies against CLDN1 suppressed cancer growth and EMT in *ex vivo* patient-derived models²⁹⁸.

In CRC, the anti-CLDN4 extracellular domain antibody 4D3 synergistically enhanced the antitumor effects of 5-FU or the anti-EGFR antibody cetuximab²⁹⁹. Overexpression of CLDN1 and CLDN2 in CRC suggests their applicability as tumor markers and targets²⁸⁹. It is worth mentioning that in

fibrosarcoma, treatment with the human-rat chimeric IgG1 1A2 CLDN2-targeting antibody attenuated tumor growth without remarkable side effects³⁰⁰.

To date, there are no commercial drugs specifically targeting CLDN2, which would be very interesting in light of the results obtained in this work.

In this work, we uncover a novel role for IKK α in the regulation of cell-cell contacts, specifically tight junctions, during the metastatic process. Functional depletion of IKK α leads to the formation of aberrant tight junction-like structures that increase cancer cell clustering and metastatic aggressiveness. In this context, the balance between pro-tumorigenic and anti-metastatic functions of IKK α needs to be re-evaluated before proposing its inhibition as a putative therapeutic strategy to fight cancer.

OBJECTIVES

OBJECTIVES

Main Objective:

Investigate the NF- κ B-dependent and independent roles of IKK α kinase in colorectal cancer cells associated to cell migration and metastasis.

Subobjectives:

- Identify potential phosphorylation and transcriptional targets of IKK α activity involved in these processes.
- Evaluate IKK α substrates as novel biomarkers for predicting metastatic risk in colorectal cancer patients.
- Depth into the development of new therapeutic strategies to eradicate metastatic cancer cells or prevent their dissemination.

MATERIALS AND METHODS

MATERIALS AND METHODS

MM1. CELL LINES AND REAGENTS

CRC cell line CaCo-2 [ATCC, Ref. HTB-37], CRC cell line HCT-116 [ATCC, Ref. CCL-247], CRC cell line HT-29 M6 [ATCC, Ref. HTB-38], CRC cell line DLD1 [ATCC, Ref. CCL-221] and HEK293T [ATCC, Ref. CRL-3216] were obtained from the American Type Culture Collection [ATCC, USA]. All adherent cells were grown in Dulbecco's modified Eagle's medium (DMEM) [Invitrogen] plus 10% fetal bovine serum (FBS) [Biological Industries], 4.5 g/L glucose [Life Technologies], 2 mM L-glutamine [Biological Industries], 56 U/mL penicillin and 56 µg/mL streptomycin [Biological Industries] and were maintained in a 5% CO₂ incubator at 37°C.

For cell treatment, BRAF inhibitors Vemurafenib (PLX4032) [Selleckchem, Ref. S1267] and AZ628 [Selleckchem, Ref. S2746], MEK inhibitor selumetinib (AZD6244) [Selleckchem, Ref. S1008] and CLDN1/2 inhibitor (CLDNi) YM201636 [Selleckchem, Ref. S1219] were used.

MM2. PDOs GENERATION

PDOs have been recently used as a cancer model, which have the capacity to resemble the original human tumour. In this study, fragments of primary or xenograft human CRC tumours were obtained from Parc de Salut MAR Biobank (MARbiobanc; <https://marbiobanc.imim.es>) with the informed consent of patients and following all recommendations of Hospital del Mar' Ethics Committee, the Spanish regulations, and the Helsinki declaration's Guide.

Table MM1. List of CRC PDOs used. Mutations of PDOs and the original tumour they come from are indicated.

PDO	Tumour subtype	PDO mutations	Original tumour mutations
PDO4	CRC metastasis in the liver	<i>TP53</i> I254T (100%) <i>EGFR</i> S464L (97.21%)	<i>TP53</i> I254T (77.96%) <i>EGFR</i> S464L (97.18%)
PDO5	CRC	<i>KRAS</i> G12D (66.43%)	<i>KRAS</i> G12D (15.52%) <i>PDGFRA</i> R293H (14.79%) <i>TP53</i> H179R (12.51%)
PDO8	CRC	<i>TP53</i> Q192stop (98.46%) <i>KRAS</i> G13C (67.27%)	<i>TP53</i> Q192stop (44.72%) <i>KRAS</i> G13C (44.26%)

Table MM2. List of DF12⁺⁺⁺ medium factors.

Factors	Stock Concentration	Final Concentration	Volume
DMEM-F12 [GIBCO Ref. 12634028]	1X	1X	50 mL
Penicillin/Streptomycin (P/S) [Thermo Scientific Ref. 15140122]	100 U/mL	1U/mL	500 µL
L-Glutamine [Thermo Scientific Ref. A2916801]	100X	1X	500 µL
Primocin [Invitrogen Ref. ant-pm-1]	100 µg/mL	200 ng/mL	100 µL

Table MM3. List of complete medium factors.

Factors	Stock Concentration	Final Concentration	Volume
DF12 ⁺⁺⁺ medium	1X	1X	40 mL
B-27 Supplement [GIBCO Ref. 17504044]	50X	1X	800 µL
N-2 Supplement [GIBCO Ref. 17502048]	100X	1X	400 µL
Nicotinamide [Sigma-Aldrich Ref. N3376]	1 M	10 mM	400 µL
N-Acetyl-L-cysteine [Sigma-Aldrich Ref. A7250]	0.5 M	1.25 mM	100 µL
Recombinant Human Noggin [PeproTech Ref. 120-10C]	100 µg/mL	100 ng/mL	40 µL
Recombinant Human R-Spondin-1 [PeproTech Ref. 120-38]	100 µg/mL	100 ng/mL	40 µL
Y-27632 dihydrochloride (ROCK inhibitor) [Sigma-Aldrich Ref. Y0503]	40 mM	10 µM	10 µL
Prostaglandin E2 [Tocris Ref. 2296]	50 µM	10 nM	8 µL
SB 202190 [Sigma-Aldrich Ref. S7067]	15 mM	3 µM	8 µL
A83-01 (ALK inhibitor) [Sigma-Aldrich Ref. SML0788]	10 mM	0.5 µM	2 µL
hEGF [Sigma-Aldrich Ref. E9644]	1 mg/mL	50 ng/mL	2 µL
Gastrin I [Tocris Ref. 3006]	500 µM	10 nM	0.8 µL
Ciprofloxacin [Sigma-Aldrich Ref. 17850]	2 mg/mL	8 µg/mL	200 µL

For PDO generation and culture, DF12⁺⁺⁺ and complete medium is needed. The preparation of these mediums is performed using the factors listed in **TABLE MM2** and **MM3**. Complete medium can be kept a maximum of 2 weeks at 4°C. The protocol used for human tumour cell isolation was adapted from³⁰¹, as follows:

1. For every human sample, perform everything for duplicate. Cut the tumor samples with a scalpel to 1-2 mm².
2. Transfer the samples with a plastic Pasteur pipette into previously prepared falcons containing the factors listed in **TABLE MM4**.
3. Incubate at 37°C for 40 min in agitation, in horizontal position, for disaggregation of the tumours.
4. Add 1 mL of FBS.
5. Filter with a 100 µm cell strainer.
6. Centrifuge at 100 rcf for 3 min.
7. Aspirate the supernatant. Resuspend the pellet with 1 mL of DF12⁺⁺⁺ medium and transfer it to an eppendorf.
8. Centrifuge at 600 rcf for 5 min.
9. Aspirate the supernatant. Resuspend the pellet with 1 mL of DF12⁺⁺⁺ medium.
10. Prepare adequate dilutions of cell suspension depending on the cell pellet, for example 1/2, 1/10 and 1/100. Make 2 wells per dilution.
11. Centrifuge the eppendorfs again and leave 50 µL of medium.
12. Resuspend the pellet and add 100 µL of Matrigel Basement Membrane Matrix [Corning Ref. 354234] (50 µL per well). Maintain the matrigel with the cells always in ice. Seed 50 µL of the mix in the middle of the well of a 24-well plate, avoiding bubble formation.
13. Incubate 10 min at 37°C.
14. Add 450 µL of complete medium, slowly against the well.

Table MM4. Factors used for tumor disaggregation.

Factors	Stock Concentration	Final Concentration	Volume
PBS + 5% P/S	1X	85%	8.5 mL
Collagenase II [Sigma-Aldrich Ref. C6885]	10 mg/mL	1.5 mg/mL	1.5 mL
Hyaluronidase [Sigma-Aldrich Ref. H3506]	10 mg/mL	20 µg/mL	20 µL
Y-27632 dihydrochloride (ROCK inhibitor) [Sigma-Aldrich Ref. Y0503]	40 mM	10 µM	2.5 µL

MM3. PDOs CULTURE AND PASSAGING

PDOs normally need to be passaged every 1-2 weeks and complete medium has to be changed at least once a week. Depending on the PDO, you should disaggregate them mechanically or produce single cells. PDOs were expanded by serial passaging and kept frozen in liquid Nitrogen for being used in subsequent experiments.

MM3.1. Mechanical disaggregation

1. Resuspend the matrigel: with 1 mL filter tips, pipetting up and down the matrigel with the medium. Avoid bubble formation. Transfer it to an eppendorf.
2. Pass the cell suspension 8 times through a 21 G needle.
3. Centrifuge at 1100 rcf for 5 min. Eliminate the supernatant, leaving 50 µL.
4. Perform the right dilutions, normally 1 well to 2-4 wells. Add the right amount of matrigel (50 µL per well) and seed them as explained before in a 24-well plate.
5. Incubate 10 min at 37°C.
6. Add 450 µL of complete medium, slowly against the wall.

MM3.2. Disaggregation to single cells

Used for passaging (24-well plate) but also for seeding PDOs to perform experiments (in 24- or 96-well plate).

1. Slowly, remove the medium and add 400 µL of PBS. Resuspend the matrigel.
2. Centrifuge at 1100 rcf for 5 min. Discard the supernatant and resuspend the cell pellet with trypsin, the same volume as medium you left.
3. Incubate at 37°C for 15 min.
4. Add DF12+++ medium + 10% FBS, the double amount of trypsin.
5. Pass the cell suspension 8 times through a 21G needle.
6. Count the cells with trypan blue.
7. Depending on the PDO, you will need to seed a different amount of cells per well. You should have 85% of matrigel and a mix of cells+DF12+++ medium up to the final volume. If you need to add more than 15% of cells, then centrifuge and count again, reducing the cell suspension volume. You should seed 50 µL per well of a 24-well plate or 10 µL per well of a 96-well plate (if seeding for an experiment).

8. Incubate 10 min at 37°C and add the complete medium: 450 µL/well in a 24-well plate and 100 µL/well in a 96-well plate. If you have seeded it in a 96-well plate for an experiment, add 100 µL of water in the wells next to your seeded wells, to avoid medium evaporation.

MM4. CELL TRANSFECTION

Cell transfection is the non-viral process that allows exogenous nucleic acids to enter eukaryotic cells, without viral infection. Polyethylenimine (PEI)-mediated [Polysciences Inc. Ref. 23996] transient transfection method was used. PEI is a high-charge cationic polymer that readily binds highly anionic substrates, such as DNA and other negatively charged molecules and it works as a carrier vector.

1. Dilute 4µl PEI per µg of DNA into 1/10 of the final volume of serum-free DMEM (1ml per plate). Mix gently and incubate 5 min at RT.
2. Add desired µg of DNA, mix and incubate 20 min at RT.
3. Add the solution to the culture plate.
4. Incubate at 37°C O/N.
5. Change the medium to DMEM + 10% FBS.
6. Analyze 48h after transfection.

MM5. CELL INFECTION

Cell lines and PDOs were infected with lentiviruses carrying the appropriate plasmids. LentiCRISPR v2 plasmid [Addgene Ref. 52961] was used for knock-out experiments, pLKO plasmid was used for knock-down experiments (MISSION shRNA Merck **TABLE MM5**) and modified PB-TRE backbone (Addgene, Cat #63800) with T2A-EGFP fragment, which was amplified from PX458 plasmid, were used to generate inducible cell lines.

Table MM5. Vectors used for knock-down virus production.

Vector	Detailed name	Description	Reference
shControl	TRC2 pLKO.5-puro Nonmammalian shRNA Control	Negative control containing a sequence that should not target any known gene, but will engage risk	Sigma-Aldrich Plasmid (SHC202)
shZO-1	TRC1.5 pLKO.1-puro MISSION shRNA	shRNA against the 3UTR of the human TJP1 gene GCAATAAAGCAGCGTTTCTAT	Sigma-Aldrich TRCN0000116252
shZO-1	TRC1.5 pLKO.1-puro MISSION shRNA	shRNA against the CDS of the human TJP1 gene GCGATCTCATAACTTCGTAA	Sigma-Aldrich TRCN0000116253
shZO-1	TRC1.5 pLKO.1-puro MISSION shRNA	shRNA against the CDS of the human TJP1 gene CGACCATTGGAACGCAAGTTT	Sigma-Aldrich TRCN0000116255
shCLDN2	TRC1.5 pLKO.1-puro MISSION shRNA	shRNA against the CDS of the human CLDN2 gene CCAGAGAAATCGCTCCAATA	Sigma-Aldrich TRCN0000108446
shCLDN2	TRC1.5 pLKO.1-puro MISSION shRNA	shRNA against the CDS of the human CLDN2 gene GATGGTGACATCCAGTGCAAT	Sigma-Aldrich TRCN0000108448
shCLDN2	TRC1.5 pLKO.1-puro MISSION shRNA	shRNA against the 3UTR of the human CLDN2 gene AGGACTCAGAGGATCCCTTTG	Sigma-Aldrich TRCN0000415862

MM5.1. Viral production

PEI-mediated transient transfection method (see **MM4**) was used to produce lentiviral particles, using HEK293T cells, as follows:

1. Seed 2.5M cells/plate of HEK293T cell line. Let them grow O/N.
2. Perform cell transfection with PEI.
 - a. Per plate you will need:
 - i. 10 µg of the DNA of interest (non-common DNA).
 - ii. 7.5 µg pCMV-dR8.2 [Addgene Ref. 8455].
 - iii. 3 µg pMD2.G [Addgene Ref. 12259].
 - iv. 1 µg pCS2EA (GFP).
 - v. PEI: 4 µL/µg DNA.
 - vi. 1 mL serum-free DMEM.
 - b. Mix the serum-free DMEM and PEI and incubate for 5 min.
 - c. Add the common plasmids. Then add 1 mL of the mix to previously.
 - d. Incubate for 20 min.
 - e. Add 1 mL to every plate, drop by drop.
3. After one day, change the medium with fresh DMEM+10% FBS.
4. After 24 h more, concentrate the viruses using Lenti-X Concentrator [Clontech Ref. 631232].
 - a. Filtrate the medium of every plate using a 0.45 µm filter and transfer it to 15 mL Falcon.
 - b. Add 1 volume of Lenti-X Concentrator per 3 volumes of supernatant. Mix per inversion.
 - c. Incubate at 4°C O/N.
 - d. Centrifuge at 1500 rcf 45 min at 4°C. Discard the supernatant.
 - e. Resuspend with 700 µL of cold PBS.
 - f. Store at -80°C.

MM5.2 Viral infection

Cell lines and PDOs infection with virus carrying plasmids described above was performed as follows:

Cell lines viral infection

Cell lines infection with viruses carrying plasmids described above was performed as follows:

1. Plate the target cells in a 6-well plate, 24h prior to viral infection.
2. Add virus-containing media or 100-200 μL of concentrated virus plus 10 $\mu\text{g}/\mu\text{L}$ Polybrene [Sigma, Ref. H9268].
3. After 24h refresh the medium.
4. Add selection, if needed, with specific antibiotic, usually Puromycin [Sigma, Ref. P8833] (1.25 $\mu\text{g}/\text{mL}$). Culture the cells with the antibiotic selection for 3-5 days.

PDOs viral infection

PDOs infection with viruses carrying plasmids described above was performed as follows:

1. Use 2-4 wells (24 wells plate) full of spheres.
2. Produce single cells as described in **MM2**.
3. Wash with DF12⁺⁺⁺ and centrifuge at 800 rcf 5 min. Eliminate the supernatant.
4. Resuspend in an adequate volume of complete medium.
5. Count the cells and prepare the mix, for every well: 15.000 cells + complete medium up to 150 μL + 100 μL of PBS (negative control) or viruses + 0.25 μL Polybrene.
6. Transfer 250 μL of the mix to a well of a 24 well-plate.
7. Seal the plate with parafilm and centrifuge it at 600 rcf for 1 h at 32°C.
8. Incubate the plate at 37°C for 5 h.
9. Transfer the content of every well to an eppendorf. Centrifuge at 800 rcf 5 min.
10. Eliminate the supernatant, add 50 μL of matrigel and seed every eppendorf in a different well.
11. Incubate at 37°C 10 min.
12. Add 450 μL of complete medium, slowly against the wall.
13. If the construct carries antibiotic resistance, put the antibiotic selection 3 days after seeding and leave it at least for 1 week.

MM6. CRISPR-Cas9 GENE MODIFICATION

The CRISPR-Cas9 (Clustered Regularly Interspaced Short Palindromic Repeats) is a nuclease system originally used by bacteria as a defence system against external DNA, which recognizes the CRISPR DNA sequences in the genome of the bacteria and Cas9 is the enzyme that uses these sequences to perform a double-strand break (DSB) in the DNA. This system has been optimized to use it in genome editing and knock-out (KO) cell line generation.

To introduce this system in mammalian cell lines, we used the plasmid *lentiCRISPRv2* [Addgene, Ref. 52961], designed by Zhang Lab³⁰². This plasmid has the Cas9 coding sequence and a cloning site to introduce the single-guide RNA (sgRNA), called sgRNA scaffold. The sgRNA of 20 bp is designed as near as TSS of the gene as possible and next to a 3' PAM sequence (NGG), which is used by the Cas9 enzyme to bind to the DNA and perform the DSB. This normally causes changes in the coding frame which leads to aberrant proteins or premature STOP codons, resulting in the impossibility to generate the targeted protein from the altered DNA. The sgRNAs for IKK α /CHUK gene were designed using Benchling [RRID:SCR_013955] (**Table MM6**) and ordered from Sigma, adding restriction enzyme sites for Esp3I [ThermoFisher, Ref. ER0451] (CACCG at 5' in the Forward primer and CAAA at 5' in the reverse one). In order to clone the sgRNAs into the different plasmids:

- Digest and dephosphorylate 5 μ g of plasmid with Esp3I restriction enzyme and FastAP (Alkaline Phosphatase) [ThermoFisher, Ref.EF0651] for 30 min at 37°C.
- Purify the 11 kb fragment and discard the 2 kb fragment using the GFX PCR DNA and Gel Band Purification Kit [GE Healthcare, Ref.28903471].
 - Run all the digestion reaction in 0,7% Agarose gel.
 - Cut the 11 kb band and add 500 μ L of Capture Buffer.
 - Incubate 15-30 min at 60 °C until agarose is completely liquid.
 - Purify the DNA using the GFX columns.
 - Elute in 50 μ L of Elution Buffer Type 6.
- In parallel, phosphorylate and anneal each pair of oligos using the T4 Polynucleotide Kinase (PNK) enzyme.
 - Use 1 μ L of each oligo (stock 100 μ M), 1 μ L of 10x T4 Ligation Buffer [New England Biolabs (NEB)], 6.5 μ L ddH₂O and 0.5 μ L T4 PNK [NEB, Ref. M0201S].
 - Leave 37°C for 30 min.

- 95° for 5 min.
 - Lower the temperature to 25°C at 5°C/min
 - Dilute the phosphorylated and annealed oligos 1/200.
- Ligate the oligos with the digested plasmid
 - 50 ng of digested plasmid, 1 µL of annealed oligos, 1 µL of 10x T4 Ligase Buffer [NEB], ddH2O up to 10 µL, 1 µL of T4 Ligase [NEB, Ref. M0202S].
 - Incubate at RT for 10 min.
 - Transform the ligation reaction into XL1 Blue bacteria (perform all steps under the hood).
 - Thaw bacterial glycerol stock on ice (100 µL).
 - Mix the ligation reaction with the bacteria.
 - Incubate 30 min on ice.
 - Add 1 mL of LB (without antibiotic) and incubate 20-30 min at 37 °C.
 - Seed 200 µL into LB-agar plate supplemented with Ampicillin and incubate at 37 °C O/N.
 - Pick some colonies and extract plasmid DNA.
 - Sequence plasmids by Sanger sequencing using U6-promoter forward primer (upstream of the sgRNA).

Table MM6. sgRNA used for IKKα KO generation.

Target	Specie	Forward	Reverse
CRISPR IKKα sgRNA	Human	CACCGACTTCCTTGATCAACATCTT	AAACAAGATGTTGATCAAGGAAGTC

Using CRISPR-Cas9 technology, viral production and cell infection procedures CaCo-2, HT-29 M6, HCT-116, PDO4, PDO5 and PDO8 IKKα KO cells were obtained. After puromycin selection, the pool of cells was plated as single cells in 96-well plates to isolate clones. Cell sorting was performed on FACS Aria [BD Biosciences]. DAPI staining [Molecular Probes] was used to exclude dead cells. All data were analyzed with FlowJo software [Tree Star]. Regarding cell lines, individual cells were placed in separated wells and allowed to expand up to have enough cells to get cell lysates to isolate genomic DNA and total proteins.

MM7. CELL LYSATES

Lysates from cells were obtained for posterior proteomic analyses. Depending on the cell fractionation desired different lysis buffers and lysis protocols are used:

Soluble/Insoluble extracts: by this method the cytoplasmatic and nuclear soluble proteins and the chromatin insoluble proteins will be separated.

1. Remove the medium and wash cells with PBS. Discard supernatant.
2. Lyse cells with ice-cold ColP lysis buffer (PBS plus 0.5% Triton X-100, 1mM EDTA, 100mM NA-orthovanadate (Na_3VO_4), 0.25mM phenyl-methylsulfonylfluoride (PMSF) and complete protease inhibitor cocktail [Roche, Ref.11836153001]. For adherent cells, scrape cells from the plate and recover the sample in an eppendorf tube.
3. Incubate 20 min on ice.
4. Centrifuge at maximum speed for 10 min at 4°C.
5. Recover the supernatant (soluble extract), keep 5 μL for measuring the protein concentration by Bradford and add the adequate volume of 6X Loading Buffer (50mM Tris-HCl pH 6.8, 1.4M β -mercaptoethanol (β -ME), 2% SDS, 0.1% bromophenol blue, 10% glycerol in H_2O).
6. Resuspend the pellet (chromatin/insoluble extract) in PBS with 1% SDS and sonicate 2-3X for 10 sec with 10% amplitude with a Digital Sonifier [Brandson].
7. Add 6X Loading buffer and boil at 95°C 10 min.
8. Keep the samples at -20°C.

Cytoplasm/Nuclear fractions: by this method proteins from the cytoplasm and the nucleus are separated. Nuclear fraction will include soluble and insoluble proteins.

1. Lyse the cells with ice-cold Buffer A pH 7.9 (10 mM Hydroxyethyl piperazineethanesulfonic acid (HEPES) [Sigma, Ref. H-3375], 1.5 mM MgCl_2 , 10mM KCl, 0.5 mM DTT, 0.05% NP40 and complete protease inhibitor cocktail.
2. Incubate on ice for 20 min.
3. Centrifuge at 1000 rcf for 10 min at 4°C.
4. Recover the supernatant (Cytoplasm fraction) and wash pellet with Buffer A (two times the amount used at the beginning) and centrifuge again.

5. Discard supernatant and resuspend the pellet (nuclear fraction) in PBS plus 1% SDS and sonicate 2-3X 10 sec with 10% amplitude.
6. Add 6X Loading Buffer to the samples and boil at 95°C for 10 min.
7. Keep the samples at -20°C and total proteins.

MM8. WOUND-HEALING ASSAY

The wound healing (or scratch) assay is a technique used to measure two-dimensional cell migration. An artificial gap is generated on a confluent cell monolayer, and movement tracked via microscopy.

1. Seed the cells in a 6-well plate.
2. Grow them at 37°C 5% CO₂ for 24-48h until they reach 100% confluence.
3. Generate a wound in the middle of the well using a tip.
4. The wound closure is monitored by imaging at different time points. Images were obtained with a Zeiss Vert.A1 microscope.
5. Using ImageJ software, measure the distance migrated based on the remaining gap opened.

MM9. TRANSWELL

Transwell assay is a popular cell migration assay that typically measures the net migration of a cell population from an upper chamber across a microporous membrane (8 µm pore size), to a lower chamber filled with a chemoattractant.

1. Generate single cells of the desired population.
2. Seed 1×10^5 cells on the upper chamber of the Transwell [Corning, Ref. 3422] in DMEM 0,1% FBS + treatment if needed.
3. Incubate 4 h at 37°C and 5% CO₂.
4. Add chemoattractant (DMEM 10% FBS) to the lower compartment.
5. Incubate 24-48 h (depending on the cell-line) at 37°C and 5% CO₂.
6. Fix the cells 10 min at -20°C with 500 µL of cold Methanol.
7. Stain the cells 15 min with 500 µL of Crystal violet.
8. Wash 3X with PBS.

9. Scrape the upper chamber membrane zone with a cotton ear swab in order to remove any cells that have not migrated through the structure.
10. Cut the membrane using a scalpel and mount in 4,6-diamino-2-phenylindole Fluoromount-G [Southern Biotech, Ref. 0100-20] onto a slide.
11. Evaluate migration by imaging. Images were obtained with an Olympus BX61 microscope.

MM10. CELL CLUSTERING *IN VITRO*

In vitro assay designed to test the ability of cultured adherent cell lines to generate 3D clusters under non-adherent conditions from single cells.

1. Generate single cells from the desired population.
2. 1×10^6 cells are seeded in a p10 plate (non-treated for cell adhesion) in 10 ml of DMEM + 10% FBS.
3. Incubate 24 h at 37°C and 5% CO₂.
4. Using ImageJ software, evaluate clustering ability by measuring the area of the clusters formed. Images were obtained with a Zeiss Vert.A1 microscope.

MM11. PDOs ADHESION AND MIGRATION ASSAY

PDOs adhesion and migration technique is an assay designed in the laboratory to evaluate the ability of PDOs to first adhere to a substrate and then migrate through the surface. The migration ability is measured by the increase in the area of the PDOs from the starting point (0 h) until the end point (24 or 48 h depending on the PDO) of the experiment.

1. Grow 15 days the PDOs in Matrigel as described in **MM3**.
2. Wash 1X with PBS each well.
3. Resuspend the matrigel with 400 µL of PBS with 1 mL filter tips, pipetting up and down the matrigel with the medium. Transfer it to an eppendorf.
4. Centrifuge at 1100 rcf 5 min.
5. Discard supernatant and resuspend the cell pellet with 400 µL of DMEM + 10% FBS.
6. Seed 100 µL in a 24-well plate (1 original well to 4 experimental wells).
7. Add 400 µL of DMEM 10% FBS + treatment if needed.
8. Incubate 24-48 h (depending on the PDO) at 37°C.

9. Evaluate migration by imaging. Images were obtained with aZeiss Vert.A1 microscope.
10. Using ImageJ software, measure the area increase of PDOs.

MM12. CHROMATIN IMMUNOPRECIPITATION ASSAY (ChIP) AND ChIPseq

ChIP is an assay used for studying the interaction of proteins to specific regions of the chromatin. ChIP and ChIP-seq following standard procedures were performed as follows:

1. Cross-linking reaction

- a. It is recommended to use 1 plate per condition of cells of interest.
- b. Wash with PBS.
- c. Dilute 1/10 cross-link solution (50 mM HEPES pH 8.0, 10 mM NaCl, 1 mM EDTA, 0.5 mM EGTA, 5.55% formaldehyde, in H₂O) to the samples to a final concentration of 0.5% formaldehyde [Sigma Ref.252549] and incubate 10 min gently rocking at RT.
- d. Dilute 1/10 stop solution (1.25 M Glycine, 10 mM Tris-HCl pH 8.0, in H₂O) and incubate 5 min gently rocking at RT.
- e. Centrifuge 5 min at 600 rcf, discard supernatant and wash x2 with cold PBS supplemented with 0.5 mM EDTA and protease inhibitor cocktail.
- f. Centrifuge 5 min at 600 rcf. Discard supernatant.

2. Cell lysis

- a. Add 1 mL of lysis buffer (10 mM Tris-HCl pH 8.0, 0.25% Triton X-100, 10 mM EDTA, 0.5 mM EGTA, 10 mM Na-butyrate, 20 mM β -glycerol-phosphate, 0.1 mM Naorthovanadate, protease inhibitor cocktail, in H₂O) and incubate 20 min on ice.
- b. Centrifuge at 1000 rcf 4°C for 4 min. Discard supernatant.
- c. Add 1.5 mL ice-cold washing buffer, which contains sonication buffer (10 mM Tris-HCl pH 8.0, 0.1 M NaCl, 1 mM EDTA, 0.5 mM EGTA, 10 mM Na-butyrate, 20 mM β -glycerol-phosphate, 0.1 mM Naorthovanadate, protease inhibitor cocktail, in H₂O) plus 0.1 M NaCl.
- d. Centrifuge at 1000 rcf 4°C for 4 min. Discard supernatant.

3. Sonication

- a. Add 800 μ L sonication buffer and 80 μ L of 10% SDS.

- b. Sonicate cells at medium power with a 0.5 interval for 10 min using a Bioruptor Sonicator [Diagenode] and 200 μ L of beads.
- c. Check with a 2% agarose gel if 500 to 1500 bp DNA fragments have been generated.
- d. Centrifuge at maximum speed for 30 min at 20°C. Collect the supernatant (soluble chromatin).

4. SDS wash

- a. Dilute the supernatant 10-fold with sonication buffer to reduce the concentration of SDS to 0.1%.
- b. Concentrate the samples using a Vivaspinn column [Sartorius Ref. VS2032], centrifuging at 1200 rcf at 20°C for 20 min.
- c. Adjust the concentrated chromatin solution to RIPA buffer by adding (for 800 μ L of sample) 9 μ L of 10% deoxycholate (DOC), 25 μ L of 5 M NaCl and 80 μ L of 10% Triton X-100.
- d. Collect 100 μ L, it will be the input sample.

5. Pre-clearing

- a. Pre-clear the chromatin by adding 1% BSA, 1 μ g salmon sperm DNA, unspecific pre-immune IgG (volume and species according to the used antibodies) and 60 μ L of 50:50 protein A/G-sepharose beads [GE Healthcare, Refs. 17-0618-01 and 17-0780-01]. Incubate rotating 2 h at 4°C.
- b. Centrifuge at 240 rcf for 2 min and recover supernatant.

6. Immunoprecipitation

- a. Add 5 μ g of target antibody (see **TABLE MM7**) to 800 μ L of chromatin.
- b. Incubate rotating O/N at 4°C.
- c. Pull down the IgG-chromatin complexes by adding 60 μ L 50:50 protein A/G-sepharose beads. Incubate rotating 2 h at 4°C.
- d. Centrifuge at 100 rcf for 2 min at 4°C. Discard the unbound fraction.

7. Washes: Rotate the samples at 4°C for 1 min, centrifuge at 100 rcf for 1 min and discard the supernatant after each washing step:

- a. 2X with ice-cold RIPA buffer.
- b. 2X with ice-cold RIPA-sodium buffer (RIPA buffer plus 1 M NaCl).

- c. 1X with LiCl buffer (0.25 M LiCl, 1% Nonidet P-40, 1% DOC, 10 mM Tris-HCl pH 8.0, 1 mM EDTA, 1 mM EGTA, 10 mM Na-butyrate, 0.1 mM Na-orthovanadate, in H₂O).
- d. 1X with TE buffer (10 mM Tris- HCl pH 8.0, 1 mM EDTA, in H₂O).

8. Elution and purification of DNA

- a. Resuspend the complexes in 100 µL of Elution buffer (10 mM Tris-HCl pH 7.5, 1% SDS, 30 mM NaCl, 80 mM β-Glycerolphosphate, 10 mM NaButyrate). Incubate rocking 1 h at RT.
- b. Centrifuge at 240 rcf for 2 min and recover supernatants.
- c. Incubate the obtained DNA and inputs O/N at 65°C, for cross-link reversion.
- d. Add 0.5 µg/µL Proteinase K [Roche Ref. 03115828001] and incubate 2 h at 55°C.
- e. Purify the DNA using the MinElute PCR purification Kit [Qiagen Ref. 28006], following the manufacturer's instructions, eluting in 50 µL of H₂O.

ChIP-seq was directly sequenced in the genomics facility of Parc de Recerca Biomèdica de Barcelona (PRBB) using Illumina® HiSeq platform. Raw single-end 50-bp sequences were filtered by quality (Q>30) and length (length>20 bp) with Trim Galore³⁰³. Filtered sequences were aligned against the reference genome (hg38) with Bowtie2³⁰⁴. MACS2 software³⁰⁵ was run first for each replicate using unique alignments (q-value<0.1). Peak annotation was performed with ChIPseeker package³⁰⁶ and peak visualisation was done with Integrative Genomics Viewer (IGV).

Table MM7. Antibodies used for ChIP and ChIP-seq.

Antibody	Company	Reference	Specie
H3K27me3	Millipore	#07-449	Rabbit
FLAG	Sigma-Aldrich	F3165	Mouse

MM13. GST-FUSION PROTEIN AND PULLDOWN ASSAY

The pull-down (PD) assay is an *in vitro* method used to determine a physical interaction between two or more proteins. It is a form of affinity purification, and is similar to immunoprecipitation, except that a "bait" protein is used instead of an antibody.

Bacteria culture:

1. Transformed BL-21 (*E.coli*) bacteria with the desired plasmid that contain a GST (Glutathione S-transferase) -fusion protein.
2. Grow one transformed BL-21 colony in 20 mL LB + Ampicillin (0.1 mg/mL) O/N at 37°C shaking.
3. Dilute 1:10 the culture by adding 180 mL fresh LB + Ampicillin to the 20 mL of O/N culture. Grow 1 h 30 min at 37°C shaking.
4. Collect 100 µL sample before induction to a 1.5 mL tube:
 - a. Centrifuge at 1500 rcf for 5 min. Discard supernatant.
 - b. Resuspend bacteria pellet in 30 µL PBS.
 - c. Add 6 µL of protein loading buffer 6x.
 - d. Boil 10 min at 100°C and spin.
 - e. Store at -20°C.
5. Induce recombinant protein production by adding 200 µL IPTG (Isopropil β-D Thiogalactopyranoside, 0.1mM) [Sigma-Aldrich, Ref. I5502]. Incubate 3h 30min at 37°C shaking.
6. Collect 100µl sample after induction (repeating previous procedure).
7. Transfer bacteria to 50 mL tubes and centrifuge at 1000 rcf for 30 min at 4°C. Pour supernatant off. Store at -20°C.
8. Run pre- and post-induction samples in an acrylamide gel and stain with Coomassie staining (Brilliant Blue G-250 [Sigma, Ref. 6104-58-1], methanol, acetic acid in water).

GST-fusion protein purification:

1. Thaw bacteria pellet on ice.
2. Resuspend in 10 mL prokaryote lysis buffer (20mM Tris HCl pH 7.4, 1M NaCl, 0.2 mM EDTA pH 8.0, 1mM PMSF, 1mM DTT, 1mg/ml lysozyme and protease inhibitor cocktail (Complete Mini) [Roche, Ref. 11836153001]) until completely homogenized.

3. Sonicate 3 times 10 sec 25% amplitude (placing at least for 10 sec on ice between each sonication step). Transfer to 12ml bacteria tube.
4. Centrifuge at 10000 rcf for 30 min at 4°C.
5. Prepare glutathione-sepharose beads (150 µL/condition): wash 2X in 10 mL PBS and 1X in 10mL prokaryote lysis buffer centrifuging at 700 rcf for 2 min at 4°C. Split in 15ml tubes.
6. Pour sonicated bacterial lysate onto previously washed glutathione-sepharose beads in a 15ml tube. Incubate for 3h at 4°C in a rotary shaker.
7. Centrifuge at 700 rcf for 5 min at 4°C and discard supernatant.
8. Wash beads 3X with 5 mL prokaryote lysis buffer, centrifuging each time at 700 rcf for 2 min at 4°C.
9. Store at 4°C in 1 mL prokaryote lysis buffer.
10. Quantify by running samples in SDS-PAGE (polyacrylamide gel electrophoresis) and staining with Coomassie staining.

Pull down assay:

1. Depending on quantification, decide comparable amounts of GST-fusion proteins to use per pull down. When needed, add an excess of previously washed free glutathione-sepharose beads to enable visualization of bead pellet.
2. Lysate cells of interest in a specific lysis buffer.
3. Wash beads 2X with lysis buffer.
4. Block each GST-fusion protein with 50µg/µL BSA O/N at 4°C in a rotary shaker.
5. Split beads carefully in tubes if necessary and centrifuge at 150 rcf for 2 min at 4°C. Discard supernatant.
6. Split cell lysates equally among each pull down.
7. Pull down: incubate 45 min at 4°C in a rotary shaker.
8. Centrifuge at 150 rcf for 2 min at 4°C. Discard supernatant.
9. Wash beads 5X with 500 µL lysis buffer mixing and centrifuging each time at 700 rcf for 2 min at 4°C. Completely aspirate remaining supernatant.
10. Add 80 µL 1x loading buffer. Boil 10 min at 100°C and spin. Store at -20°C.
11. Analyze by Western Blot.

MM14. CO-IMMUNOPRECIPITATION

Co-Immunoprecipitation (Co-IP) assay is a widely used technique to identify physiologically relevant protein-protein interactions by using specific antibodies to indirectly capture proteins that are bound to a specific target protein. The immune complex formed by the specific antibody and target protein is precipitated on a beaded support to which an antibody-binding protein is immobilized (Protein A or G). Then the precipitated proteins are analyzed by WB. Protein-protein interactions can be strengthened by crosslinking the binding partners.

1. Use 3×10^6 cells per condition.
2. Remove the medium and wash cells with PBS.
3. Crosslink proteins by using the reversible crosslinker DSP (1mM) [Thermo scientific, Ref. 22586] for 10 min at RT.
4. Lysate cells with 1 mL ice-cold lysis buffer following the protocol described in **MM7**.
5. From each fraction separate 100 μ L as input.
6. Add 2-5 μ g of specific antibody or unspecific IgG and leave rotating O/N at 4°C.
7. Add 1000 μ L Sepharose A beads [Cytiva, Ref. 17078001] (previously hydrated and blocked with lysis buffer with 10% BSA 100 mg/mL).
8. Incubate 1 h 30 min at 4°C rotating.
9. Centrifuge at 300 rcf for 2 min. Discard the unbound fraction.
10. Wash 5X with lysis buffer, centrifuging between washes at 1200 rpm for 2 min.
11. Add 100 μ L 1x Loading Buffer and boil for 10 min at 95°C. Store at -20°C.

Table MM8. Antibodies used in Co-IP experiments.

Antibody	Company	Reference	Specie
p65	Abcam	ab32536	Rabbit
I κ B α	Cell Signalling	4814	Mouse
p50	Cell Signalling	13586	Rabbit
Ha hybridoma 12CA5	Homemade		Mouse
Mouse IgG	Sigma	I8765	Mouse
Rabbit IgG	Sigma	I8140	Rabbit

MM15. WESTERN BLOT

Western blot (WB) is a common method used in molecular biology to detect specific proteins in cell lysates. In brief, denatured proteins are separated by gel electrophoresis based on their molecular weight and transferred to a membrane where they are detected using specific antibodies. For protein visualization, membranes are incubated with secondary antibodies conjugated to HRP, which catalyze the reaction to generate a light signal.

1. Carry out protein separation using standard SDS-polyacrylamide gel electrophoresis (SDS-PAGE) at 120V.
2. Transfer the proteins to a Polyvinylidene difluoride (PVDF) membrane [Millipore, Ref. IPVH00010] at 400mA for 1h.
3. Block the membrane with 5% non-fat milk in Tris buffered saline plus Tween20 (TBS-T) buffer (50mM Tris-HCl pH 8.0, 150 mM NaCl, 0.05% Tween 20 [VWR, Ref. 8.22184], in H₂O) rocking 1h at RT.
4. Incubate the membrane with the primary antibody in blocking solution (**Table MM9**) rocking O/N at 4°C.
5. Wash 6X in TBS-T buffer rocking 5 min at RT.
6. Incubate the membrane with the secondary antibody (HRP-conjugated) in blocking solution (**Table MM9**) rocking 1h 30 min at RT.
7. Wash 6X in TBS-T buffer rocking 5 min at RT.
8. Peroxidase activity is visualized following the incubation of the membranes with ECL solution [Biological Industries, Ref. 20-500-120] or [GE Healthcare, Ref. RPN2232], which contains a chemiluminescent HRP substrate.
9. The chemiluminescent signal is developed in an autoradiography film [GE Healthcare, Ref. 28906844].

Table MM9. Antibodies used in WB.

Antibody	Company	Reference	Specie	Dilution
IKK α	Abcam	ab32041	Rabbit	1:1000
pIKK α /β (Ser 176/180)	Cell Signalling	#2697	Rabbit	1:1000
IKKβ	Abcam	ab32135	Rabbit	1:1000
ZO-1	Merck-Millipore	AB2272	Rabbit	1:1000
ZO-1	Merck-Millipore	MABT339	Mouse	1:1000
Claudin-2	Cell Signalling	#48120	Rabbit	1:1000
p-ERK1/2 (Thr202/Tyr204)	Cell Signalling	#4370	Rabbit	1:1000
ERK1/2	Cell Signalling	#9102	Rabbit	1:1000
p-BRAF(Ser445)	Cell Signalling	#2696	Rabbit	1:1000
BRAF	Cell Signalling	#14814	Rabbit	1:1000
p-MEK1/2 (Ser217/221)	Cell Signalling	#9154	Rabbit	1:1000
MEK1/2	Santa Cruz	sc-81504	Mouse	1:1000
IκB α	Cell Signalling	#4814	Mouse	1:1000
p65	Abcam	ab32536	Rabbit	1:1000
p50	Cell Signalling	#13586	Rabbit	1:1000
Ha Hybridoma 12CA5	Homemade		Mouse	1:1000
Muc5Ac	Abcam	ab3649	Mouse	1:5000
Lamin B	Santa Cruz	sc-6216	Goat	1:1000
PP1	Santa Cruz	sc-7482	Mouse	1:10000
Histone H3	Abcam	ab1791	Rabbit	1:5000
Tubulin- α	Sigma Aldrich	T6074	Mouse	1:10000
Polyclonal Goat anti-Rabbit Immunoglobulins/HRP	Dako	P0448	Rabbit	1:2000
Polyclonal Rabbit anti-Mouse Immunoglobulins/HRP	Dako	P0260	Mouse	1:2000
Polyclonal Rabbit anti-Goat Immunoglobulins /HRP	Dako	P0449	Goat	1:2000
Veriblot for IP detection Reagent HRP	Abcam	ab131366	Rabbit	1:2000
Monoclonal Rat anti-Mouse Immunoglobulins /HRP	Abcam	ab131368	Mouse	1:2000

MM16. IMMUNOFLUORESCENCE

Immunofluorescence (IF) is employed for the direct visualization of protein expression and localization. Proteins are detected through the use of specific antibodies, and then a secondary antibody with a conjugated fluorochrome is used to detect protein levels. In the case of adherent cell lines, cells are cultured in a glass coverslip, and all the steps are performed in the same coverslip, which is then mounted on a slide in the final step.

1. Seed 1×10^6 cells per condition.
2. Remove the medium and wash with PBS.
3. Fix the cells with Paraformaldehyde (PFA) 4% [Sigma, Ref. P6148, 4% in PBS] for 30 min at 4°C.
4. Wash 3X with PBS rocking 5 min at RT.
5. Permeabilization and blockage with 4% milk and 0.3% Triton X-100 [Surfactant Amps, Thermo Scientific, Ref. 28340] in PBS for at least 1 h at 4°C.
6. Incubate with the appropriate dilutions of primary antibodies in the same permeabilization solution and leave O/N at 4°C (**Table MM10**).
7. Wash 5X with PBS 5 min at RT.
8. Incubate with the secondary antibodies, diluted in PBS plus 4% milk for 1 h 30 min at RT (**Table MM10**).
9. Wash 5X with PBS at RT.
10. Mount in 4,6-diamino-2-phenylindole (DAPI) Fluoromount-G [Southern Biotech, Ref. 0100-20] onto a slide.
11. Images were taken in an SP5 upright confocal microscope [Leica], using the Leica Application Suite software.

Table MM10. Antibodies used in IF/IHC.

Antibody	Company	Reference	Specie	Dilution
Ki-67	Novocastra	NCL-Ki67-MM1	Mouse	1:500
IKK α	Abcam	ab32041	Rabbit	1:500
pIKK α / β (Ser 176/180)	Cell Signalling	#2697	Rabbit	1:500
ZO-1	Millipore	AB2272	Rabbit	1:300
	Millipore	MABT339	Mouse	1:300
	Sigma-Aldrich	HPA001636	Rabbit	1:100
CLDN2	Invitrogen	516100	Rabbit	1:100
	Cell Signalling	#28530	Rabbit	1:100
pERK (Thr202/Tyr204)	Cell Signalling	#4370S	Rabbit	1:300
SMA	Sigma-Aldrich	A2547	Mouse	1:400
CD31	Abcam	ab231436	Rabbit	1:100
Alexa Fluor 488 donkey-anti-rabbit IgG	Invitrogen	A21206	Donkey anti-rabbit	1:1000
Alexa Fluor 488 donkey-anti-mouse IgG	Invitrogen	A21202	Donkey anti-mouse	1:1000
Alexa Fluor 647 donkey-anti-rabbit IgG	Invitrogen	A31573	Donkey anti-rabbit	1:1000
Alexa Fluor 647 donkey-anti-mouse IgG	Invitrogen	A31571	Donkey anti-mouse	1:1000

MM17. RNA ISOLATION

Adherent cell lines: total RNA was extracted with the RNeasy Mini Kit [Qiagen, Ref. 74106], following manufacturer's instructions:

1. Lysate cells with 350 μ L RLT buffer plus 3.5 μ L β -mercaptoethanol.
2. Homogenise with a 21G needle.
3. Add 1 volume of 70% ethanol and transfer it to a RNeasy MinElute spin column.
4. Centrifuge at 8000 rcf for 20 sec.
5. Add 350 μ L of RW1 Buffer. Centrifuge at 8000 rcf for 20 sec.
6. Add 10 μ L of diluted DNase I. Incubate 15 min at RT.
7. Add 350 μ L of RW1 Buffer. Centrifuge at 8000 rcf for 20 sec.
8. Add 500 μ L of RPE Buffer. Centrifuge at 8000 rcf for 2 min.

9. Centrifuge at 20000 rcf for 5 min and discard the supernatant.
10. For elution, add 15 μ L of H₂O. Centrifuge at 20000 rcf for 1 min.
11. RNA concentration is quantified with a NanoDrop spectrophotometer [Thermo Scientific].

PDOs: total RNA was extracted with the RNeasy Micro Kit [Qiagen, Ref. 74004], following manufacturer's instructions:

1. Use 2-4 wells (24-wells plate) full of spheres
2. Resuspend wells with 400 μ L of PBS, 2 wells per eppendorf.
3. Produce single cells as described in **MM3**.
4. Centrifuge at 600 rcf for 5 min and discard supernatant.
5. Prepare 1 mL of RLT buffer plus 10 μ L of β -ME and add 350 μ L to PDOs.
6. Homogenise with a 21 G needle.
7. Add 1 volume of 70% ethanol and transfer it to a RNeasy MinElute spin column.
8. Centrifuge at 8000 rcf for 20 sec.
9. Add 350 μ L of RW1 Buffer. Centrifuge at 8000 rcf for 20 sec.
10. Add 10 μ L of diluted DNase I. Incubate for 15 min at RT.
11. Add 350 μ L of RW1 Buffer. Centrifuge at 8000 rcf for 20 sec.
12. Add 500 μ L of RPE Buffer. Centrifuge at 8000 rcf for 20 sec.
13. Add 500 μ L of 80% ethanol. Centrifuge at 8000 rcf for 2 min.
14. Centrifuge at 20.000 rcf for 5 min and discard supernatant.
15. For elution, add 15 μ L of H₂O. Centrifuge at 20.000 rcf for 1 min.
16. RNA concentration is quantified with a NanoDrop spectrophotometer [Thermo Scientific].

MM18. RT-qPCR

Quantitative real time polymerase chain reaction (RT-qPCR) is a technique used to amplify and simultaneously quantify specific DNA regions. First, complementary DNA (cDNA) has to be synthesised from RNA sample by retrotranscription, using the Transcriptor First Strand cDNA Synthesis Kit [Roche, Ref. 04897030001].

1. Mix 2 µg of extracted RNA (**see MM12**) with H₂O up to 11 µL.
2. Add 2 µL of anchored-oligo(dT)18 primer.
3. Denature the template-primer mixture by heating the tube for 10 min at 65°C in a block cycler with a heated lid. This step ensures denaturation of RNA secondary structures.
4. Cool the tube on ice immediately.
5. Add 7 µL of a mix containing (x1 reaction): 4 µL of buffer, 2 µL of dNTPs, 0.5 µL RNase inhibitor and 0.5 µL Transcriptor Reverse Transcriptase.
6. Incubate at 30 min at 55°C in the block cycler.
7. Inactivate Transcriptor Reverse Transcriptase by heating to 85°C for 5 min and keep at 4°C.
8. Dilute the sample 1:20 with H₂O and store at -20°C.

After cDNA synthesis, RT-qPCR was performed in the LightCycler480 system, using a SYBR Green I Master Kit [Roche, Ref. 04887352001]. Samples were normalised to the mean expression of the housekeeping genes GAPDH and TBP. Primers used are listed in **Table MM11**.

1. Prepare the mix containing (x1 reaction): 5 µL of SYBR Green I Master Kit, 2 µL of H₂O, 0.5 µL (10 µM) of forward primer and 0.5 µL of reverse primer (10 µM).
2. Add 8 µL of the mix to a 384-well plate.
3. Add 2 µL of diluted cDNA.
4. Seal the plate and centrifuge at 150 rcf for 1 min.
5. Perform the RT-qPCR in LightCycler 480 machine [Roche].

Table MM11. Primers used for RT-qPCR.

Target	Specie	Forward	Reverse
TBP	Human	TGCCCCGAAACGCCGAATATAATC	GTCTGGACTGTTCTTCACTCTTGG
GAPDH	Human	GTCATCCCTGAGCTGAACG	CTCCTTGGAGGCCATGTG
ZO-1	Human	CCACCCTGAGTCTGGTGAGT	AAGGCCTTTTCACTGACGAA
CLDN2	Human	ATTCCTCAGGCCCTTTGACT	TACACACTGCCTTCCCTTCC
CHUK	Human	ATGTGTTTTTCCCCATGAA	AGGCAAATGTGTCGTGATGA
Lgr5	Human	ATGGTCGCTCTCATCTTGCTC	ATATTCTCCAGGTCTCCCTTGTC
E-cadherin	Human	TGCCCAGAAAATGAAAAAGG	GTGTATGTGGCAATGCGTTC
DUSP1	Human	CTGCCTTGATCAACGTCTCA	ACCCTTCCTCCAGCATTCTT
DUSP3	Human	TAAAAACCCCAACATTTGGA	CTTCCCTGCTTGTCTTCTGG
DUSP5	Human	TCCTGCTAAACTGGGATGG	ACCTACCCTGAGGTCCGTCT
IκBα	Human	AAATACCCCCCTACACCTTGCC	CATCAGCCCCACACTTCAACAG
A20	Human	GAGAGGCGGCAAAAGAATCAAAAC	TGAACAGAAAAGGGCTGGGTGC

MM19. TUMOR INITIATING CAPACITY *IN VITRO*

Tumor initiating capacity (TIC) *in vitro* assay is a technique used to measure the ability of tumoral cells to generate 3D tumoral structures from single cells.

- 300 cells (cell lines or PDOs) are plated in 96-well plates in 10μL Matrigel with 100 μL of complete medium.
- After 7 days in culture, the number of 3D structures in each well was counted, photographs were taken for diameter determination with ImageJ and cell viability was measured using CellTiter-Glo 3D Cell Viability Assay [Promega, Ref. G7571]:
 - Equilibrate the plate and CellTiter Glo Reagent at RT for approximately 40-45 min.
 - Add 15 μL of CellTiter-Glo Reagent to every well.
 - Mix contents for 5 min on an orbital shaker to induce cell lysis.
 - Allow the plate to incubate at room temperature for 25 min.
 - Record luminescence (measurement of 1 second per well) in an Orion II multiplate luminometer.

MM20. CRYSTAL VIOLET STAINING

Crystal violet staining is a widely used method for cell colony visualization. The amount of crystal violet staining is directly proportional to the cell biomass that is attached to the plate. It is a rapid and reliable assay which relies on the detachment of adherent cells from cell culture plates during cell death.

1. Gently aspirate supernatant of cells in 24-well plates.
2. Rinse once with 1 mL PBS
3. Fix with ice-cold 100% methanol for 10 min (keep in freezer)
4. Gently cover the cells with 0.5% crystal violet [Sigma-Aldrich, Ref. C0775] solution in 25% methanol. Incubate for 15 min at RT.
5. Remove the crystal violet and wash cells with water several times.
6. Allow the cells to dry at RT.

MM21. PARAFFIN EMBEDDING OF TUMOR SAMPLES

For long-term conservation of samples and to perform immunohistochemistry and immunofluorescence analysis, samples have to be paraffin embedded.

1. Collect the tissues from the organs of interest in ice-cold PBS and place them in a cassette.
2. Fix in 4% PFA rocking O/N at RT. Wash 2X in PBS 15 min rocking at RT.
3. Wash in 25% and 50% ethanol rocking 15 min each at RT.
4. Wash in 75% ethanol rocking O/N at 4°C.
5. Wash in 90% ethanol rocking 30 min at RT.
6. Wash 3X in absolute ethanol and xylene rocking 1 h each at RT.
7. Place tissue in embedding moulds and incubate in paraffin 1 h at 65°C.
8. Change paraffin and incubate O/N at 65°C.
9. Change paraffin and cool down at -20°C.
10. Unmould the block and store it at 4°C.

MM22. IMMUNOHISTOCHEMISTRY

Immunohistochemistry (IHC) combines histological, immunological and biochemical techniques for the identification of specific tissue components by means of a specific antigen/antibody reaction tagged (directly or most commonly indirectly) with a visible label. IHC enables the visualization of the distribution and localization of specific cellular components within cells and in the proper tissue context. The starting material is usually 2.5 or 4 µm paraffin sections.

1. Dewax the slides heating them at 65°C, for 1 h or O/N if they have been re-paraffined, to melt all the paraffin.
2. Rehydration battery: xylene I and II 15 min each, absolute ethanol I and II, 96%, 70% and 50% ethanol 10 min each and distilled water for 10 min.
3. Antigen retrieval: citrate-based antigen retrieval (sodium citrate pH 6.0) was used, at 100°C for 20 min with pressure. Then, retain in buffer 1 h allowing cooling down.
4. Wash 3X with PBS 5 min at RT.
5. Blockage of endogenous peroxidase activity with 1.5% H₂O₂ [Sigma, Ref. H1009] for 20 min at RT.
6. Wash 3X with PBS rocking 5 min at RT.
7. Permeabilization and blockage with 1% BSA in PBS for 1 h at RT.
8. Incubate the appropriate dilutions of the primary antibodies in PBS containing 1% BSA, O/N at 4°C (**Table MM10**).
9. Wash 3X with PBS 5 min at RT.
10. Incubate with the secondary antibodies diluted in BSA 1% in PBS, using the Envision+ System HRP Labelled Polymer anti-Rabbit [Dako, Ref. K4003] or anti-Mouse [Dako, Ref. K4001] for 90 min at RT.

In order to achieve optimal visualization of the protein, an amplification cascade reaction may be required:

- a. Incubate with the secondary antibody Polyclonal Goat Anti-Rabbit Immunoglobulins/Biotinylated [Dako, Ref. E0432] for 1 h at RT.
 - b. Wash 3X with PBS 5 min at RT.
 - c. Incubate with Streptavidin-Peroxidase Polymer, Ultrasensitive [Merck, Ref. S2438] for 1h at RT.
11. Wash 3X with PBS 5 min at RT.

12. Develop the samples with 3,3'-diaminobenzidine (DAB) [Dako, Ref. K3468] or EnVision FLEX HRP Magenta Substrate Chromogen System (Dako Omnis) [Dako, Ref. GV925] in the case of double IHC, for the appropriate time.
13. Wash 3X in PBS 5 min at RT and counterstain with haematoxylin [Merck, Ref. 1092530500] and mount with DPX [Merck, Ref. 1.01979.0500] or Aquatex [Merck, Ref. 108562] if Magenta developing is used.
14. Images were obtained with an Olympus BX61 microscope.

MM23. HAEMATOXYLIN AND EOSIN STAINING

Haematoxylin and eosin (H&E) staining is widely used for correct visualisation of cell structures. Cell nucleus is stained by haematoxylin (dark purple) and cytoplasm by eosin (pink), although other cell structures can also be stained, such as components from the extracellular matrix. With this objective, tissue paraffin embedded samples were sectioned appropriately and stained with HE.

1. Dewax the slides, heating them at 65°C, for 1 h or O/N if they have been re-paraffined, to melt all the paraffin.
2. Rehydration battery: xylene I and II 15 min each, absolute ethanol I and II, 96%, 70% and 50% ethanol 10 min each and distilled water for 10 min.
3. Staining with haematoxylin for 30 sec [Merck, Ref. 1092530500]. Wash with tap water for 5 min.
4. 80% ethanol 0.15% HCl for 30 sec. Wash with distilled water for 30 sec.
5. Ammonia water [NH₃(aq)] 0.3% for 30 sec. Wash with distilled water for 30 sec.
6. 96% ethanol for 5 min.
7. Counterstaining with eosin for 3 sec [Bio-Optica, Ref. 05-10003/L].
8. Wash x3 with absolute ethanol 1 min each.
9. Dehydration battery: absolute ethanol I and II 5 min each and xylene I and II 5 min each.
10. Mount in DPX [Merck, Ref. 1.01979.0500].
11. Images were obtained with an Olympus BX61 microscope.

MM24. ANIMAL STUDIES

Animal models or model organisms are widely used in biomedical research to investigate human diseases or biological processes. The classical vertebrate model is the house mouse (*Mus musculus*), which shares around 95% of its genome with humans. Mice can be genetically manipulated to mimic human diseases or conditions and can be inbred to maintain uniformity within strains, allowing for more accurate and repeatable experiments. They have an accelerated lifespan, and an entire life cycle can be studied within 2-3 years. They are cost-effective and efficient research tool: they are small, reproduce quickly and are relatively easy to house and transport. In all procedures, animals were kept under pathogen-free conditions and all animal work was conducted according to the guidelines from the Animal Care Committee at the Generalitat de Catalunya. These studies were approved by the Committee for Animal Experimentation at the Institute of Biomedical Research of Bellvitge (Barcelona) and were carried out within the framework of procedure 11973 of Dr. Alberto Villanueva, approved by the Generalitat de Catalunya. Sacrifice of adult mice was done using exposure to CO₂. For intrasplenic injection experiments, nude mice were anaesthetized using isoflurane inhalation and then secured in right lateral recumbency. The skin beneath the left costal margin was disinfected, layers were clipped incrementally up to the peritoneum, and the tail of the spleen was exposed and injected with PDO cells resuspended in 50 µL of saline serum. Subsequently, the abdominal cavity was closed with surgical staples. 24 hours later, a splenectomy is performed to minimize the possibility of local growth and peritoneal dissemination. After 2 months, mice were euthanized, the livers were excised and fixed for subsequent H&E staining and IHC analysis. Vemurafenib (50mg/kg) and selumetinib (50mg/kg) were administered by oral gavage following a 5 day on/2 day off schedule.

MM25. BULK RNA-seq DATA ANALYSIS

Libraries for both primary tumor and metastasis were simultaneously prepared and sequenced using Illumina HiSeq2500 platform (50bp paired-end reads). Samples sequencing depth ranged between 24M and 41M reads (average 31M reads) per sample.

Colorectal Tumoroid (primary tumor) samples

Quality control was performed on raw data with FASTQC tool (v0.11.9). Raw reads were trimmed to remove adapters presence with Trimgalore (v0.6.6)³⁰⁷. Default parameters were used except for a minimum quality of 15 (Phred score) and an adapter removal stringency of 3bp overlap. Trimmed

reads were aligned to reference genome with STAR aligner tool (v2.7.8). STAR was executed with default parameters except for the number of allowed mismatches which was set to 1. Required genome index was built with corresponding hg38 gtf and fasta files retrieved from Ensembl (<http://ftp.ensembl.org/pub/release-106/>). Obtained BAM files with uniquely mapped reads were considered for further analysis. Raw gene expression was quantified using featureCounts tool from subRead software (v2.0.1) with exon as feature³⁰⁸. Obtained raw counts matrix was imported into R Statistical Software environment (v4.3.1) for downstream analysis. Raw expression matrix included 61,552 genes per 4 samples in total. Experimental design considered two existing conditions: 2xIKK α WT and 2xIKK α KO. Prior to statistical analysis, those genes with less than 5 raw counts across the 4 samples under test were removed. After pre-filtering, 20,826 genes were available for testing. For visualization purposes, counts were normalized by variance-stabilizing transformation method as implemented in DESeq2 R package³⁰⁹ (v1.40.2). Differential expression analysis (DEA) was conducted with DESeq2. Fitted statistical model included sample condition as covariable with WT as the reference. Primary tumor samples were separately tested from metastasis samples since the latter showed larger within-group variability than the primary ones. Obtained log₂ fold change values were shrunk with apegglm shrinkage estimator R package (v1.22.1)³¹⁰. Raw p-values were adjusted for multiple testing using the Benjamini-Hochberg False Discovery Rate (FDR) (Benjamini & Hochberg, 1995). Differentially Expressed Genes (DEGs) between KO and WT samples were called with adjusted p-values (FDR) < 0.05 and shrunk $|\log_2 \text{Fold change}| > 1$.

Hepatic Metastases derived from PDX samples

Same general methodology as in previous paragraph was applied for the hepatic metastasis derived samples except for the reference genome. Since these samples were derived from PDX, an in-silico combine human-mouse reference genome was used instead as described by other authors³¹¹. Specifically, hg38 and mm39, both retrieved from Ensembl (release 106) were combined. After alignment, only those reads mapping to human assembly were considered for further analysis. Raw expression matrix included 61,552 genes per 6 samples in total (3xIKK α met-WT and 3xIKK α met-KO). This matrix was combined with raw counts from primary tumor samples for conducting differential expression analysis. Since both types of samples were simultaneously processed, no technical batch effect was expected. Experimental design considered one variable with four levels from the combination of samples origin and condition, specifically, 2xIKK α prim-WT, 2xIKK α KO, 3xIKK α met-WT and 3xIKK α met-KO. Prior to statistical analysis, those genes with less than 5 raw

counts across the 10 samples under test were removed. After pre-filtering, 23,036 genes were available for testing. Following contrasts were explored: met-KO vs prim-KO, met-WT vs prim-WT and met-KO vs prim-WT.

MM26. SINGLE CELL RNA-seq DATA ANALYSIS

Data pre-processing

10x sequencing raw reads were demultiplexed and aligned with 10x Genomics CellRanger v7.2.0 (cellranger count) under default parameters which includes intronic reads³¹². Sequences were aligned against the mouse pre-built reference transcriptome *refdata-gex-GRCh38-2020-A* provided by 10x Genomics. Features, barcodes and expression matrices were separately obtained per sample: 1xIKK α WT, 1xIKK α KO and 1xIKK α KO + inhibited CLDN2. Respectively for WT, KO and KO+inh CLDN2 conditions, (i) the recovered cells were 7,746, 5,367 and 6,751 cells, (ii) the median genes per cell was 6,160, 6,756 and 6,353 genes and, (iii) the mean reads per cell was 51,439, 77,820 and 60,624 reads.

Quality control

Generated filtered matrices were imported and merged into R (v4.3.1) using Seurat package (v5.0.0)³¹³. A Seurat object with a total of 36,601 genes and 19,864 cells was obtained. Doublets were separately detected by sample with scDblFinder package (v1.14.0)³¹⁴. For this purpose, random and cluster-based approaches, implemented in the same package, were used. Additionally, the latter was considered with the clusters identified by CellRanger software (graph-based). Those cells detected as doublets by two out of the three cases were finally labelled as doublets and removed from the dataset. Next, cells were filtered based on the number of genes removing those with less than 500 or more than 10k genes. Cells with more than 15% of mitochondrial gene content or with less than 3500 counts were also discarded. Genes not present in at least 10 cells were filtered out. Ribosomal genes were as well discarded. After quality control, a Seurat object with a total of 25,642 genes and 14,074 cells was used for downstream analysis.

Samples Integration and Clustering

Samples were normalized using the SCTransform function regressing the mitochondrial content out and with the method glmGamPoi (package v1.12.2). After normalization, samples were integrated with the anchor-based CCA integration method implemented in Seurat. The integrated dataset was

used for downstream analysis. For dimensionality reduction and visualization, runPCA and runUMAP functions were executed considering 37 principal components which corresponded to a cumulative captured data variance > 85%. Cell phase score was computed with CellCycleScoring function and available S and G2M genes in Seurat package. Clustering analysis was performed with FindNeighbors (37 dimensions) and FindClusters (resolution 0.3) obtaining a total of 10 clusters. Cluster representative genes were obtained from SCT assay with FindConservedMarkers function (adjusted p-value < 0.05, $|\log FC| > 0.5$, cell percentage cluster of interest > 0.25). Additionally, from SCT assay, differentially expressed genes were obtained per cluster and testing KO or KO+inh CLDN2 against WT. For this purpose, FindMarkers function was used (adjusted p-value < 0.05, $\log FC > 0.5$, cell percentage > 0.25). Normalized expression values were imputed and smoothed with MAGIC algorithm through Rmagic package (v2.0.3.999)³¹⁵.

EpiHR and Tight Junction signatures scoring

Score values were computed for 'Tight Junction Organization' (GO:0120193) GO BP term and the High-Relapse (EpiHR) signature of Cañellas-Socias et al. For this purpose, UCell R package was used (v2.4.0)³¹⁶ based on expression values from MAGIC. Additionally, per signature, cells were classified as 'Low' or 'High' based on their obtained UCell scores (High > Q3, Low for the rest of cases). Cutoff was independently obtained per condition.

MM27. CRC PATIENTS METACOHORT

To generate a CRC patients metacohort³¹⁷, raw gene expression data was downloaded (19th March 2024) from different colon cancer datasets with following GEO series: GSE14333, GSE143985, GSE17536, GSE17537, GSE33114, GSE37892, GSE38832, GSE39582, GSE92921. All selected datasets were using HG-U133_Plus_2 Array platform from Affymetrix. For this purpose, the *getGEOSuppFiles* function from the *GEOquery* package (v2.70.0) was used³¹⁸. A total of 1660 samples was retrieved. Clinical data was extracted from the series matrix found in each dataset and merged into a phenotype data file. Following clinical information, if existing, was included: (i) patient age and gender, (ii) BRAF, KRAS and TP53 mutations, (iii) tumor-related information (stage and location), (iv) treatment information (surgery, radiotherapy and chemotherapy), (v) survival data (Disease-Free Survival, Overall Survival and Disease-Specific Survival) and (vi) other features (ethnicity, grade and risk group). We excluded duplicated samples among datasets and filtered out samples without Disease-Free Survival information. A final set with 1118 samples was available. Corresponding .CEL

files were imported to R environment (v4.3.3) using the *ReadAffy* function from the *Affy* package (v1.80.0)³¹⁹. Probe intensities were background corrected and normalized with the *frozen Robust Multiarray Analysis* (fRMA) algorithm from the *frma* package (v1.54.0) per original dataset³²⁰. Normalized datasets were aggregated into one metacohort. Remaining batch effect due to original datasets was removed with the *ComBat* function from the *sva* package (v3.50.0)³²¹. Finally, gene annotation was added to each probe identifier by means of *hgu133plus2.db* package (v3.13.0). Additionally, Jetset scores were added. using the *jscores* function from the *jetset* package (v3.4.0)³²². Required custom R scripts together with the final CRC patients metacohort are available at [https://github.com/BigaSpinosoLab/ RESOURCES_CRC_metacohort_generation](https://github.com/BigaSpinosoLab/RESOURCES_CRC_metacohort_generation).

Survival analysis over CRC patients metacohort

Association of the gene expression levels with relapse was assessed using Kaplan-Meier curve estimates in the custom CRC patients metacohort. For this purpose, only those patients in Stage II or III were considered. Patients were classified into two subgroups, 'High' or 'Low', based on the expression of specific genes (IKK α or ZO-1) of the mean expression of those genes within a signature as cluster marker genes from scRNA-seq data. Cutoff point was set to Q3. Right-censoring was applied for saturating survival curves up to 60 months. A Log-rank test was applied to assess statistical significance between both subgroups. All the survival analyses and graphs were performed with the *survival* (v.3.5-5)³²³ and *survminer* (v0.4.9, <https://github.com/kassambara/survminer>) R packages. A p-value<0.05 was considered statistically significant.

Mouse scRNA-seq data exploration from Cañellas-Socias et al. 2022

The AKTP MTOs scRNA-seq dataset from Cañellas-Socias et al.⁷² was downloaded from Synapse (<https://www.synapse.org/#!Synapse:syn35000645>). An already preprocessed .RData file was retrieved referring to all stages. This included merged data from four Smart-Seq2 experiments, each corresponding to: primary tumor, micro-, small- and macro-metastases. Data was imported into R Statistical Software (v.4.3.1) by means of Seurat R package (v5.0.0)³¹³. MAGIC SCT assay (non-integrated data) was used for visualization purpose. Specifically, the expression levels from genes annotated to 'Tight Junction Organization' (GO:0120193) GO BP term was explored³²⁴. Heatmap was generated with ComplexHeatmap R package (v2.16.0)³²⁵.

Data availability

Single-cell and bulk RNA-seq datasets generated in this study have been deposited in NCBI Gene Expression Omnibus (GEO) repository under GEO SuperSeries accession no. GSE274368, composed in three SubSeries GSE274321 (10x scRNA-seq data), GSE274325 (bulk RNA-seq Primary Tumor) and GSE274326 (bulk RNA-seq Hepatic Metastasis derived from PDX).

Code availability

Scripts that have been used to process the in house scRNA-seq and bulk RNA-seq datasets are deposited in Github repository: [https://github.com/BigaSpinosaLab/ PAPER_IKKα_metastasis_modulator_CRC_Tight_Junctions](https://github.com/BigaSpinosaLab/PAPER_IKKα_metastasis_modulator_CRC_Tight_Junctions)

MM28. QUANTIFICATION AND STATISTICAL ANALYSIS

Statistical parameters, including number of events quantified, standard deviation and statistical significance, are reported in the figures and in the figure legends. GraphPad Prism 9 software was used for statistical analysis and p -value <0.05 is considered significant (**** p -value <0.0001 , *** p -value <0.001 , ** p -value <0.01 and n.s. p -value > 0.05). Statistical significance among groups was determined by Student's t-test (data fitting normal distribution) or Mann Whitney U test (data not fitting normal distribution) for two-group comparison or one-way ANOVA with Tukey's correction for multiple comparison testing.

RESULTS

RESULTS: PART I

R1. Regulation of the tight junction proteins ZO-1 and CLDN2 by the IKK α kinase.

Taking advantage of phosphor-proteomic analysis data previously performed in the laboratory, we were able to identify ZO-1 and occludin (**Table R1**) as potential new direct phosphorylation targets²⁴⁹ of the IKK α kinase (raw data available at PRIDE: PXD008932).

Table R1. Tight junction elements identified as putative direct phosphorylation targets of IKK α . Table indicating the residues of ZO-1 and OCLN that were identified as differentially phosphorylated by MS analysis of CRC cell lysates from the indicated conditions. We considered these residues as candidates to be phosphorylated by IKK α or kinases downstream of IKK α .

Annotated Sequence	Protein	Positions	Log2 FC WT (UV) vs WT	Log2 FC KD(UV) vs KD
[R].SVASSQPAKPTK.[V]	ZO-1	[175-186]	0.55	-0.59
[K].SREDLSAQPVQTK.[F]	ZO-1	[617-629]	2.41	0.38
[K].AEASSPVYPYLPETNPASSTSAVNHNVNLTNVR.[L]	ZO-1	[923-955]	2.37	NA
[K].STPVPEVVQELPLTSPVDDFRQPR.[Y]	OCLN	[344-367]	100	NA
[R].YSSGGNFETPSK.[R]	OCLN	[368-379]	1.35	0.52

Our results indicated that ZO-1 was differentially phosphorylated in cell lacking IKK α . We investigated whether IKK α activity affected tight junction properties. By immunofluorescence analysis of ZO-1 in Caco-2 CRC colonies, we detected ZO-1 at the membranes localized between adjacent cells, as expected, and in agreement with tight junctions function. However, in IKK α KO cells (**Figure R1A**) ZO-1 protein was also present in the cell membranes at the edge of colonies, where cell-cell contact elements are normally absent. Abrogation of IKK α activity by AZ628^{249,326} (**Figure R1B**) imposed a change in ZO-1 distribution comparable to IKK α KO (**Figure R1C**).

We also observed changes in the ZO-1 distribution pattern of HCT-116 and HT-29 M6 CRC cells. Specifically, HCT-116 AZ628-treated cells showed aberrant tight junction-like structures were found between adjacent cells (**Figure R1C**). In HT-29 M6 AZ628-treated cells, ZO-1 positive junctions were less restricted to the center of the colonies compared to untreated cells (**Figure R1D**). The efficiency of IKK α inhibition by AZ628 was confirmed by WB using the antibody against p-IKK α / β (**Figure R1E**).

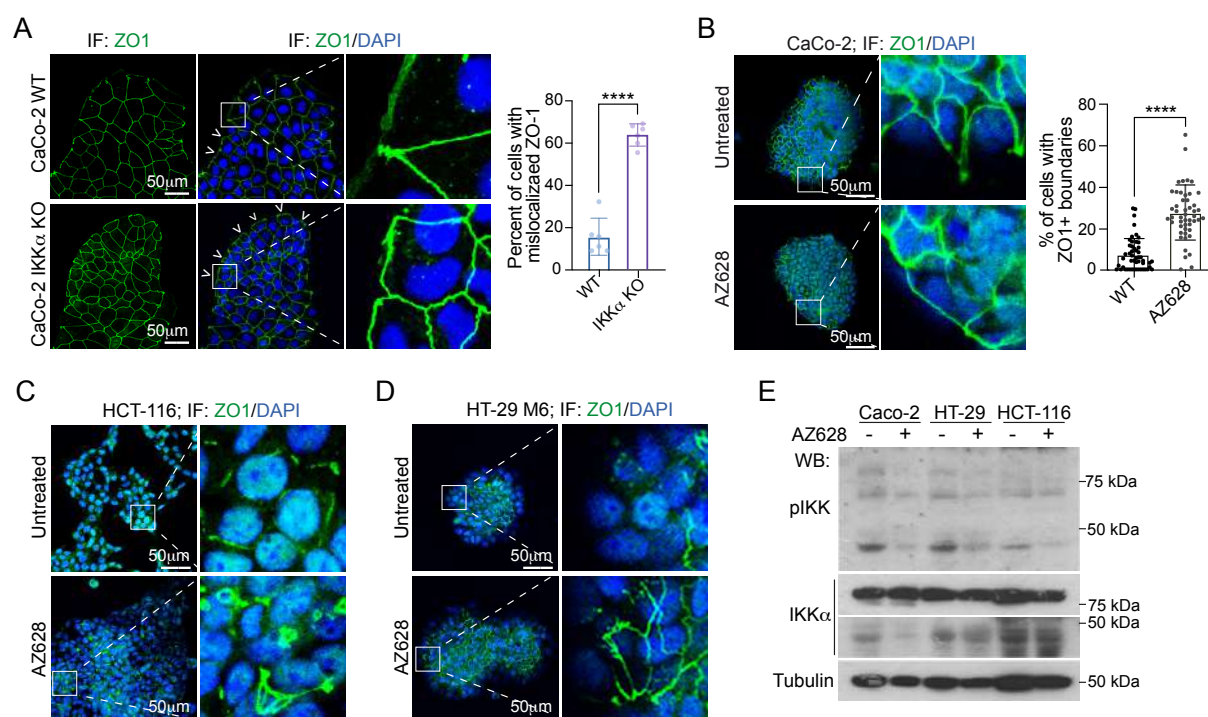


Figure R1. ZO-1 distribution is altered, in CRC cell lines, in response to IKK α depletion, either genetically or pharmacologically. **(A-D)** Representative images of immunofluorescence staining of ZO-1 in different cell types, WT and IKK α KO CaCo-2 cells untreated **(A)** or AZ628-treated (10 μ M O/N) CaCo-2 **(B)**, HCT-116 **(C)** and HT-29 M6 **(D)** cells. **(E)** Western blot analysis of the indicated cell lines untreated or treated with the BRAF inhibitor AZ628.

Altered ZO-1 distribution after IKK α KO was similarly observed in CRC patient-derived organoid (PDO) cells **(Figure R2)**.

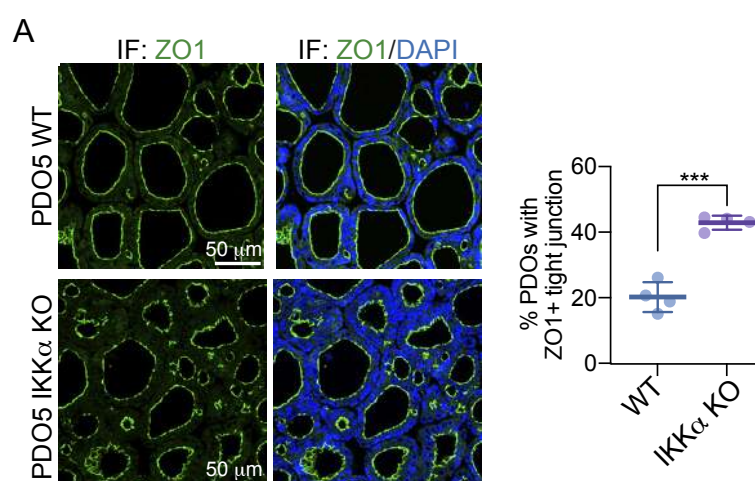


Figure R2. ZO-1 distribution is altered in IKK α KO CRC PDOs. **(A)** Representative images of immunofluorescence staining of ZO-1 in PDO5 WT and IKK α KO cells and quantification.

To investigate whether differences in ZO-1 distribution were associated with changes in ZO-1 protein levels, we performed western blot (WB) analysis of WT and IKK α KO cells. IKK α depletion led to an increase in ZO-1 protein levels in the different cellular systems tested (**Figure R3A**). However, increase in ZO-1 protein was not consistently associated with an increase in RNA levels, as determined by qPCR analysis (**Figure R3B**), suggestive of higher protein stability.

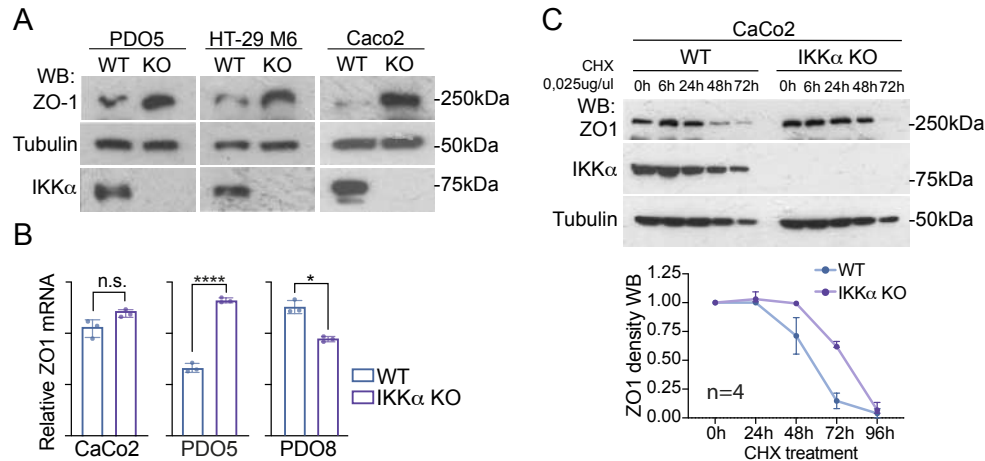


Figure R3. IKK α modulates ZO-1 levels at protein level. (A) WB analysis of ZO-1 levels in the indicated WT and IKK α KO cells. **(B)** RT-qPCR analysis of TJP1/ZO-1 in WT and IKK α KO cell lines and PDOs. **(C)** WB analysis of CaCo-2 cells treated with cycloheximide (0,025 μ g/ μ L) and collected at the indicated time points. Densitometric quantification of the ZO-1 band from 3 independent experiments performed.

Treatment of CaCo-2 cells with the protein synthesis inhibitor cycloheximide followed by western blot analysis revealed an increased half-life of ZO-1 protein after IKK α depletion (**Figure R3C**), providing further evidence of the role of IKK α in regulating ZO-1 protein. These results, together with the altered distribution of ZO-1 determined by IF, suggest that IKK α -dependent phosphorylation may favor ZO-1 destabilization at specific cellular domains. Consistent with this possibility, both IKK α (**Figure R4A**) and active p-IKK (**Figure R4B**) co-localized with the residual ZO-1 detected at the cell membranes in the periphery of IKK α WT CaCo-2 colonies.

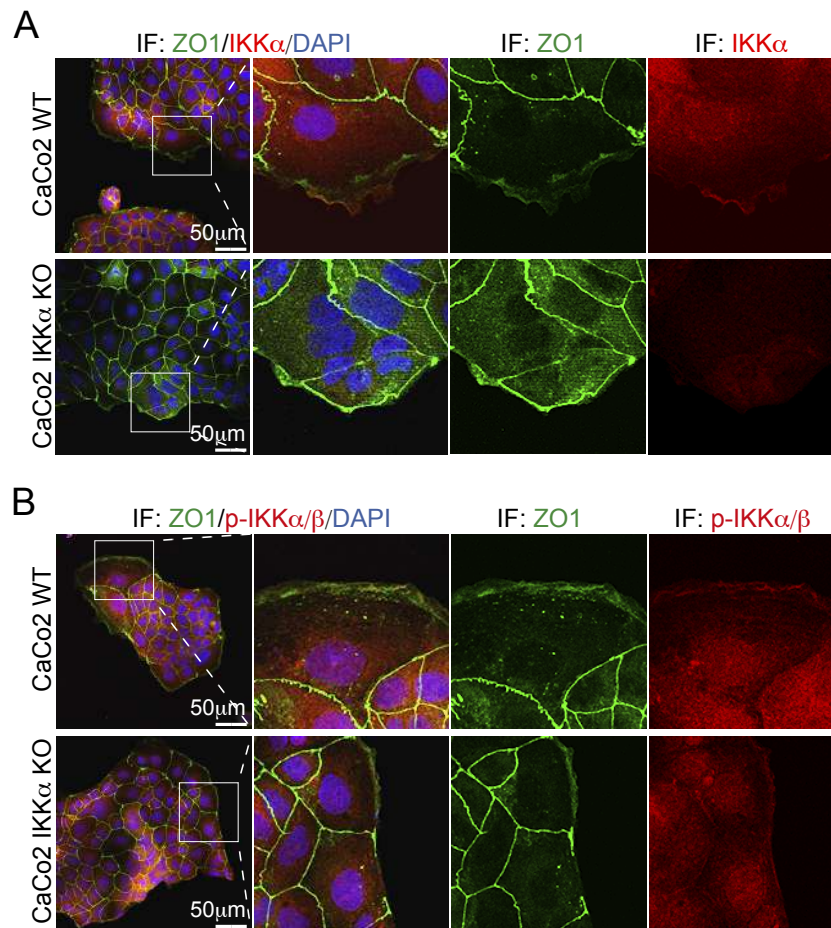


Figure R4. IKKα and pIKK co-localize with residual ZO-1 at the cell membrane of peripheral WT cells. (A, B) Representative images of double immunofluorescence analysis of IKKα **(A)** or active pIKK **(B)** and ZO-1 in WT and IKKα KO CaCo-2 cells.

Cell-cell contacts comprise multiple components and different protein families and are essential regulators of cell behavior. Thus, we aimed to study whether other elements of the cell-cell contacts were affected upon IKKα depletion. To tackle these questions, we performed bulk RNA-seq of WT and IKKα KO PDO5 cells. We found that several cell-cell contact elements were transcriptionally downregulated in IKKα including the three tight junction protein (TJP) homologues ZO-1, ZO-2 and ZO-3, OCLN and the canonical adherens junction component CDH1 (E-Cadherin), among others. In contrast, the tight junction element Claudin 2 (CLDN2) was slightly but significantly upregulated in IKKα KO cells (**Table R2** and **Figure R7A**).

Table R2. IKKα KO cells present altered expression in several tight junction elements and canonical adherens junction component. Table indicating the cell-cell contact elements dysregulated in IKKα KO PDO5 cells identified by bulk RNA-seq.

Gene Name	Log2 Fold Change	padj
TJP3	0,781647870	9,5238E-27
TJAP1	-0,620110007	1,3005E-06
TJP1	-0,544858071	1,662E-17
TJP2	-0,362578453	5,15664E-07
JUP	-0,731080359	1,8778E-34
CLDN3	-0,601630121	1,23508E-07
CTNND1	-0,344893229	2,95621E-08
CTNNA1	-0,121926621	0,063894147
CTNNB1	0,213497085	0,000545858
CTNNBL1	0,263972696	0,012971486
CTNNA2	-0,852479492	0,009822973
CTNNBIP1	-0,351328917	0,000129869
OCLN	-1,103022268	8,27139E-19
CLDN2	0,531315227	1,06059E-24
CDH1	-0,824031893	2,69772E-45

The transcriptional upregulation of CLDN2 upon IKKα KO, as detected in bulk RNA-seq, was subsequently validated by qPCR in multiple cell lines and PDOs (**Figure R5A**). Furthermore, by WB analysis we demonstrated that CRC IKKα KO cell lines and PDOs presented increased CLDN2 levels (**Figure R5B**). In addition, IF and IHC analysis revealed an increased amount of CLDN2 positive cell-cell contacts in IKKα KO CaCo-2 cells (**Figure R5C**) and PDO5 cells (**Figure R5D**).

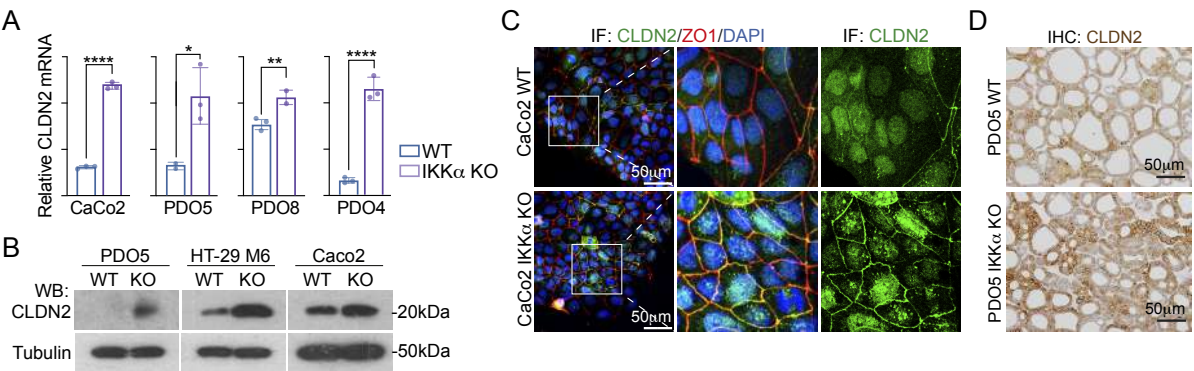


Figure R5. IKKα KO cells showed increased CLDN2 levels. (A-B) RT-qPCR (**A**) and Western blotting analysis

(B) of CLDN2 in the indicated WT and IKK α KO cell lines and PDOs. **(C)** Representative images of a double immunofluorescence staining of CLDN2 and ZO-1 in WT and IKK α KO CaCo-2 cells. **(D)** Representative images of CLDN2 immunohistochemistry in WT and IKK α KO PDO5.

The reduction of CDH1 expression was confirmed in several IKK α KO models by qPCR (**Figure R6A**) and IF (**Figure R6B**). Moreover, IF analysis of CDH1 in CaCo-2 WT and IKK α KO cells revealed an altered pattern of distribution characterized by a significant decrease at the edge of the colonies (**Figure R6B**), a pattern that was opposed to that observed for ZO-1 (that was accumulated at the edge of the colonies in the absence of IKK α).

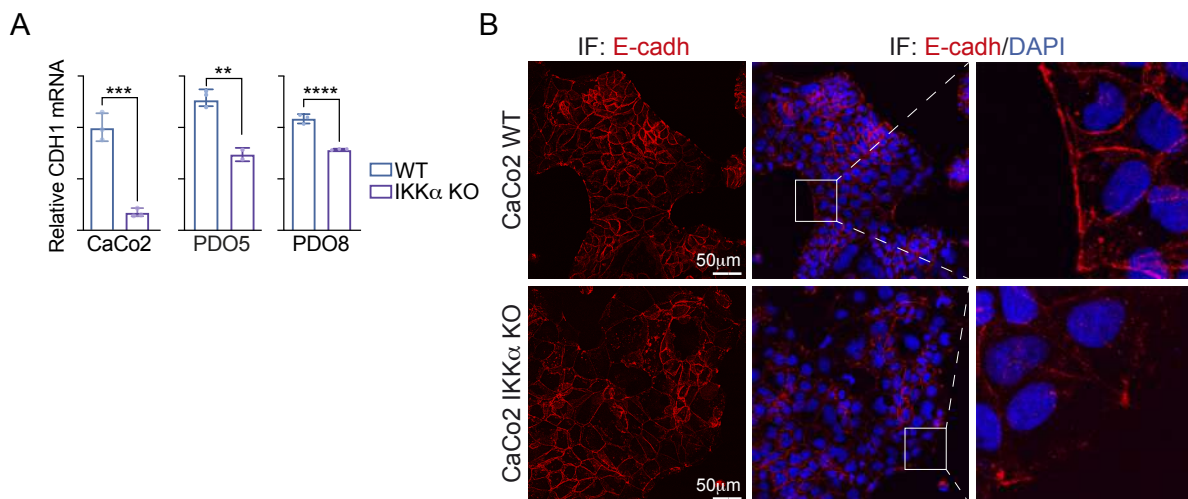


Figure R6. CDH1 is downregulated and re-localized upon IKK α depletion. (A) RT-qPCR analysis of CDH1 in the indicated WT and IKK α KO cell lines and PDOs. **(B)** Representative images of CLDN2 immunofluorescence of WT and IKK α KO CaCo-2 cells.

In general, the presence of well-established cell-cell contacts in the epithelial cancer cells is associated with higher degree of differentiation, which correlates with reduced malignancy³²⁷. Counterintuitively, increases in ZO-1 and CLDN2 were associated with decreased expression of differentiation markers and increased expression of stemness markers (**Figure R7A**), as well as higher clonogenic activity in 3D (Matrigel) cultures (**Figure R7B**).

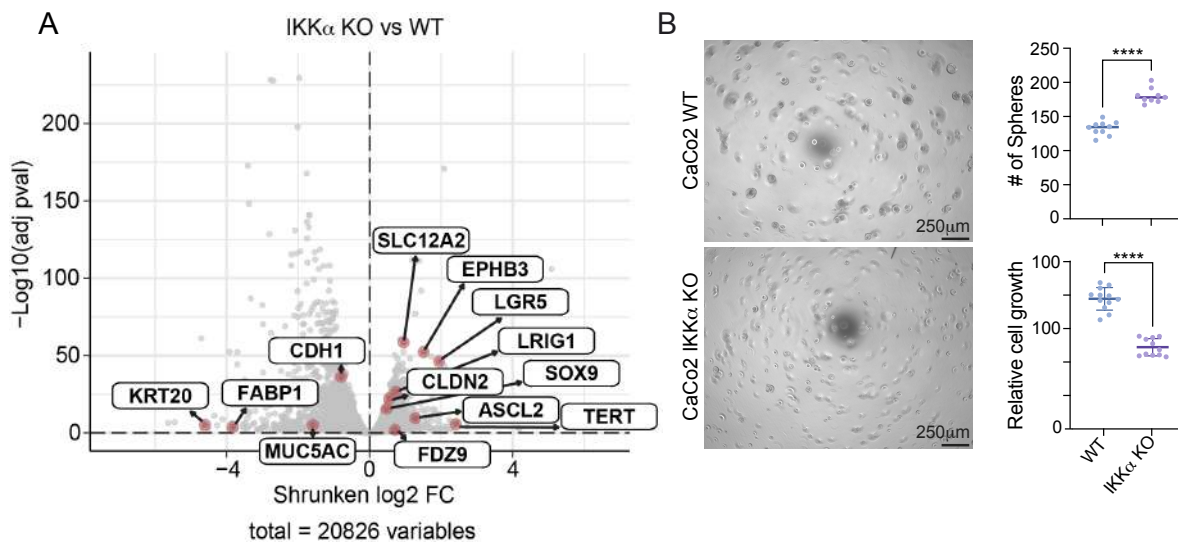


Figure R7. IKK α KO cells showed increased stemness and reduced differentiation. (A) Volcano plot representation of the bulk RNA-seq data from WT and IKK α KO PDO5 cells, indicating the distribution of canonical intestinal differentiation and stemness genes, as well as CLDN2. **(B)** Clonogenic assay from WT and IKK α KO CaCo-2 cells. Representative microscopic images, and quantification of the number of spheres obtained and relative cell growth (CellTiter-Glo).

R2. Functional depletion of IKK α alters the migratory behavior of cancer cells.

As a dynamic behavior of cell-cell contacts is essential for successful cell migration, we postulated that alterations in cell-cell contacts present in IKK α KO cells might be affecting cell motility. To investigate this, wound-healing assays were conducted in different CRC cell lines known to carry activated IKK α ²⁴⁹. Migration of IKK α KO DLD-1 and CaCo-2 cells was significantly reduced after 12 and 24 hours compared with WT cells (**Figure R8A** and **R8B**). Equivalent phenotype was observed following IKK α inhibition by AZ628. No differences were observed between untreated or AZ628-treated IKK α KO cells, indicating that the effect of AZ628 on cell migration is primarily related to its activity on IKK α . Same results were obtained using HCT-116 and HT-29 M6 cells (data not shown).

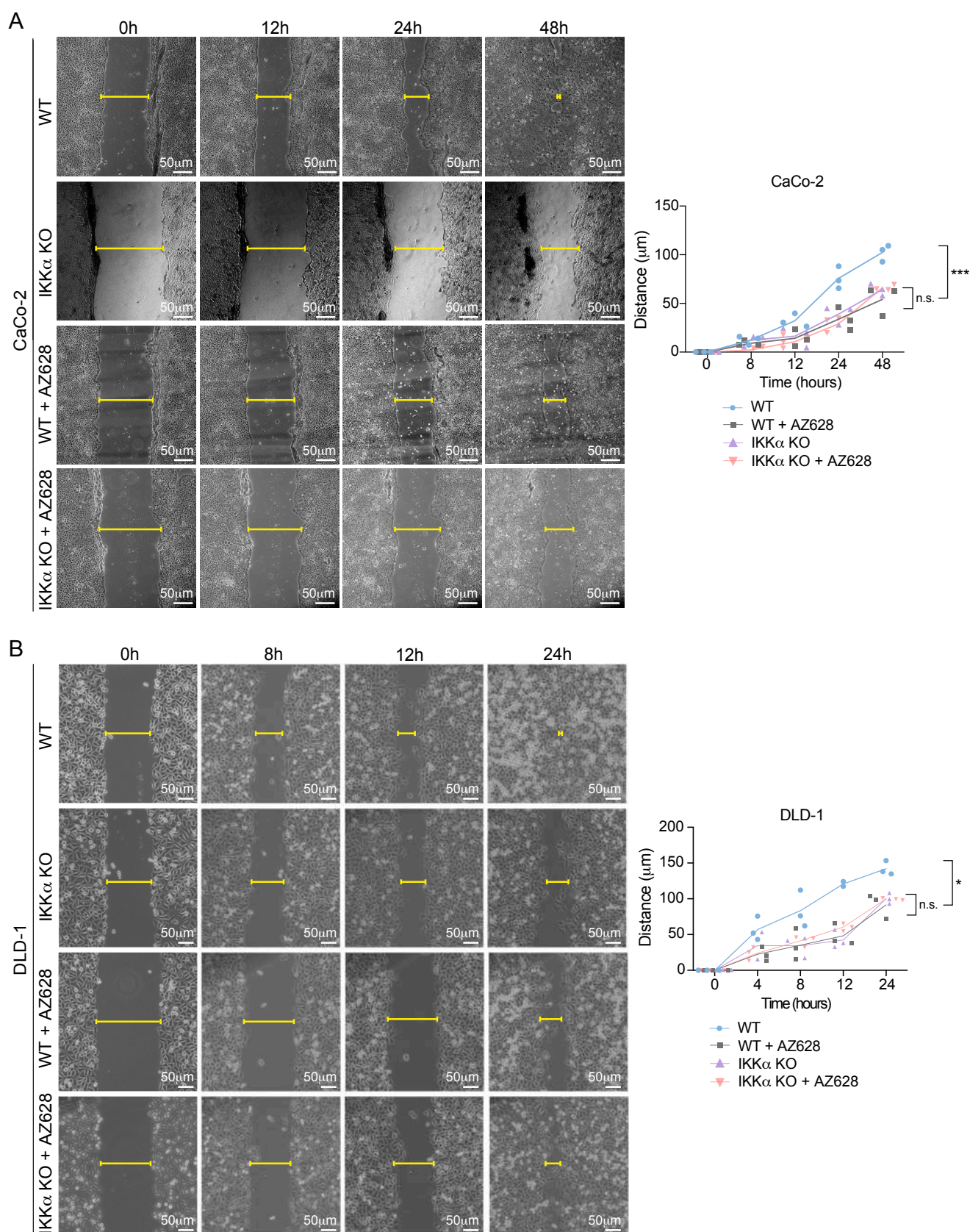


Figure R8. IKK α depleted CRC cell lines, either genetically or pharmacologically, showed decreased cell migration *in vitro*. **(A, B)** Representative images of wound-healing assay of CaCo-2 **(A)** and DLD-1. **(B)** WT and IKK α KO untreated cells plus AZ628-treated (10 μ M O/N) cells. Quantification of wound closure at each time point.

We next tested whether IKK α depletion was also affecting the migratory capacity of PDO cells in culture. PDO cells, which normally grow as 3D cultures produced flat colonies that adhered and spread over the plastic plates when adapted to grow in 2D conditions. Depletion of IKK α virtually abrogated the ability of both, PDO5 and PDO8 cells, to adhere and spread on culture plates, thus remaining as spherical structures (**Figure R9A and R9B**). Defective migratory ability of PDO5 cells was also observed upon different doses of AZ628-treatment (**Figure R9C**). Similar to that found in the wound healing assay, we did not detect differences in the migratory capacity of IKK α KO PDO cells after AZ628 treatment, reinforcing the concept that the effects of AZ628 on cell migration are linked to IKK α

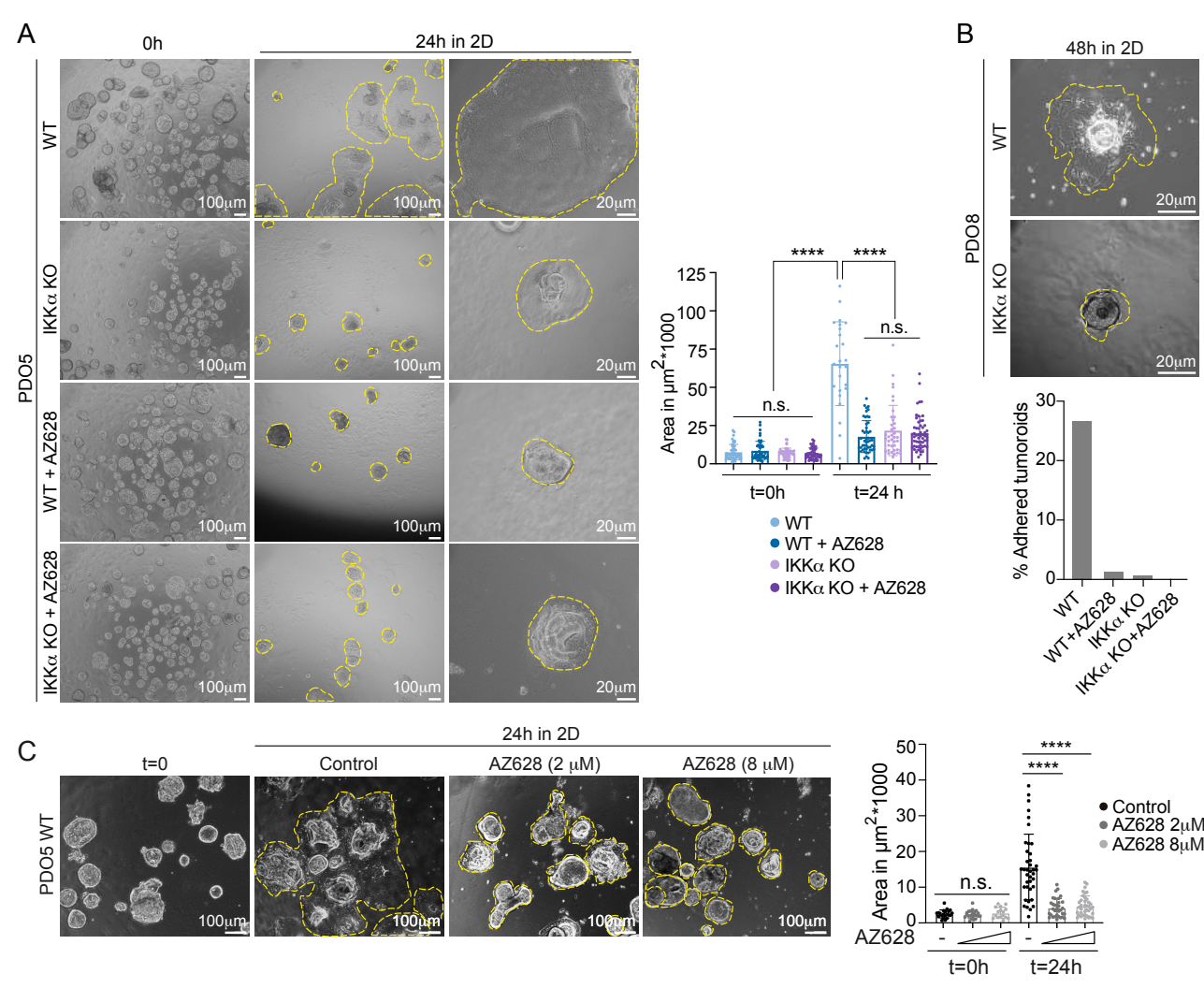


Figure R9. IKK α depleted CRC PDOs, either genetically or pharmacologically, showed decreased cell migration *in vitro*. **(A-C)** Representative images of WT and IKK α KO PDO5 **(A)** and PDO8 **(B)** cells seeded in 2D conditions and quantification of the area covered by the colonies at the indicated time points and experimental conditions (WT and IKK α KO, untreated or AZ628-treated, 2-8 μ M).

To further study the effects of functional IKK α depletion on the migratory capacity of CRC cells, we performed transwell *in vitro* cell migration assay using HCT-116 and DLD-1 cell lines. Similar to that observed in the wound-healing assay, the capacity of CRC cells to migrate across the transwell filters was highly reduced in AZ628-treated HCT-116 and DLD-1 cells (**Figure R10A and R10C**). However, the majority of AZ628-treated cells that migrated through the membrane were distributed in clusters compared to control cells that migrated mainly as single cells (**Figure R10B and R10D**).

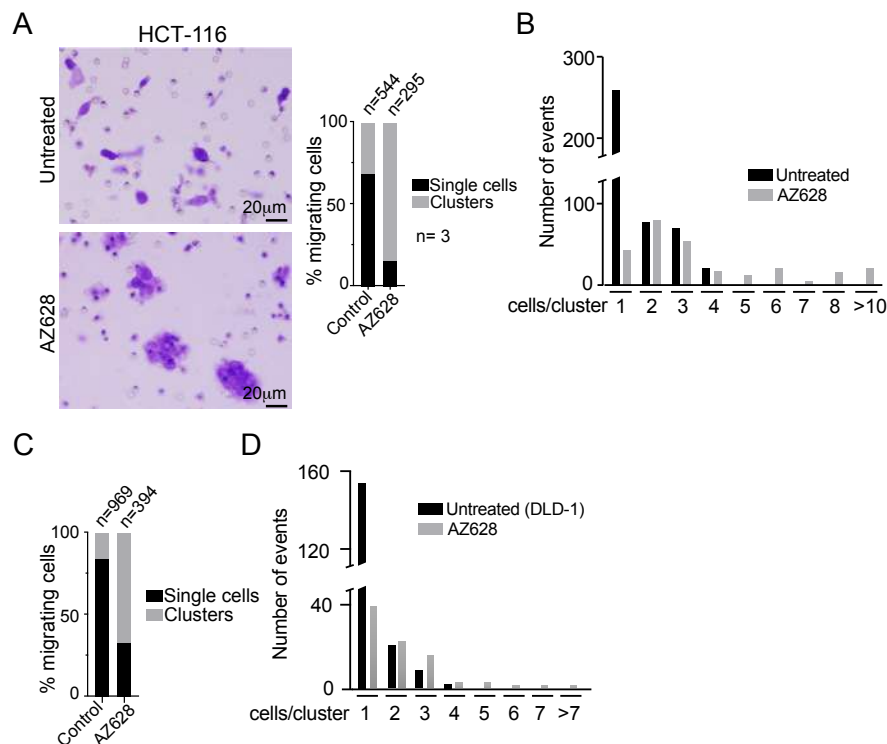


Figure R10. Pharmacological inhibition of IKK α in CRC cells imposes a collective cell migration behavior. (A) Representative images of untreated or AZ628-treated HCT-116 cells in the transwell inserts at 24h and quantification of the number of single cells or cell clusters in the filter. **(B)** Quantification of the number of HCT-116 cells per cluster in each condition. **(C)** Quantification of the number of DLD-1 single cells or cell clusters in the filter. **(D)** Quantification of the number of DLD-1 cells per cluster in each condition. Cells were treated with AZ628 at 10 μ M O/N.

Increased cellular clustering was also detected by simply seeding single IKK α KO CaCo-2 cells under non-adherent conditions (**Figure R11A**). In agreement with results from **Figure R1**, we detected increased ZO-1 staining in the cell-cell contacts and outer membranes of IKK α KO CaCo-2 clusters (**Figure R11B**).

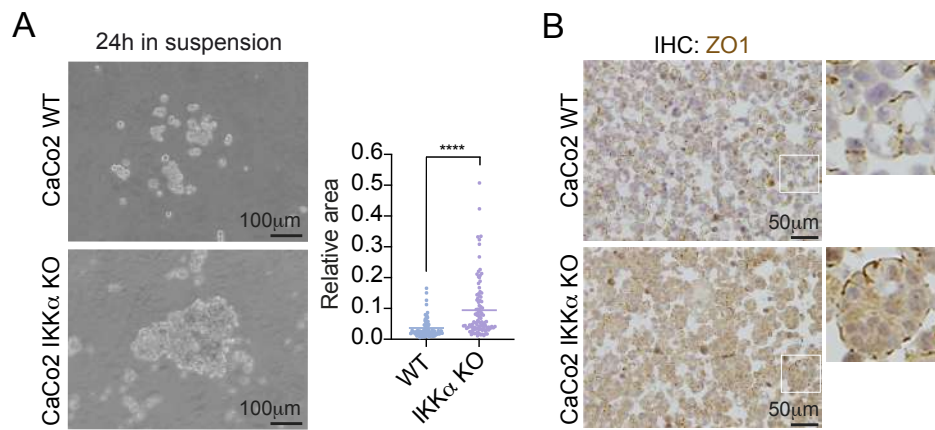


Figure R11. Intrinsic cell clustering ability is enhanced upon IKK α depletion. (A) Representative microscopic images of the clusters generated after 24h of seeded single WT or IKK α KO CaCo-2 cells in suspension in non-adhesive plates. Quantification of the area of the clusters obtained by analyzing multiple images taken from randomly selected fields. **(B)** Representative IHC images of ZO-1 in the CaCo-2 WT and IKK α KO cell clusters.

R3. Accumulation of the tight junction signature in CRC IKK α KO cells is linked to a higher metastatic activity.

We investigated whether cells with higher tight junction activity, which is the phenotype observed after IKK α depletion, displayed a distinct metastatic activity in CRC. We took advantage of publicly available scRNA-seq data from a mouse model of CRC metastatic relapse developed by Dr. Eduard Batlle lab⁷² that include different tumor stages: primary tumor, micro metastases, small metastases, and macro metastases (**Figure R12A**). Analysis of these data revealed a progressive accumulation of multiple tight junction elements, including TJP1 (ZO-1), OCLN (Occludin) and CLDN2, from the primary tumor to micro- and small metastases (**Figure R12B**). In the Uniform Manifold Approximation and Projection (UMAP) (**Figure R12C**), TJP1 and CLDN2 were detected at low levels in cell clusters of micro metastases that were negative for the stem cell marker Lgr5, but were significantly elevated in the Lgr5-positive small metastasis cluster together with OCLN. We did not detect a robust accumulation of CHUK (IKK α) levels in any particular cluster. Taken together, these results were counterintuitive but consistent with the notion that cancer cells enriched in tight junction elements are the origin of metastatic recurrence.

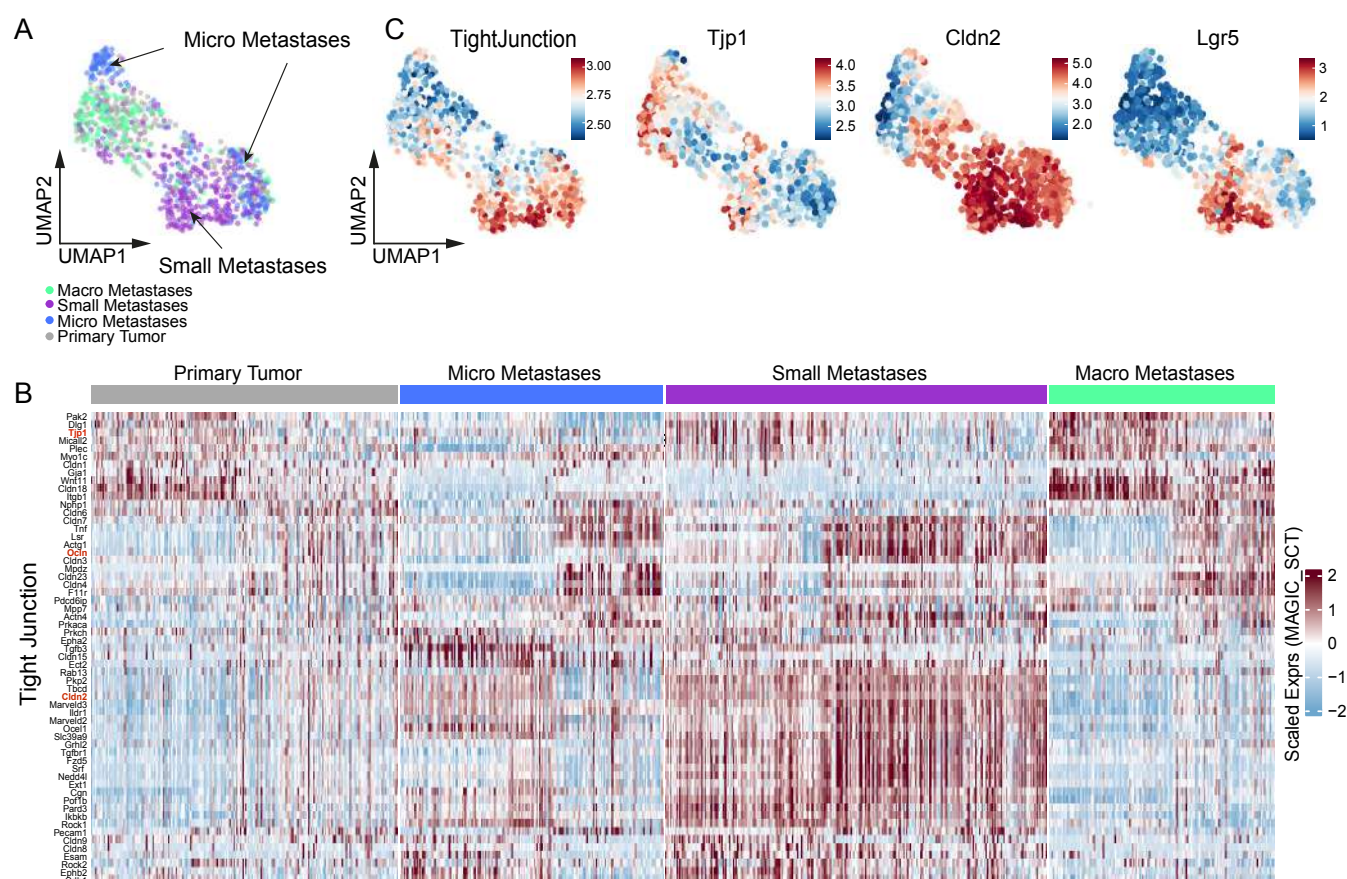


Figure R12. Metastatic populations in mice are enriched in tight junction elements. (A) UMAP layout of the CRC scRNA-seq data from Cañellas-Socias et al. colored by tumor stage (Primary Tumor and Micro/Small/Macro Metastases). Dataset obtained from AKTP mouse tumor organoids. **(B)** Heatmap representing the scaled expression levels of genes annotated to 'Tight Junction Organization' term (GO:0120193) of previously mentioned scRNA-seq data. Unsupervised hierarchical clustering is only performed on genes (rows) based on Pearson correlation. **(C)** UMAP representation based on previously mentioned scRNA-seq data colored by the mean expression levels of genes annotated to 'Tight Junction Organization' term from Gene Ontology database (GO:0120193) or the individual gene expression levels of: the tight junction components TJP1 and CLDN2 or the stem cell marker LGR5.

We then experimentally tested the metastatic capacity of WT and IKK α KO PDO5 cells upon intrasplenic transplantation in nude mice. Consistent with the idea that cell enriched in tight junction elements are the source of metastasis, IKK α -depleted PDO5 cells showed significantly higher metastatic activity than WT PDO cells, and comparable to that observed in mice treated with vemurafenib that inhibits BRAF-dependent IKK α activity^{326,328,329} (Figure R13A and R13B). Specifically, we detected not only an increase in the area covered by tumoral tissue but also in the number of metastatic lesions.

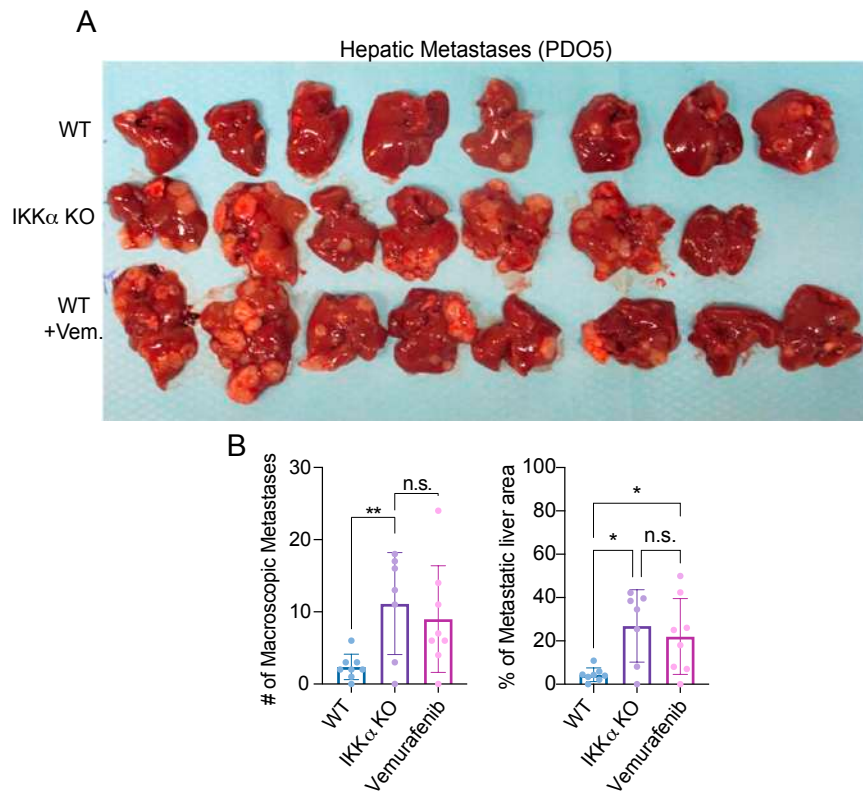


Figure R13. IKK α depleted PDO5 cells showed higher metastatic ability. (A) Photograph of the hepatic metastases developed in nude mice after intrasplenic injection of WT, IKK α KO PDO5 cells. A third group correspond to mice injected with WT PDO5 cells and then treated with vemurafenib. **(B)** Quantification of metastatic area and number of metastases.

By histopathologic examination and IHC analysis of the hepatic metastases, we found that lesions derived from IKK α KO PDO5 cells were organized as larger glandular structures with a significant occurrence of ZO-1- and CLDN2-positive tight junction cell-cell contacts (**Figure R14A and R14B**). IKK α KO-derived metastases were characterized by less infiltration by SMA-positive fibroblasts (Smooth Muscle Actin) and increased levels of the mitochondrial marker ATP5A, suggestive of altered metabolism (**Figure 14C**).

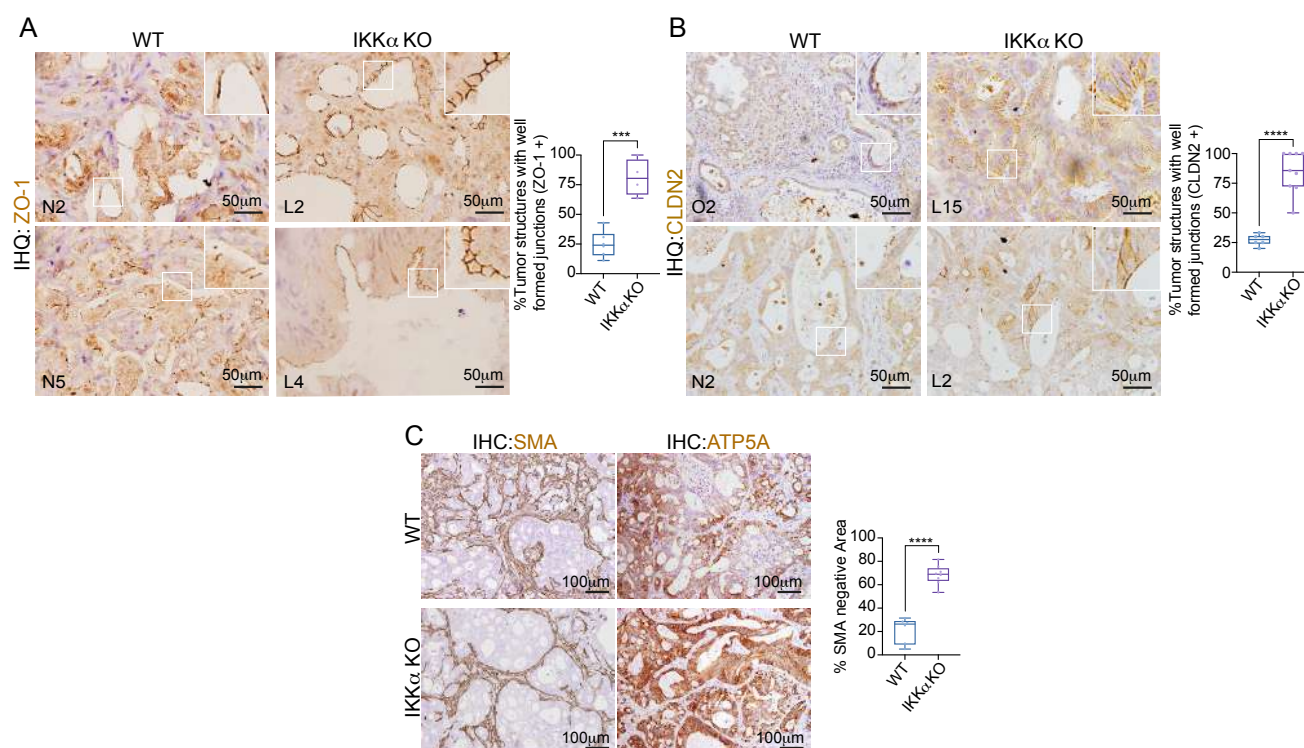


Figure R14. Characterization of IKK α KO PDO5-derived hepatic metastases. (A-C) Representative images of the immunohistochemistry analysis of ZO-1 **(A)**, CLDN2 **(B)**, SMA and ATP5A **(C)** in WT and IKK α KO-derived metastases. Quantification of the tumor structures with well-formed cell-cell contacts positive for ZO-1 or CLDN2 and SMA negative tumoral areas.

PDO4 was used as an independent patient-derived CRC model to further validate the results obtained with PDO5 *in vivo*. Metastatic colonization of the liver was again higher when injecting IKK α KO PDO4 (**Figure R15A**) and these metastases accumulated tight junction protein ZO-1 (**Figure R15B**).

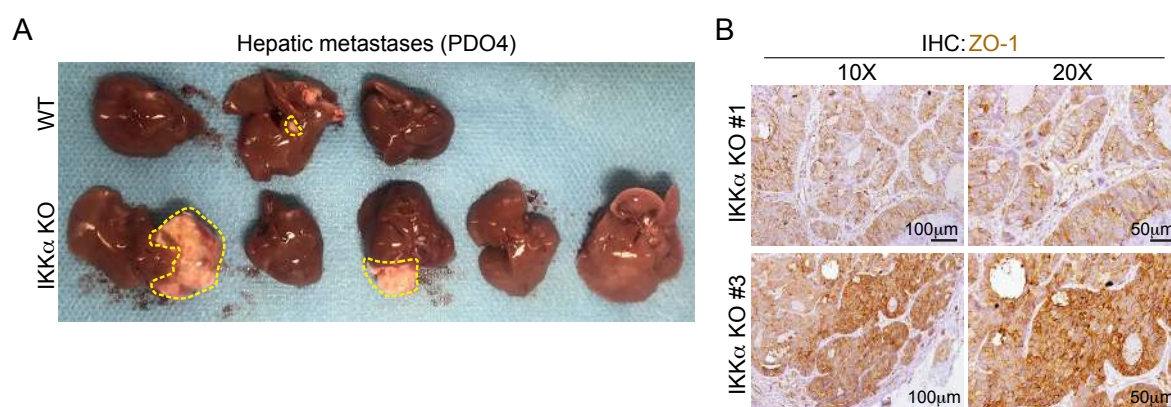


Figure R15. IKK α depleted PDO4 cells showed higher metastatic ability and tight junction accumulation. (A) Photograph of the hepatic metastases developed in nude mice after intrasplenic injection of WT or IKK α KO PDO4 cells. **(B)** Representative IHC images of ZO-1 in the hepatic metastases derived from IKK α KO PDO4 cells.

R4. Accumulation of high relapse and tight junction signatures in two different clusters of PDO5 cells, that are characterized by TFF3 expression and are increased in IKK α KO cells.

To better understand the mechanisms underlying the higher metastatic activity of IKK α KO cells, we performed scRNA-seq analysis of PDO5 cells WT, IKK α KO and IKK α KO treated with YM201636, which was found to perturbs CLDN2 recycling and function³³⁰. Integration of these data allowed the identification of 10 distinct cell clusters (**Figure R16A**) that are all represented in the different experimental conditions. The percentage of cells identified in each cluster were different in each condition (**Figure R16B**). Inhibition of CLDN2 activity by YM201636 had little effect in terms of gene transcription but imposed a significant reduction in the percent of cells contributing to cluster C8 (**Figure R16B**).

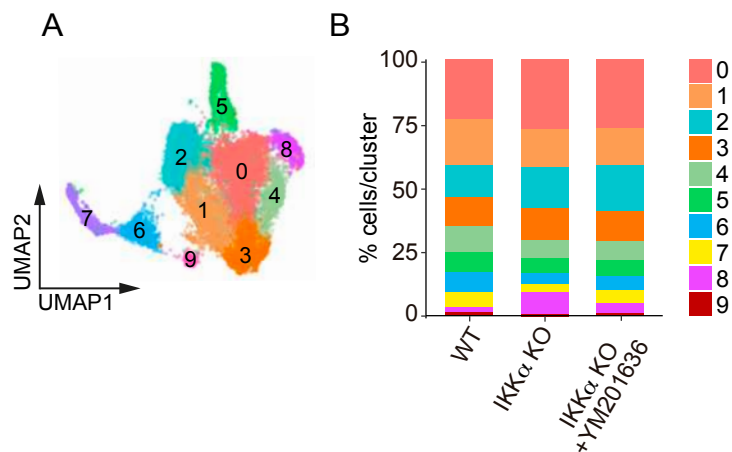


Figure R16. PDO5 scRNA-seq clustering data. (A) UMAP representation of integrated scRNA-seq data from PDO5 cells in three experimental conditions (WT, IKK α KO, and IKK α KO treated with CLDN2 inhibitor for 16h) showing the 10 identified clusters. **(B)** Stacked bar plot shows the percentage of cells annotated to each cluster per experimental condition.

We first analyzed the distribution of several key factors such as the epithelial marker EpCAM (**Figure R17A**), the intestinal stem cell marker LGR5 (**Figure R17B**) and the proliferation marker KI67 (**Figure R17C**) in the different cell clusters. The detection of EpCAM expression in almost all of the sequenced cells further indicated that the 10 distinct clusters corresponded to epithelial cells.

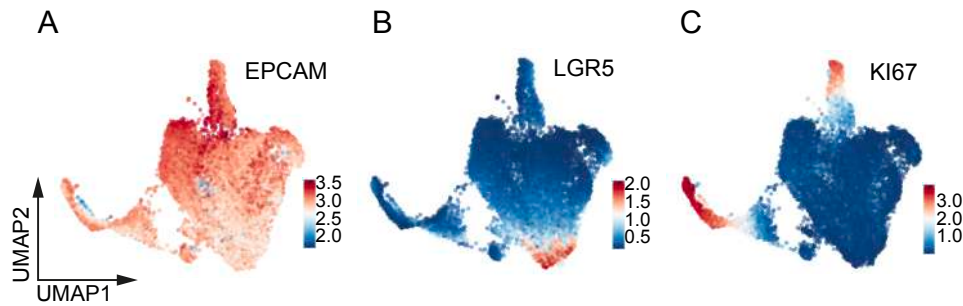


Figure R17. PDO5 scRNA-seq data, cluster characterization. (A-C) UMAP layouts showing the expression levels of the epithelial marker EPCAM **(A)**, the intestinal stem cell marker LGR5 **(B)** and the proliferation marker KI67 **(C)**.

We then represented in our clusters the High-Relapse (EpiHR) signature of Cañellas-Socias et al., which identifies early metastatic populations⁷². The EpiHR signature was preferentially enriched in clusters 2 (C2), 4 (C4) and 8 (C8) (**Figure R18A**), with more than 50% of all cells classified as EpiHR-high (**Figure R18B**), being LGR5 and KI67 primarily absent from these clusters (**Figure R17B** and **R17C**). We also detected an enrichment of the tight junction signature in C2 and C8 (**Figure R18C**), being EpiHR and the tight junction signatures significantly correlated in the different PDO5 lines and experimental conditions (**Figure R18D**).

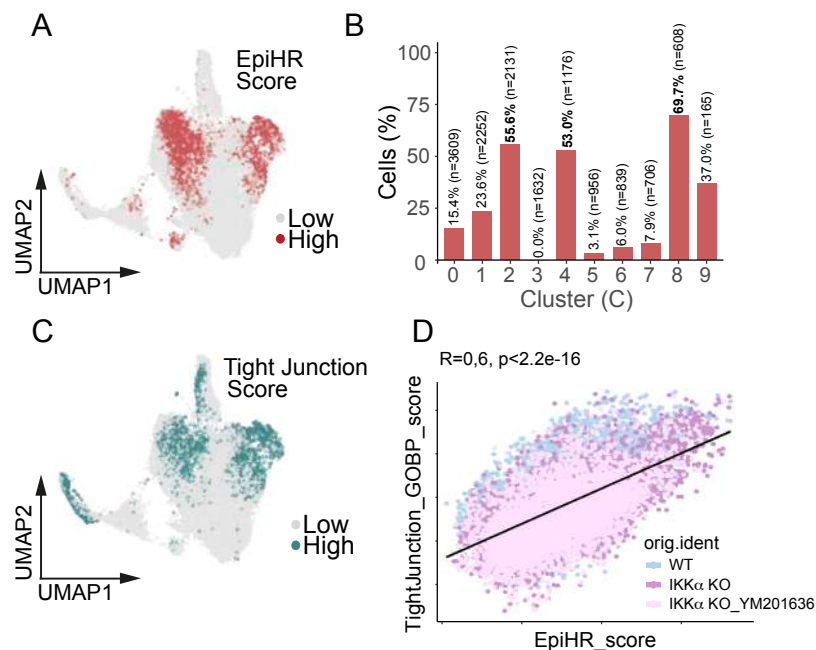


Figure R18. EpiHR and tight junction signature scores represented in PDO5 scRNA-seq data. (A-B) UMAP showing the cell classification into high or low score levels of the **(A)** 'Tight Junction Organization' term from Gene Ontology database (GO:0120193) and the **(B)** High-Relapse (EpiHR) signature of Cañellas-Socias et al., which identify early metastatic populations⁷². **(C)** Bar plot showing the percentage of cells labeled as High

EpiHR score per identified cluster. The number of cells per cluster is indicated. Clusters C2, C4 and C8 show percentages > 50%. **(D)** Correlation analysis of the tight junction and EpiHR scores in the scRNA-seq data of the indicated cellular models.

Importantly, genes specifically defining C2, C4 and C8 (not present in other clusters) did not overlap with genes of the EpiHR signature (**Figure R19A**). We performed a Kaplan-Meier analysis of a meta-cohort of public CRC data using the transcriptomic signatures (top upregulated genes) specifically present in C2, C4 and C8. All three signatures were predictive of poor prognosis, with C2 showing the highest significance (**Figure R19B**). Heatmap representation showed upregulation of C2, C4 and C8 signatures in IKK α KO cells, with C2 being more predominant (**Figure R19C**).

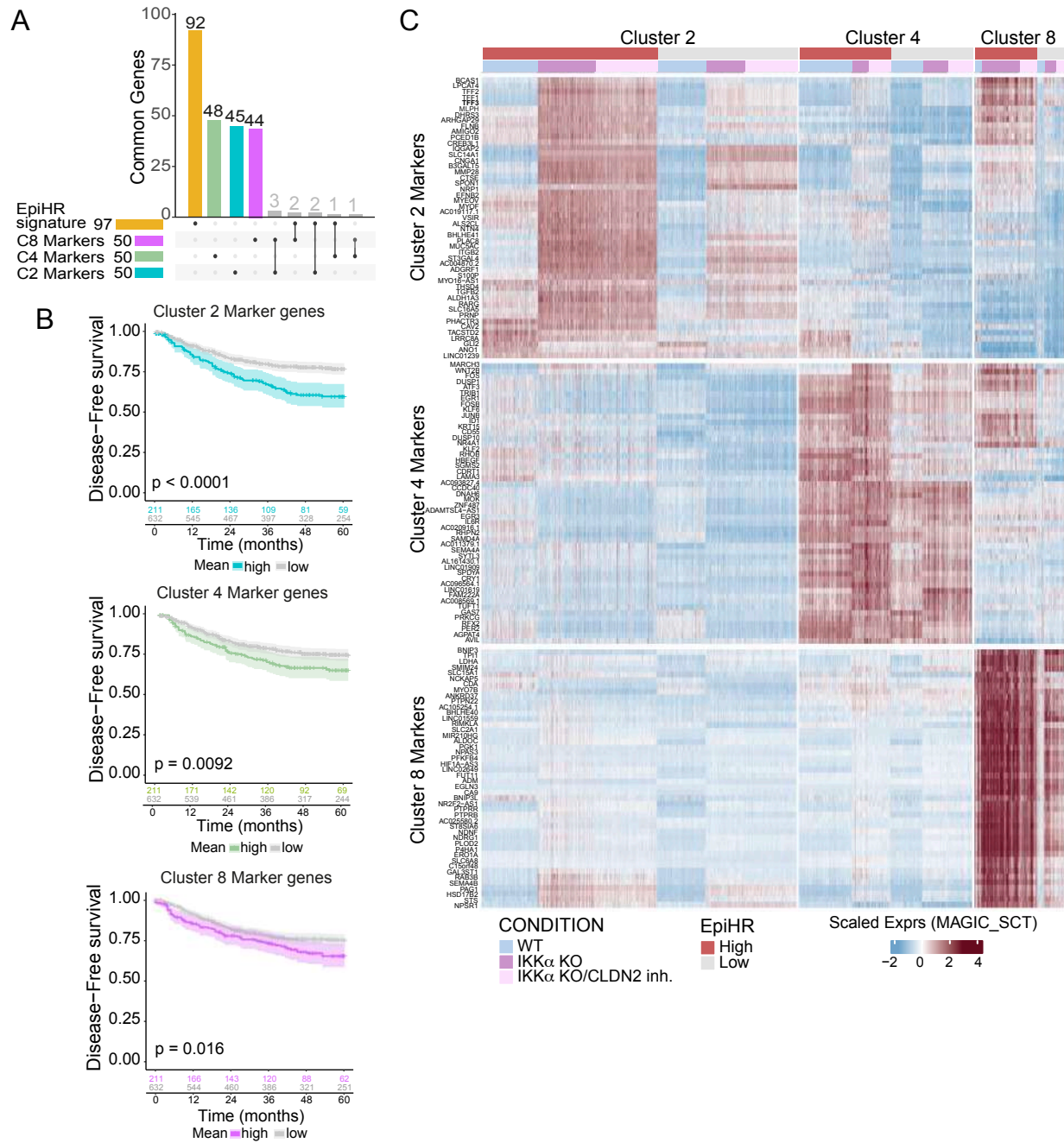


Figure R19. C2, C4 and C8 marker gene signatures predict poor prognosis in CRC. (A) Representation of the

number of top-50 genes from C2, C4 and C8 that were exclusive or shared between them and compared to the 97 genes of the EpiHR signature. **(B)** Kaplan-Meier survival curves showing disease-free survival of patients stratified based on the C2, C4 or C8 signatures. **(C)** Heatmap representation of the expression levels of the genes defining the C2, C4 and C8 signatures in PDO5 cells WT, IKK α KO and IKK α KO treated with the CLDN2 inhibitor YM201636. Expression levels are presented to distinguish cells from different experimental conditions and high or low scores for the EpiHR signature.

We performed bulk RNA-seq analysis of liver metastases derived from WT and IKK α KO PDO5 cells. We found a significant enrichment of the C2 (**Figure R20A**), C4 (**Figure R20B**) and C8 (**Figure R20C**) signatures in the metastatic outgrowths compared with the original PDO5 cells.

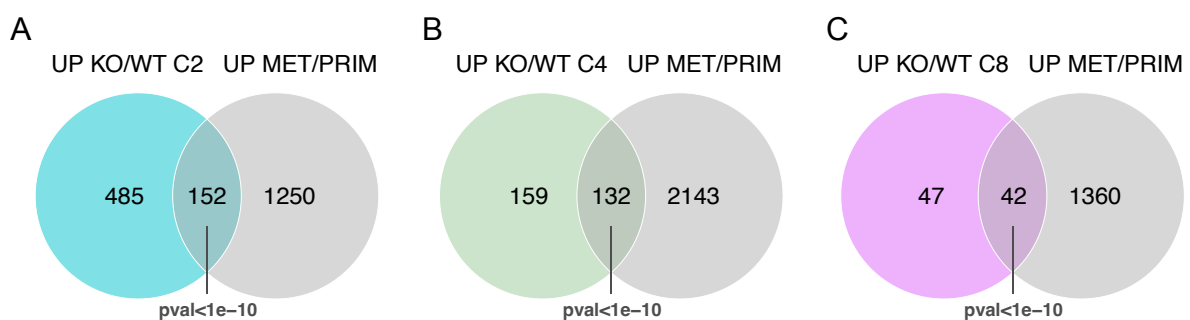


Figure R20. C2, C4 and C8 marker gene signatures are enriched in PDO5-derived metastases. **(A-C)** Venn diagrams depicting differentially expressed genes of clusters C2 **(A)**, C4 **(B)** and C8 **(C)** that are upregulated in both IKK α KO conditions compared to WT (from scRNA-seq) and genes that are upregulated in the metastases compared to primary tumors of both WT and IKK α KO (bulk RNA-seq). Some of the most representative overlapping genes from each signature are shown. Associated p-value determined by Chi-square test considering a background of 20,000 genes for both sets.

Genes enriched in the PDO5 IKK α KO metastases, and restricted to C2 and C8 clusters, comprise several trefoil factors (TFF) (**Figure R21A**). TFF3 has been identified as a factor that enables CD147 and CD44 signaling leading to activation of the pro-tumorigenic STAT3 and arachidonic acid pathways associated with SRC³³¹. All these TFF3-related elements were detected in C2 and/or C8 (**Figure R21B**).

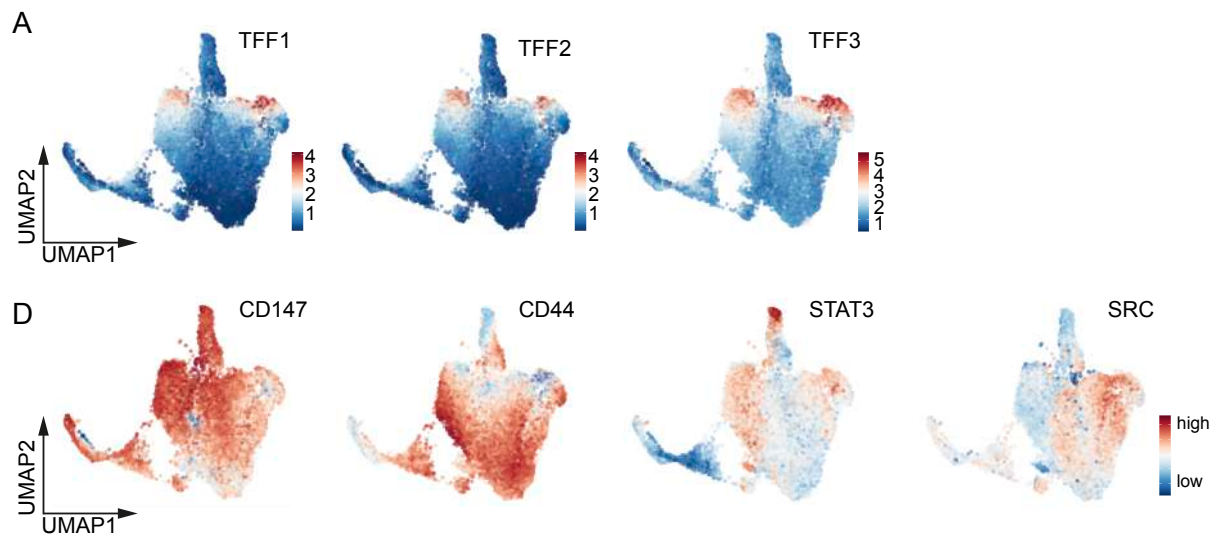


Figure R21. C2 and C8 marker genes are not enriched in the general IKK α KO cell populations. (A) UMAP analysis of PDO5 cells colored by TFF1 (left), TFF2 (center) and TFF3 (right) expression. **(B)** UMAP layouts showing the expression levels of TFF3-related elements expression (left to right): CD147, CD44, STAT3 and SRC.

R5. Targeting CLDN2 activity reverts the migratory mode imposed by IKK α deficiency

Expression of the tight junction protein CLDN18.2 in gastric cancer cells correlates with liver metastasis and blocking antibodies to CLDN18.2 have demonstrated their efficacy in the treatment of metastatic gastric cancer^{296,297}. We used several strategies to test whether interfering with CLDN2 could affect the migratory phenotype imposed by IKK α depletion in CRC. First, we performed wound healing assays in IKK α KO CaCo-2 and HT-29 M6 cells untreated or treated with YM201636, that blocks the continuous recycling of CLDN2 in the junctions and causes intracellular accumulation³³⁰. CLDN2 inhibition by YM201636 was sufficient to restore their migratory activity in wound healing assays to the level of WT cells, both after chronic treatment or after 16h treatment followed by drug washout (**Figure R22A and R22B**).

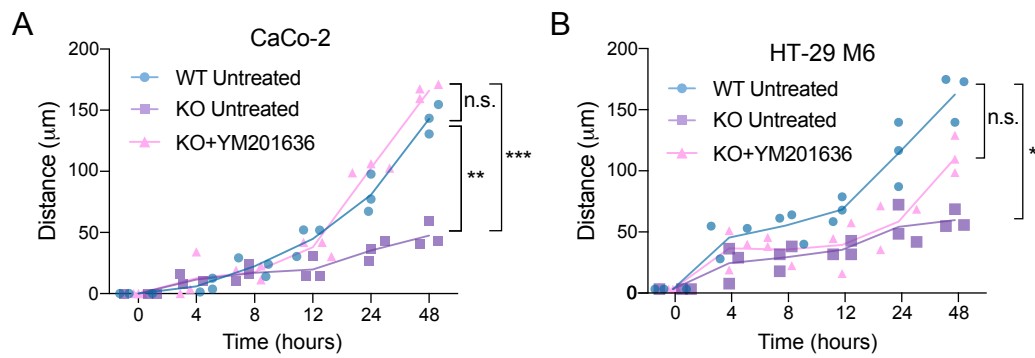


Figure R22. YM201636 treatment restores the migratory properties of IKK α KO CRC cell lines. (A-B) Quantification of wound-healing migration assay of CaCo-2 **(A)** and HT-29 M6 **(B)** cells WT, IKK α KO and IKK α KO treated with the CLDN2 inhibitor YM201636 at 0,5 μ M O/N.

Similarly, YM201636 treatment (both, maintaining the inhibitor throughout the experiment or performing a washout prior to 2D growth) reverted the adhesive/migratory properties of IKK α KO PDO5 cells adapted to grow in 2D cultures (**Figure R23A and R23B**).

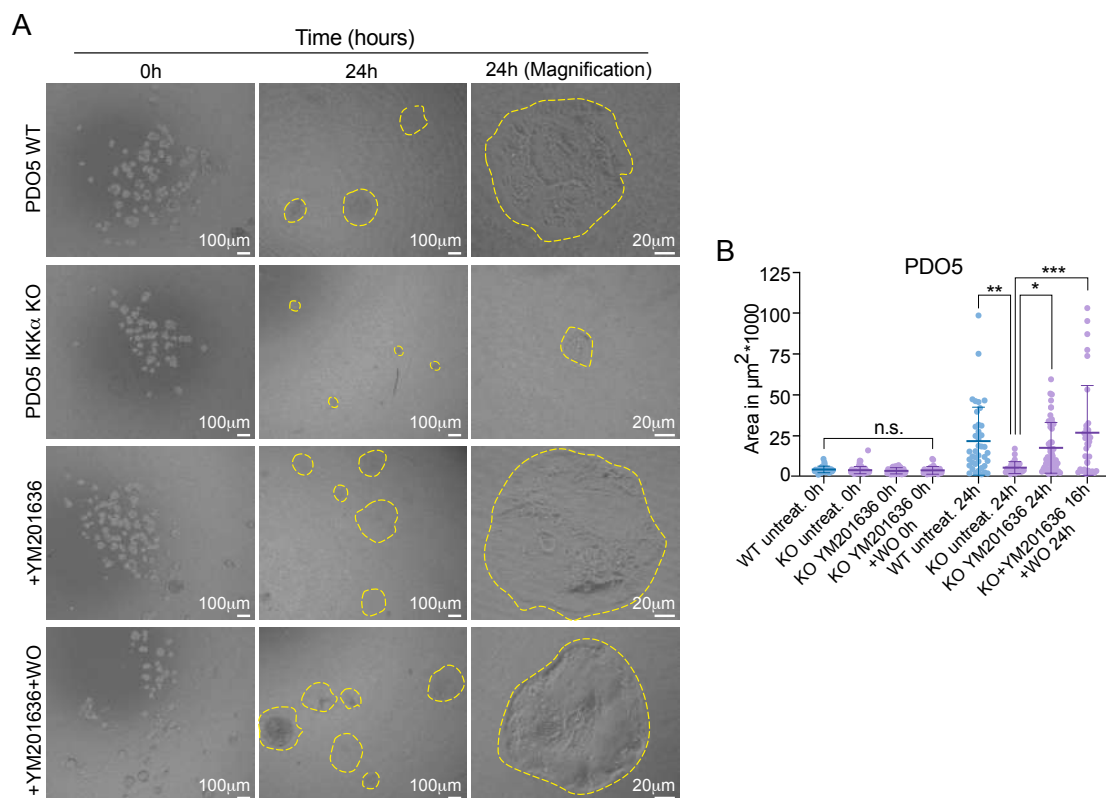


Figure R23. YM201636 treatment reverts the adhesive/migratory properties of IKK α KO PDO5 cells. (A-B) Representative images of the 2D adaptation assay in WT, IKK α KO and IKK α KO PDO5 cells treated with YM201636 at 0,5 μ M O/N. **(B)** Quantification of the area covered by the colonies at the indicated time points and conditions.

To confirm that the effects observed were due to CLDN2 inhibition, we knocked down CLDN2 in IKK α KO cells by three different shRNAs (**Figure R24A**). Reducing CLDN2 levels by shRNAs in CaCo-2 cells was sufficient to reverse the migratory phenotype of IKK α KO cells, comparable to WT cells (**Figure R24B and R24C**).

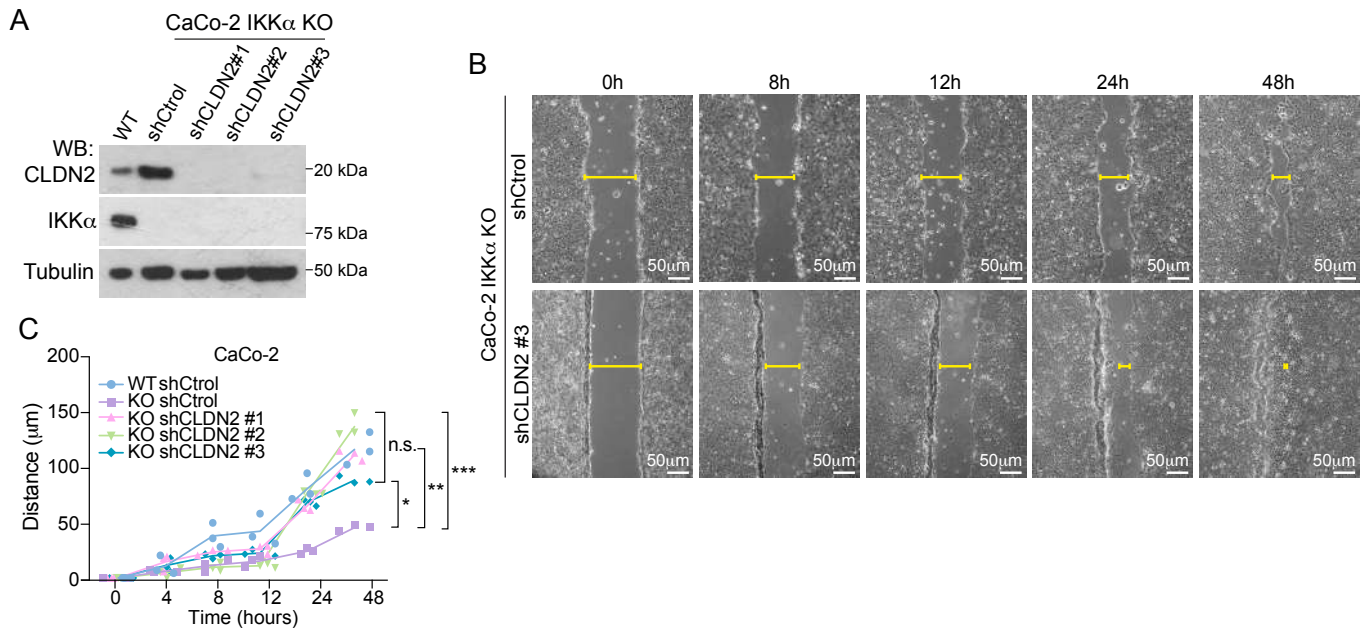


Figure R24. CLDN2 knockdown restores the migratory properties of IKK α KO CaCo-2 cells. (A) Western blot validation of CLDN2 knockdown. **(B)** Representative images and quantification of wound-healing assay of CaCo-2 IKK α KO untreated cells or YM201636-treated (0,5 μ M O/N) cells. **(C)** Quantification of wound-healing migration assay.

To obtain a proof of concept for the potential use of CLDN2 inhibition in CRC therapy, we performed *in vivo* metastasis assays by intrasplenic implantation of IKK α KO PDO5 cells untreated or treated with the CLDN2 inhibitor for 16 hours. Metastatic colonization of the liver was completely abolished when IKK α KO PDO5 cells were treated with CLDN2 inhibitor (**Figure R25A**).

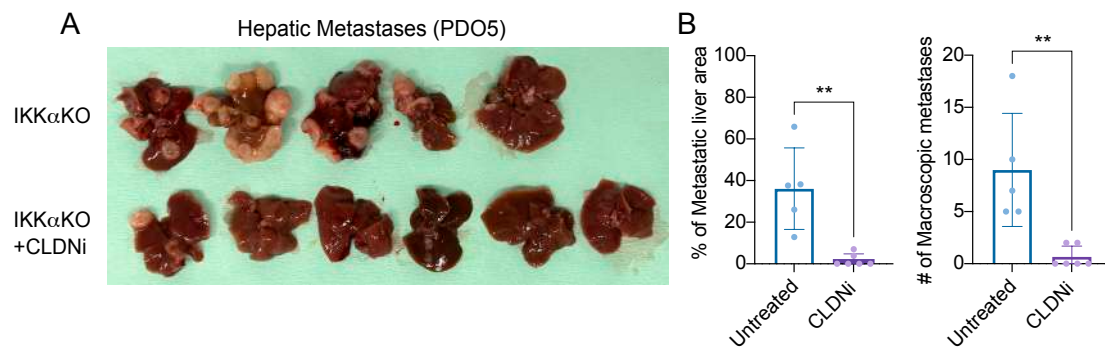


Figure R25. Metastatic potential of PDO5 IKK α -depleted cells is reduced upon YM201636 treatment. (A) Photograph of the hepatic metastases developed in nude mice after intrasplenic injection of IKK α KO PDO5 cells untreated or pre-treated with YM201636 at 0,5 μ M O/N. **(B)** Quantification of metastatic area and number of metastases.

To confirm that the *in vivo* effects observed with CLDNi were due to CLDN2 inhibition and not to other side effects, we knocked down CLDN2 in IKK α KO PDO5 cells using three different shRNAs (**Figure R26A**). Metastatic colonization of the liver was drastically reduced upon CLDN2 knockdown, regardless of the shRNA used (**Figure R26B**).

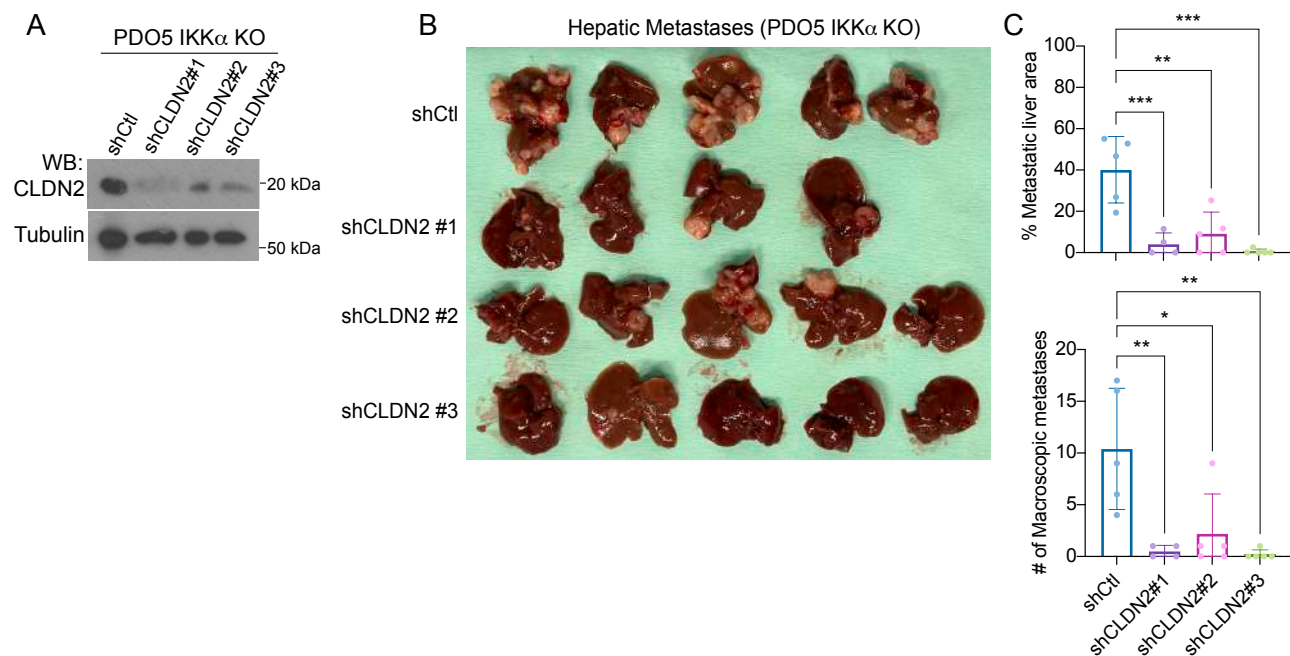


Figure R26. CLDN2 knockdown reduces the metastatic potential of PDO5 IKK α -depleted cells. (A) Western blot validation of CLDN2 knockdown. **(B)** Photograph of the hepatic metastases developed in nude mice after intrasplenic injection of IKK α KO PDO5 cells infected with shControl or shCLDN2 (#1, #2 or #3). **(C)** Quantification of metastatic area and number of metastases.

These results provide initial evidence supporting the possibility of interfering with cell-cell contact elements (i.e., CLDN2) in the treatment of mCRC.

R6. Different modes of vascular invasion and tight junction distribution are detected in primary human CRC samples. ZO-1 and CLDN2 as candidate IHC biomarkers in the invasive clusters.

Circulating tumor cell clusters, also known as micro emboli, has been successfully isolated from several metastatic murine and human cancers and shown to be associated with their superior metastatic potential^{138,184,187}. However, this type of analysis is time consuming and expensive, making it difficult to implement as a diagnostic tool. In this context, we evaluated the possibility of studying the migration mode of cancer cells from paraffin sections obtained at the time of tumor resection. To this end, 150 samples diagnosed with vascular infiltration by histopathological analysis of H&E-stained tumor sections were selected and re-examined. We identified four different well-defined infiltration patterns: single cells/small clusters (≤ 5 cells), large solid clusters (>5 cells), glandular and cribriform (**Figure R27A**).

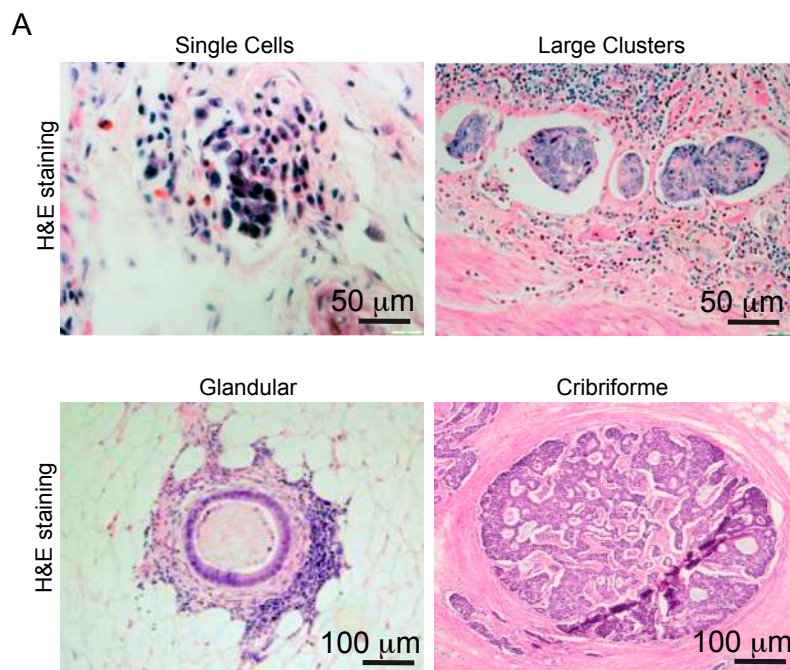


Figure R27. Different observed patterns of tumor vascular infiltration. (A) Microscopic images of H&E-stained paraffin-embedded CRC samples including different patterns of tumor vascular infiltration.

Sequential sections were then processed for double IHC analysis of CD31 (endothelial cells) plus ZO-1 or CLDN2. Collectively migrating vascular tumor infiltrates were observed with a high prevalence, many of which showed well-established ZO-1 and/or CLDN2-positive tight junctions (**Figure R28A and R28B**).

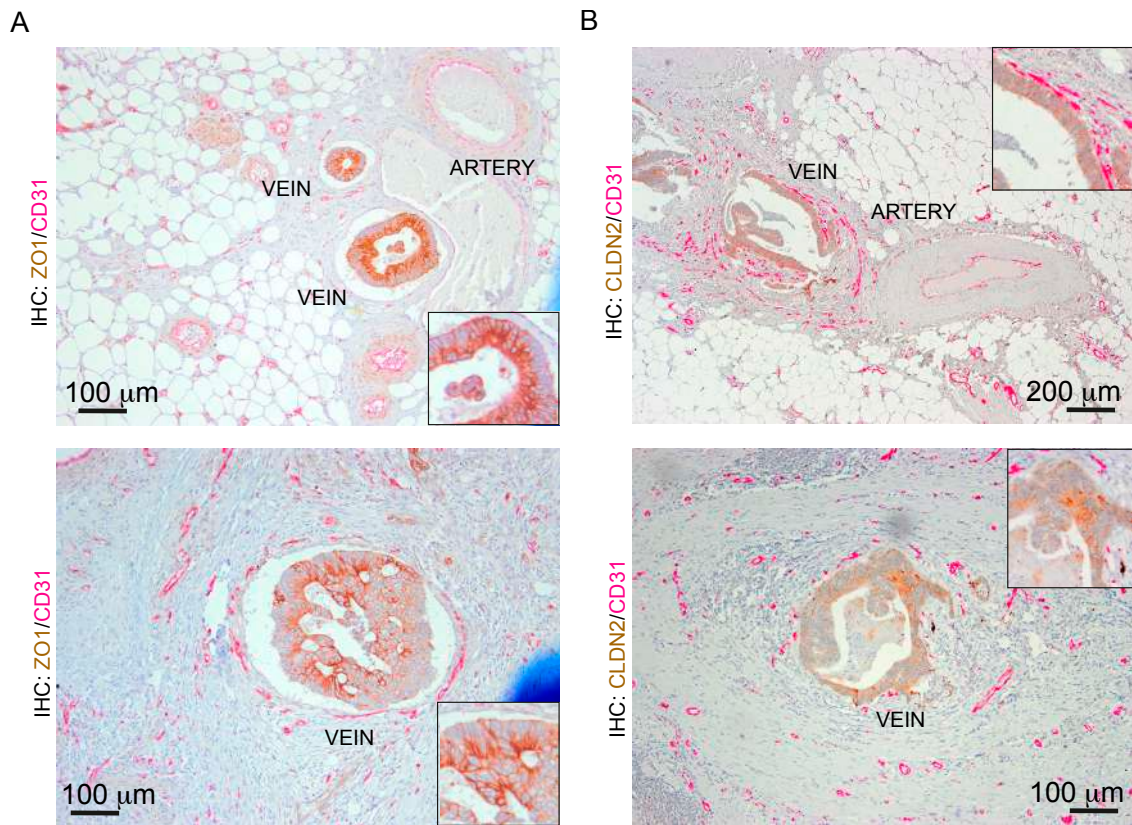


Figure R28. Tight junction proteins ZO-1 and CLDN2 as candidate IHC biomarkers in the invasive clusters of CRC patients. (A-B) Representative images of double IHC of paraffin-embedded CRC samples, stained for CD31 (endothelial) in pink and ZO-1 **(A)** or CLDN2 **(B)** in brown.

Furthermore, and suggesting that IKK α activity also impacts tight junctions and tumor malignancy in CRC patients, we found that low levels of CHUK (codifying for IKK α) together with high levels of TJP1 is the combination of biomarkers that provides the poorest prognostic in stage II/III patients **(Figure R29A)**.

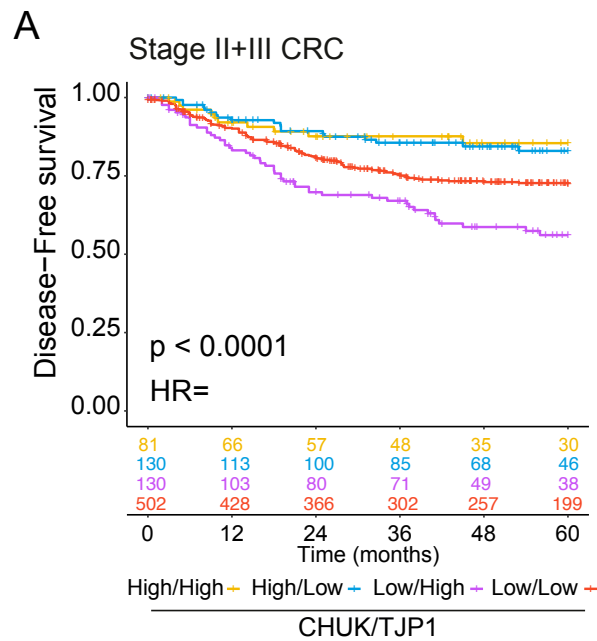


Figure R29. ZO-1 and IKK α predict the risk of metastasis of CRC patients. (A) Kaplan-Meier survival curves showing the disease-free survival of stages II-III CRC patients classified according to the expression levels of CHUK and TJP1 in the tumors. Statistical analysis was performed using a two-sided Wald test. Note the poorest outcome of patients with CHUK-low/TJP1-high tumors.

R7. Activation of the MAPK pathway linked to downregulation of DUSPs in IKK α KO tumor cells increases metastatic growth.

Since hepatic metastases produced by IKK α KO PDO cells were not only superior in number (**Figure R13**) but also bigger, we further characterized their proliferative status in the WT and KO conditions. We noticed increased levels of Ki67 proliferation marker in IKK α KO-derived metastases (**Figure R30A**). We then checked the activation status of the MAPK pathway, which is one of the main regulators of cell proliferation³³² as previously mentioned. By IHC of PDO5-derived liver metastases, we observed a clear accumulation of pERK staining in the invasive front of both WT and IKK α KO metastases, consistent with previous publications^{333,334}. However, pERK staining in the IKK α KO-derived lesions was not restricted to the periphery of the metastatic lesions, but spread throughout the whole tumor area (**Figure R30A**). By WB analysis, we also detected increased pERK levels in the protein lysates from IKK α KO-derived metastases (**Figure R30C**). Notably, we found that vemurafenib treatment also increased pERK levels in WT-derived metastases (**Figure R30C**). This partially counterintuitive result has been previously reported and has been associated with a paradoxical feedback loop activation of the pathway upon BRAF inhibition^{59–61}.

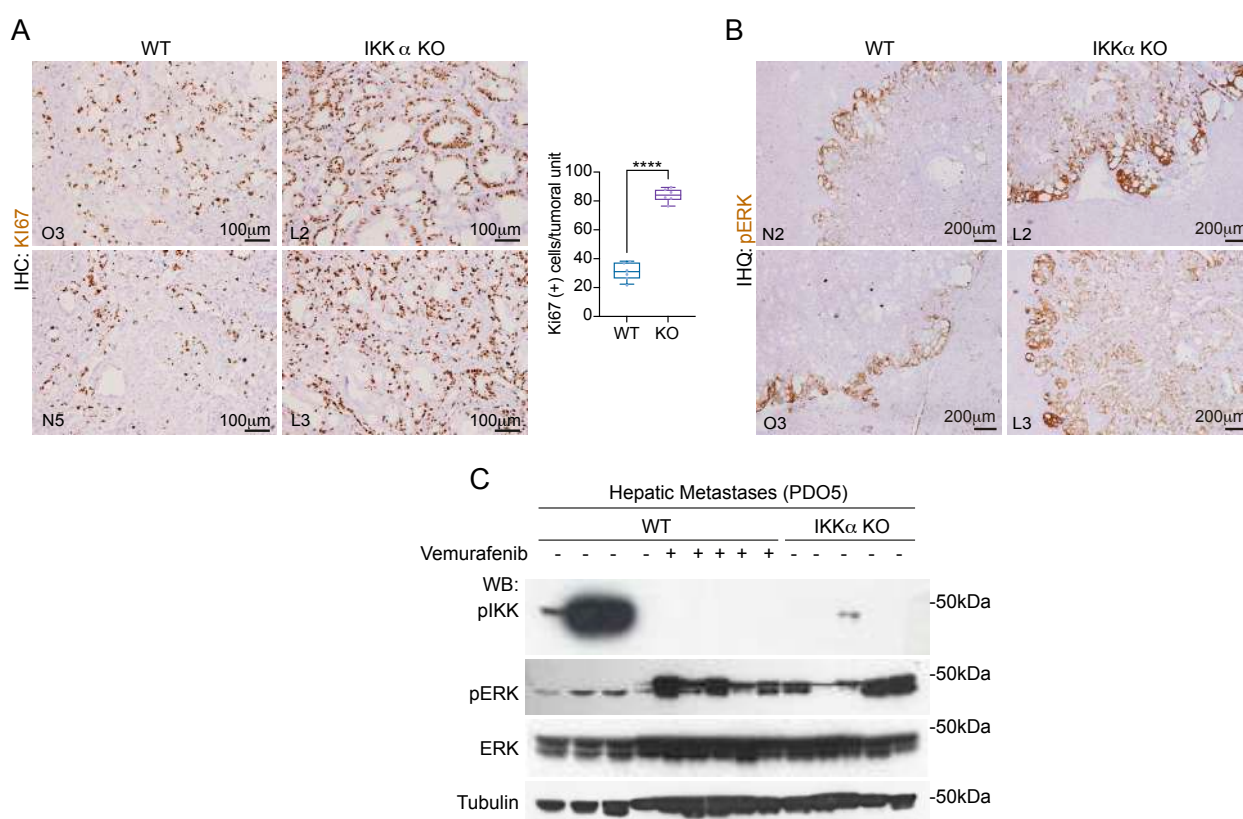


Figure R30. IKK α KO PDO5-derived metastases present increased MAPK pathway signaling. (A-B) Representative IHC images of Ki67 **(A)** and pERK **(B)** in the hepatic metastases derived from PDO5 WT or IKK α KO cells. **(C)** WB analysis of pERK levels in WT untreated, WT-treated with vemurafenib or IKK α KO PDO5-derived metastases.

We then investigated whether IKK α depletion could be affecting one or more MAPK pathway regulators. The Dual-Specificity Phosphatases (DUSP) family of proteins comprises several enzymes that dephosphorylate specific elements in the MAPK pathway, including MEK1/2, ERK, p38 or JNK, thereby inhibiting its activity³³⁵. Bulk RNA-seq data of WT and IKK α KO PDO5 cells revealed a clear downregulation of DUSP1, DUSP5 and DUSP10 (**Figure R31A**). We focused on DUSP1 and DUSP5 since both directly target ERK, the MAPK member that appeared affected in our IKK α KO models. DUSP3 was employed as a control for all related experiments, given that it does not target ERK or any other MAPK-related protein.

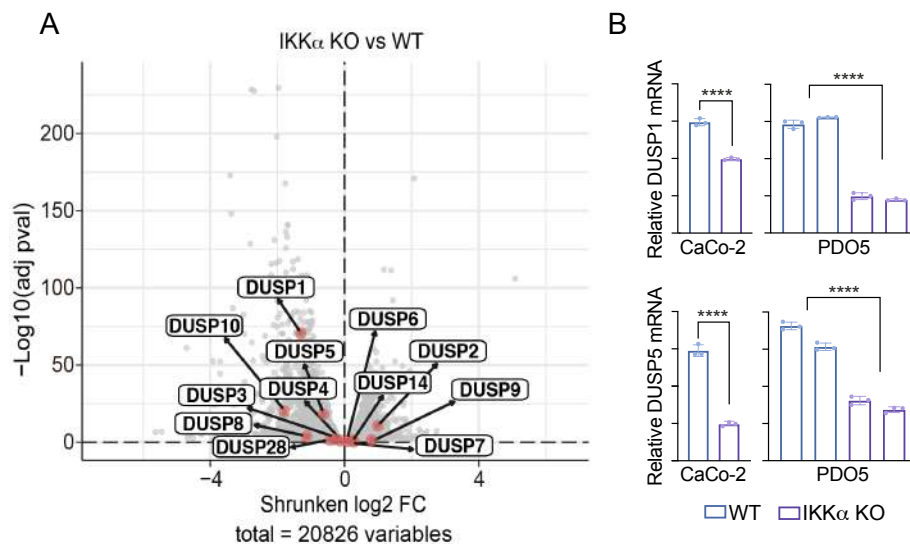


Figure R31. IKK α depletion influences the transcriptional status of DUSPs in different CRC cell types. (A) Volcano plot representation of the bulk RNA-seq data from WT and IKK α KO PDO5 cells, indicating the distribution of DUSP family members detected. **(B)** RT-qPCR analysis of DUSP1 (top) and DUSP5 (bottom) in the indicated WT and IKK α KO cells.

A ChEA (ChIP Enrichment Analysis) from publicly available ChIP data using the Enrichr tool³³⁶ revealed RelA as the top candidate transcription factors regulating the DUSP1, DUSP5, and DUSP10 expression, suggesting their NF- κ B/IKK α -dependent regulation (**Figure R32A**). In agreement with this possibility, the top heat of the analysis, NUCKS1, has been recently linked with NF- κ B/RelA transcriptional regulation in different models^{337–339}. To evaluate the hypothesis that DUSPs are regulated via NF- κ B/RelA, we treated CaCo-2 CRC cells with the canonical NF- κ B-activating factor tumor necrosis factor alpha (TNF α) or TNF α plus BAY65 (IKK β inhibitor). Our results demonstrated that TNF α treatment induced the upregulation of DUSP1 and DUSP5, which was reverted by BAY65 pre-incubation (**Figure R32B**).

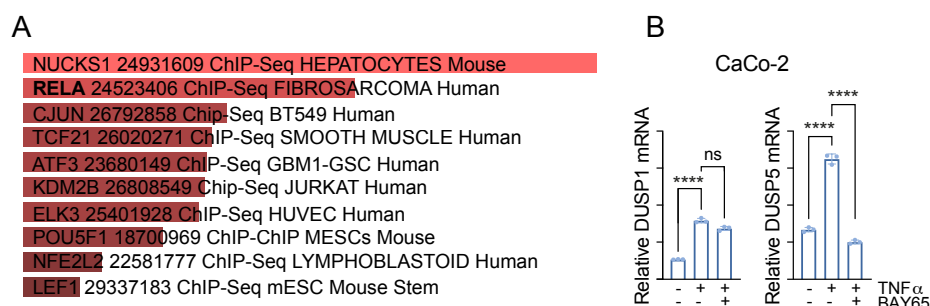


Figure R32. DUSPs transcriptional regulation is NF- κ B/RelA-dependent. (A) Bar graph representing ChEA analysis of DUSP1, DUSP5 and DUSP10 using Enrichr tool (public data). **(B)** RT-qPCR analysis of DUSP1 (left), DUSP3 (center) and DUSP5 (right) in CaCo-2 cells upon treatment with TNF α and BAY65.

We then analyzed DUSPs protein levels in PDO5-derived metastases. We detected lower DUSP1 (**Figure R33A**) and DUSP5 (**Figure R33B**) staining in IKK α KO-derived metastases, in line with RNA downregulation and the higher pERK protein levels.

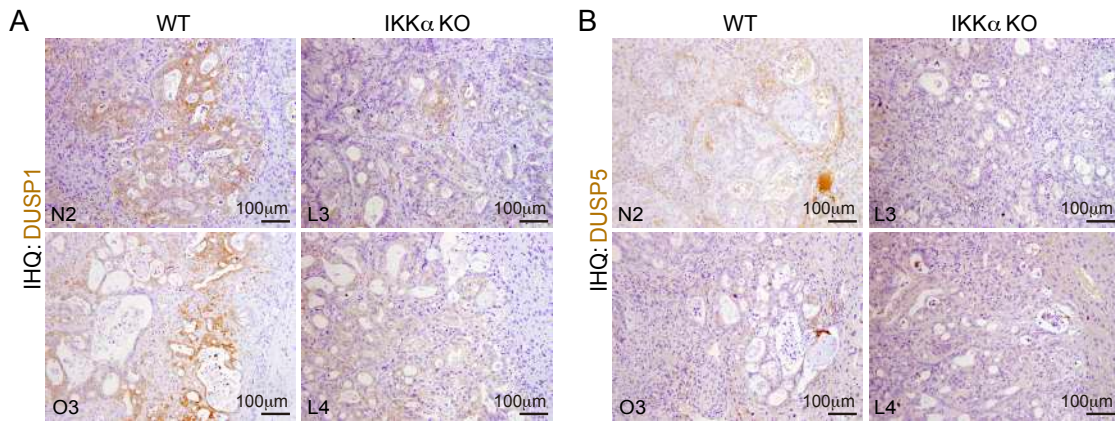


Figure R33. DUSP1 and DUSP5 staining is increased in PDO5 IKK α KO-derived metastases. (A-B) Representative images of the immunohistochemistry analysis of DUSP1 (**A**) and DUSP5 (**B**) in WT and IKK α KO-derived metastases.

To further confirm that the aberrant MAPK activation observed in IKK α KO cells was the result of DUSP1/5 downregulation, we generated doxycycline-inducible DUSP constructs (i-DUSP1, i-DUSP5, and i-DUSP3) and transduced them into IKK α KO cells. All transfected cells were successfully reconstituted (**Figures R34A, R34B and R34C**). Ectopic expression of DUSP1 or DUSP5 after doxycycline treatment was sufficient to abrogate pERK activation in CaCo-2 IKK α KO cells (**Figure R34A and R34B**). In addition, DUSP1/5 expression resulted in increased pMEK levels, likely as a mechanism to attempt to compensate for defective ERK phosphorylation (which is its phosphorylation substrate). Consistent with previously published studies³³⁵, DUSP3 was unable to reduce pERK because it does not target the ERK protein (**Figure R34C**).

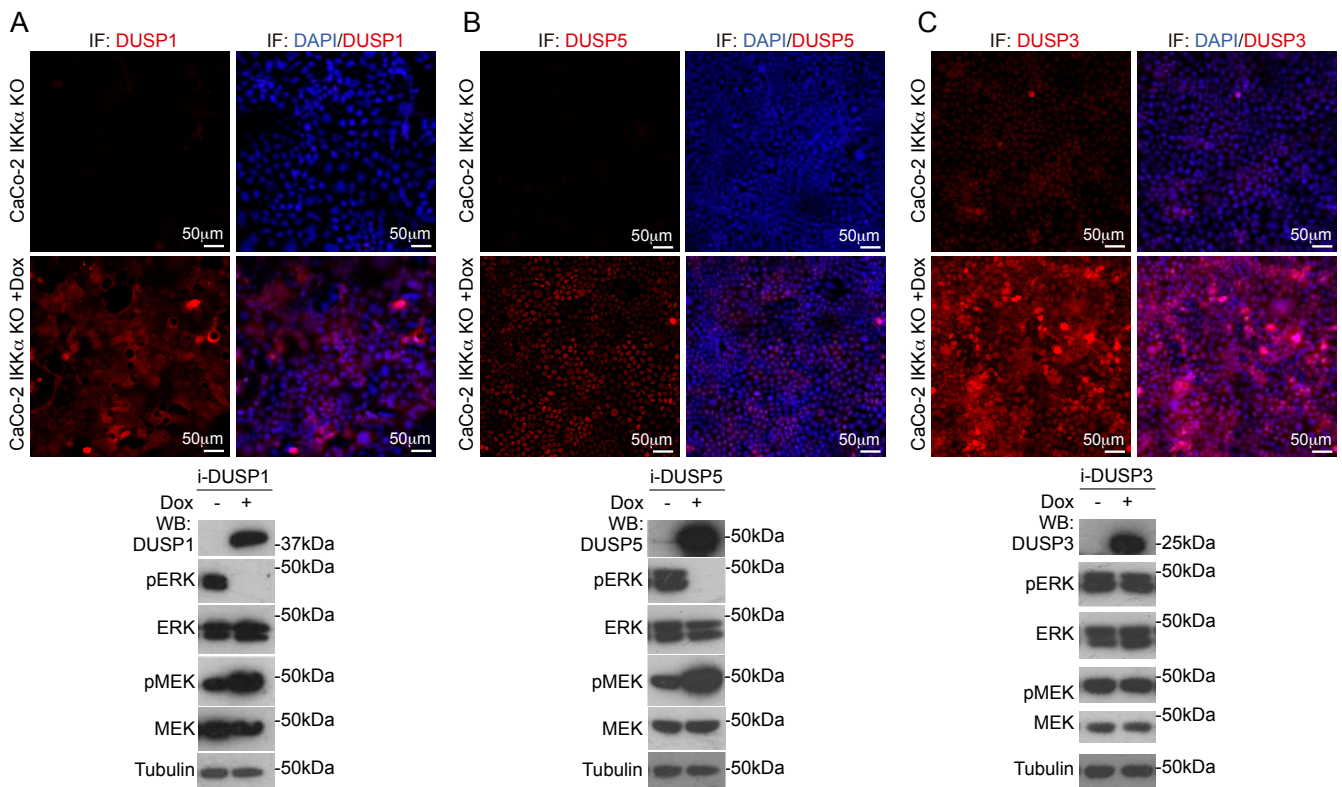


Figure R34. i-DUSPs constructs increase DUSPs presence in CaCo-2 IKK α depleted cells and block pERK activation. (A-C) Representative images of the immunohistochemistry analysis of DUSP1 (A), DUSP5 (B) and DUSP3 (C) in CaCo-2 IKK α KO cells transfected with i-DUSP1, i-DUSP5 and i-DUSP3 respectively and WB validation for each cell line.

In **Figure R7B**, we showed that IKK α KO cells exhibited increased TIC activity *in vitro*. We further investigated the role of DUSPs in this process. Overexpression of DUSP1 or DUSP5 in IKK α KO CaCo-2 cells resulted in a reduction in the growth of 3D structures generated without affecting the number of spheres formed (**Figure R35A and R35B**).

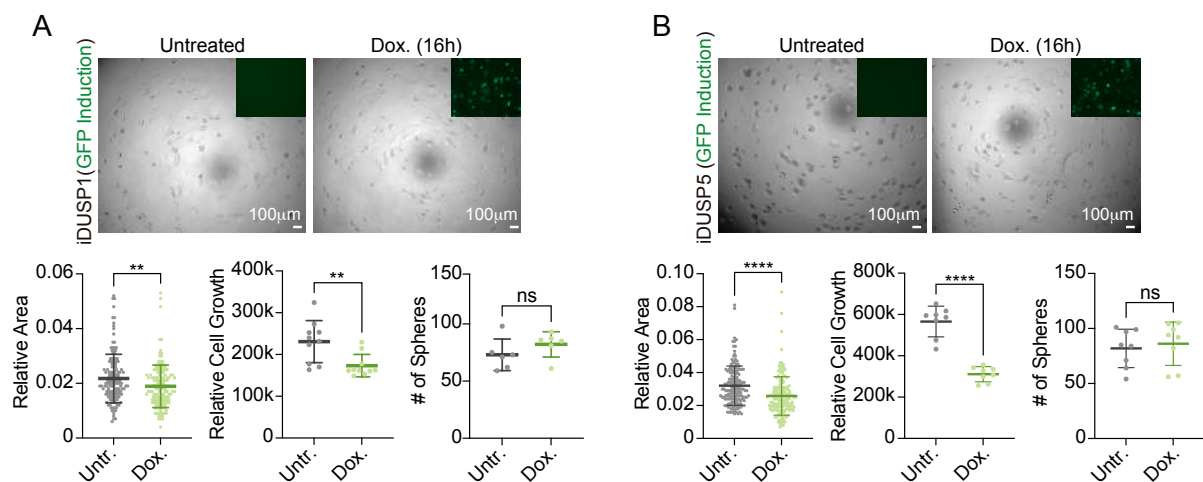


Figure R35. DUSP1 or DUSP5 overexpression reduce tumoral growth *in vitro*. (A-B) Clonogenic assay from

i-DUSP1 **(A)** and i-DUSP5 **(B)** of IKK α KO CaCo-2 cells. Representative microscopic images, and quantification of the spheres area, cell growth and number of spheres obtained per well.

Since DUSP1 and DUSP5 have been demonstrated to suppress pERK and subsequently inhibit the growth of 3D tumoral structures *in vitro*, we hypothesized that pharmacological blockade of ERK phosphorylation may potentially reduce metastatic growth *in vivo*. First, we established an *in vitro* strategy to block ERK activation by treating CRC cells with selumetinib, which completely abrogates ERK activation (**Figure R36A**). *In vivo*, selumetinib treatment reverted the metastatic growth of IKK α KO PDO5 (**Figure R36B**). These data indicate that elevated MAPK activity (in particular of the ERK pathway) in IKK α KO cells facilitates metastatic growth once tumor cells have colonized the target organs.

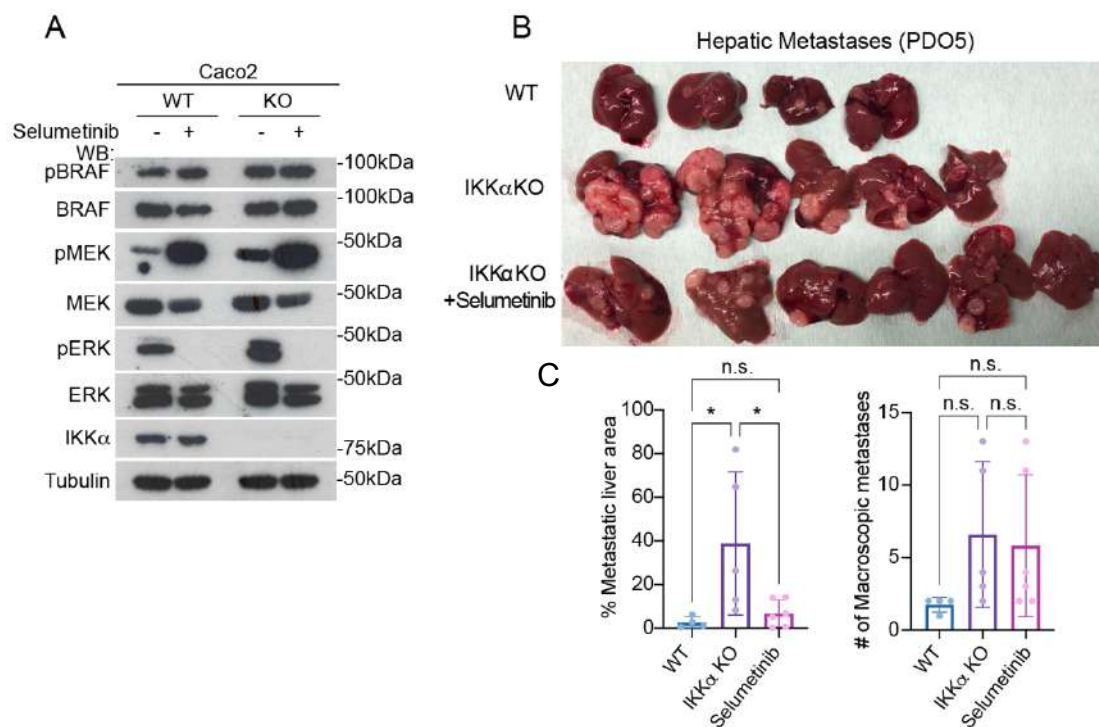


Figure R36. MEK inhibition abrogates pERK activation and reduces the growth of PDO5 IKK α KO-derived metastases. (A) WB analysis of MAPK members in CaCo-2 WT and IKK α KO cells untreated or treated with selumetinib at 0,5 μ M O/N. **(B)** Photograph of the hepatic metastases developed in nude mice after intrasplenic injection of WT or IKK α KO PDO5 cells. One experimental group was treated with selumetinib. Quantification of metastatic area and number of metastases. **(C)** Quantification of metastatic area and number of metastases.

Finally, we focused on the clinical setting of MAPK-targeted therapies. Currently, BRAF inhibitors are most commonly used in combination with MEK inhibitors in different tumor types^{62,340–344}. We found that vemurafenib plus selumetinib combination reduced the number of microscopic metastases developed by WT PDO5 in nude mice (**Figure R37A** and **R37B**). These results confirm that the increased metastatic growth observed upon vemurafenib treatment was caused by the paradoxical feedback loop activation of MAPK.



Figure R37. Combination of BRAFi plus MEKi reduces metastatic potential of WT PDO5 cells. (A) Photograph of the hepatic metastases developed in nude mice after intrasplenic injection of WT PDO5. One experimental group was treated with vemurafenib, and another experimental group was treated with vemurafenib plus selumetinib. **(B)** Quantification of the number of microscopic hepatic metastases.

RESULTS: PART II

R8. A common domain of I κ B α binds to p65 and histones H2A and H4.

We aimed to investigate the determinants of I κ B α association with NF- κ B or chromatin/histones. Based on the strict evolutionary conservation of histone tails, we hypothesized that residues of I κ B α involved in histone binding would also be similarly conserved. To differentiate I κ B α residues that are conserved because they participate in other functions besides protein folding (e.g., in protein-protein binding, for surface exposed residues), we derived a classification score named FEEC (fold-excluded evolutionary conservation) that allows identifying conserved residues with functional roles beyond maintaining the structural fold of the protein (see Methods for the FEEC score definition). From the set of 213 I κ B α residues in the crystallographic structure (PDB code: 1NFI, encompassing residues 70 to 282 in the I κ B α sequence; Uniprot entry P25963), we considered 132 residues to have positive FEEC values (**Figure R38A**, upper panels), of which around half (65) are solvent-exposed — solvent-accessible surface area (SASA) higher than 0.2 nm²— and could putatively participate in protein-protein interactions. To validate our model, we classified which residues in the I κ B α /NF- κ B interface could be predicted using the FEEC score alone —interface residues were defined as having more than 20% of their SASA hidden (SASA_h) upon complexation. For the interaction with NF- κ B, 83% (30/36) and 73% (8/11) of I κ B α interface residues interacting with the p65 and p50 subunits, respectively, were correctly included in the set of positive FEEC residues. While SASA_h is derived from a geometric definition of residues belonging to the interface, it does not account for chemical interactions or their strength; residues not participating in significant interactions are still expected to be included in the interface just because nearby interface residues occlude them. Therefore, we repeated our interface analysis considering per-residue interface scores (for details, see Methods) to define their role in the I κ B α and NF- κ B interface more quantitatively. Our method shows that all strongly interacting residues were correctly included in our set of positive FEEC residues (**Figure R39A**). We then mapped the positive FEEC scores to the protein surface to compare their distribution with the location of the residues of the I κ B α /NF- κ B interfaces (obtained from the crystal structure of this complex³⁴⁵), defined either by the per-residue SASA_h, or the interface binding score values. Interestingly, there is a strikingly similar distribution pattern between surface residues with positive FEEC scores and residues participating at the interface (**Figure R38A**), validating the FEEC metric as a predictor of putative binding sites for the I κ B α protein. The N-terminal tail of histone H4 includes many positively charged residues. Thus, logical surface positions for its binding should

include charge complementarity (i.e., negatively charged residues). To identify hot spots for interaction with H4, we considered all the negatively charged surface IκBα residues having positive FEEC scores. Importantly, sequence alignment between the p65-NF-κB Nuclear Localization Signal (NLS) and the H4 N-terminal tail revealed an alpha-helical motif conserved between the two proteins (**Figure 38B**), with different secondary structure prediction methods showing a comparable helical character for the region between K16 and K20 of histone H4 (**Figure R39B**). Based on these data, the most likely IκBα region for binding to histone H4 is coincident with the one binding the p65-NF-κB NLS (**Figure R38C**). Inside this region, NLS of p65-NF-κB makes contact with many IκBα charged and polar residues with positive FEEC scores, including D73, D75, H84, E85, E86, N108 and Q112 that belong to the ANK1 and ANK2 subdomains (**Figure R38D**).

We propose that the same IκBα interface patch that interacts with the p65-NF-κB NLS could mediate the interactions with histone H4.

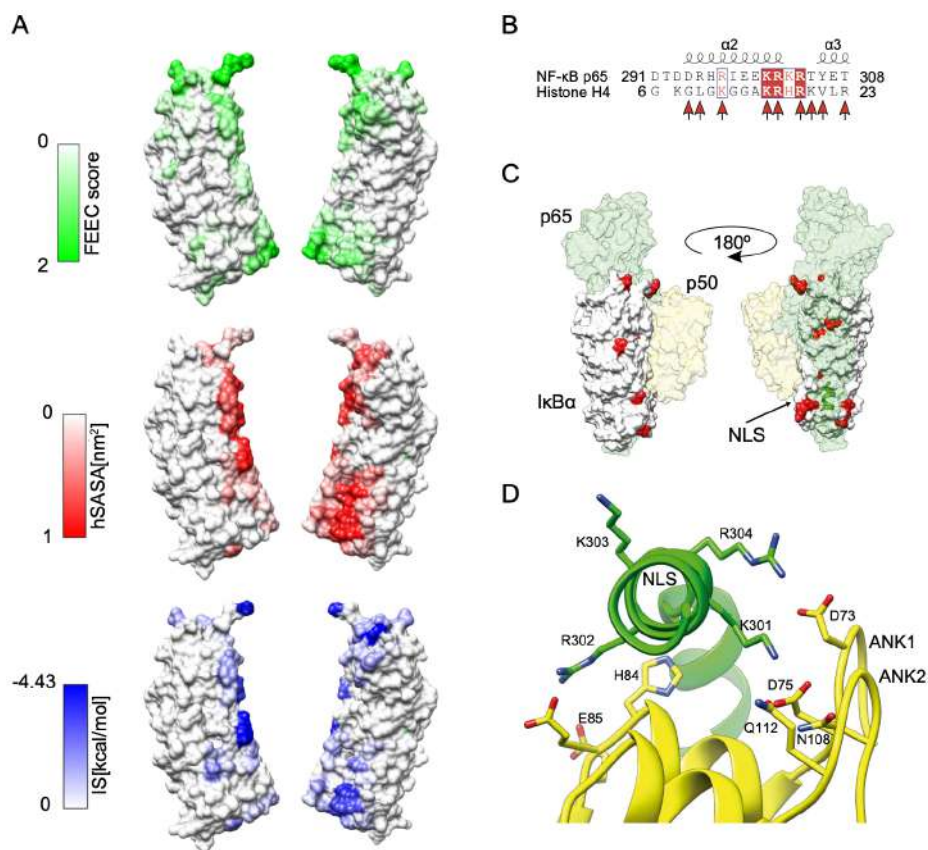


Figure R38. A common domain of IκBα binds to p65 and histones H2A and H4. (A) (Upper) Surface mapping of residues with positive fold-excluded evolutionary conservation scores (maximum value capped at 2 to exclude outliers). (Middle) Fraction of the solvent-accessible surface area hidden upon complexation of the IκBα and NF-κB complex structure. (Bottom) Per-residue interface scores of the IκBα and NF-κB complex structure. The structures are related by a 180o turn— PDB structure 1NFI. **(B)** Alignment of the NF-κB/p65 NLS region to H4 N-terminal tail. Similar positions are indicated in blue rectangles; similar and identical

residues, inside a position, are in red and white letters respectively. Red arrows indicate NF- κ B/p65 residues participating in I κ B α binding. Secondary structure is from PDB structure 3UW9. **(C)** I κ B α (white) and NF- κ B/p65 (green) and p50 (yellow) complex. All negatively charged I κ B α residues with a positive FEEC score appear as red surfaces. The NF- κ B/p65 Nuclear Localization Signal (NLS) region is indicated. **(D)** Interaction of NF- κ B/p65 NLS motif with I κ B α ANK1 and ANK2 repeats. Polar I κ B α residues interacting with the NLS are depicted in yellow, NLS motif, KRKR, is shown in green. They are numbered according to Uniprot entries Q04206 (NF- κ B/p65) and P25963 (I κ B α) — PDB structure 1NFI.

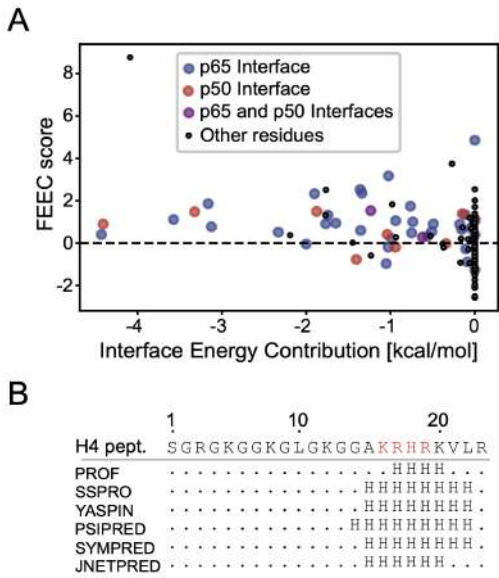


Figure R39. Structural characterization of the N-terminal tail of histone H4. (A) Classification of I κ B α and NF- κ B interface residues based on the Fold- excluded Evolutionary Conservation (FEEC) score. All I κ B α residue energy contributions to the interface with NF- κ B are plotted against their respective FEEC scores. Interface residues between I κ B α and NF- κ B subunits appear in blue (p65 subunit), red (p50 subunit), or purple (p65 and p50 subunits), all remaining residues appear in black circles. **(B)** Secondary structure prediction of the N-terminal peptide of the H4 Histone (H4p). Positions indicated with an H have a helical character according to the prediction method. The NLS motif is displayed as red letters in the H4p sequence.

R9. Two different aminoacidic clusters in IκBα define NF-κB and chromatin interaction.

Consistent with their putative functional relevance, residues D73, D75, H84, E85, E86, N108 and Q112 of IκBα (corresponding to the human sequence, Uniprot entry P25963) are highly conserved from nematodes to humans (**Figure R40A**) and among different IκBα homologues, with the exception of E85 and E86 that were specific for IκBα (**Figure R40B**). To investigate the contribution of these residues to NF-κB and histone binding, we first carried out an in-silico mutagenesis to determine the effect of changing these positions to non- synonymous residues over the structure of IκBα. According to a mutation penalty matrix, all positions will accept an alanine substitution without significantly changing the energy of the system (**Figure R40C**).

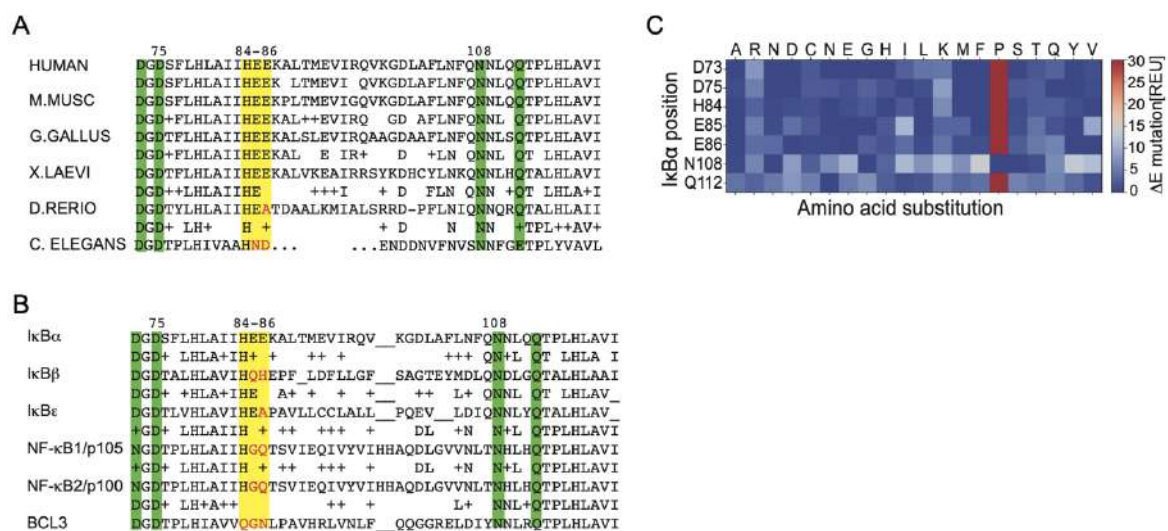


Figure R40. Two different evolutionary conserved Aa clusters of IκBα define NF-κB or histone H2A and H4 binding. (A) Sequence alignment of the IκBα sequence (Aa. 73 to 121 in the human orthologue) in the indicated species. Notice the absolute conservation of residues D75 and N108 (essential for NF-κB binding) and the cluster formed by the acidic residues HEE (essential for histone H4 and PRC2 binding). **(B)** Sequence alignment of the IκBα sequence (Aa. 73 to 121 in the human orthologue) with the indicated IκB homologs. **(C)** Analysis of the energy differences produced by mutating the WT amino acid in the indicated position to any of the other 20 amino acids.

Therefore, we generated different composite mutants carrying alanine substitutions of residues D73, D75, H84, E85, E86, N108 and Q112 (**Figure R41A**) and tested them functionally in pull-down (PD) and co-precipitation (Co-IP) assays. By PD assay of HEK-293T cell lysates, we found that mutating N72, D73, and D75 to alanine (M2 mutant) did not reduce IκBα binding to histones H2A and H4, which was almost abolished by the H84, E85, E86 to alanine mutations (**Figures R41B and R41D**).

Defective association of M3 to histones, which is imposed by H84, E85 and E86 to A mutations, was reverted by the additional substitution of N108 and Q112 to A (see M1 in **Figure R41B**), suggesting that N108 or Q112 positions may favor the competing NF- κ B association. Identical results were obtained by Co-IP with a peptide corresponding to the N terminal tail of histone H4 (aa 1-23) (**Figure R41C**). Notably, histone binding-proficient I κ B α proteins enhanced SUZ12 association to histone H4 *in vitro* (**Figure R41B**), as we previously shown for WT I κ B α ⁹, further supporting the concept that chromatin-bound I κ B α modulates PRC2 function. We then tested the binding capacity of HA-I κ B α mutants expressed in HEK-293T cells to endogenous NF- κ B subunits. We found reduced association of the M3 mutant to p65/NF- κ B compared with wildtype (WT) I κ B α , whereas mutants M1 (N72A, D73A, D75A) and M2 (H84A, E85A, E86A, N108A, Q112A) displayed an absolute lack of p65- and p50-NF- κ B binding (**Figure R41D**). We then generated single-point mutants for residue candidates to impose I κ B α binding specificity. By PD and Co-IP experiments, we found that D75A (**Figure R41E**) and N108A (**Figure R41F**) mutations were sufficient to disrupt I κ B α association to the NF- κ B subunits. In contrast, single mutations of H84, E85 or E86 to alanine failed to preclude histone H4 binding compared with the triple H84A, E85A and E86A mutant (not depicted).

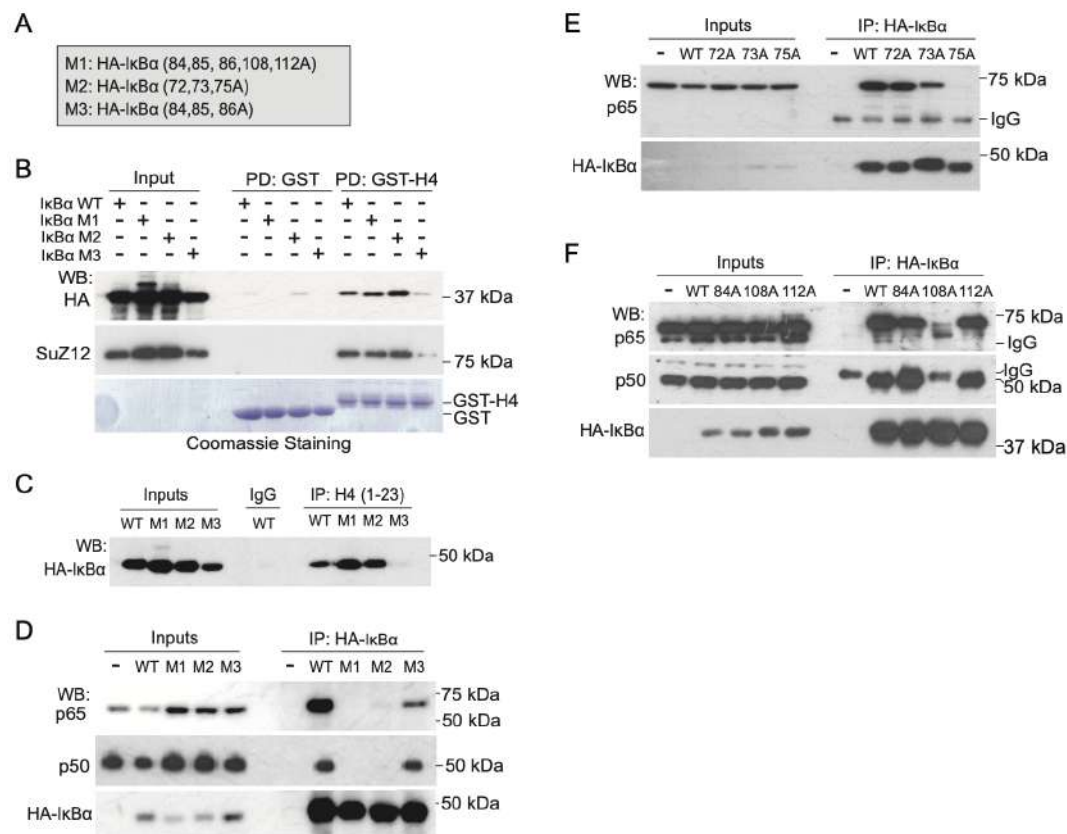


Figure R41. Two different aminoacidic clusters in I κ B α define NF- κ B and histone H4 interaction. (A) Compose mutants generated for evaluation of binding affinity with NF- κ B and histone H4. **(B, C)** Precipitation assays using GST, GST-H4 as bait **(C)** or biotinylated peptides corresponding to amino acids 1-23 of H4 **(D)** and

the indicated compose IκBα mutants expressed in HCT-116 or HEK-293T cells. We determined the presence of IκBα in the precipitates by WB with anti-HA antibody. Coomassie staining in C shows comparable amount of GST or GST-H4 in the assays. **(D)** WB analysis of the indicated NF-κB subunits in the precipitates of the indicated HA-IκBα mutants expressed in HCT-116 cells.

We generated a new mutant, which we called IκBα/β-mimic, that incorporated the changes in the Aa84-86 domain that are present in IκBα (HEE to HQH). By PD assay, we found that IκBα/β-mimic bound to p65 comparable to IκBα (**Figure R42A**), as expected, but showed defective association to histone H4 (**Figure R42B**). In the same pull-down assay, we did not detect any association between histone H4 and endogenous IκBα (**Figure R42B**), which shows a single E46 to A substitution in the histone binding motif relative to IκBα (see **Figure R40B**). From now on, we will refer to IκBα SOF^{ΔNF-κB} as the mutants that display defective NF-κB binding (but retain histone binding) (M1, M2, D75A and N108A) and SOF^{ΔH2A/H4} as the IκBα mutants that fail to bind histones but associate with p65 and p50 (M3 and IκBα/β-mimic).



Figure R42. IκBα/β-mimic *in vitro* characterization. **(A, B)** Co-IP using the anti-IκBα antibody **(A)** and PD assay using GST-H4 as bait **(B)** to determine the relative binding capacity of the IκBα (β-mimic) to p65 (NF-κB) and histones. Notice the high reduction in the binding capacity of the mutant to histone H4 when compared with WT IκBα. Ponceau staining in E is shown to demonstrate comparable amount of GST and GST-H2A/GST-H4 in the assays.

Together, these results support the concept that p65-NF-κB and histone H4 compete for binding to the same IκBα region with specific residues differentially influencing its association with NF-κB and histones.

R10. I κ B α mutants display separation of function (SOF) activity in intestinal cells.

To investigate the functional activity of I κ B α mutants, we reconstituted I κ B α knockout (KO) HT-29 M6 cells (CRC cells) with doxycycline-inducible (i) I κ B α WT, I κ B α SOF $^{\Delta NF-\kappa B}$ (we used N108A) and SOF $^{\Delta H2A/H4}$ (M3) constructs. We first tested the capacity of i-I κ B α WT or SOF mutants (induced by 16 hours of doxycycline treatment) to prevent nuclear translocation of NF- κ B subunits induced by TNF α treatment. As determined by immunofluorescence (IF) analysis, sustained expression of i-I κ B α WT or i-I κ B α SOF $^{\Delta H2A/H4}$ completely abrogated nuclear p65 translocation after 30 and 60 minutes of TNF α treatment. In contrast, i-I κ B α SOF $^{\Delta NF-\kappa B}$ failed to prevent p65 translocation (**Figures R43A and R43B**), consistent with their defective association to NF- κ B factors. We validated the differential effect of i-I κ B α mutants on nuclear translocation of NF- κ B by subcellular fractionation followed by WB analysis of TNF α -treated HT-29 M6 cells (**Figure 3C**). Next, we tested the impact of ectopic i-I κ B α WT or SOF mutants in the TNF α -induced transcription of the canonical NF- κ B target A20 (**Figure 3D**). Consistent with their inhibitory activity on NF- κ B, both I κ B α WT and the SOF $^{\Delta H2A/H4}$ mutant significantly reduced A20 transcriptional activity after 30 and 60 minutes of TNF α treatment when compared with I κ B α SOF $^{\Delta NF-\kappa B}$ (**Figure 3D**).

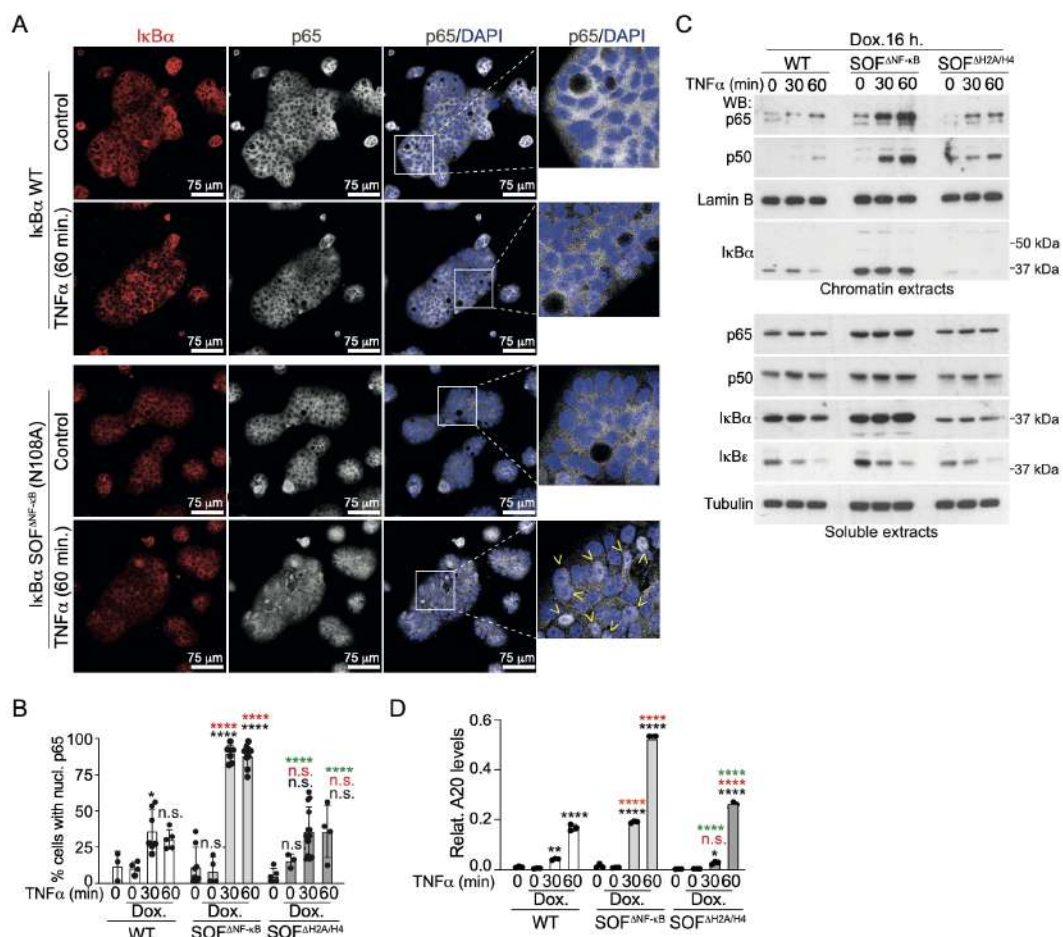


Figure R43. I κ B α mutants display separation of function (SOF) activity in intestinal cells. (A) IF analysis of p65/NF- κ B of I κ B α -deficient HT-29 M6 cells reconstituted (by 16 hours doxycycline treatment) with the SOF $^{\Delta$ NF- κ B mutant N108A or WT I κ B α proteins and then treated with TNF α as indicated. **(B)** Quantification of the percent of cells displaying nuclear p65 in a minimum of 5 colonies per condition counted. **(C)** Western blot analysis of cytoplasmic and chromatin fractions from i-I κ B α WT and SOF reconstituted HT-29 M6 cells. **(D)** qPCR analysis of the canonical NF- κ B target gene A20 in I κ B α KO HT-29 M6 cells reconstituted as indicated. Expression levels of the different genes were calculated relative to GAPDH. In B and D, statistical analysis of differences was determined by Two-way Anova test comparing treatments with no-treatment (black labels), same treatments in WT (red labels) or same treatments in SOF $^{\Delta$ NF- κ B (green labels). ****p-value < 0.0001, ***p-value < 0.0005, **p-value < 0.0025 *p-value < 0.05; n.s.: no significant.

Comparable expression levels of i-I κ B α WT, SOF $^{\Delta$ NF- κ B and SOF $^{\Delta$ H2A/H4 were confirmed by qPCR analysis (**Figure R44**).

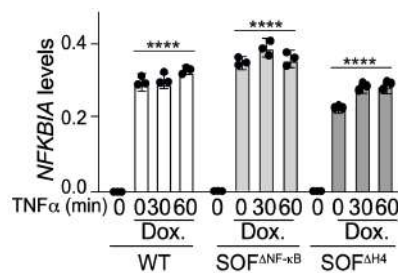


Figure R44. Similar transcriptional induction of I κ B α WT and SOF mutants after doxycycline treatment. qPCR analysis of I κ B α expression (NFKBIA gene) in I κ B α KO HT-29 M6 cells reconstituted with i-I κ B α WT or the indicated SOF mutants, left untreated or treated for 16 hours with doxycycline (Dox.). NFKBIA levels were calculated relative to GAPDH. Bars represent mean values \pm standard error of the mean (s.e.m) from at least 3 independent experiments performed; p values were derived from an unpaired two-tailed t-test, ****p-value<0.0001.

These results support the notion that I κ B α SOF $^{\Delta$ NF- κ B, but not SOF $^{\Delta$ H2A/H4, is defective on NF- κ B regulation.

R11. The $\text{I}\kappa\text{B}\alpha$ $\text{SOF}^{\Delta\text{NF-}\kappa\text{B}}$ mutant N108A rescues the Goblet Cell differentiation $\text{I}\kappa\text{B}\alpha$ depleted cells linked to repression of the ISC program.

HT-29 M6 CRC cells acquire a goblet-cell phenotype upon confluence³⁴⁶, which is precluded by $\text{I}\kappa\text{B}\alpha$ depletion²¹⁰. Defective goblet-cell differentiation in $\text{I}\kappa\text{B}\alpha$ KO HT-29 M6 cells is illustrated by the reduced MUC5AC expression at 7 days post-confluence (dpc) (**Figure 45A**). We tested whether ectopic expression of i- $\text{I}\kappa\text{B}\alpha$ mutants rescued the differentiation capacity of $\text{I}\kappa\text{B}\alpha$ KO HT-29 M6 cells. We initially tested two different $\text{I}\kappa\text{B}\alpha$ induction protocols: i) 16 hours of doxycycline treatment at pre-confluence and culture in fresh medium up to 7 dpc and ii) dox. treatment for the whole period of the experiment. We found that 16 hours of $\text{I}\kappa\text{B}\alpha$ $\text{SOF}^{\Delta\text{NF-}\kappa\text{B}}$ induction were sufficient to restore MUC5AC levels in $\text{I}\kappa\text{B}\alpha$ KO HT-29 M6 cells at levels comparable to i- $\text{I}\kappa\text{B}\alpha$ WT. However, $\text{SOF}^{\Delta\text{H2A/H4}}$ did not revert the defective differentiation of $\text{I}\kappa\text{B}\alpha$ KO cells (**Figure R45B, R45C and R45D**), indicating that $\text{I}\kappa\text{B}\alpha$ chromatin function was the only required for goblet-cell differentiation.

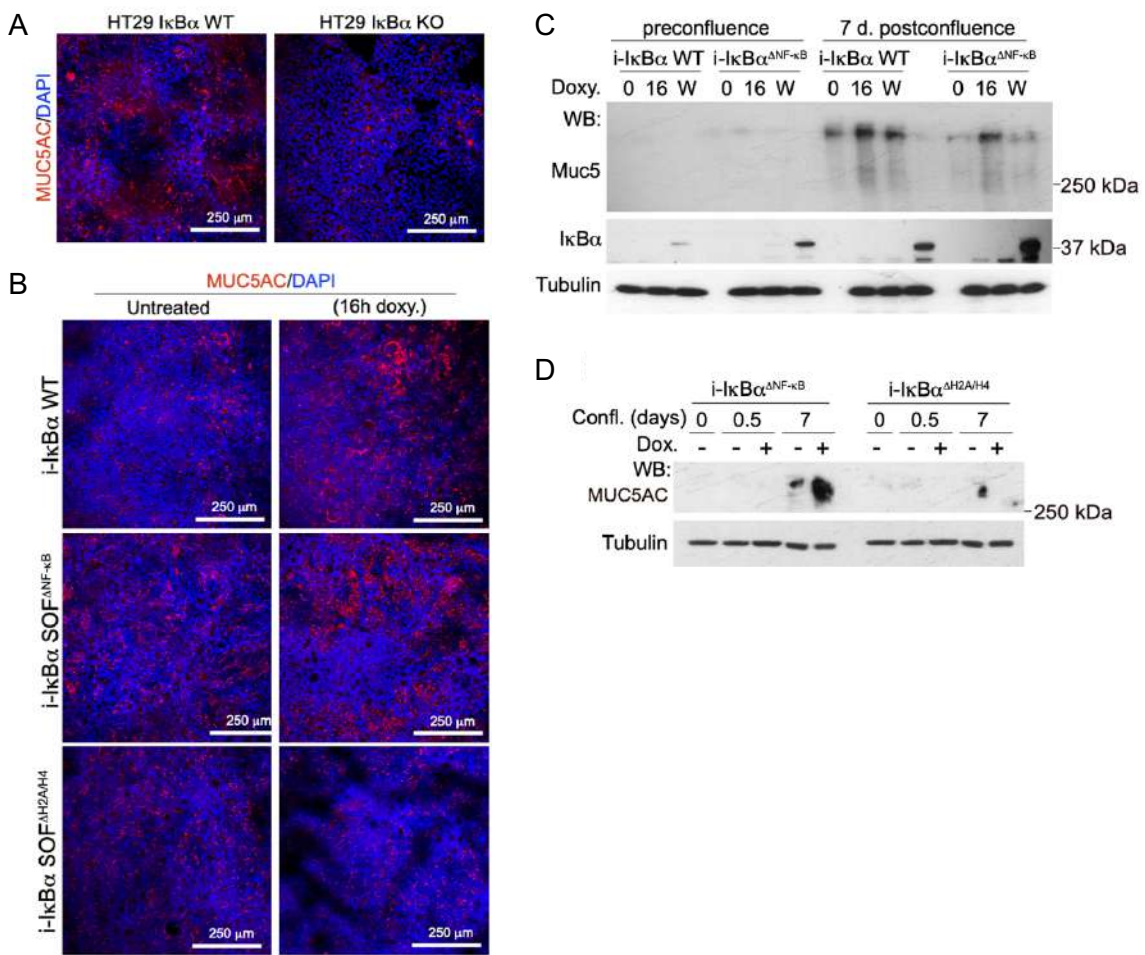


Figure R45. The $\text{I}\kappa\text{B}\alpha$ $\text{SOF}^{\Delta\text{NF-}\kappa\text{B}}$ mutant N108A rescues the Goblet Cell differentiation blockage imposed by $\text{I}\kappa\text{B}\alpha$ deletion. (A, B) IF analysis of WT and $\text{I}\kappa\text{B}\alpha$ KO HT-29 M6 cells (A) and doxycycline-inducible $\text{I}\kappa\text{B}\alpha$ WT, $\text{I}\kappa\text{B}\alpha$ $\text{SOF}^{\Delta\text{NF-}\kappa\text{B}}$ and $\text{SOF}^{\Delta\text{H2A/H4}}$ lines (B). (C, D) Western blot analysis of the differentiation marker MUC5AC in

HT-29 M6 $\text{I}\kappa\text{B}\alpha$ KO cells reconstituted as indicated and collected at pre-confluence or at 0.5 and 7 days of post-confluence. In C, $\text{i-I}\kappa\text{B}\alpha$ expression was induced by treating cells with doxycycline for 16 hours (16), for the whole period of the experiment (W), or left uninduced (0). In D, doxycycline was added for 16 hours at pre- confluence.

To uncover the molecular bases by which $\text{I}\kappa\text{B}\alpha$ regulates cell differentiation, we performed RNA-seq analysis of HT-29 M6 cells reconstituted with $\text{i-I}\kappa\text{B}\alpha$ WT, $\text{SOF}^{\Delta\text{NF-}\kappa\text{B}}$ and $\text{SOF}^{\Delta\text{H2A/H4}}$ for 16 hours (**Figures R46A**). When considering the entire transcriptome, the first two principal components from the PCA grouped each cell line separately (**Figure R46B**). However, PC3 captured the variance associated with doxycycline-treated and untreated cells (**Figure R46C**).

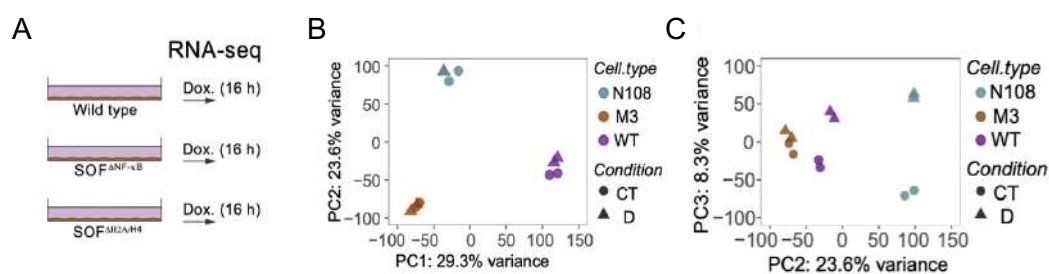


Figure R46. RNA-seq characterization of $\text{i-I}\kappa\text{B}\alpha$ cell lines. **(A)** Scheme of the strategy used to study the transcriptional impact of $\text{i-I}\kappa\text{B}\alpha$ WT and SOF expression. **(B)** Principal Component Analysis of the RNA-seq data from untreated and doxycycline-treated SOF reconstituted HT29 cells. **(C)** Principal Component Analysis (PCA) results over whole transcriptome from bulk RNA-seq data (22,993 genes) for the complete dataset showing second and third PCs.

Further evaluation of differentially expressed genes (DEGs) following doxycycline induction demonstrated that $\text{SOF}^{\Delta\text{NF-}\kappa\text{B}}$ imposed the highest transcriptional effect leading to downregulation of 652 genes and upregulation of 278 genes, considering an adjusted p-value of $p < 0.05$. With these criteria, we did not detect any differentially expressed gene upon ectopic expression of $\text{SOF}^{\Delta\text{NF-}\kappa\text{B}}$, indicating that transcriptional control by $\text{I}\kappa\text{B}\alpha$ in HT-29 M6 cells is $\text{I}\kappa\text{B}\alpha$ dependent but $\text{NF-}\kappa\text{B}$ independent. $\text{I}\kappa\text{B}\alpha$ WT expression imposed an intermediate effect on gene transcription (**Figures R47A, R47B and R47C**). Gene Set Enrichment Analysis (GSEA) from $\text{i-I}\kappa\text{B}\alpha$ WT and $\text{SOF}^{\Delta\text{NF-}\kappa\text{B}}$ revealed a significant inverse correlation ($p < 0.05$) between $\text{i-I}\kappa\text{B}\alpha$ WT expression and $\text{TNFA_SIGNALING_VIA_NF}\kappa\text{B}$, as expected, whereas we did not detect any alteration associated with $\text{NF-}\kappa\text{B}$ signaling in $\text{i-I}\kappa\text{B}\alpha$ $\text{SOF}^{\Delta\text{NF-}\kappa\text{B}}$ -expressing cells (**Figures R47D and R47E**). Overrepresentation analysis of downregulated DEGs against the ENCODE/ChEA Transcription Factors dataset identified RelA (p65) and NFE2L2/NRF2, the latter of which has pleiotropic roles in

the immune response³⁴⁷ and NF- κ B regulation in multiple systems^{347–351}, as the factors most likely associated with i-IkBa WT-mediated gene repression (**Figure R47F**). In contrast, NF- κ B-related factors were not found to be associated with i-IkBa SOF^{ΔNF- κ B}-mediated repression, but we identified the EZH2-related factors SOX2 and MYC^{352,353}, the PRC2 subunit SUZ12 and the chromatin repressor PPAR delta³⁵⁴ in this analysis (**Figure R47G**). By GSEA, we found that transcriptional changes imposed by i-IkBa WT and SOF^{ΔNF- κ B} inversely correlated with the intestinal stem cell (ISC) signature of Muñoz et al³⁵⁵ (**Figures R47H and R47I**). Stem cell genes specifically repressed by i-IkBa SOF^{ΔNF- κ B} includes CD44, ADRA2A, SLC12A2 or MYC (**Figure R47B**).

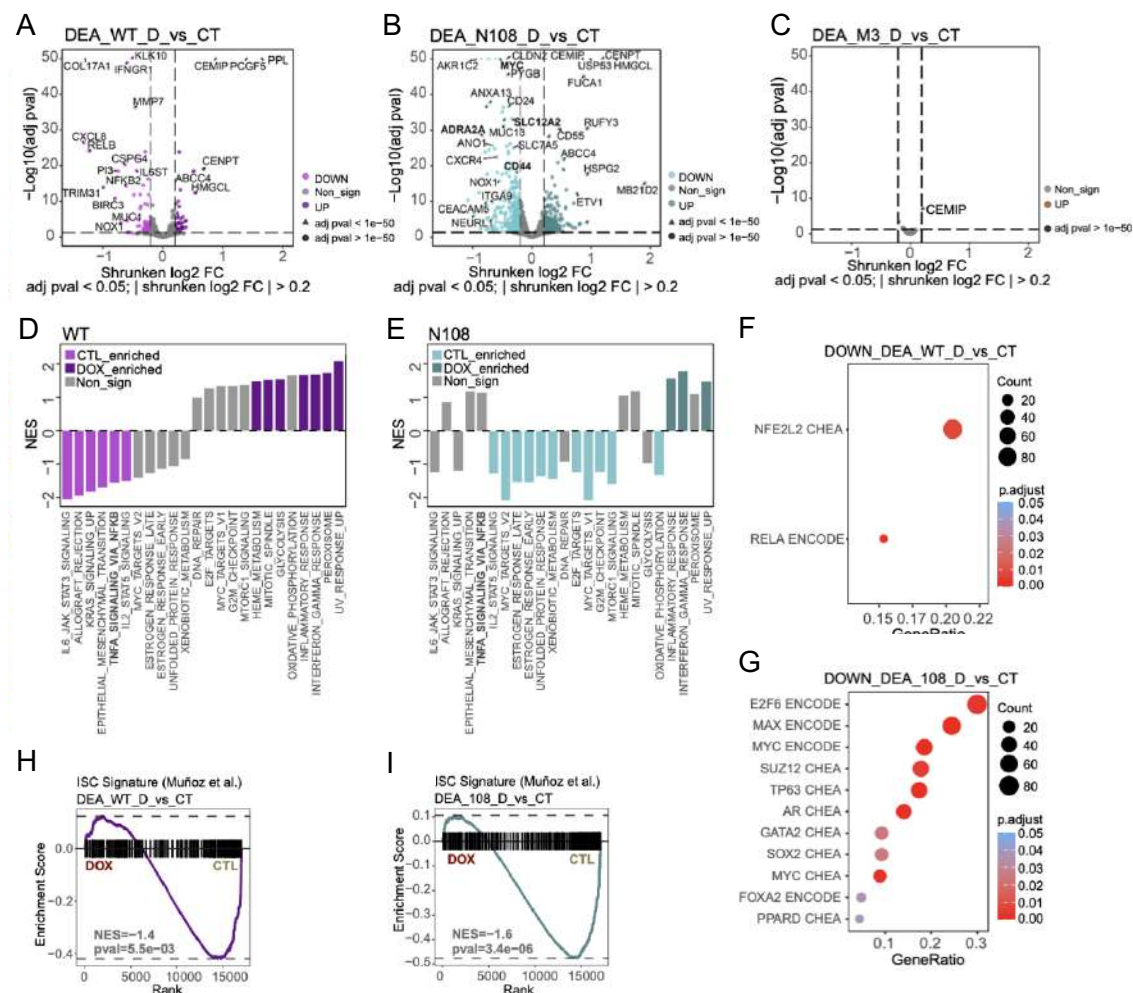


Figure R47. Transcriptional characterization of the rescue of goblet cell differentiation by the IkBa SOF^{ΔNF- κ B} mutant 108A. (A, B, C) Volcano plots from RNA-seq differential expression analysis of i-IkBa WT (A), IkBa SOF^{ΔNF- κ B} (N108A) (B) and IkBa SOF^{H2A/H4} (C) when comparing doxycycline-treated and untreated samples. Representative genes are highlighted (FDR adjusted p-value < 0.05 and absolute shrunken log2 fold change > 0.2). Some relevant NF- κ B-related genes (i.e. RelB, MMP7 or CXCL8) and intestinal stem cell genes (i.e. CD44, CD24 or MYC) are shown. (D, E) Barplot showing GSEA results from doxycycline-treated compared with untreated IkBa WT (D) and IkBa SOF^{ΔNF- κ B} (N108A) (E) samples against MSigDB Hallmark database. Colored

bars refer to enriched pathways (FDR adjusted p-value < 0.05) while grey bars indicate non-significant pathways. Only those statistically significant pathways in any of the two cell types are included. **(F, G)** Analysis of transcription factors (TFs) likely contributing to the differential gene transcription upon i-IkB α SOF^{ΔNF-κB} and WT expression. Dotplot showing overrepresented TFs from the ENCODE and ChEA Consensus TFs database when considering differentially down-regulated genes (DEGs) upon doxycycline treatment of i-IkB α WT **(F)** and SOF^{ΔNF-κB} (N108) **(G)** cell lines against untreated samples (FDR adjusted p-value < 0.05). GeneRatio refers to the DEGs ratio within a particular TF set (target genes). Count refers to the absolute DEGs number within a particular TF set. **(H, I)** GSEA results from doxycycline-treated (16 hours) and untreated i-IkB α WT **(H)** or i-IkB α SOF^{ΔNF-κB} (N108A) **(I)** samples against an Intestinal Stem Cell (ISC) signature composed of 510 genes (Muñoz et al³⁵⁵).

Together these data suggest that the ability of chromatin-competent IκBs (WT and SOF^{ΔNF-κB}) to restore goblet cell differentiation of HT-29 M6 cells is associated with their ability to negatively regulate the intestinal stem cell program.

R12. IκB α binds to genomic regions at genes involved in cell development and neuronal signaling

Finally, we investigated whether the transcriptional regulation imposed by IκB α was actually related to its ability to bind the chromatin at specific genomic regions or genes. Since commercially available anti-IκB α antibodies gave variable results in the ChIP assay, we knocked-in a 3xFLAG tag into the endogenous IκB α locus in HCT-116 and HT-29 M6 cells, and used the anti-FLAG antibody for ChIP-seq analysis. Considering 3 biological replicates per cell line performed, we obtained a consensus peakset of 2,489 IκB α -FLAG peaks in HCT-116 cells (1,484 of which with fold-change > 6, relative to the input), and 610 peaks in HT-29 M6 cells (410 of which with fold-change > 6) corresponding to 807 and 364 annotated genes, respectively (286 genes in common). However, we also noticed a high number of promoter regions in the IκB α -FLAG precipitates (16.4%). Compared with the average distribution of different genomic regions, 74% intergenic, 24% intronic and 1-2% exonic/promoter³⁵⁶, these results suggest that IκB α -FLAG is mainly located in gene-enriched regions (**Figure R48A**). Overrepresentation analysis of annotated genes to identified IκB α -FLAG peaks against Gene Ontology biological terms revealed overrepresented biological functions highly specific such as neuronal signaling, which is being increasingly implicated in colorectal tumor growth and metastasis (reviewed in ³⁰¹), and cell development (**Figure R48B**). We confirmed IκB α recruitment to the stem cell genes EPHA2, LRIG1 and WNT3A^{355,357–359} and a subset of the genes repressed upon i-IκB α SOF^{ΔNF-κB} expression including ANXA13, SLC12A2, TRIM29 or AXIN2 (**Figure**

R48C), previously identified as regulators of intestinal homeostasis and cancer^{355,360–363}. Collectively, we have here provided, for the first time, the identification of the IκBα domains that define its association with NF-κB or histones, and used this information to generate mutant molecules defective in either NF-κB or histone binding.

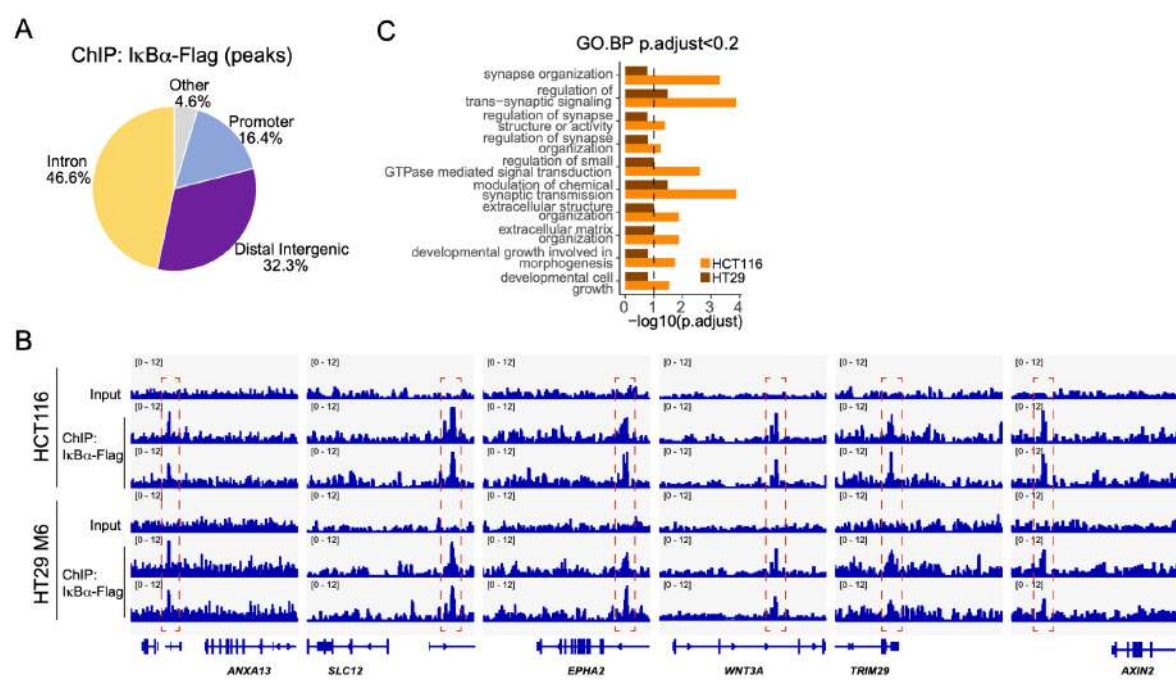


Figure R48. i-IκBα WT and SOF^{ΔNF-κB} expression regulates a specific intestinal stem cell program with impact on intestinal cell differentiation. **(A)** Pie chart depicting the genomic distribution of the IκBα peaks identified in HT-29 cells. Results obtained from HCT-116 were primarily identical and are not included in the figure. **(B)** Barplot with overrepresented (FDR adjusted p-value < 0.2 in at least one cell line) Gene Ontology Biological Processes (GO BP) terms obtained from testing genes annotated to IκBα peaks. Vertical line refers to an adjusted p-value of 0.1. **(C)** Tracks visualization from Integrative Genomics Browser (IGV) tool showing called IκBα peaks in selected genes.

Taking advantage of these separation-of-function (SOF) IκBα mutants, we demonstrated that the NF-κB-independent functions of IκBα are sufficient to regulate specific gene transcription with implications for intestinal differentiation.

DISCUSSION

DISCUSSION: PART I

This study reveals a novel function of IKK α kinase in regulating cell-cell contacts, particularly tight junctions, during the metastatic process. The deficiency of IKK α leads to the formation and accumulation of abnormal tight junction-like structures. Elevated levels of tight junction proteins in CRC cells promote collective migration, enhancing their pro-metastatic potential, which can be detected in vascular infiltrates at time of diagnosis. This Increased clustering of cancer cells correlates with greater metastatic aggressiveness. However, disrupting tight junctions through interfering by two different approaches (CLDNi and shCLDN2) has proven effective in significantly reducing the metastatic capacity and aggressiveness of CRC cells, nearly abolishing their ability to spread *in vivo*. These findings provide preliminary evidence for the potential of targeting cell-cell contact components, such CLDN2, in treating mCRC. Moving forward, we plan to further investigate the development of novel therapies targeting CLDN2 for the treatment and prevention of metastasis in CRC patients. This discussion highlights the most significant findings of the study within the context of current knowledge in the field, while also addressing key limitations and outlining future directions for this work.

D1. Pro-tumorigenic vs anti-metastatic functions of IKK α .

The IKK α kinase, as well as other members of the NF- κ B pathway, are generally considered to be drivers of tumorigenesis^{364–366} and metastasis^{220,221,367}, making IKK α inhibitors potential candidate targets for cancer treatment^{328,368–370}. Nevertheless, these compounds showed critical toxicity *in vivo*, precluding their use for cancer treatment. In this work, using multiple experimental strategies and different IKK α KO CRC models, we found that, in addition to its canonical NF- κ B roles, IKK α activity is required for the proper regulation of cell-cell contacts. Thus, IKK α depletion or inhibition led to a general disorganization of tight and adherens junctions, which resulted in a reduction of cell migration and a change in the migratory mode of cancer cells from single-cell migration (classically associated with EMT and single CTCs) towards collective migration (CTC clusters). A reduced migratory and invasive capacity *in vitro* has also been observed in prostate cancer cells using general IKK inhibitors³⁷¹ which was interpreted, without a formal demonstration, as an anti-metastatic effect. These results are consistent with that obtained in this work. Altered ZO-1 distribution leading to increased collective migration is also observed in CRC cell lines expressing high levels of proteolipid protein 2 (PLP2)³⁷². As a possible mechanism, an interaction between ZO-1 and PLP2 has

been proposed in addition to the involvement of the Rac family small GTPase 1 (Rac1). Interestingly, PLP2 is significantly increased in the liver metastases derived from PDO5 cells (data not shown), suggesting that altered ZO-1 activity is still required during the metastatic colonization process and not only for the process of dissemination, most likely, as CTC clusters.

Depletion of IKK α has been shown to be tumor promoting not only in CRC but also in other cancer systems. For example, lung-specific IKK α deletion induced by intratracheally injected adenovirus-Cre causes spontaneous lung adenocarcinoma³⁷³. Reintroduction of IKK α reduced tumor incidence and tumor cell-derived burden in the lung and suppressed the expression of several cytokines, suggesting that impaired IKK α expression in cancer cells also regulates the tumor microenvironment. However, our findings indicating that IKK α acts as a metastasis suppressor have only been described in CRC. Therefore, it would be of great interest to investigate this IKK α function in other tumor types.

D2. Tight junction elements as key modulators of cancer cell migration mode.

Tight junctions are the most apical intercellular junctions found in epithelial and endothelial cells. Here, we have experimentally demonstrated that changes in the migratory mode associated with differential tight junction activity, downstream of IKK α regulation, have a more pronounced impact than the speed of cancer cells migration on the *in vivo* metastatic capacity of cancer cells. This concept, supported by work from several groups^{138,146,374–376}, contrasts with the classical view of loss of epithelial features and acquisition of mesenchymal features (EMT) as the main pathway for metastasis^{116–118}, which has recently been modulated by incorporating the concept of EMT transition states, also known as hybrid states^{123,124,377}. The cumulative evidence that collective cancer cell migration is more efficient in producing metastasis may require a rethinking not only of the concept of pure EMT as a metastatic driver, which is still in the minds of many researchers, but also of the well-established concept that poorly differentiated tumors with a clear EMT phenotype should by definition be more metastatic. In this sense, we have shown that more cohesive patient-derived organoids are more metastatic in preclinical *in vivo* assays (**Figure R15 and R16 and R17**), but we have also robustly detected large tumor clusters and glandular structures invading the vasculature adjacent to well-differentiated primary tumors from CRC patient samples.

It is worth noting that after discovering that PDO cells with higher clustering capacity were more metastatic in our preclinical mouse model, we discussed the possibility of isolating CTCs, both from

our *in vivo* experiments and from patient samples (liquid biopsy) to further study their properties. However, this idea was discarded when we realized that all these CTCs sorting technologies⁷⁰ are extremely expensive and would be highly difficult to translate into clinical routine. In addition, the results obtained for both sensitivity and specificity will vary widely between different approaches, making translation and standardization complex.

The histopathological characterization of paraffin-embedded surgical tumor specimens at time of diagnosis is the standard for CRC diagnosis. The presence of vascular tumor infiltrates is a highly relevant part of the information provided by pathologist's report. We believe that identifying the presence of these infiltrating tumor clusters in the vessels surrounding the tumor tissue at the time of diagnosis may represent a prognostic factor in CRC. Therefore, the incorporation of this relevant information into routine histopathological reports would be a useful tool for the follow-up of patients at high risk of metastasis. Currently, we are retrospectively re-analyzing paraffin blocks of embedded colorectal tumor samples that present vascular tumor infiltration. In this sense, we aim to establish the correlation between the presence of CTCs clusters of different morphologies (e.g., solid, glandular, or cribriform) with CRC patient outcome, survival, progression disease-free survival or even chemotherapeutic treatment response. In addition, we will investigate by IHC whether the levels and expression patterns of specific tight junction proteins in these samples (initially focusing on ZO-1 and CLDN2) allow for better patient prognosis and stratification.

D3. CHUK and TJP1 as novel biomarkers of relapse risk in CRC patients.

In this work, we described the role of IKK α in regulating tight junction proteins ZO-1 and CLDN2 with impact in CRC cells metastatic potential. To date, it has not been studied whether a decrease of IKK α activity/expression has a role in the stabilization of the tight junction contacts in circulating metastatic precursors. Thus, with the aim of evaluating potential relationships, we have generated a CRC patients metacohort using multiple public data sets³¹⁷. Patients with low expression levels of IKK α gene (CHUK) combined with high levels of ZO-1 gene (TJP-1), are those who present a higher risk of recurrence. (**Figure R31**). Although the results obtained are very robust and have been validated in several patient datasets, it is important to remark that the conclusions are only applicable to CRC patients. To extend the results to other tumor types, it would be necessary both to generate additional metacohorts with data from other tumor types and to characterize in depth tight junction members regulated downstream of IKK α .

Regarding CLDN2, when we analyzed its expression levels in our CRC metacohort, they do not fit a normal distribution, a fact that makes it difficult to obtain conclusive results as well as to establish optimal cut-off criteria.

Consequently, we focused on other markers that could be incorporated into clinical practice, both as biomarkers and as potential therapeutic targets. We therefore set out to further investigate the genes in cluster 2 from our scRNA-seq data (**Figure R21**). In this regard, we paid special attention to those genes that have previously been linked to cancer, metastasis or therapy resistance, such as TFF1^{378–380}, TFF3^{331,381}, matrix metalloproteinase 28 (MMP28)^{382–384}, beta-1,3-galactosyltransferase 5 (B3GALT5)³⁸⁵ and placenta associated 8 (PLAC8)^{386–389}. We are currently investigating the implication of these members in the metastatic aggressiveness of our PDO models *in vivo*.

D4. CLDN2 inhibition as a potential new anti-metastatic therapeutic strategy in CRC.

As shown in **Figure R27** and **R28**, inhibition of CLDN2 function, either pharmacologically or genetically, correlated in *in vivo* assays with a reduction in the ability of PDO cells to develop liver metastases when injected intrasplenically. These results suggest a crucial dependence of CRC cells on CLDN2 function to generate CTC clusters that could generate metastasis.

Based on these results, we will investigate in the future the potential of using anti-CLDN2 blocking antibodies for the treatment of selected CRC patients with vascular tumor infiltration in form of CTC clusters. Antibodies that, in addition to their potential to inhibit CLDN2, could be used as antibody-drug conjugates (ADCs) to deliver chemotherapeutic treatments selectively and specifically to the clusters of metastatic cells traveling through the bloodstream. In fact, a similar strategy using the anti-CLDN18.2 blocking antibody is in clinical trials for advanced gastric tumors^{296,297}. However, it is important to note, unlike CLDN18.2 is restricted to the gastric mucosa, CLDN2 is highly expressed not only in the intestine but also in the liver and kidney. This may present a challenge because of the potential side effects of the drug. Possible solutions include low-affinity ADCs, which may target only CTCs due to their highest expression.

Further research is needed regarding the effect on the primary tumor, as the role of CLDN2 and tight junctions has not been explored in this context. In this sense, we believe that treating primary tumors with CLDN2-blocking compounds could potentially alter their compactness. This change could either improve the penetration of chemotherapeutic agents, such as those used in first-line cancer treatment, thereby increasing their efficacy, or enhance the infiltration of anti-tumor

immune cells and other cell types that target the malignancy from within. Concerning this last point, combination with immunotherapy should be explored to try to enhance the effectiveness of the strategy by leveraging the potential synergistic effects of the compounds. However, the potential use of any of these combinations for cancer treatment requires thorough preclinical *in vitro* and *in vivo* characterization and validation to assess both efficacy and toxicity. For *in vivo* validation, PDOs and patient-derived xenografts (PDXs) orthotopically implanted in nude mice represents our best current option. Indeed, this is our ongoing strategy, leveraging both approved drugs and new compounds for future personalized medicine. Regardless of the therapeutic approach used, the ability to eliminate CTC clusters may prevent disease recurrence if applied before metastatic disease becomes overt.

D5. MEK inhibitors slow the growth of hepatic metastases but do not reduce liver colonization.

MEK inhibitors, including selumetinib, are widely used in clinical practice for the treatment of various malignancies, particularly skin cancer^{62,63}. However, as shown in **Figure R38**, treatment with selumetinib only slowed metastatic growth without reducing the number of liver metastases developed by PDO5 when injected intrasplenically in mice. These data suggest that inhibition of the MAPK pathway is insufficient to prevent cancer cells from metastasizing but is effective in reducing metastatic growth. Regarding the impact of MAPK in CRC metastatic growth, we observed an even greater inhibitory effect upon stimulation of DUSP phosphatases, which completely shut down MAPK signaling in the different CRC cell models tested (**Figure R36**). To date, no specific compound has been described to induce or promote DUSP activity, making the development of DUSP-specific activators or small molecules that block their proteasomal degradation by polyubiquitination a highly appealing area of research. In particular, in line with our results, we propose DUSP1 and DUSP5 as promising targets for the development of such small molecules.

In the case of DUSP1, several factors are known to promote its degradation, including ERK, which induces the activity of the transcription factor forkhead box M1 (FoxM1)³⁹⁰ and the E3 ligase Atrogin-1³⁹¹. Additionally, stimuli such as glutamate-induced oxidative stress have been shown to reduce DUSP1 levels³⁹², while PGE2 and PGE1 can induce DUSP1 expression by attenuating MAPK signaling in non-cancer contexts³⁹³. In contrast, ubiquitin-specific peptidase 49 (USP49) directly interacts with DUSP1, promoting its deubiquitination and subsequent stabilization³⁹⁴.

Similarly, DUSP5 degradation is mediated by the proteasome and regulated by ERK³⁹⁵, but independently of kinase activity. However, our understanding of DUSP5 interactions and regulation is limited and warrants further investigation. Consistent with the findings of this study, a preliminary link between NF- κ B and DUSP5 has already been described³⁹⁶.

We propose that the identification of the key residues responsible for the proteasomal degradation of DUSP1 and DUSP5 in the context of CRC would be extremely useful for the development of new therapies, such as small molecules, aimed at inhibiting the MAPK pathway through DUSP stabilization.

D6. A deeper understanding of CTC vulnerabilities could lead to more precise treatments for mCRC.

In recent years, significant efforts have been dedicated to study both individual and clustered CTCs. While the scientific community has made remarkable progress in the understanding of CTCs, the mechanisms by which they intravasate, persist in circulation and extravasate to colonize other organs remain poorly understood at multiple levels. One of the most intriguing questions is how CTCs after surviving in circulation, acquire the ability to colonize distant organs and establish a niche that will allow the establishment of a new tumor.

Here, we have uncovered a mechanism responsible for CTC clustering in the context of CRC, which may enhance tumor cell survival in the bloodstream. Our proposed working model (**Figure D1**) implicates IKK α activity in this process but also the presence of a tumoral cell population with high tight junction signature. Thus, under normal conditions, IKK α phosphorylates the tight junction protein ZO-1, facilitating the proper dynamic assembly and disassembly of cell-cell contacts. This regulation is essential for cancer cells to migrate and invade blood vessels as single cells. While single-cell migration is more efficient in terms of number of cells, these cells are easily cleared from the bloodstream and require a reverse epithelial-mesenchymal transition (EMT) process to colonize target organs, resulting in lower metastatic potential.

When IKK α activity is diminished, either through reduced expression levels or increased protein degradation induced by a yet-to-be-discovered factors, tight junctions become less dynamic and begin to accumulate in areas where such cell-cell contacts should not be formed. This leads to increased tumor compactness and facilitates collective cell migration and invasion. Although we might expect that the entry of tumor clusters into circulation would be more challenging compared

to single cells, CTC clusters reach circulation and become protected from anoikis and immune system attack. Homotypic clusters are the most common type of CTC clusters found in tumoral surrounding vessels of our CRC patients cohort (**Figure R29 and R30**). However, we cannot exclude the presence of heterotypic clusters containing neutrophils and platelets described in other studies^{100,149,152,155–158}. Here, we propose CLDN2 inhibition as a novel therapeutic strategy to prevent metastatic colonization. As discussed in D4, this can be achieved through several approaches, but in this study, we demonstrated that pharmacological inhibition of CLDN2 recycling at the junctions or protein knockdown significantly reduced the generation of hepatic metastases in nude mice.

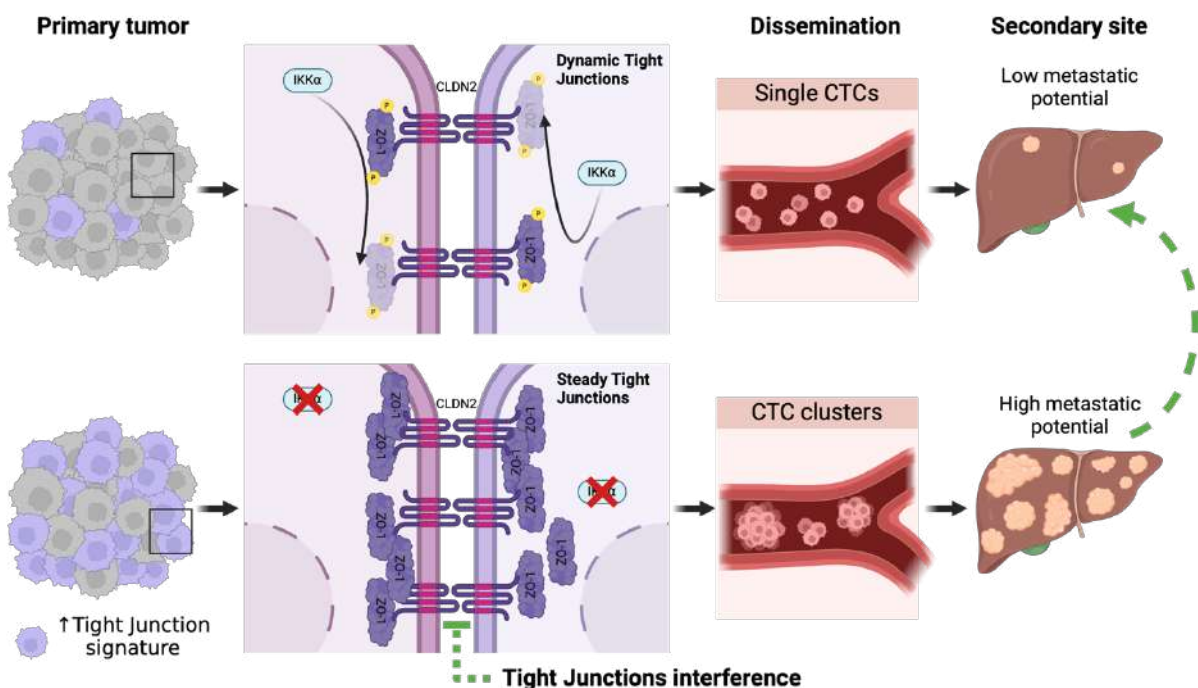


Figure D1. Proposed CTC clustering mechanism in CRC. Schematic representation of the key findings of this study relating IKKα activity to tight junction stability, which dictates the migration mode of cancer cells during dissemination and their metastatic potential. Created with Biorender.com.

D7. Following steps: how CT affects CTC cluster formation and tight junction dynamics?

One of the major unsolved questions of this work is the role of first-line CT in the formation of CTC clusters. We have observed a clear accumulation of ZO-1 and CLDN2 in CTC clusters located in the surrounding vessels of the primary tumor of CRC patients; however, we have yet to elucidate the expression dynamics of these proteins in response to various chemotherapeutic drugs. Several scenarios are possible: i) Toxic agents may induce a response in cancer cells leading to cellular compaction, allowing them to overcome toxicity in primary tumor cells. This could reduce cell

motility while increasing cell clustering, potentially making these tumors more metastatic. ii) Tumor cells may decrease the expression of tight junction proteins in response to CT. If this occurs, it could reduce or even prevent the formation of CTC clusters. This possibility might also enhance the expression of other contact elements, such as various integrins, which could mediate cell-matrix interactions³⁹⁷, and also potentially regulate cell-cell contacts under different conditions and stimuli. iii) Many other unexpected responses may occur that are currently unpredictable.

In addition, the impact of CT on IKK α expression and dynamics requires further investigation in response to the wide range of drugs used for CRC treatment. Some of these compounds may reduce kinase activity without directly affecting tight junction components. However, as demonstrated in this study using IKK α knockout models, the lack of regulation of these junctions can lead to the accumulation of tight junction elements, resulting in increased clustering and, ultimately, enhanced metastatic potential of cancer cells.

Our group has proposed several potential chemotherapy combinations for the treatment of colorectal tumors based on preclinical PDX models. In particular, CT+BRAFi²⁴⁹ and CT+BRAFi+JAK/STATi²⁵⁰ combinations demonstrated superior antitumor effects compared to CT alone. It would be valuable to assess the sensitivity of these metastatic lesions to these combinations, which have shown improved efficacy in treating primary tumor PDX models in nude mice.

Furthermore, the characteristics of metastatic lesions are highly dependent on the target organ. The microenvironment can vary significantly when a primary tumor disseminates to the lung compared to the liver or brain (e.g., differences in oxygen levels, tissue density, metabolites or proximity to the circulation). Therefore, it is crucial to test therapeutic strategies in multiple models. We propose to further validate new CLDN2-targeting therapies in different metastatic PDX models orthotopically implanted in the same metastatic organ. This approach will allow us to closely mimic the conditions under which metastatic lesions arise in patients.

In the near future, we hope to address these challenges, enhancing our understanding of CTC characteristics, expanding the options to prevent metastatic spread, and improving treatment outcomes for mCRC patients.

DISCUSSION: PART II

D8. Following steps: how CT affects CTC cluster formation and tight junction dynamics?

For years, NF- κ B inhibition has been considered the only I κ B α function, which is shared by all other I κ B homologs. However, I κ B α deletion in mice imposes a striking phenotype that is not compensated by I κ B β , I κ B ϵ or p100 (I κ B δ), suggesting that I κ B α may exert additional NF- κ B-unrelated functions. In support of this possibility, we previously demonstrated the presence of SUMOylated I κ B α in the nuclear compartment of specific cell populations, including adult stem cells of the skin and intestine. Binding of SUMOylated I κ B α to the chromatin takes place through direct association with histones H2A and H4 and provides cytokine responsiveness to a subset of PRC2 target genes, which are cell-type specific. For example, whereas SUMOylated I κ B α regulates multiple genes of the HOX and IRX families as well as NEUROG2 and NEUROD4 in keratinocytes, it regulates MEX3A or BMI1 in intestinal cells, thus controlling tissue stem cell maturation and lineage cell differentiation^{208,209}. Further supporting the concept that I κ B α exerts both NF- κ B-related and -unrelated functions, two I κ B α homologs are present and functional in the nematode *C.elegans*³⁹⁸, which lacks recognizable NF- κ B factors (see <https://www.bu.edu/nf-kb>). Moreover, the homeotic phenotype imposed by Cactus (I κ B α) hemizygous deletion in *Drosophila* is not rescued by reducing dorsal (p65-NF- κ B) levels²⁰⁸. In pathology, loss of nuclear I κ B α and accumulation of cytoplasmic I κ B α correlates with cancer progression in the human skin and is associated with aberrant transcription of HOX genes²⁰⁸, which are canonical targets of PRC2 activity. In addition to skin cancer, loss of a single I κ B α allele in human glioblastoma is associated with adverse patient outcome independent of any clinicopathologic predictor³⁹⁹. However, the prominent function of NF- κ B in gene regulation and the multiple cross-talks between NF- κ B and polycomb^{208,400,401} have precluded, until now, the study of NF- κ B-independent I κ B α functions (i.e., PRC2 related) not only in cancer but also in the different physiological systems where it plays a role. We have now performed a sophisticated bioinformatic analysis of the evolutionary conserved residues of the I κ B α protein to uncover the most likely contributors to relevant protein-protein interactions. This analysis indicated that I κ B α binds to NF- κ B and histones through the same region, which we had already suggested based on its mutually exclusive binding to either partner²⁰⁸. Strikingly, residues essential for NF- κ B binding were conserved during evolution and among the different I κ B α homologs including BCL3. However, residues involved in histone binding were exclusively found in the I κ B α homolog but are still

evolutionary conserved, indicating that the chromatin function of I κ B α represents an exclusive but ancestral NF- κ B-independent function. Using separation-of-function I κ B α mutants, we have shown that goblet cell differentiation requires the chromatin function of I κ B α (rescued by I κ B α WT and the SOF^{ΔNF- κ B} mutant), which parallels the transcriptional repression of ISC genes. In contrast, repression of TNFA_SIGNALING_VIA_NFKB is detected in cells expressing the I κ B α WT but lost in the SOF^{ΔNF- κ B} mutant N108A (**Figures R47D** and **R47E**). To our view, the I κ B α SOF mutants represent a unique tool for basic research (i.e., in the stem cell and development field) and clinical research, including the more specific cancer models where I κ B α deletions are highly prevalent such as Hodgkin lymphoma^{402,403} or glioblastoma^{399,404} and also neuronal disorders where defective I κ B α function plays a role.

The design of a new tools to reconstitute either NF- κ B or PRC2 regulation in I κ B α -depleted cancers will allow a diagnosis refinement (i.e., stratification of tumors fueled by aberrant NF- κ B or PRC2 activity) and a better therapeutic prescription for specific groups of patients.

CONCLUSIONS

CONCLUSIONS

PART I- The impact of IKK α in CRC regulating cell clustering and metastasis through tight junctions

1. IKK α activity is required for the proper regulation of different cell-cell adhesion elements in CRC cells.
2. Defective IKK α activity promotes cellular clustering while reducing the migratory capacity of CRC cells.
3. The depletion of IKK α confers superior metastatic activity to PDO cells, which is likely related to their different migratory mode and the enrichment of tight junction signature.
4. We identified 3 distinct cell clusters in PDO5 as potential contributors to the higher metastatic activity observed in IKK α KO cells.
5. We provide initial evidence supporting the utility of interfering with cell-cell contact elements (i.e., CLDN2) in the treatment of metastatic CRC.
6. Tumor clusters with tight junction cell-cell contacts (ZO-1 and CLDN2) are detectable in CRC samples at diagnosis, which could be used as prognostic and prescriptive biomarkers in the near future.

PART II- Separation-of-function mutants reveal the NF- κ B-independent involvement of I κ B α in the regulation of intestinal stemness

1. The same I κ B α interface patch that interacts with the p65-NF- κ B NLS mediate the interaction with histone H4.
2. p65-NF- κ B and histone H4 compete for binding to the same I κ B α region with specific residues differentially influencing its association.
3. NF- κ B-independent functions of I κ B α are sufficient to regulate specific gene transcription with implications for intestinal differentiation.

BIBLIOGRAPHY

BIBLIOGRAPHY

1. Sung, H. *et al.* Global Cancer Statistics 2020: GLOBOCAN Estimates of Incidence and Mortality Worldwide for 36 Cancers in 185 Countries. *CA Cancer J Clin* **71**, 209–249 (2021).
2. Dekker, E., Tanis, P. J., Vleugels, J. L. A., Kasi, P. M. & Wallace, M. B. Colorectal cancer. *The Lancet* **394**, 1467–1480 (2019).
3. Dow, L. E. *et al.* Apc Restoration Promotes Cellular Differentiation and Reestablishes Crypt Homeostasis in Colorectal Cancer. *Cell* **161**, 1539–1552 (2015).
4. Keum, N. & Giovannucci, E. Global burden of colorectal cancer: emerging trends, risk factors and prevention strategies. *Nat Rev Gastroenterol Hepatol* **16**, 713–732 (2019).
5. Kuipers, E. J. *et al.* Colorectal cancer. *Nat Rev Dis Primers* **1**, 15065 (2015).
6. Chen, S. *et al.* The Function of RAS Mutation in Cancer and Advances in its Drug Research. *Curr Pharm Des* **25**, 1105–1114 (2019).
7. ZHAI, X. *et al.* Dual specificity phosphatase 6 suppresses the growth and metastasis of prostate cancer cells. *Mol Med Rep* **10**, 3052–3058 (2014).
8. Lin, S., Hsiao, K., Chang, N., Hou, P. & Tsai, S. Loss of dual-specificity phosphatase-2 promotes angiogenesis and metastasis via up-regulation of interleukin-8 in colon cancer. *J Pathol* **241**, 638–648 (2017).
9. Zhang, Y. *et al.* DUSP2 recruits CSNK2A1 to suppress AKT1-mediated apoptosis resistance under hypoxic microenvironment in pancreatic cancer. *Cancer Lett* **568**, 216288 (2023).
10. Zou, F. *et al.* DUSP2 affects bladder cancer prognosis by down-regulating MEK/ERK and P38 MAPK signaling pathways through PTPN7. *Cell Signal* **112**, 110893 (2023).
11. Wong, V. C. L. *et al.* Tumor suppressor dual-specificity phosphatase 6 (DUSP6) impairs cell invasion and epithelial-mesenchymal transition (EMT)-associated phenotype. *Int J Cancer* **130**, 83–95 (2012).
12. de la Peña Avalos, B., Tropée, R., Duijf, P. H. G. & Dray, E. EYA4 promotes breast cancer progression and metastasis through its role in replication stress avoidance. *Mol Cancer* **22**, 158 (2023).
13. Yang, Z. *et al.* BAF53A drives colorectal cancer development by regulating DUSP5-mediated ERK phosphorylation. *Cell Death Dis* **13**, 1049 (2022).
14. Buffet, C. *et al.* Dual Specificity Phosphatase 5, a Specific Negative Regulator of ERK Signaling, Is Induced by Serum Response Factor and Elk-1 Transcription Factor. *PLoS One* **10**, e0145484 (2015).
15. Karakashev, S. V. & Reginato, M. J. Hypoxia/HIF1 α induces lapatinib resistance in ERBB2-positive breast cancer cells via regulation of DUSP2. *Oncotarget* **6**, 1967–1980 (2015).
16. Lin, S.-C. *et al.* Suppression of dual-specificity phosphatase–2 by hypoxia increases chemoresistance and malignancy in human cancer cells. *Journal of Clinical Investigation* **121**, 1905–1916 (2011).

17. Hou, P.-C. *et al.* Hypoxia-Induced Downregulation of DUSP-2 Phosphatase Drives Colon Cancer Stemness. *Cancer Res* **77**, 4305–4316 (2017).
18. Nguyen, H. & Duong, H. The molecular characteristics of colorectal cancer: Implications for diagnosis and therapy (Review). *Oncol Lett* (2018) doi:10.3892/ol.2018.8679.
19. Fearon, E. R. Molecular Genetics of Colorectal Cancer. *Annual Review of Pathology: Mechanisms of Disease* **6**, 479–507 (2011).
20. Li, S. K. H. & Martin, A. Mismatch Repair and Colon Cancer: Mechanisms and Therapies Explored. *Trends Mol Med* **22**, 274–289 (2016).
21. Bakhoum, S. F. & Cantley, L. C. The Multifaceted Role of Chromosomal Instability in Cancer and Its Microenvironment. *Cell* **174**, 1347–1360 (2018).
22. Shen, L. *et al.* Integrated genetic and epigenetic analysis identifies three different subclasses of colon cancer. *Proceedings of the National Academy of Sciences* **104**, 18654–18659 (2007).
23. Huang, Z. & Yang, M. Molecular Network of Colorectal Cancer and Current Therapeutic Options. *Front Oncol* **12**, (2022).
24. Schmitt, M. & Greten, F. R. The inflammatory pathogenesis of colorectal cancer. *Nat Rev Immunol* **21**, 653–667 (2021).
25. Brenner, H., Kloor, M. & Pox, C. P. Colorectal cancer. *The Lancet* **383**, 1490–1502 (2014).
26. O’Connell, J. B., Maggard, M. A. & Ko, C. Y. Colon Cancer Survival Rates With the New American Joint Committee on Cancer Sixth Edition Staging. *JNCI Journal of the National Cancer Institute* **96**, 1420–1425 (2004).
27. Nagtegaal, I. D., Quirke, P. & Schmoll, H.-J. Has the new TNM classification for colorectal cancer improved care? *Nat Rev Clin Oncol* **9**, 119–123 (2012).
28. Cañellas-Socias, A., Sancho, E. & Batlle, E. Mechanisms of metastatic colorectal cancer. *Nat Rev Gastroenterol Hepatol* (2024) doi:10.1038/s41575-024-00934-z.
29. Guinney, J. *et al.* The consensus molecular subtypes of colorectal cancer. *Nat Med* **21**, 1350–1356 (2015).
30. Dick, J. E. Stem cell concepts renew cancer research. *Blood* **112**, 4793–4807 (2008).
31. Plaks, V., Kong, N. & Werb, Z. The Cancer Stem Cell Niche: How Essential Is the Niche in Regulating Stemness of Tumor Cells? *Cell Stem Cell* **16**, 225–238 (2015).
32. Driessens, G., Beck, B., Caauwe, A., Simons, B. D. & Blanpain, C. Defining the mode of tumour growth by clonal analysis. *Nature* **488**, 527–530 (2012).
33. Batlle, E. & Clevers, H. Cancer stem cells revisited. *Nat Med* **23**, 1124–1134 (2017).
34. Yang, L. *et al.* Targeting cancer stem cell pathways for cancer therapy. *Signal Transduct Target Ther* **5**, 8 (2020).

35. Dalerba, P. *et al.* Phenotypic characterization of human colorectal cancer stem cells. *Proceedings of the National Academy of Sciences* **104**, 10158–10163 (2007).
36. O’Brien, C. A., Pollett, A., Gallinger, S. & Dick, J. E. A human colon cancer cell capable of initiating tumour growth in immunodeficient mice. *Nature* **445**, 106–110 (2007).
37. Ricci-Vitiani, L. *et al.* Identification and expansion of human colon-cancer-initiating cells. *Nature* **445**, 111–115 (2007).
38. Schepers, A. G. *et al.* Lineage Tracing Reveals Lgr5⁺ Stem Cell Activity in Mouse Intestinal Adenomas. *Science* (1979) **337**, 730–735 (2012).
39. Shimokawa, M. *et al.* Visualization and targeting of LGR5⁺ human colon cancer stem cells. *Nature* **545**, 187–192 (2017).
40. Cui, G. *et al.* Temporal and spatial changes of cells positive for stem-like markers in different compartments and stages of human colorectal adenoma-carcinoma sequence. *Oncotarget* **8**, 45311–45322 (2017).
41. Levin, T. G. *et al.* Characterization of the Intestinal Cancer Stem Cell Marker CD166 in the Human and Mouse Gastrointestinal Tract. *Gastroenterology* **139**, 2072–2082.e5 (2010).
42. Vermeulen, L. *et al.* Single-cell cloning of colon cancer stem cells reveals a multi-lineage differentiation capacity. *Proceedings of the National Academy of Sciences* **105**, 13427–13432 (2008).
43. de Sousa e Melo, F. *et al.* A distinct role for Lgr5⁺ stem cells in primary and metastatic colon cancer. *Nature* **543**, 676–680 (2017).
44. Morral, C. *et al.* Zonation of Ribosomal DNA Transcription Defines a Stem Cell Hierarchy in Colorectal Cancer. *Cell Stem Cell* **26**, 845–861.e12 (2020).
45. Clevers, H. What is an adult stem cell? *Science* (1979) **350**, 1319–1320 (2015).
46. Bartram, I. & Jeschke, J. M. Do cancer stem cells exist? A pilot study combining a systematic review with the hierarchy-of-hypotheses approach. *PLoS One* **14**, e0225898 (2019).
47. Pérez-González, A., Bévant, K. & Blanpain, C. Cancer cell plasticity during tumor progression, metastasis and response to therapy. *Nat Cancer* **4**, 1063–1082 (2023).
48. Chu, X. *et al.* Cancer stem cells: advances in knowledge and implications for cancer therapy. *Signal Transduct Target Ther* **9**, 170 (2024).
49. Zhu, L. *et al.* Prominin 1 marks intestinal stem cells that are susceptible to neoplastic transformation. *Nature* **457**, 603–607 (2009).
50. Vermeulen, L. *et al.* Wnt activity defines colon cancer stem cells and is regulated by the microenvironment. *Nat Cell Biol* **12**, 468–476 (2010).
51. Schwitalla, S. *et al.* Intestinal Tumorigenesis Initiated by Dedifferentiation and Acquisition of Stem-Cell-like Properties. *Cell* **152**, 25–38 (2013).

52. Kreso, A. & Dick, J. E. Evolution of the Cancer Stem Cell Model. *Cell Stem Cell* **14**, 275–291 (2014).
53. McQuade, R. M., Stojanovska, V., Bornstein, J. C. & Nurgali, K. Colorectal Cancer Chemotherapy: The Evolution of Treatment and New Approaches. *Curr Med Chem* **24**, (2017).
54. Moiseyenko, V. M. *et al.* First-Line Cetuximab Monotherapy in KRAS/NRAS/BRAF Mutation-Negative Colorectal Cancer Patients. *Clin Drug Investig* **38**, 553–562 (2018).
55. Janani, B. *et al.* EGFR-Based Targeted Therapy for Colorectal Cancer-Promises and Challenges. *Vaccines (Basel)* **10**, (2022).
56. Seeber, A., Gunsilius, E., Gastl, G. & Pircher, A. Anti-Angiogenics: Their Value in Colorectal Cancer Therapy. *Oncol Res Treat* **41**, 188–193 (2018).
57. Xie, Y.-H., Chen, Y.-X. & Fang, J.-Y. Comprehensive review of targeted therapy for colorectal cancer. *Signal Transduct Target Ther* **5**, 22 (2020).
58. Ganesh, K. *et al.* Immunotherapy in colorectal cancer: rationale, challenges and potential. *Nat Rev Gastroenterol Hepatol* **16**, 361–375 (2019).
59. Janku, F. Advances on the BRAF Front in Colorectal Cancer. *Cancer Discov* **8**, 389–391 (2018).
60. Poulikakos, P. I., Zhang, C., Bollag, G., Shokat, K. M. & Rosen, N. RAF inhibitors transactivate RAF dimers and ERK signalling in cells with wild-type BRAF. *Nature* **464**, 427–430 (2010).
61. Zhang, C. *et al.* RAF inhibitors that evade paradoxical MAPK pathway activation. *Nature* **526**, 583–586 (2015).
62. Flaherty, K. T. *et al.* Combined BRAF and MEK Inhibition in Melanoma with BRAF V600 Mutations. *New England Journal of Medicine* **367**, 1694–1703 (2012).
63. Hu-Lieskovan, S. *et al.* Improved antitumor activity of immunotherapy with BRAF and MEK inhibitors in *BRAF*^{V600E} melanoma. *Sci Transl Med* **7**, (2015).
64. Sundar, R., Hong, D. S., Kopetz, S. & Yap, T. A. Targeting *BRAF* -Mutant Colorectal Cancer: Progress in Combination Strategies. *Cancer Discov* **7**, 558–560 (2017).
65. Siegel, R. L., Wagle, N. S., Cercek, A., Smith, R. A. & Jemal, A. Colorectal cancer statistics, 2023. *CA Cancer J Clin* **73**, 233–254 (2023).
66. Van Cutsem, E. *et al.* ESMO consensus guidelines for the management of patients with metastatic colorectal cancer. *Ann Oncol* **27**, 1386–422 (2016).
67. Fidler, I. J. Metastasis: quantitative analysis of distribution and fate of tumor emboli labeled with 125 I-5-iodo-2'-deoxyuridine. *J Natl Cancer Inst* **45**, 773–82 (1970).
68. Butler, T. P. & Gullino, P. M. Quantitation of cell shedding into efferent blood of mammary adenocarcinoma. *Cancer Res* **35**, 512–6 (1975).
69. Sznurkowska, M. K. & Aceto, N. The gate to metastasis: key players in cancer cell intravasation. *FEBS J* **289**, 4336–4354 (2022).

70. Ring, A., Nguyen-Sträuli, B. D., Wicki, A. & Aceto, N. Biology, vulnerabilities and clinical applications of circulating tumour cells. *Nat Rev Cancer* **23**, 95–111 (2023).
71. Gkoutela, S. & Aceto, N. Stem-like features of cancer cells on their way to metastasis. *Biol Direct* **11**, 33 (2016).
72. Cañellas-Socias, A. *et al.* Metastatic recurrence in colorectal cancer arises from residual EMP1+ cells. *Nature* **611**, 603–613 (2022).
73. Birkbak, N. J. & McGranahan, N. Cancer Genome Evolutionary Trajectories in Metastasis. *Cancer Cell* **37**, 8–19 (2020).
74. Priestley, P. *et al.* Pan-cancer whole-genome analyses of metastatic solid tumours. *Nature* **575**, 210–216 (2019).
75. Pierce, S. E. *et al.* LKB1 inactivation modulates chromatin accessibility to drive metastatic progression. *Nat Cell Biol* **23**, 915–924 (2021).
76. Yaeger, R. *et al.* RAS mutations affect pattern of metastatic spread and increase propensity for brain metastasis in colorectal cancer. *Cancer* **121**, 1195–1203 (2015).
77. Hu, Z. *et al.* Quantitative evidence for early metastatic seeding in colorectal cancer. *Nat Genet* **51**, 1113–1122 (2019).
78. Bockhorn, M., Jain, R. K. & Munn, L. L. Active versus passive mechanisms in metastasis: do cancer cells crawl into vessels, or are they pushed? *Lancet Oncol* **8**, 444–448 (2007).
79. Follain, G. *et al.* Hemodynamic Forces Tune the Arrest, Adhesion, and Extravasation of Circulating Tumor Cells. *Dev Cell* **45**, 33–52.e12 (2018).
80. Follain, G. *et al.* Fluids and their mechanics in tumour transit: shaping metastasis. *Nat Rev Cancer* **20**, 107–124 (2020).
81. Donato, C. *et al.* Hypoxia Triggers the Intravasation of Clustered Circulating Tumor Cells. *Cell Rep* **32**, 108105 (2020).
82. Jin, F., Brockmeier, U., Otterbach, F. & Metzen, E. New Insight into the SDF-1/CXCR4 Axis in a Breast Carcinoma Model: Hypoxia-Induced Endothelial SDF-1 and Tumor Cell CXCR4 Are Required for Tumor Cell Intravasation. *Molecular Cancer Research* **10**, 1021–1031 (2012).
83. Mazzone, M. *et al.* Heterozygous Deficiency of PHD2 Restores Tumor Oxygenation and Inhibits Metastasis via Endothelial Normalization. *Cell* **136**, 839–851 (2009).
84. King, M. R. *et al.* A physical sciences network characterization of circulating tumor cell aggregate transport. *American Journal of Physiology-Cell Physiology* **308**, C792–C802 (2015).
85. Haemmerle, M. *et al.* Platelets reduce anoikis and promote metastasis by activating YAP1 signaling. *Nat Commun* **8**, 310 (2017).

86. Schumacher, D., Strilic, B., Sivaraj, K. K., Wettschureck, N. & Offermanns, S. Platelet-Derived Nucleotides Promote Tumor-Cell Transendothelial Migration and Metastasis via P2Y2 Receptor. *Cancer Cell* **24**, 130–137 (2013).
87. Anderson, K. J., de Guillebon, A., Hughes, A. D., Wang, W. & King, M. R. Effect of circulating tumor cell aggregate configuration on hemodynamic transport and wall contact. *Math Biosci* **294**, 181–194 (2017).
88. Leong, H. S. *et al.* Invadopodia Are Required for Cancer Cell Extravasation and Are a Therapeutic Target for Metastasis. *Cell Rep* **8**, 1558–1570 (2014).
89. Coussens, L. M. & Werb, Z. Inflammation and cancer. *Nature* **420**, 860–867 (2002).
90. Rahn, J. J. *et al.* MUC1 Mediates Transendothelial Migration in vitro by Ligating Endothelial Cell ICAM-1. *Clin Exp Metastasis* **22**, 475–483 (2005).
91. Osmani, N. *et al.* Metastatic Tumor Cells Exploit Their Adhesion Repertoire to Counteract Shear Forces during Intravascular Arrest. *Cell Rep* **28**, 2491–2500.e5 (2019).
92. Teicher, B. A. & Fricker, S. P. CXCL12 (SDF-1)/CXCR4 Pathway in Cancer. *Clinical Cancer Research* **16**, 2927–2931 (2010).
93. Fu, Q. *et al.* Primary tumor-derived exosomes facilitate metastasis by regulating adhesion of circulating tumor cells via SMAD3 in liver cancer. *Oncogene* **37**, 6105–6118 (2018).
94. Padua, D. *et al.* TGFβ Primes Breast Tumors for Lung Metastasis Seeding through Angiopoietin-like 4. *Cell* **133**, 66–77 (2008).
95. Reymond, N., d'Água, B. B. & Ridley, A. J. Crossing the endothelial barrier during metastasis. *Nat Rev Cancer* **13**, 858–870 (2013).
96. Wolf, M. J. *et al.* Endothelial CCR2 Signaling Induced by Colon Carcinoma Cells Enables Extravasation via the JAK2-Stat5 and p38MAPK Pathway. *Cancer Cell* **22**, 91–105 (2012).
97. Strilic, B. *et al.* Tumour-cell-induced endothelial cell necroptosis via death receptor 6 promotes metastasis. *Nature* **536**, 215–218 (2016).
98. Chen, M. B. *et al.* Inflamed neutrophils sequestered at entrapped tumor cells via chemotactic confinement promote tumor cell extravasation. *Proceedings of the National Academy of Sciences* **115**, 7022–7027 (2018).
99. Spiegel, A. *et al.* Neutrophils Suppress Intraluminal NK Cell–Mediated Tumor Cell Clearance and Enhance Extravasation of Disseminated Carcinoma Cells. *Cancer Discov* **6**, 630–649 (2016).
100. Cools-Lartigue, J. *et al.* Neutrophil extracellular traps sequester circulating tumor cells and promote metastasis. *Journal of Clinical Investigation* **123**, 3446–3458 (2013).
101. Denève, E. *et al.* Capture of Viable Circulating Tumor Cells in the Liver of Colorectal Cancer Patients. *Clin Chem* **59**, 1384–1392 (2013).

102. Müller, A. *et al.* Involvement of chemokine receptors in breast cancer metastasis. *Nature* **410**, 50–56 (2001).
103. Labelle, M., Begum, S. & Hynes, R. O. Direct Signaling between Platelets and Cancer Cells Induces an Epithelial-Mesenchymal-Like Transition and Promotes Metastasis. *Cancer Cell* **20**, 576–590 (2011).
104. Sosa, M. S., Bragado, P. & Aguirre-Ghiso, J. A. Mechanisms of disseminated cancer cell dormancy: an awakening field. *Nat Rev Cancer* **14**, 611–622 (2014).
105. Correia, A. L. *et al.* Hepatic stellate cells suppress NK cell-sustained breast cancer dormancy. *Nature* **594**, 566–571 (2021).
106. Croucher, P. I., McDonald, M. M. & Martin, T. J. Bone metastasis: the importance of the neighbourhood. *Nat Rev Cancer* **16**, 373–386 (2016).
107. Lawson, M. A. *et al.* Osteoclasts control reactivation of dormant myeloma cells by remodelling the endosteal niche. *Nat Commun* **6**, 8983 (2015).
108. Dai, J. *et al.* Astrocytic laminin-211 drives disseminated breast tumor cell dormancy in brain. *Nat Cancer* **3**, 25–42 (2021).
109. Zhang, X. H.-F. *et al.* Latent Bone Metastasis in Breast Cancer Tied to Src-Dependent Survival Signals. *Cancer Cell* **16**, 67–78 (2009).
110. Albregues, J. *et al.* Neutrophil extracellular traps produced during inflammation awaken dormant cancer cells in mice. *Science* (1979) **361**, (2018).
111. Wang, H. *et al.* The Osteogenic Niche Is a Calcium Reservoir of Bone Micrometastases and Confers Unexpected Therapeutic Vulnerability. *Cancer Cell* **34**, 823–839.e7 (2018).
112. Chambers, A. F., Groom, A. C. & MacDonald, I. C. Dissemination and growth of cancer cells in metastatic sites. *Nat Rev Cancer* **2**, 563–572 (2002).
113. Mehlen, P. & Puisieux, A. Metastasis: a question of life or death. *Nat Rev Cancer* **6**, 449–458 (2006).
114. Lambert, A. W., Pattabiraman, D. R. & Weinberg, R. A. Emerging Biological Principles of Metastasis. *Cell* **168**, 670–691 (2017).
115. Nieto, M. A., Huang, R. Y.-J., Jackson, R. A. & Thiery, J. P. EMT: 2016. *Cell* **166**, 21–45 (2016).
116. Batlle, E. *et al.* The transcription factor Snail is a repressor of E-cadherin gene expression in epithelial tumour cells. *Nat Cell Biol* **2**, 84–89 (2000).
117. Lu, W. & Kang, Y. Epithelial-Mesenchymal Plasticity in Cancer Progression and Metastasis. *Dev Cell* **49**, 361–374 (2019).
118. Mani, S. A. *et al.* The Epithelial-Mesenchymal Transition Generates Cells with Properties of Stem Cells. *Cell* **133**, 704–715 (2008).
119. Ocaña, O. H. *et al.* Metastatic Colonization Requires the Repression of the Epithelial-Mesenchymal Transition Inducer Prrx1. *Cancer Cell* **22**, 709–724 (2012).

120. Tsai, J. H., Donaher, J. L., Murphy, D. A., Chau, S. & Yang, J. Spatiotemporal Regulation of Epithelial-Mesenchymal Transition Is Essential for Squamous Cell Carcinoma Metastasis. *Cancer Cell* **22**, 725–736 (2012).
121. Yang, J. *et al.* Twist, a Master Regulator of Morphogenesis, Plays an Essential Role in Tumor Metastasis. *Cell* **117**, 927–939 (2004).
122. Revenco, T. *et al.* Context Dependency of Epithelial-to-Mesenchymal Transition for Metastasis. *Cell Rep* **29**, 1458-1468.e3 (2019).
123. Bakir, B., Chiarella, A. M., Pitarresi, J. R. & Rustgi, A. K. EMT, MET, Plasticity, and Tumor Metastasis. *Trends Cell Biol* **30**, 764–776 (2020).
124. Löönd, F. *et al.* Distinct contributions of partial and full EMT to breast cancer malignancy. *Dev Cell* **56**, 3203-3221.e11 (2021).
125. Pastushenko, I. *et al.* Identification of the tumour transition states occurring during EMT. *Nature* **556**, 463–468 (2018).
126. Pastushenko, I. *et al.* Fat1 deletion promotes hybrid EMT state, tumour stemness and metastasis. *Nature* **589**, 448–455 (2021).
127. Cheung, K. J. & Ewald, A. J. A collective route to metastasis: Seeding by tumor cell clusters. *Science* (1979) **352**, 167–169 (2016).
128. Friedl, P., Locker, J., Sahai, E. & Segall, J. E. Classifying collective cancer cell invasion. *Nat Cell Biol* **14**, 777–783 (2012).
129. Einenkel, J., Braumann, U.-D., Horn, L.-C., Kuska, J.-P. & Höckel, M. 3-D analysis of the invasion front in squamous cell carcinoma of the uterine cervix: histopathologic evidence for collective invasion per continuitatem. *Anal Quant Cytol Histol* **29**, 279–90 (2007).
130. Christiansen, J. J. & Rajasekaran, A. K. Reassessing Epithelial to Mesenchymal Transition as a Prerequisite for Carcinoma Invasion and Metastasis. *Cancer Res* **66**, 8319–8326 (2006).
131. Tarin, D. The Fallacy of Epithelial Mesenchymal Transition in Neoplasia. *Cancer Res* **65**, 5996–6001 (2005).
132. Liotta, L. A., Saidel, M. G. & Kleinerman, J. The significance of hematogenous tumor cell clumps in the metastatic process. *Cancer Res* **36**, 889–94 (1976).
133. Cleary, A. S., Leonard, T. L., Gestl, S. A. & Gunther, E. J. Tumour cell heterogeneity maintained by cooperating subclones in Wnt-driven mammary cancers. *Nature* **508**, 113–117 (2014).
134. Gudem, G. *et al.* The evolutionary history of lethal metastatic prostate cancer. *Nature* **520**, 353–357 (2015).
135. Maddipati, R. & Stanger, B. Z. Pancreatic Cancer Metastases Harbor Evidence of Polyclonality. *Cancer Discov* **5**, 1086–1097 (2015).

136. McFadden, D. G. *et al.* Genetic and Clonal Dissection of Murine Small Cell Lung Carcinoma Progression by Genome Sequencing. *Cell* **156**, 1298–1311 (2014).
137. Eirew, P. *et al.* Dynamics of genomic clones in breast cancer patient xenografts at single-cell resolution. *Nature* **518**, 422–426 (2015).
138. Aceto, N. *et al.* Circulating Tumor Cell Clusters Are Oligoclonal Precursors of Breast Cancer Metastasis. *Cell* **158**, 1110–1122 (2014).
139. Liu, X. *et al.* Homophilic CD44 Interactions Mediate Tumor Cell Aggregation and Polyclonal Metastasis in Patient-Derived Breast Cancer Models. *Cancer Discov* **9**, 96–113 (2019).
140. Aceto, N., Toner, M., Maheswaran, S. & Haber, D. A. En Route to Metastasis: Circulating Tumor Cell Clusters and Epithelial-to-Mesenchymal Transition. *Trends Cancer* **1**, 44–52 (2015).
141. Cheung, K. J. *et al.* Polyclonal breast cancer metastases arise from collective dissemination of keratin 14-expressing tumor cell clusters. *Proceedings of the National Academy of Sciences* **113**, (2016).
142. Padmanaban, V. *et al.* E-cadherin is required for metastasis in multiple models of breast cancer. *Nature* **573**, 439–444 (2019).
143. Rejniak, K. A. Circulating Tumor Cells: When a Solid Tumor Meets a Fluid Microenvironment. in 93–106 (2016). doi:10.1007/978-3-319-42023-3_5.
144. Au, S. H. *et al.* Clusters of circulating tumor cells traverse capillary-sized vessels. *Proceedings of the National Academy of Sciences* **113**, 4947–4952 (2016).
145. Chimonidou, M. *et al.* DNA Methylation of Tumor Suppressor and Metastasis Suppressor Genes in Circulating Tumor Cells. *Clin Chem* **57**, 1169–1177 (2011).
146. Gkoutela, S. *et al.* Circulating Tumor Cell Clustering Shapes DNA Methylation to Enable Metastasis Seeding. *Cell* **176**, 98–112.e14 (2019).
147. Taftaf, R. *et al.* ICAM1 initiates CTC cluster formation and trans-endothelial migration in lung metastasis of breast cancer. *Nat Commun* **12**, 4867 (2021).
148. Zhao, Q. *et al.* Interaction between circulating galectin-3 and cancer-associated MUC1 enhances tumour cell homotypic aggregation and prevents anoikis. *Mol Cancer* **9**, 154 (2010).
149. Labelle, M. & Hynes, R. O. The Initial Hours of Metastasis: The Importance of Cooperative Host–Tumor Cell Interactions during Hematogenous Dissemination. *Cancer Discov* **2**, 1091–1099 (2012).
150. Rachidi, S. *et al.* Platelets subvert T cell immunity against cancer via GARP-TGF β axis. *Sci Immunol* **2**, (2017).
151. Placke, T. *et al.* Platelet-Derived MHC Class I Confers a Pseudonormal Phenotype to Cancer Cells That Subverts the Antitumor Reactivity of Natural Killer Immune Cells. *Cancer Res* **72**, 440–448 (2012).
152. Szczerba, B. M. *et al.* Neutrophils escort circulating tumour cells to enable cell cycle progression. *Nature* **566**, 553–557 (2019).

153. Labelle, M., Begum, S. & Hynes, R. O. Platelets guide the formation of early metastatic niches. *Proceedings of the National Academy of Sciences* **111**, (2014).
154. Coffelt, S. B. *et al.* IL-17-producing $\gamma\delta$ T cells and neutrophils conspire to promote breast cancer metastasis. *Nature* **522**, 345–348 (2015).
155. Schuster, E. *et al.* Better together: circulating tumor cell clustering in metastatic cancer. *Trends Cancer* **7**, 1020–1032 (2021).
156. Sprouse, M. L. *et al.* PMN-MDSCs Enhance CTC Metastatic Properties through Reciprocal Interactions via ROS/Notch/Nodal Signaling. *Int J Mol Sci* **20**, 1916 (2019).
157. Gaggioli, C. *et al.* Fibroblast-led collective invasion of carcinoma cells with differing roles for RhoGTPases in leading and following cells. *Nat Cell Biol* **9**, 1392–1400 (2007).
158. Labernadie, A. *et al.* A mechanically active heterotypic E-cadherin/N-cadherin adhesion enables fibroblasts to drive cancer cell invasion. *Nat Cell Biol* **19**, 224–237 (2017).
159. Diamantopoulou, Z. *et al.* The metastatic spread of breast cancer accelerates during sleep. *Nature* **607**, 156–162 (2022).
160. Zhu, X. *et al.* In vivo flow cytometry reveals a circadian rhythm of circulating tumor cells. *Light Sci Appl* **10**, 110 (2021).
161. Schernhammer, E. S. *et al.* Rotating Night Shifts and Risk of Breast Cancer in Women Participating in the Nurses' Health Study. *JNCI Journal of the National Cancer Institute* **93**, 1563–1568 (2001).
162. Schernhammer, E. S. *et al.* Night-Shift Work and Risk of Colorectal Cancer in the Nurses' Health Study. *JNCI Journal of the National Cancer Institute* **95**, 825–828 (2003).
163. Straif, K. *et al.* Carcinogenicity of shift-work, painting, and fire-fighting. *Lancet Oncol* **8**, 1065–1066 (2007).
164. Lauriola, M. *et al.* Diurnal suppression of EGFR signalling by glucocorticoids and implications for tumour progression and treatment. *Nat Commun* **5**, 5073 (2014).
165. Sephton, S. E. *et al.* Diurnal cortisol rhythm as a predictor of lung cancer survival. *Brain Behav Immun* **30**, S163–S170 (2013).
166. Giacchetti, S. *et al.* Phase III Trial Comparing 4-Day Chronomodulated Therapy Versus 2-Day Conventional Delivery of Fluorouracil, Leucovorin, and Oxaliplatin As First-Line Chemotherapy of Metastatic Colorectal Cancer: The European Organisation for Research and Treatment of Cancer Chronotherapy Group. *Journal of Clinical Oncology* **24**, 3562–3569 (2006).
167. Lévi, F. Circadian chronotherapy for human cancers. *Lancet Oncol* **2**, 307–315 (2001).
168. Lévi, F., Zidani, R. & Misset, J.-L. Randomised multicentre trial of chronotherapy with oxaliplatin, fluorouracil, and folinic acid in metastatic colorectal cancer. *The Lancet* **350**, 681–686 (1997).

169. Anderson, R. L. *et al.* A framework for the development of effective anti-metastatic agents. *Nat Rev Clin Oncol* **16**, 185–204 (2019).
170. Eisenhauer, E. A. *et al.* New response evaluation criteria in solid tumours: Revised RECIST guideline (version 1.1). *Eur J Cancer* **45**, 228–247 (2009).
171. Scheidmann, M. C. *et al.* An *In Vivo* CRISPR Screen Identifies Stepwise Genetic Dependencies of Metastatic Progression. *Cancer Res* **82**, 681–694 (2022).
172. Xu, X. R., Yousef, G. M. & Ni, H. Cancer and platelet crosstalk: opportunities and challenges for aspirin and other antiplatelet agents. *Blood* **131**, 1777–1789 (2018).
173. Wei, R. *et al.* CTC clusters induced by heparanase enhance breast cancer metastasis. *Acta Pharmacol Sin* **39**, 1326–1337 (2018).
174. Cooke, N. M., Spillane, C. D., Sheils, O., O’Leary, J. & Kenny, D. Aspirin and P2Y₁₂ inhibition attenuate platelet-induced ovarian cancer cell invasion. *BMC Cancer* **15**, 627 (2015).
175. Choi, J. W. *et al.* Urokinase Exerts Antimetastatic Effects by Dissociating Clusters of Circulating Tumor Cells. *Cancer Res* **75**, 4474–4482 (2015).
176. Elia, I. *et al.* Breast cancer cells rely on environmental pyruvate to shape the metastatic niche. *Nature* **568**, 117–121 (2019).
177. Elia, I. *et al.* Proline metabolism supports metastasis formation and could be inhibited to selectively target metastasizing cancer cells. *Nat Commun* **8**, 15267 (2017).
178. Chen, H.-N. *et al.* EpCAM Signaling Promotes Tumor Progression and Protein Stability of PD-L1 through the EGFR Pathway. *Cancer Res* **80**, 5035–5050 (2020).
179. Müller, P. *et al.* Trastuzumab emtansine (T-DM1) renders HER2⁺ breast cancer highly susceptible to CTLA-4/PD-1 blockade. *Sci Transl Med* **7**, (2015).
180. Parkins, K. M. *et al.* Engineering Circulating Tumor Cells as Novel Cancer Theranostics. *Theranostics* **10**, 7925–7937 (2020).
181. Aggarwal, C. *et al.* Relationship among circulating tumor cells, CEA and overall survival in patients with metastatic colorectal cancer. *Annals of Oncology* **24**, 420–428 (2013).
182. Allard, W. J. *et al.* Tumor Cells Circulate in the Peripheral Blood of All Major Carcinomas but not in Healthy Subjects or Patients With Nonmalignant Diseases. *Clinical Cancer Research* **10**, 6897–6904 (2004).
183. Cristofanilli, M. *et al.* Circulating Tumor Cells, Disease Progression, and Survival in Metastatic Breast Cancer. *New England Journal of Medicine* **351**, 781–791 (2004).
184. Hou, J.-M. *et al.* Clinical Significance and Molecular Characteristics of Circulating Tumor Cells and Circulating Tumor Microemboli in Patients With Small-Cell Lung Cancer. *Journal of Clinical Oncology* **30**, 525–532 (2012).

185. Scher, H. I. *et al.* Circulating tumour cells as prognostic markers in progressive, castration-resistant prostate cancer: a reanalysis of IMMC38 trial data. *Lancet Oncol* **10**, 233–239 (2009).
186. Cohen, S. J. *et al.* Isolation and Characterization of Circulating Tumor Cells in Patients with Metastatic Colorectal Cancer. *Clin Colorectal Cancer* **6**, 125–132 (2006).
187. Larsson, A.-M. *et al.* Longitudinal enumeration and cluster evaluation of circulating tumor cells improve prognostication for patients with newly diagnosed metastatic breast cancer in a prospective observational trial. *Breast Cancer Research* **20**, 48 (2018).
188. Krol, I. *et al.* Detection of clustered circulating tumour cells in early breast cancer. *Br J Cancer* **125**, 23–27 (2021).
189. Smerage, J. B. *et al.* Circulating Tumor Cells and Response to Chemotherapy in Metastatic Breast Cancer: SWOG S0500. *Journal of Clinical Oncology* **32**, 3483–3489 (2014).
190. Edge, S. B. & Compton, C. C. The American Joint Committee on Cancer: the 7th Edition of the AJCC Cancer Staging Manual and the Future of TNM. *Ann Surg Oncol* **17**, 1471–1474 (2010).
191. Sen, R. & Baltimore, D. Inducibility of κ immunoglobulin enhancer-binding protein NF- κ B by a posttranslational mechanism. *Cell* **47**, 921–928 (1986).
192. Karin, M. Nuclear factor- κ B in cancer development and progression. *Nature* **441**, 431–436 (2006).
193. Zhang, Q., Lenardo, M. J. & Baltimore, D. 30 Years of NF- κ B: A Blossoming of Relevance to Human Pathobiology. *Cell* **168**, 37–57 (2017).
194. Gilmore, T. D. & Herscovitch, M. Inhibitors of NF- κ B signaling: 785 and counting. *Oncogene* **25**, 6887–6899 (2006).
195. Hayden, M. S. & Ghosh, S. Shared Principles in NF- κ B Signaling. *Cell* **132**, 344–362 (2008).
196. Pasparakis, M., Luedde, T. & Schmidt-Supprian, M. Dissection of the NF- κ B signalling cascade in transgenic and knockout mice. *Cell Death Differ* **13**, 861–872 (2006).
197. Perkins, N. D. Integrating cell-signalling pathways with NF- κ B and IKK function. *Nat Rev Mol Cell Biol* **8**, 49–62 (2007).
198. Ghosh, S. & Karin, M. Missing Pieces in the NF- κ B Puzzle. *Cell* **109**, S81–S96 (2002).
199. Hayden, M. S. & Ghosh, S. NF- κ B, the first quarter-century: remarkable progress and outstanding questions. *Genes Dev* **26**, 203–234 (2012).
200. Smale, S. T. Dimer-specific regulatory mechanisms within the NF- κ B family of transcription factors. *Immunol Rev* **246**, 193–204 (2012).
201. Yamamoto, Y. & Gaynor, R. B. I κ B kinases: key regulators of the NF- κ B pathway. *Trends Biochem Sci* **29**, 72–79 (2004).
202. Tam, W. F., Lee, L. H., Davis, L. & Sen, R. Cytoplasmic Sequestration of Rel Proteins by I κ B α Requires CRM1-Dependent Nuclear Export. *Mol Cell Biol* **20**, 2269–2284 (2000).

203. Arenzana-Seisdedos, F. *et al.* Nuclear localization of I kappa B alpha promotes active transport of NF-kappa B from the nucleus to the cytoplasm. *J Cell Sci* **110** (Pt 3), 369–78 (1997).
204. Karin, M. & Ben-Neriah, Y. Phosphorylation Meets Ubiquitination: The Control of NF-κB Activity. *Annu Rev Immunol* **18**, 621–663 (2000).
205. Espinosa, L. & Marruecos, L. NF-κB-Dependent and -Independent (Moonlighting) IκBα Functions in Differentiation and Cancer. *Biomedicines* **9**, 1278 (2021).
206. Viatour, P. *et al.* Cytoplasmic IκBα increases NF-κB-independent transcription through binding to histone deacetylase (HDAC) 1 and HDAC3. *J Biol Chem* **278**, 46541–8 (2003).
207. Aguilera, C., Hoya-Arias, R., Haegeman, G., Espinosa, L. & Bigas, A. Recruitment of IκBα to the *hes1* promoter is associated with transcriptional repression. *Proceedings of the National Academy of Sciences* **101**, 16537–16542 (2004).
208. Mulero, M. C. *et al.* Chromatin-Bound IκBα Regulates a Subset of Polycomb Target Genes in Differentiation and Cancer. *Cancer Cell* **24**, 151–166 (2013).
209. Marruecos, L. *et al.* IκBα deficiency imposes a fetal phenotype to intestinal stem cells. *EMBO Rep* **21**, (2020).
210. Marruecos, L. *et al.* Dynamic chromatin association of IκBα is regulated by acetylation and cleavage of histone H4. *EMBO Rep* **22**, (2021).
211. Israel, A. The IKK Complex, a Central Regulator of NF- B Activation. *Cold Spring Harb Perspect Biol* **2**, a000158–a000158 (2010).
212. Zandi, E., Rothwarf, D. M., Delhase, M., Hayakawa, M. & Karin, M. The IκB Kinase Complex (IKK) Contains Two Kinase Subunits, IKKα and IKKβ, Necessary for IκB Phosphorylation and NF-κB Activation. *Cell* **91**, 243–252 (1997).
213. Chen, G., Cao, P. & Goeddel, D. V. TNF-Induced Recruitment and Activation of the IKK Complex Require Cdc37 and Hsp90. *Mol Cell* **9**, 401–410 (2002).
214. Hinz, M. *et al.* Signal Responsiveness of IκB Kinases Is Determined by Cdc37-assisted Transient Interaction with Hsp90. *Journal of Biological Chemistry* **282**, 32311–32319 (2007).
215. Sigala, J. L. D. *et al.* Activation of Transcription Factor NF-κB Requires ELKS, an IκB Kinase Regulatory Subunit. *Science* (1979) **304**, 1963–1967 (2004).
216. Scheidereit, C. IκB kinase complexes: gateways to NF-κB activation and transcription. *Oncogene* **25**, 6685–6705 (2006).
217. May, M. J., Marienfeld, R. B. & Ghosh, S. Characterization of the IκB-kinase NEMO Binding Domain. *Journal of Biological Chemistry* **277**, 45992–46000 (2002).
218. Yamamoto, Y., Verma, U. N., Prajapati, S., Kwak, Y.-T. & Gaynor, R. B. Histone H3 phosphorylation by IKK-α is critical for cytokine-induced gene expression. *Nature* **423**, 655–659 (2003).

219. Anest, V. *et al.* A nucleosomal function for I κ B kinase- α in NF- κ B-dependent gene expression. *Nature* **423**, 659–663 (2003).
220. Luo, J.-L. *et al.* Nuclear cytokine-activated IKK α controls prostate cancer metastasis by repressing Maspin. *Nature* **446**, 690–694 (2007).
221. Toll, A. *et al.* Active nuclear IKK correlates with metastatic risk in cutaneous squamous cell carcinoma. *Arch Dermatol Res* **307**, 721–729 (2015).
222. Descargues, P. *et al.* IKK α is a critical coregulator of a Smad4-independent TGF β -Smad2/3 signaling pathway that controls keratinocyte differentiation. *Proc Natl Acad Sci U S A* **105**, 2487–92 (2008).
223. Zhu, F. *et al.* IKK α Shields 14-3-3 σ , a G2/M Cell Cycle Checkpoint Gene, from Hypermethylation, Preventing Its Silencing. *Mol Cell* **27**, 214–227 (2007).
224. Zandi, E., Chen, Y. & Karin, M. Direct Phosphorylation of I κ B by IKK α and IKK β : Discrimination Between Free and NF- κ B-Bound Substrate. *Science* (1979) **281**, 1360–1363 (1998).
225. Delhase, M., Hayakawa, M., Chen, Y. & Karin, M. Positive and Negative Regulation of I κ B Kinase Activity Through IKK β Subunit Phosphorylation. *Science* (1979) **284**, 309–313 (1999).
226. Häcker, H. & Karin, M. Regulation and Function of IKK and IKK-Related Kinases. *Science's STKE* **2006**, (2006).
227. Mercurio, F. *et al.* IKK-1 and IKK-2: Cytokine-Activated I κ B Kinases Essential for NF- κ B Activation. *Science* (1979) **278**, 860–866 (1997).
228. Meylan, E. *et al.* RIP1 is an essential mediator of Toll-like receptor 3-induced NF- κ B activation. *Nat Immunol* **5**, 503–507 (2004).
229. Yang, J. *et al.* The essential role of MEKK3 in TNF-induced NF- κ B activation. *Nat Immunol* **2**, 620–624 (2001).
230. Ea, C.-K., Deng, L., Xia, Z.-P., Pineda, G. & Chen, Z. J. Activation of IKK by TNF α Requires Site-Specific Ubiquitination of RIP1 and Polyubiquitin Binding by NEMO. *Mol Cell* **22**, 245–257 (2006).
231. Pobezinskaya, Y. L. *et al.* The function of TRADD in signaling through tumor necrosis factor receptor 1 and TRIF-dependent Toll-like receptors. *Nat Immunol* **9**, 1047–1054 (2008).
232. Wang, C. *et al.* TAK1 is a ubiquitin-dependent kinase of MKK and IKK. *Nature* **412**, 346–351 (2001).
233. Kanarek, N. & Ben-Neriah, Y. Regulation of NF- κ B by ubiquitination and degradation of the I κ Bs. *Immunol Rev* **246**, 77–94 (2012).
234. Claudio, E., Brown, K., Park, S., Wang, H. & Siebenlist, U. BAFF-induced NEMO-independent processing of NF- κ B2 in maturing B cells. *Nat Immunol* **3**, 958–965 (2002).
235. Coope, H. J. CD40 regulates the processing of NF- κ B2 p100 to p52. *EMBO J* **21**, 5375–5385 (2002).

236. Dejardin, E. *et al.* The Lymphotoxin- β Receptor Induces Different Patterns of Gene Expression via Two NF- κ B Pathways. *Immunity* **17**, 525–535 (2002).
237. Senftleben, U. *et al.* Activation by IKK α of a Second, Evolutionary Conserved, NF- κ B Signaling Pathway. *Science* (1979) **293**, 1495–1499 (2001).
238. He, J. Q., Saha, S. K., Kang, J. R., Zarnegar, B. & Cheng, G. Specificity of TRAF3 in Its Negative Regulation of the Noncanonical NF- κ B Pathway. *Journal of Biological Chemistry* **282**, 3688–3694 (2007).
239. Cildir, G., Low, K. C. & Tergaonkar, V. Noncanonical NF- κ B Signaling in Health and Disease. *Trends Mol Med* **22**, 414–429 (2016).
240. Sun, S.-C. The non-canonical NF- κ B pathway in immunity and inflammation. *Nat Rev Immunol* **17**, 545–558 (2017).
241. Hinz, M. & Scheidereit, C. The I κ B kinase complex in NF- κ B regulation and beyond. *EMBO Rep* **15**, 46–61 (2014).
242. Park, K.-J., Krishnan, V., O'Malley, B. W., Yamamoto, Y. & Gaynor, R. B. Formation of an IKK α -Dependent Transcription Complex Is Required for Estrogen Receptor-Mediated Gene Activation. *Mol Cell* **18**, 71–82 (2005).
243. Tu, Z. *et al.* IKK α Regulates Estrogen-induced Cell Cycle Progression by Modulating E2F1 Expression. *Journal of Biological Chemistry* **281**, 6699–6706 (2006).
244. Zhang, W. *et al.* A NIK-IKK α Module Expands ErbB2-Induced Tumor-Initiating Cells by Stimulating Nuclear Export of p27/Kip1. *Cancer Cell* **23**, 647–659 (2013).
245. Huang, W.-C., Ju, T.-K., Hung, M.-C. & Chen, C.-C. Phosphorylation of CBP by IKK α Promotes Cell Growth by Switching the Binding Preference of CBP from p53 to NF- κ B. *Mol Cell* **26**, 75–87 (2007).
246. Fernández-Majada, V. *et al.* Aberrant Cytoplasmic Localization of N-CoR in Colorectal Tumors. *Cell Cycle* **6**, 1748–1752 (2007).
247. Fernández-Majada, V. *et al.* Nuclear IKK activity leads to dysregulated Notch-dependent gene expression in colorectal cancer. *Proceedings of the National Academy of Sciences* **104**, 276–281 (2007).
248. Colomer, C. *et al.* IKK α is required in the intestinal epithelial cells for tumour stemness. *Br J Cancer* **118**, 839–846 (2018).
249. Colomer, C. *et al.* IKK α Kinase Regulates the DNA Damage Response and Drives Chemo-resistance in Cancer. *Mol Cell* **75**, 669–682.e5 (2019).
250. Pecharromán, I. *et al.* I κ B kinase- α coordinates BRD4 and JAK/STAT signaling to subvert DNA damage-based anticancer therapy. *EMBO J* **42**, (2023).
251. Gilmore, T. D. & Garbati, M. R. Inhibition of NF- κ B Signaling as a Strategy in Disease Therapy. in 245–263 (2010). doi:10.1007/82_2010_105.

252. Karin, M., Yamamoto, Y. & Wang, Q. M. The IKK NF- κ B system: a treasure trove for drug development. *Nat Rev Drug Discov* **3**, 17–26 (2004).
253. Cereijido, M., Contreras, R. G., Shoshani, L., Flores-Benitez, D. & Larre, I. Tight junction and polarity interaction in the transporting epithelial phenotype. *Biochimica et Biophysica Acta (BBA) - Biomembranes* **1778**, 770–793 (2008).
254. Martin-Belmonte, F. & Perez-Moreno, M. Epithelial cell polarity, stem cells and cancer. *Nat Rev Cancer* **12**, 23–38 (2012).
255. Van Itallie, C. M. & Anderson, J. M. Architecture of tight junctions and principles of molecular composition. *Semin Cell Dev Biol* **36**, 157–165 (2014).
256. Balda, M. S., Gonzalez-Mariscal, L., Matter, K., Cereijido, M. & Anderson, J. M. Assembly of the tight junction: the role of diacylglycerol. *J Cell Biol* **123**, 293–302 (1993).
257. Gumbiner, B., Lowenkopf, T. & Apatira, D. Identification of a 160-kDa polypeptide that binds to the tight junction protein ZO-1. *Proceedings of the National Academy of Sciences* **88**, 3460–3464 (1991).
258. Haskins, J., Gu, L., Wittchen, E. S., Hibbard, J. & Stevenson, B. R. ZO-3, a Novel Member of the MAGUK Protein Family Found at the Tight Junction, Interacts with ZO-1 and Occludin. *J Cell Biol* **141**, 199–208 (1998).
259. Dobrosotskaya, I., Guy, R. K. & James, G. L. MAGI-1, a Membrane-associated Guanylate Kinase with a Unique Arrangement of Protein-Protein Interaction Domains. *Journal of Biological Chemistry* **272**, 31589–31597 (1997).
260. Ide, N. *et al.* Localization of membrane-associated guanylate kinase (MAGI)-1/BAI-associated protein (BAP) 1 at tight junctions of epithelial cells. *Oncogene* **18**, 7810–7815 (1999).
261. Hamazaki, Y., Itoh, M., Sasaki, H., Furuse, M. & Tsukita, S. Multi-PDZ Domain Protein 1 (MUPP1) Is Concentrated at Tight Junctions through Its Possible Interaction with Claudin-1 and Junctional Adhesion Molecule. *Journal of Biological Chemistry* **277**, 455–461 (2002).
262. Zihni, C., Mills, C., Matter, K. & Balda, M. S. Tight junctions: from simple barriers to multifunctional molecular gates. *Nat Rev Mol Cell Biol* **17**, 564–580 (2016).
263. Lemmers, C. *et al.* hINADL/PATJ, a Homolog of Discs Lost, Interacts with Crumbs and Localizes to Tight Junctions in Human Epithelial Cells. *Journal of Biological Chemistry* **277**, 25408–25415 (2002).
264. Stevenson, B. R., Heintzelman, M. B., Anderson, J. M., Citi, S. & Mooseker, M. S. ZO-1 and cingulin: tight junction proteins with distinct identities and localizations. *American Journal of Physiology-Cell Physiology* **257**, C621–C628 (1989).
265. Steed, E. *et al.* MarvelD3 couples tight junctions to the MEKK1–JNK pathway to regulate cell behavior and survival. *Journal of Cell Biology* **204**, 821–838 (2014).
266. Fredriksson, K. *et al.* Proteomic Analysis of Proteins Surrounding Occludin and Claudin-4 Reveals Their Proximity to Signaling and Trafficking Networks. *PLoS One* **10**, e0117074 (2015).

267. Zihni, C., Balda, M. S. & Matter, K. Signalling at tight junctions during epithelial differentiation and microbial pathogenesis. *J Cell Sci* **127**, 3401–3413 (2014).
268. González-Mariscal, L. *et al.* Tight junctions and the regulation of gene expression. *Semin Cell Dev Biol* **36**, 213–223 (2014).
269. Quiros, M. & Nusrat, A. RhoGTPases, actomyosin signaling and regulation of the Epithelial Apical Junctional Complex. *Semin Cell Dev Biol* **36**, 194–203 (2014).
270. Furuse, M. *et al.* Overexpression of occludin, a tight junction-associated integral membrane protein, induces the formation of intracellular multilamellar bodies bearing tight junction-like structures. *J Cell Sci* **109**, 429–435 (1996).
271. Furuse, M., Sasaki, H., Fujimoto, K. & Tsukita, S. A Single Gene Product, Claudin-1 or -2, Reconstitutes Tight Junction Strands and Recruits Occludin in Fibroblasts. *J Cell Biol* **143**, 391–401 (1998).
272. Kubota, K. *et al.* Ca²⁺-independent cell-adhesion activity of claudins, a family of integral membrane proteins localized at tight junctions. *Current Biology* **9**, 1035-S1 (1999).
273. Morita, K., Furuse, M., Fujimoto, K. & Tsukita, S. Claudin multigene family encoding four-transmembrane domain protein components of tight junction strands. *Proceedings of the National Academy of Sciences* **96**, 511–516 (1999).
274. Itallie, C. M. Van & Anderson, J. M. Occludin confers adhesiveness when expressed in fibroblasts. *J Cell Sci* **110**, 1113–1121 (1997).
275. Osler, M. E., Chang, M. S. & Bader, D. M. Bves modulates epithelial integrity through an interaction at the tight junction. *J Cell Sci* **118**, 4667–4678 (2005).
276. Luissint, A.-C., Nusrat, A. & Parkos, C. A. JAM-related proteins in mucosal homeostasis and inflammation. *Semin Immunopathol* **36**, 211–226 (2014).
277. Martín-Padura, I. *et al.* Junctional Adhesion Molecule, a Novel Member of the Immunoglobulin Superfamily That Distributes at Intercellular Junctions and Modulates Monocyte Transmigration. *J Cell Biol* **142**, 117–127 (1998).
278. Cohen, C. J. *et al.* The coxsackievirus and adenovirus receptor is a transmembrane component of the tight junction. *Proceedings of the National Academy of Sciences* **98**, 15191–15196 (2001).
279. Higashi, T. *et al.* Analysis of the angulin family consisting of LSR, ILDR1 and ILDR2: tricellulin recruitment, epithelial barrier function and implication in deafness pathogenesis. *J Cell Sci* (2012) doi:10.1242/jcs.116442.
280. Leech, A. O., Cruz, R. G. B., Hill, A. D. K. & Hopkins, A. M. Paradigms lost-an emerging role for over-expression of tight junction adhesion proteins in cancer pathogenesis. *Ann Transl Med* **3**, 184 (2015).
281. Gowrikumar, S., Singh, A. B. & Dhawan, P. Role of Claudin Proteins in Regulating Cancer Stem Cells and Chemoresistance-Potential Implication in Disease Prognosis and Therapy. *Int J Mol Sci* **21**, 53 (2019).

282. Nehme, Z., Roehlen, N., Dhawan, P. & Baumert, T. F. Tight Junction Protein Signaling and Cancer Biology. *Cells* **12**, 243 (2023).
283. Balda, M. S., Garrett, M. D. & Matter, K. The ZO-1-associated Y-box factor ZONAB regulates epithelial cell proliferation and cell density. *J Cell Biol* **160**, 423–432 (2003).
284. Singh, A. B., Sharma, A. & Dhawan, P. Claudin-1 expression confers resistance to anoikis in colon cancer cells in a Src-dependent manner. *Carcinogenesis* **33**, 2538–2547 (2012).
285. Wu, J. *et al.* RBM38 is involved in TGF- β -induced epithelial-to-mesenchymal transition by stabilising zonula occludens-1 mRNA in breast cancer. *Br J Cancer* **117**, 675–684 (2017).
286. Nito, M. *et al.* Par3 and ZO-1 Membrane Clustering is an Indicator of Poor Prognosis in Lung Squamous Cell Carcinoma. *Tokai J Exp Clin Med* **46**, 110–117 (2021).
287. Kim, T. H. *et al.* Down-regulation of claudin-2 in breast carcinomas is associated with advanced disease. *Histopathology* **53**, 48–55 (2008).
288. Aung, P. P. *et al.* Differential expression of claudin-2 in normal human tissues and gastrointestinal carcinomas. *Virchows Archiv* **448**, 428–434 (2006).
289. Kinugasa, T. *et al.* Selective up-regulation of claudin-1 and claudin-2 in colorectal cancer. *Anticancer Res* **27**, 3729–34 (2007).
290. Dhawan, P. *et al.* Claudin-2 expression increases tumorigenicity of colon cancer cells: role of epidermal growth factor receptor activation. *Oncogene* **30**, 3234–3247 (2011).
291. Hichino, A. *et al.* Down-regulation of Claudin-2 Expression and Proliferation by Epigenetic Inhibitors in Human Lung Adenocarcinoma A549 Cells. *Journal of Biological Chemistry* **292**, 2411–2421 (2017).
292. Chang, F. *et al.* Involvement of PI3K/Akt pathway in cell cycle progression, apoptosis, and neoplastic transformation: a target for cancer chemotherapy. *Leukemia* **17**, 590–603 (2003).
293. Ikari, A. *et al.* Claudin-2 knockdown decreases matrix metalloproteinase-9 activity and cell migration via suppression of nuclear Sp1 in A549 cells. *Life Sci* **88**, 628–633 (2011).
294. Paquet-Fifield, S. *et al.* Tight Junction Protein Claudin-2 Promotes Self-Renewal of Human Colorectal Cancer Stem-like Cells. *Cancer Res* **78**, 2925–2938 (2018).
295. Mezheyeuski, A. *et al.* Treatment-related survival associations of claudin-2 expression in fibroblasts of colorectal cancer. *Virchows Archiv* **472**, 395–405 (2018).
296. Nakayama, I. *et al.* Claudin 18.2 as a novel therapeutic target. *Nat Rev Clin Oncol* **21**, 354–369 (2024).
297. van Laarhoven, H. W. M. & Derks, S. Claudin-18.2 targeting by zolbetuximab: results of SPOTLIGHT in perspective. *The Lancet* **401**, 1630–1631 (2023).
298. Colpitts, C. C. *et al.* Humanisation of a claudin-1-specific monoclonal antibody for clinical prevention and cure of HCV infection without escape. *Gut* gutjnl-2016-312577 (2017) doi:10.1136/gutjnl-2016-312577.

299. Fujiwara-Tani, R. *et al.* Anti-claudin-4 extracellular domain antibody enhances the antitumoral effects of chemotherapeutic and antibody drugs in colorectal cancer. *Oncotarget* **9**, 37367–37378 (2018).
300. Hashimoto, Y. *et al.* Safety evaluation of a human chimeric monoclonal antibody that recognizes the extracellular loop domain of claudin-2. *European Journal of Pharmaceutical Sciences* **117**, 161–167 (2018).
301. Sato, T. *et al.* Long-term Expansion of Epithelial Organoids From Human Colon, Adenoma, Adenocarcinoma, and Barrett's Epithelium. *Gastroenterology* **141**, 1762–1772 (2011).
302. Shalem, O. *et al.* Genome-scale CRISPR-Cas9 knockout screening in human cells. *Science* **343**, 84–87 (2014).
303. Krueger, B. *et al.* Different evolutionary modifications as a guide to rewire two-component systems. *Bioinform Biol Insights* **6**, 97–128 (2012).
304. Langmead, B. & Salzberg, S. L. Fast gapped-read alignment with Bowtie 2. *Nat Methods* **9**, 357–9 (2012).
305. Zhang, Y. *et al.* Model-based analysis of ChIP-Seq (MACS). *Genome Biol* **9**, R137 (2008).
306. Yu, G., Wang, L.-G. & He, Q.-Y. ChIPseeker: an R/Bioconductor package for ChIP peak annotation, comparison and visualization. *Bioinformatics* **31**, 2382–3 (2015).
307. Krueger, F., James, F., Ewels, P., Afyounian, E., & Schuster-Boeckler, B. (2020). FelixKrueger/TrimGalore - DOI via Zenodo. <https://doi.org/https://zenodo.org/record/7598955#.ZGOKAi8RpR4>.
308. Liao, Y., Smyth, G. K. & Shi, W. featureCounts: an efficient general purpose program for assigning sequence reads to genomic features. *Bioinformatics* **30**, 923–930 (2014).
309. Love, M. I., Huber, W. & Anders, S. Moderated estimation of fold change and dispersion for RNA-seq data with DESeq2. *Genome Biol* **15**, 550 (2014).
310. Zhu, A., Ibrahim, J. G. & Love, M. I. Heavy-tailed prior distributions for sequence count data: removing the noise and preserving large differences. *Bioinformatics* **35**, 2084–2092 (2019).
311. Callari, M. *et al.* Computational approach to discriminate human and mouse sequences in patient-derived tumour xenografts. *BMC Genomics* **19**, 19 (2018).
312. Zheng, G. X. Y. *et al.* Massively parallel digital transcriptional profiling of single cells. *Nat Commun* **8**, 14049 (2017).
313. Hao, Y. *et al.* Dictionary learning for integrative, multimodal and scalable single-cell analysis. *Nat Biotechnol* **42**, 293–304 (2024).
314. Germain, P.-L., Lun, A., Garcia Meixide, C., Macnair, W. & Robinson, M. D. Doublet identification in single-cell sequencing data using scDblFinder. *F1000Res* **10**, 979 (2022).

315. van Dijk, D. *et al.* Recovering Gene Interactions from Single-Cell Data Using Data Diffusion. *Cell* **174**, 716–729.e27 (2018).
316. Andreatta, M. & Carmona, S. J. UCell: Robust and scalable single-cell gene signature scoring. *Comput Struct Biotechnol J* **19**, 3796–3798 (2021).
317. A.Bigas and L.Espinosa Lab. (2024). CRC Metacohort [Data set]. Zenodo. <https://doi.org/10.5281/zenodo.13303050>.
318. Davis, S. & Meltzer, P. S. GEOquery: a bridge between the Gene Expression Omnibus (GEO) and BioConductor. *Bioinformatics* **23**, 1846–1847 (2007).
319. Gautier, L., Cope, L., Bolstad, B. M. & Irizarry, R. A. affy—analysis of *Affymetrix GeneChip* data at the probe level. *Bioinformatics* **20**, 307–315 (2004).
320. McCall, M. N., Bolstad, B. M. & Irizarry, R. A. Frozen robust multiarray analysis (fRMA). *Biostatistics* **11**, 242–253 (2010).
321. Leek, J. T., Johnson, W. E., Parker, H. S., Jaffe, A. E. & Storey, J. D. The `sva` package for removing batch effects and other unwanted variation in high-throughput experiments. *Bioinformatics* **28**, 882–883 (2012).
322. Li, Q., Birkbak, N. J., Györfy, B., Szallasi, Z. & Eklund, A. C. Jetset: selecting the optimal microarray probe set to represent a gene. *BMC Bioinformatics* **12**, 474 (2011).
323. Therneau, T. M. (2024). A Package for Survival Analysis in R <https://CRAN.R-project.org/package=survival>.
324. Ashburner, M. *et al.* Gene Ontology: tool for the unification of biology. *Nat Genet* **25**, 25–29 (2000).
325. Gu, Z., Eils, R. & Schlesner, M. Complex heatmaps reveal patterns and correlations in multidimensional genomic data. *Bioinformatics* **32**, 2847–2849 (2016).
326. Margalef, P. *et al.* BRAF-induced tumorigenesis is IKK α -dependent but NF- κ B-independent. *Sci Signal* **8**, (2015).
327. Halvorsen, T. B. & Seim, E. Degree of differentiation in colorectal adenocarcinomas: a multivariate analysis of the influence on survival. *J Clin Pathol* **41**, 532–537 (1988).
328. Colomer, C., Pecharroman, I., Bigas, A. & Espinosa, L. Targeting IKK α kinase to prevent tumor progression and therapy resistance. *Cancer Drug Resist* **3**, 482–490 (2020).
329. Alonso-Marañón, J. *et al.* Combination of chemotherapy with BRAF inhibitors results in effective eradication of malignant melanoma by preventing ATM-dependent DNA repair. *Oncogene* **40**, 5042–5048 (2021).
330. Dukes, J. D., Whitley, P. & Chalmers, A. D. The PIKfyve inhibitor YM201636 blocks the continuous recycling of the tight junction proteins claudin-1 and claudin-2 in MDCK cells. *PLoS One* **7**, e28659 (2012).

331. Cui, H.-Y. *et al.* CD147 receptor is essential for TFF3-mediated signaling regulating colorectal cancer progression. *Signal Transduct Target Ther* **6**, 268 (2021).
332. Zhang, W. & Liu, H. T. MAPK signal pathways in the regulation of cell proliferation in mammalian cells. *Cell Res* **12**, 9–18 (2002).
333. Karamitopoulou, E. *et al.* Systematic analysis of proteins from different signaling pathways in the tumor center and the invasive front of colorectal cancer. *Hum Pathol* **42**, 1888–96 (2011).
334. Kim, H.-S. *et al.* Expression of phosphorylated extracellular signal-regulated kinase at the invasive front of hepatic colorectal metastasis. *Oncol Lett* **9**, 1261–1265 (2015).
335. Chen, H.-F., Chuang, H.-C. & Tan, T.-H. Regulation of Dual-Specificity Phosphatase (DUSP) Ubiquitination and Protein Stability. *Int J Mol Sci* **20**, (2019).
336. Xie, Z. *et al.* Gene Set Knowledge Discovery with Enrichr. *Curr Protoc* **1**, (2021).
337. Tran, K. *et al.* SIRT7 regulates NUCKS1 chromatin binding to elicit metabolic and inflammatory gene expression in senescence and liver aging. *bioRxiv* (2024) doi:10.1101/2024.02.05.578810.
338. Li, B. *et al.* Roles of increased NUCKS1 expression in endometriosis. *BMC Womens Health* **23**, 432 (2023).
339. Poon, M.-W. *et al.* Inhibition of NUCKS Facilitates Corneal Recovery Following Alkali Burn. *Sci Rep* **7**, 41224 (2017).
340. Subbiah, V., Baik, C. & Kirkwood, J. M. Clinical Development of BRAF plus MEK Inhibitor Combinations. *Trends Cancer* **6**, 797–810 (2020).
341. Atefi, M. *et al.* Combination of pan-RAF and MEK inhibitors in NRAS mutant melanoma. *Mol Cancer* **14**, 27 (2015).
342. Adamopoulos, C. *et al.* Exploiting Allosteric Properties of RAF and MEK Inhibitors to Target Therapy-Resistant Tumors Driven by Oncogenic BRAF Signaling. *Cancer Discov* **11**, 1716–1735 (2021).
343. Larkin, J. *et al.* Combined vemurafenib and cobimetinib in BRAF-mutated melanoma. *N Engl J Med* **371**, 1867–76 (2014).
344. Robert, C. *et al.* Improved overall survival in melanoma with combined dabrafenib and trametinib. *N Engl J Med* **372**, 30–9 (2015).
345. Huxford, T., Huang, D.-B., Malek, S. & Ghosh, G. The Crystal Structure of the I κ B α /NF- κ B Complex Reveals Mechanisms of NF- κ B Inactivation. *Cell* **95**, 759–770 (1998).
346. Mayo, C., Lloreta, J., Real, F. X. & Mayol, X. In vitro differentiation of HT-29 M6 mucus-secreting colon cancer cells involves a trychostatin A and p27^{KIP1}-inducible transcriptional program of gene expression. *J Cell Physiol* **212**, 42–50 (2007).
347. He, F., Ru, X. & Wen, T. NRF2, a Transcription Factor for Stress Response and Beyond. *Int J Mol Sci* **21**, 4777 (2020).

348. Casper, E. The crosstalk between Nrf2 and NF- κ B pathways in coronary artery disease: Can it be regulated by SIRT6? *Life Sci* **330**, 122007 (2023).
349. Liu, S. *et al.* Pseudolaric acid B exerts an antifungal effect and targets SIRT1 to ameliorate inflammation by regulating Nrf2/NF- κ B pathways in fungal keratitis. *Inflammopharmacology* **32**, 1133–1146 (2024).
350. Matouk, A. I., Awad, E. M., El-Tahawy, N. F. G., El-Sheikh, A. A. K. & Anter, A. Dihydromyricetin Modulates Nrf2 and NF- κ B Crosstalk to Alleviate Methotrexate-Induced Lung Toxicity. *Pharmaceuticals* **16**, 481 (2023).
351. Gao, W. *et al.* Dissecting the Crosstalk Between Nrf2 and NF- κ B Response Pathways in Drug-Induced Toxicity. *Front Cell Dev Biol* **9**, (2022).
352. Wang, L. *et al.* EZH2 depletion potentiates MYC degradation inhibiting neuroblastoma and small cell carcinoma tumor formation. *Nat Commun* **13**, 12 (2022).
353. Rao, R. A. *et al.* Ezh2 mediated H3K27me3 activity facilitates somatic transition during human pluripotent reprogramming. *Sci Rep* **5**, 8229 (2015).
354. Adhikary, T. *et al.* Genomewide Analyses Define Different Modes of Transcriptional Regulation by Peroxisome Proliferator-Activated Receptor- β/δ (PPAR β/δ). *PLoS One* **6**, e16344 (2011).
355. Muñoz, J. *et al.* The Lgr5 intestinal stem cell signature: robust expression of proposed quiescent ‘+4’ cell markers. *EMBO J* **31**, 3079–3091 (2012).
356. Battaglin, F. *et al.* Neurotransmitter signaling: a new frontier in colorectal cancer biology and treatment. *Oncogene* **41**, 4769–4778 (2022).
357. Wong, V. W. Y. *et al.* Lrig1 controls intestinal stem-cell homeostasis by negative regulation of ErbB signalling. *Nat Cell Biol* **14**, 401–408 (2012).
358. Husain, A. *et al.* Ephrin-A3/EphA2 axis regulates cellular metabolic plasticity to enhance cancer stemness in hypoxic hepatocellular carcinoma. *J Hepatol* **77**, 383–396 (2022).
359. Jiang, G. *et al.* Annexin A13 promotes tumor cell invasion *in vitro* and is associated with metastasis in human colorectal cancer. *Oncotarget* **8**, 21663–21673 (2017).
360. Chen, D. *et al.* Comprehensive analyses of solute carrier family members identify SLC12A2 as a novel therapy target for colorectal cancer. *Sci Rep* **14**, 4459 (2024).
361. Xu, W. *et al.* RNA interference against TRIM29 inhibits migration and invasion of colorectal cancer cells. *Oncol Rep* **36**, 1411–1418 (2016).
362. Wesley, T., Berzins, S., Kannourakis, G. & Ahmed, N. The attributes of plakins in cancer and disease: perspectives on ovarian cancer progression, chemoresistance and recurrence. *Cell Communication and Signaling* **19**, 55 (2021).
363. Bredel, M. *et al.* Haploinsufficiency of NFKBIA reshapes the epigenome antipodal to the IDH mutation and imparts disease fate in diffuse gliomas. *Cell Rep Med* **4**, 101082 (2023).

364. Hu, M. C.-T. *et al.* I κ B Kinase Promotes Tumorigenesis through Inhibition of Forkhead FOXO3a. *Cell* **117**, 225–237 (2004).
365. Karin, M. & Greten, F. R. NF- κ B: linking inflammation and immunity to cancer development and progression. *Nat Rev Immunol* **5**, 749–759 (2005).
366. Vreka, M. *et al.* I κ B Kinase α Is Required for Development and Progression of *KRAS* -Mutant Lung Adenocarcinoma. *Cancer Res* **78**, 2939–2951 (2018).
367. Xie, W. *et al.* IKBKE phosphorylates and stabilizes Snail to promote breast cancer invasion and metastasis. *Cell Death Differ* **29**, 1528–1540 (2022).
368. Awasthee, N. *et al.* Targeting I κ B kinases for cancer therapy. *Semin Cancer Biol* **56**, 12–24 (2019).
369. Lee, D.-F. & Hung, M.-C. Advances in targeting IKK and IKK-related kinases for cancer therapy. *Clin Cancer Res* **14**, 5656–62 (2008).
370. Mauro, C., Zazzeroni, F., Papa, S., Bubici, C. & Franzoso, G. The NF- κ B Transcription Factor Pathway as a Therapeutic Target in Cancer: Methods for Detection of NF- κ B Activity. in 169–207 (2009). doi:10.1007/978-1-60327-530-9_10.
371. Ping, H., Yang, F., Wang, M., Niu, Y. & Xing, N. IKK inhibitor suppresses epithelial-mesenchymal transition and induces cell death in prostate cancer. *Oncol Rep* **36**, 1658–1664 (2016).
372. Ghosh, D., Dutta, A., Kashyap, A., Upmanyu, N. & Datta, S. PLP2 drives collective cell migration via ZO-1-mediated cytoskeletal remodeling at the leading edge in human colorectal cancer cells. *J Cell Sci* **134**, (2021).
373. Song, N.-Y. *et al.* IKK α inactivation promotes Kras-initiated lung adenocarcinoma development through disrupting major redox regulatory pathways. *Proceedings of the National Academy of Sciences* **115**, (2018).
374. DeCamp, S. J. *et al.* Epithelial layer unjamming shifts energy metabolism toward glycolysis. *Sci Rep* **10**, 18302 (2020).
375. Friedl, P. & Gilmour, D. Collective cell migration in morphogenesis, regeneration and cancer. *Nat Rev Mol Cell Biol* **10**, 445–457 (2009).
376. Labuschagne, C. F., Cheung, E. C., Blagih, J., Domart, M.-C. & Vousden, K. H. Cell Clustering Promotes a Metabolic Switch that Supports Metastatic Colonization. *Cell Metab* **30**, 720-734.e5 (2019).
377. Pastushenko, I. & Blanpain, C. EMT Transition States during Tumor Progression and Metastasis. *Trends Cell Biol* **29**, 212–226 (2019).
378. Arumugam, T. *et al.* Trefoil Factor 1 Stimulates Both Pancreatic Cancer and Stellate Cells and Increases Metastasis. *Pancreas* **40**, 815–822 (2011).
379. Bougen, N. M. *et al.* Trefoil factor 1 suppression of E-CADHERIN enhances prostate carcinoma cell invasiveness and metastasis. *Cancer Lett* **332**, 19–29 (2013).

380. Spadazzi, C. *et al.* Trefoil factor-1 upregulation in estrogen-receptor positive breast cancer correlates with an increased risk of bone metastasis. *Bone* **144**, 115775 (2021).
381. Ahmed, A. R. H., Griffiths, A. B., Tilby, M. T., Westley, B. R. & May, F. E. B. TFF3 Is a Normal Breast Epithelial Protein and Is Associated with Differentiated Phenotype in Early Breast Cancer but Predisposes to Invasion and Metastasis in Advanced Disease. *Am J Pathol* **180**, 904–916 (2012).
382. Li, Y. *et al.* KLF9 suppresses gastric cancer cell invasion and metastasis through transcriptional inhibition of MMP28. *The FASEB Journal* **33**, 7915–7928 (2019).
383. Zhang, J. *et al.* Overexpression of MMP21 and MMP28 is associated with gastric cancer progression and poor prognosis. *Oncol Lett* **15**, 7776–7782 (2018).
384. Zhou, J. *et al.* Upregulated MMP28 in Hepatocellular Carcinoma Promotes Metastasis via Notch3 Signaling and Predicts Unfavorable Prognosis. *Int J Biol Sci* **15**, 812–825 (2019).
385. Liao, Y.-M. *et al.* High B3GALT5 expression confers poor clinical outcome and contributes to tumor progression and metastasis in breast cancer. *Breast Cancer Research* **23**, 5 (2021).
386. Fu, H. *et al.* Integrated analysis of colorectal cancer metastasis identifies characteristics of tumor cell during metastasis. *Gastroenterol Rep (Oxf)* **12**, (2023).
387. Jia, Y. *et al.* The novel KLF4/PLAC8 signaling pathway regulates lung cancer growth. *Cell Death Dis* **9**, 603 (2018).
388. Kaistha, B. P. *et al.* PLAC8 Localizes to the Inner Plasma Membrane of Pancreatic Cancer Cells and Regulates Cell Growth and Disease Progression through Critical Cell-Cycle Regulatory Pathways. *Cancer Res* **76**, 96–107 (2016).
389. Kinsey, C. *et al.* Plac8 Links Oncogenic Mutations to Regulation of Autophagy and Is Critical to Pancreatic Cancer Progression. *Cell Rep* **7**, 1143–1155 (2014).
390. Ma, R. Y. M. *et al.* Raf/MEK/MAPK signaling stimulates the nuclear translocation and transactivating activity of FOXM1c. *J Cell Sci* **118**, 795–806 (2005).
391. Xie, P. *et al.* Atrogin-1/MAFbx Enhances Simulated Ischemia/Reperfusion-induced Apoptosis in Cardiomyocytes through Degradation of MAPK Phosphatase-1 and Sustained JNK Activation. *Journal of Biological Chemistry* **284**, 5488–5496 (2009).
392. Choi, B.-H., Hur, E.-M., Lee, J.-H., Jun, D.-J. & Kim, K.-T. Protein kinase C δ -mediated proteasomal degradation of MAP kinase phosphatase-1 contributes to glutamate-induced neuronal cell death. *J Cell Sci* **119**, 1329–1340 (2006).
393. Kusakabe, T. *et al.* DUSP-1 Induced by PGE2 and PGE1 Attenuates IL-1 β -Activated MAPK Signaling, Leading to Suppression of NGF Expression in Human Intervertebral Disc Cells. *Int J Mol Sci* **23**, 371 (2021).
394. Zhang, W. *et al.* USP49 inhibits ischemia–reperfusion-induced cell viability suppression and apoptosis in human AC16 cardiomyocytes through DUSP1–JNK1/2 signaling. *J Cell Physiol* **234**, 6529–6538 (2019).

395. Kucharska, A., Rushworth, L. K., Staples, C., Morrice, N. A. & Keyse, S. M. Regulation of the inducible nuclear dual-specificity phosphatase DUSP5 by ERK MAPK. *Cell Signal* **21**, 1794–1805 (2009).
396. Seo, H. *et al.* Dual-specificity phosphatase 5 acts as an anti-inflammatory regulator by inhibiting the ERK and NF- κ B signaling pathways. *Sci Rep* **7**, 17348 (2017).
397. Desgrosellier, J. S. & Cheresch, D. A. Integrins in cancer: biological implications and therapeutic opportunities. *Nat Rev Cancer* **10**, 9–22 (2010).
398. Brena, D. *et al.* Ancestral function of Inhibitors-of-kappaB regulates *Caenorhabditis elegans* development. *Sci Rep* **10**, 16153 (2020).
399. Cabannes, E., Khan, G., Aillet, F., Jarrett, R. F. & Hay, R. T. Mutations in the I κ B α gene in Hodgkin's disease suggest a tumour suppressor role for I κ B α . *Oncogene* **18**, 3063–3070 (1999).
400. Iannetti, A. *et al.* Regulation of p53 and Rb Links the Alternative NF- κ B Pathway to EZH2 Expression and Cell Senescence. *PLoS Genet* **10**, e1004642 (2014).
401. Lee, S. T. *et al.* Context-Specific Regulation of NF- κ B Target Gene Expression by EZH2 in Breast Cancers. *Mol Cell* **43**, 798–810 (2011).
402. Emmerich, F. *et al.* Inactivating I kappa B epsilon mutations in Hodgkin/Reed–Sternberg cells. *J Pathol* **201**, 413–420 (2003).
403. Lesuffleur, T., Barbat, A., Dussaulx, E. & Zweibaum, A. Growth adaptation to methotrexate of HT-29 human colon carcinoma cells is associated with their ability to differentiate into columnar absorptive and mucus-secreting cells. *Cancer Res* **50**, 6334–43 (1990).
404. Bredel, M. *et al.* NFKBIA Deletion in Glioblastomas. *New England Journal of Medicine* **364**, 627–637 (2011).